Multiphase fuel combustion in a swirl diffusion burner: an operational and performance study

By

Ogbonnaya Agwu

A thesis submitted in partial fulfilment of the requirements for the degree of Doctor of Philosophy in Mechanical Engineering

School of Engineering

Cardiff University

August 2020

Summary

Meeting the ever-growing energy demands of the world while not sacrificing energy security/environmental sustainability by relying on a single fuel source means that combustion systems must demonstrate fuel flexibility. Currently, the gas turbine burns a wide range of fuels and fuel combinations. However, there seems to be a limit to an exploration of its fuel flexibility. Whereas there are numerous investigations into multiphase fuel combustion in other internal combustion engines like the diesel engine, there is a dearth of such studies for the gas turbine. Consequently, this thesis investigates the simultaneous combustion of practical liquid and gaseous fuels in a 20 kW swirl-stabilised gas turbine relevant combustor.

The investigation involved developing a dual-phase fuel injection system capable of handling diesel/methane, diesel/syngas, biodiesel/methane, biodiesel/syngas and blends of methanol/glycerol co-combusted with methane. The effect of partly replacing the liquid fuel with a gaseous type fuel on combustion characteristics like flammability limits, flame stability, flame structure and exhaust emissions were studied for the diesel and biodiesel blends. The gas substitution ratio was based on heat energy contribution in such a manner that a certain percentage of a desired heat output is contributed by the gaseous fuel and the balance by the liquid fuel. The nature of non-reacting flows in the system, including air flow and liquid fuel spray was also investigated using CFD while experimental measurements were supported using numerical chemical kinetics modelling.

Flame extinction tests proved that as gas substitution ratio increases, flammability limits decrease owing to changing non-reacting and reacting flow dynamics. Intermediate combustion species chemiluminescence imaging was key to the investigations and was used in evaluating reaction zone characteristics and flame stability. These parameters as well as exhaust emissions were assessed as test conditions were varied. It was important, for the methanol/glycerol blends, to establish the feasibility of its combustion without retrofitting the burner used for the other blends in order to prove its practicality. Thereafter, the influence of methane addition on flame structure and stability was investigated.

Table of Contents

List of Tables

List of Figures

List of Publications

Journals

1. **Ogbonnaya Agwu**, Jon Runyon, Burak Goktepe, Cheng Tung Chong, Jo-Han Ng, Anthony Giles, Agustin Valera-Medina. "Visualisation and performance evaluation of biodiesel/methane co-combustion in a swirl-stabilised gas turbine combustor". *Fuel,* 277 (2020).
2. **Ogbonnaya Agwu**, Agustin Valera-Medina. "Diesel/syngas co-combustion in a swirl-stabilised gas turbine combustor. *International Journal of Thermofluids,* 3-4, (2020). https://doi.org/10.1016/j.ijft.2020.100026.

3. Aniekan Okon, Osvaldo Vigueras-Zuniga, **Ogbonnaya Agwu**, Cheng Tung Chong, Agustin Valera-Medina. "Stable combustion under carbon dioxide enriched methane blends for Exhaust Gas Recirculation (EGR)". *Journal of Thermal Science,* (2020), In press, Journal Pre-proof.

4. **Ogbonnaya Agwu**, Jon Runyon, Burak Goktepe, Cheng Tung Chong, Jo-Han Ng, Anthony Giles, Agustin Valera-Medina. "Dual phase fuel combustion under gas turbine conditions". *Combustion Science and Technology* (Under editorial review).

5. **Ogbonnaya Agwu**, Agustin Valera-Medina, Tomaz Katrasnik, Tine Seljak. "Flame characteristics of glycerol/methanol blends in a swirl-stabilised gas turbine burner". *Fuel* (Under editorial review).

Conferences

1. **Ogbonnaya Agwu**, Agustin Valera-Medina, Cheng Tung Chong. "Assessing emission characteristics of multiphase fuel combustion under gas turbine conditions". *9th European Combustion Meeting 2019*. 14 – 17 April, 2019. Lisboa, Portugal.

2. **Ogbonnaya Agwu**, Jon Runyon, Agustin Valera-Medina. Operability and Emission Characteristics of Swirl-stabilised Dual-fuel Flames. *Cardiff School of Engineering PGR Research Conference*. 19 – 21 June, 2019. Gregynog, Wales, UK.

3. Aniekan Okon, **Ogbonnaya Agwu**, Agustin Valera-Medina, Ali Al-Zughaibi, Cheng Tung Chong. "Stable combustion under carbon dioxide enriched methane blends for Exhaust Gas Recirculation (EGR)". *International Conference on Energy, Ecology and Environment (ICEEE 2019)*. 23 – 26 July, 2019. Stavanger, Norway.

4. **Ogbonnaya Agwu**, Agustin Valera-Medina, Tomaz Katrasnik, Tine Seljak. "Flame characteristics of glycerol/methanol blends in a swirl-stabilised gas turbine burner". *Low Carbon Combustion Conference* May 2020, Lille, France (Postponed)

Nomenclature

Abbreviations

AFR	–	Air-to-fuel ratio
ALR	–	Air-to-liquid ratio
ASTM	–	American Society for Testing and Materials
ATJ	–	Alcohol-to-jet
BTL	–	Biomass-to-liquid
CAAFI	–	Commercial Aviation Alternative Fuels Initiative
CCD	–	Charged couple device
CFD	–	Computational fluid dynamics
CI	–	Compression-ignition
CP	–	Commercially pure
CRZ	–	Central recirculation zone
CTL	–	Coal-to-liquid
DLN	–	Dry low- NO_X
DPM	–	Discrete Phase Model
D/M	–	Diesel/methane blend
D/SG	–	Diesel/syngas blend
ER	–	Equivalence ratio
FAME	–	Fatty Acid Methyl Esters
FAR	–	Fuel-to-air ratio
FBN	–	Fuel-bound nitrogen
FSD	–	Full scale deflection
FT	–	Fisher-Tropsch
FWHM	–	Full width half maximum
GPH	–	Gallons per hour
GT	–	Gas turbine
GTL	–	Gas-to-liquid
HEFA	–	Hydroprocessed Esters and Fatty Acids
HRJ	–	Hydroprocessed Renewable Jet
IGCC	–	Integrated gasification combined cycle
II	–	Integral Intensity
LDI	–	Lean direct injection
LES	–	Large Eddy Simulation
LHE	–	Lean head end
LHV	–	Lower heating value
LIF	–	Laser induced florescence
LNG	–	Liquefied natural gas
LPM	–	Lean-premixed
LPP	–	Lean-premixed prevporized
MFC	–	Mass flow controller
MOD	–	Ministry of Defence
NG	–	Natural gas

NO_X	–	Oxides of nitrogen
OECD	–	Organisation for Economic Co-operation and Development
OEM	–	Original Equipment Manufacturer
PAH	–	Polycyclic aromatic hydrocarbon
PDA	–	Phase Doppler anemometry
PIV	–	Particle image velocimetry
PM	–	Particulate matter
PME	–	Palm methyl ester
RANS	–	Reynolds Averaged Navier-Stokes simulation
RME	–	Rapeseed methyl ester
RQL	–	Rich-burn quick-quench lean-burn
RTD	–	Resistive thermal device
SCR	–	Selective catalytic reduction
SMD	–	Sauter mean diameter
SPK	–	Synthetic paraffinic kerosene
SVO	–	Straight vegetable oil
TET	–	Turbine entry temperature
THO	–	Total heat output
UHC	–	Unburnt Hydrocarbons
VO	–	Vegetable oil
VOC	–	Volatile organic compound
WI	–	Wobbe Index

Symbols

c_p	–	Specific heat of the mixture at constant pressure
C_D	–	Drag coefficient
$C_{j,r}$	–	Molar concentration of species j in reaction r
d_p	–	Particle diameter
$\bar{d}$	–	Size constant
g_i	–	Component's gravity acceleration
h_0	–	Stagnation enthalpy
h_j	–	Component's enthalpy
J_i	–	Component's diffusion flow
J_{ji}	–	Component j flow in the direction i
$k_{f,r}$	–	Forward rate constant for reaction r
$k_{b,r}$	–	Backward rate constant for reaction r
k_m	–	Coefficient of molecular thermal conductivity
k_t	–	Coefficient of effective thermal conductivity
$M_{w,i}$	–	Molecular weight of species i
N	–	Number of chemical species in the system
n	–	Size distribution parameter
p	–	pressure

$\dot{F}^s, \dot{Q}^s$	–	Sources for interaction of the gas and liquid phases
R_i	–	Component's rate of formation or destruction
$R_{i,r}$	–	Arrhenius molar rate of formation or destruction of species i in reaction r
S_h	–	Source term from the chemical reaction
t	–	time
u	–	velocity
u_p	–	Particle velocity
x_i, x_j	–	coordinates
Y_i	–	Component's mass fraction

Greek letters

$\gamma_{j,r}$	–	Third-body efficiency of the j-th species in the reaction r
δ_i	–	Dirac delta function
$\eta'_{j,r}$	–	Rate exponent for reactant species j in reaction r
$\eta''_{j,r}$	–	Rate exponent for product species j in reaction r
μ	–	Dynamic viscosity
υ	–	Kinematic viscosity
$\nu'_{i,r}$	–	Stoichiometric coefficient for reactant i in reaction r
$\nu''_{i,r}$	–	Stoichiometric coefficient for product i in reaction r
ρ	–	density
σ	–	Surface tension
τ_p	–	Particle relaxation time
φ	–	Equivalence ratio

Acknowledgement

A work of this magnitude cannot be done by one person without assistance. From conceptualisation to experimental rig commissioning, from data acquisition and interpretation to thesis write up, help was sought and obtained from several sources. One source of help that was constant from start to finish was my Supervisor, Dr. Agustin Valera-Medina. An incredibly knowledgeable yet personable and positive-minded man, he provided not only reliable guidance relevant to the project but also offered me opportunities for personal/professional development pertinent for the future. In the same vein, thanks are due to my co-supervisor, Prof. Richard Marsh. Every meeting with him had an interesting and memorable aspect to it.

The endless assistance of the post-doctoral researchers: Jon Runyon, Burak Goktepe, Anthony Giles and Dan Pugh are gratefully acknowledged. Their involvement by way of material sourcing, equipment training, ideas development, encouragement and constructive criticism fuelled the fire by which my research skills were refined. Also, I had the pleasure of working with excellent technicians in the department of Mechanical Engineering to bring designs to reality. In that regard, I am full of gratitude to Malcolm Seaborne, Paul Malpas, Andrew Rankmore and Amie Parnell. I am equally indebted to Gareth Castle who I could rely on for diesel supply; Jose Ladera for the brilliant flame photographs; Franck Lacan for 3D printing of the swirler; Cheng Chong and Jo-Han Ng for biodiesel supply from overseas; and Seljak Tine for instigating the glycerol question (from Slovenia) and spending a week physically with me in Cardiff to solve it. There are scores of other people I did not and may never meet but who collectively contributed immensely to this work – members of the research community. Every care has been taken to give credit, by means of referencing, to these ones whose works preceded hence laid the foundation and inspired mine.

Then there are colleagues whose perseverance in their individual struggles for a PhD boosted my confidence and energised me in my own low moments. They also provided invaluable company and encouragement. This group includes Seif, Syed, Ianos, Ali, Victor, Haydee, Najlaa, Sally, Martin, Abdulkarim, Yeobong, and Godwin. The friends who, in their different ways, showed love and support from Nigeria: Idorenyin Markson, Mfon Umana, Samuel Asuquo and Praise Akpanobong are well appreciated. I will not fail to mention the love of the members of the Cardiff East Christian Congregation – my spiritual family. To the Agwu's that raised me and instilled in me the values of hard work and humility, I love you all.

The role of the Nigeria government through the PTDF in funding this PhD cannot be overemphasised. I will always remain grateful to them. The ultimate thanks, of course, goes to Jehovah God for the gift of life, good health and mercies over the years.

1

INTRODUCTION

This chapter provides an introduction to the work carried for this thesis. It gives a background to the study as well as the motivation for it. Further, it brings out the aim and objectives of the study and describes how the thesis is organised.

1.1 The global energy scenario

The total primary energy consumption, shown in Fig. 1.1 and that refers to the direct use of naturally occurring energy that has not undergone any conversion of transformation process, grew by 2.9% in 2018 across the globe – the fastest expansion since 2010 [1]. In the past such growth has been attributed to world economic expansion. For instance, over a consecutive ten-year period ending in 2017, primary energy consumption growth averaged 1.7% per year. In 2017, the fastest growth since 2013 – an average growth of 2.2% in primary energy consumption – was recorded, the developing world accounting for 80% of the expansion [2]. In the same ten-year period just mentioned, global GDP grew by an average of 2.3%; the biggest growth in six years of 3.1% being recorded in 2017 [3]. However, the climb in energy demand in 2018 was not reflective of the modest growth in the global economy. Weather effects – long periods of hot and cold days requiring heating/cooling – in the top energy demand areas of the world are said to have contributed to the spike in energy demand [1]. Apart from industrial activity and weather-related effects, population growth, rising standards of living and urbanisation of society would encourage increased energy demand in the residential and commercial sector [4]. Also, wider use of air conditioners, heaters, clean cooking facilities, computers, smart devices and other electrical appliances as a result of an increase in the number of people with access to electricity impacts on energy consumption [5, 6]. The International Energy Agency [7] estimates that the number of people without access to electricity fell to 1.1 billion for the first time in 2016, with about 1.2 billion gaining access since 2000.

This increased electricity access occurred mostly in the so-called non-OECD countries, a group mainly made up of less-developed nations as per The Organisation for Economic Co-operation and Development (OECD) classification, and projections into the future is that these countries will account for almost all of the nearly 50% increase in energy consumption between 2018 and 2050 (Fig. 1.2). It is speculated that in addition to improved access to energy, rapid population growth and an unprecedented increase in economic activity will be the key drivers of rising energy consumption in the non-OECD region [8]. The highlighted factors that drive energy demand – economic expansion, weather effects, population growth, urbanisation and better standard of living occasioned by access to electricity – are natural consequences of evolving societies that can hardly be halted therefore energy must be sourced somehow to assuage this need.

Going by the experience of China and India (incidentally non-OECD countries) both of which has undergone tremendous economic and social development in the recent past, meeting the huge energy demands of the future in developing nations will invariably involve heavy utilisation of non-renewable primary energy sources at least in the preliminary stages.

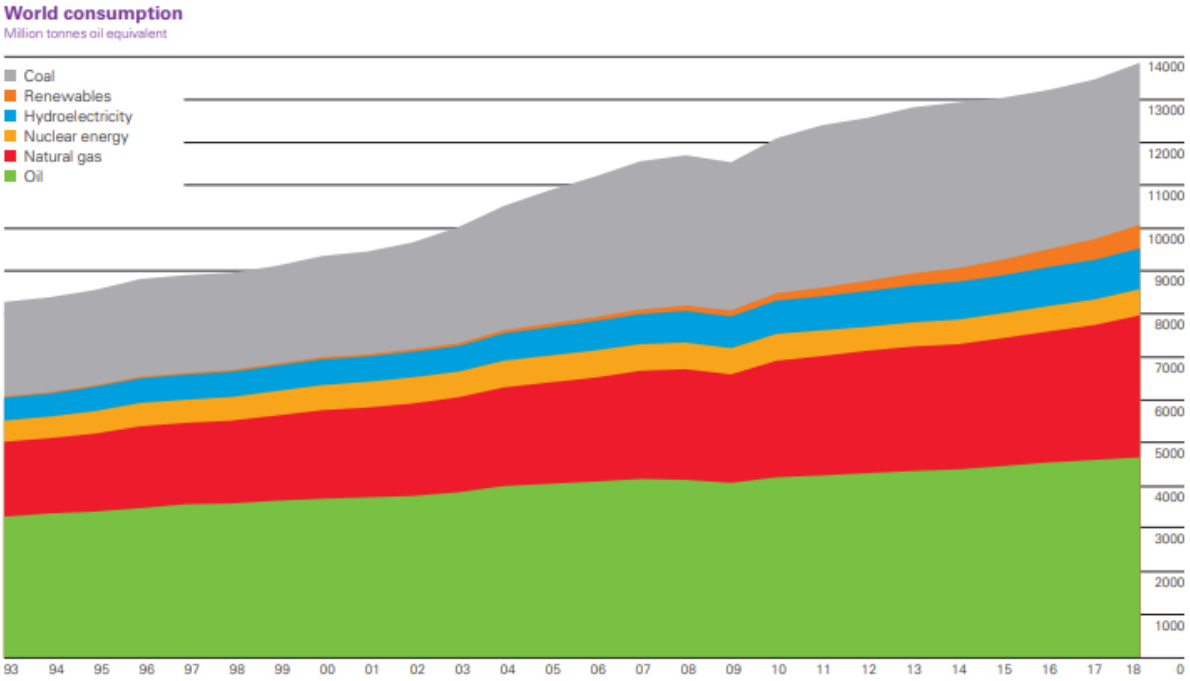

Fig. 1.1.. World primary energy consumption from 1993 – 2018 [1].

This experiential assertion has historical backing as Fig. 1.1 shows that despite the increased relevance of renewables in the last ten years, conventional energy sources still dominate the global energy consumption scene.

As a consequence of continued reliance on fossil fuels, greenhouse gas emissions remain an unfading brushstroke in the global energy utilisation portrait. Take for instance carbon emissions from energy use, which notwithstanding the raised societal awareness and calls for urgent action, rose by 2% in 2018, the fastest expansion in seven years [1]. It would seem then that even a well-publicised threat of severe health and environmental consequences from climate change did not serve to discourage fossil fuel utilisation especially where such fuel use is economically expedient at least in the short term. This is hardly surprising as energy development and energy security are both firmly linked to economic growth hence poverty reduction across the globe [9]. Whereas the concept of energy security often encompasses policy goals like sustainability and economic efficiency or competitiveness, the focus is on energy supply continuity i.e. the uninterrupted physical availability of energy [10, 11]. Clearly, there is a linkage between both agendas of energy security and environmental sustainability (in the context of climate change mitigation) thus these agendas must be pursued as integrated themes. Balancing these three challenges – energy accessibility and affordability, energy security and energy sustainability – is the energy trilemma of our time.

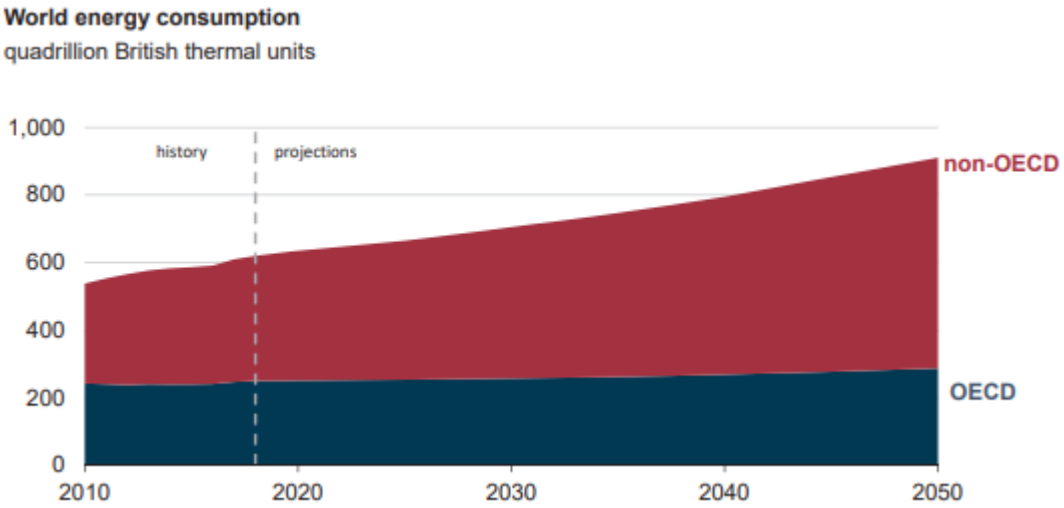

Fig. 1.2. World energy consumption forecast [8].

For secondary energy generating systems like internal combustion engines, the interplay between security of energy supply and environmental sustainability means that engine fuel flexibility is important. This has led to investigations not only of alternative fuel usage in combustion engines but also the utilisation of fuel blends that potentially impact positively on emissions while promoting energy security. The main motivation behind this thesis is in exploring the feasibility, technical and otherwise, of expanding the fuel flexibility of the gas turbine engine to include co-combustion of liquid and gaseous fuels. Of interest as well is how multiphase fuel combustion (using practical fuels) in gas turbine engines impacts on its performance. But why the gas or combustion turbine?

1.2 Power generation: the enduring role of the gas turbine

Taking into account environmental concerns while enhancing supply security, secondary energy generation in the power sector is increasingly obtained from sustainable primary sources. However, in certain cases such as in the rapidly growing aviation sector, jet engines powered by gas turbines still burn traditional fuels. In the non-aviation sector that includes marine and mechanical drive applications, electric power gas turbines dominate. This continues to be the case because the gas turbine plant typically powered by fossil fuels has: (1) remarkably high efficiencies particularly in the combined-cycle units (2) cheaper averaged 'levelised' and 'overnight' costs compared to nuclear and renewable plants and (3) considerable advantage of dispatch-able power generation over the other technologies [12].

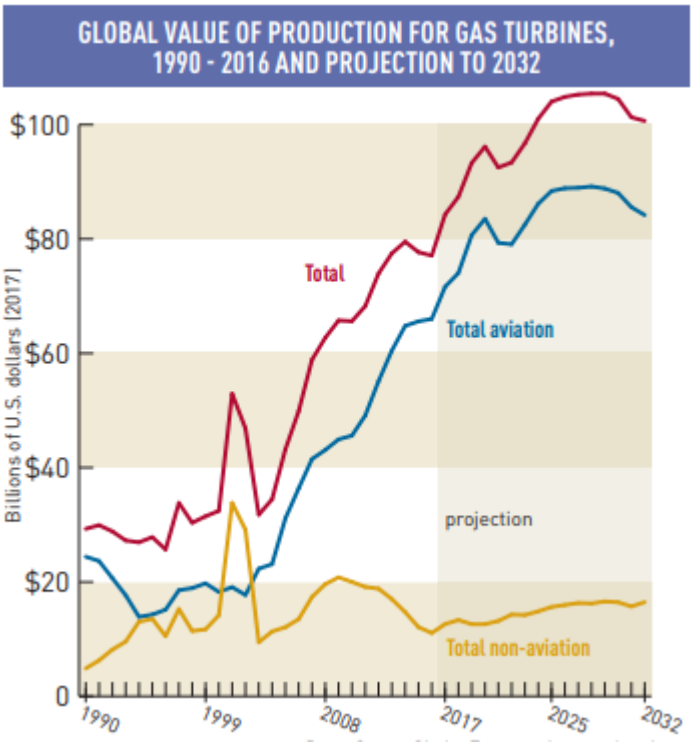

Fig. 1.3. Global value of gas turbine manufacturing

Noble though it is, renewable energy power plants based on wind or solar energy can only be trusted to deliver satisfactorily when fast-reacting technologies like the gas turbine are employed to cushion against variability of electrical supply from the renewable plants. And in the developing world where the need to access electric power far outweighs environmental concerns, the gas turbine with its simple yet robust design rules supreme [13]. These and other factors such as gas turbine technology advancement and rising engine efficiencies – as highlighted in Section 1.2.1 – contribute to healthy predictions for future market trends of the gas turbine. For instance, Forecast International (FI), a market research firm in Newtown, Connecticut utilised computer models and an extensive database to provide the value of gas turbine manufacturing from 1990 and projected through to 2032. The historical production values as well as the projections for the future is shown in Fig. 1.3 as reproduced from [14]. Focusing on the non-aviation type gas turbines which consists of electrical power, mechanical and marine engines, a more or less steady increase in production is expected over the coming 12 years. It is noted by [14] that in the data for 2017, over 80% of the non-aviation gas turbine market belonged to electric power gas turbines. Given such historical dominance one would expect that this sub-division

contributes greatly to the future projections as the gas turbine continues to be a workhorse in the power generation industry.

1.3 Brief overview of the gas turbine

The gas turbine is a rotary engine that extracts energy from the flow of hot pressurised gas generated from the combustor, which has an upstream compressor and a downstream turbine. As a power generating unit, it has exceptional reliability, is relatively easy to maintain and is one of the most cost effective dispatch-able power sources for the grid. Over and above that, because it is almost instantly available, reaching full load within a few minutes, the gas turbine often provides a necessary backup to the variability of renewable power plants [12]. The attractiveness of the gas turbine further lies in its versatility. It enjoys wide application including as standby generators, in flexible distributed power grid systems and in industrial mechanical drive applications [15]. This is partly down to its variability of power output which ranges from the multi-MW range down to micro gas turbine (<200 kW) mobile systems (see Fig. 1.3).

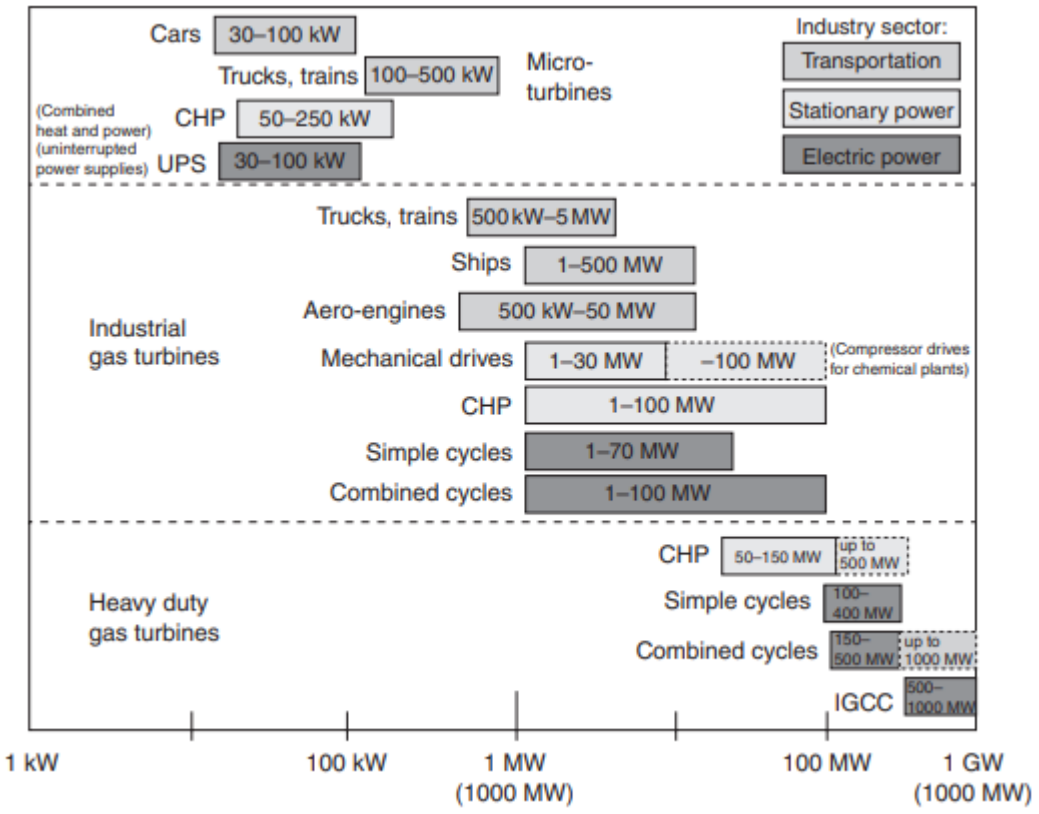

Fig. 1.4. Gas turbine application vs power output [16].

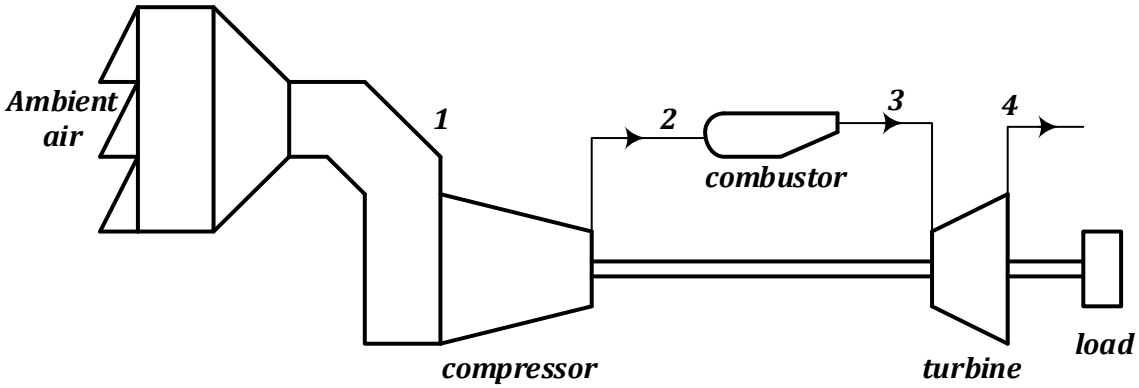

Fig. 1.5. Schematic of simple cycle gas turbine machine

A simple cycle gas turbine unit is sketched in Fig. 1.4, with the three main parts (the gas generator) indicated by station numbers 1-2, 2-3 and 3-4. The compressor and turbine of this simplest version of a gas turbine engine are linked by a common shaft making it a single spool engine. Of course, there are variants of this configuration leading to two and three spool machines.

Also, modifications of the simple cycle to include components like a heat exchanger to channel exhaust gases to preheat air entering the combustor (regenerative cycle) or into a heat recovery steam generator to raise process steam (cogeneration) results in improved efficiency.

The most efficient electric power gas turbines are those working on the combined cycle whereby the Brayton-cycle gas turbine delivers its hot exhaust to a boiler to make steam to drive a Rankine-cycle electric power steam turbine. This further heat extraction from the otherwise wasted gas generator exhaust essentially means wringing two units of work from one unit of fuel and results in combined cycle thermal efficiencies in excess of 60%. In 2016, GE reported that its most advanced combined cycle plant, the 9HA.01 engine, is the world's most efficient power plant with an efficiency of 62.22% while producing over 605 MW of electricity [17]. To put that in context, a standard steam turbine plant has an efficiency of about 30% and the largest single cycle gas turbine units are efficient to the tune of 30 – 45%. Gas turbine combined cycle power plants are therefore the most efficient heat engines ever made. Obtaining higher efficiencies from the gas turbine and hence the combined cycle plant primarily involves increasing turbine inlet temperatures.

The highest turbine inlet temperature attainable is limited by material integrity. Consequently, turbine blades and vanes immediately downstream of the combustor are made of special high melting point nickel-base alloys (superalloys) because they maintain good strength and resist hot corrosion at extreme temperatures [18]. Even so, these superalloys require effective cooling since their melting points are often exceeded in practice. Turbine entry temperatures of modern high-performance commercial jet engines reach 1649°C; electric power gas turbines typically operate at 1482°C or lower; and military jet engines experience temperatures in the 1982°C range so that the melting point of the superalloy is exceeded by anywhere between 278 and 778°C [19]. To endure these temperature excesses and still maintain good integrity, turbine blades and vanes are cooled often by any or a combination of internal passage heat transfer (convective cooling), protective effect of cooling air over external airfoil surfaces (film/effusion cooling) and thermal barrier coatings [20, 21]. Also, progress in manufacturing technology has resulted in directionally solidified and single crystal blades that possess superior qualities adding to overall performance improvement of the gas turbine [18].

Performance enhancement by utilising the combined cycle approach and by advancement in material science and turbine blade cooling technology makes an already popular electric generator, the gas turbine, even more appealing. However, the need to match growing global energy demands with reduced pressure on the environment (green growth) means that the appeal of the gas turbine can only be sustained if its combustion process is fuel-flexible. This thesis explores an area of gas turbine fuel flexibility that is relatively uncharted – multiphase fuel burn. The goal is to investigate the technical feasibility and performance (on different combustion indices) of, say, biodiesel/methane or diesel/syngas co-combustion. And for micro-turbines, utilisation of low heating value fuels like glycerol, a by-product of biodiesel production, in the combustion process is examined. In all cases, the aim is to use standard parts of conventional combustion systems in order to ensure the practicability of using such fuel blends in existing systems without major modification/retrofitting. Such fuel combinations would relieve the pressure/reliance on each fuel while shining some light on a potential value-added use for glycerol in the power generation process.

1.4 Thesis aim and objectives

Currently, gas turbines have demonstrated the capability of burning a wide range of fuels in different phases and from various feedstock [22]. Also, the gas turbine, being a continuous flow device with a universal combustion system, accepts fuels over a wide range of specific energies. For instance, a particular OEM [23] states that its machines operate on "most" of the fuels shown in Fig. 1.5. Moreover, as shown in greater detail in Chapter 2, there is no shortage of literature on utilisation of single-phase blends of these fuels in gas turbine combustion research.

However, there is a noticeable limitation regarding gas turbine fuel combustion. Whereas there are scores of studies on multiphase fuel combustion in other internal combustion systems like the diesel engine, research into multiphase fuel burn in the versatile gas (combustion) turbine engine is severely limited. It is the aim of this thesis to fill that gap by attempting multiphase fuel combustion in a 20 kW swirl-stabilised gas turbine relevant combustor rig. This is achieved by a systematic parametric investigation of liquid fuel spray flames burning in a swirling premixed gas fuel-air flow. Selected liquid fuels were introduced into the burner using a standard injection nozzle for practicability and reproducibility. To draw a relatively like-for-like optical and post combustion emissions comparison, the fuels were split so that total power output and equivalence ratio is maintained for different test cases.

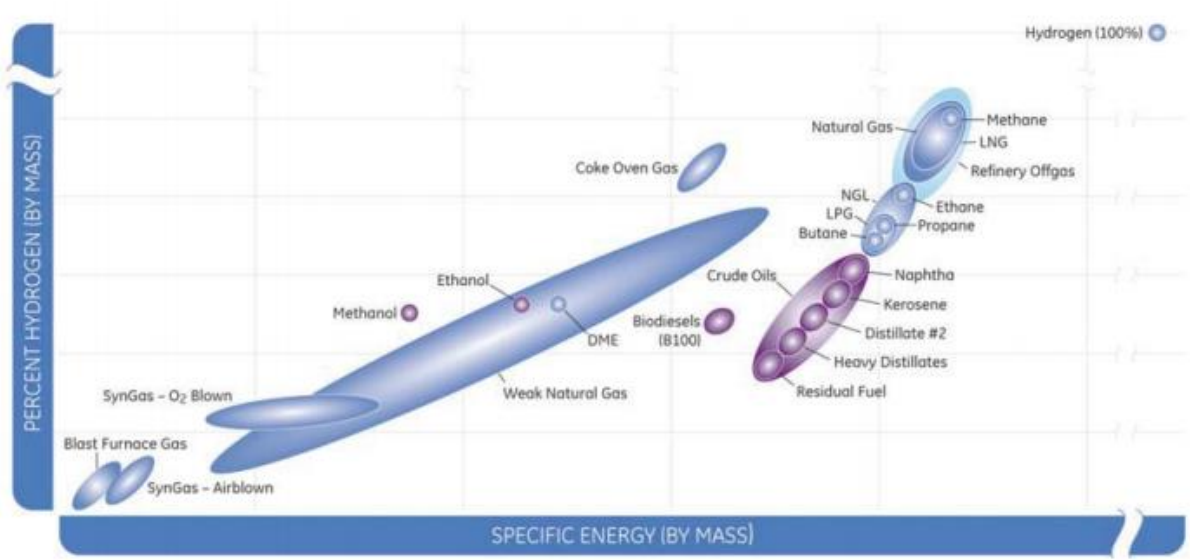

Fig. 1.6. Fuel used by high efficiency gas turbines [23].

To realise the aim of the thesis, the following specific objectives were set out:

1. Design and construct a 20 kW swirl-stabilised gas turbine relevant combustion rig capable of reliable operation using a dual phase (liquid/gas) fuel combination.
2. Perform a CFD analysis utilising the experimental burner set-up to understand, from a numerical stand-point, the reacting and non-reacting flow characteristics obtainable from the system.
3. Test the dual fuel burner with several blends of
    a. Diesel/methane
    b. Diesel/syngas
    c. Biodiesel/methane
    d. Biodiesel/syngas
4. Investigate the effect of multiphase fuel combustion of the blends in (3) on operable (flammability) range of a swirl-stabilised gas turbine with respect to both neat liquid fuel combustion and the extent of liquid fuel substitution.
5. Investigate the effect of multiphase fuel combustion of the blends in (3) on flame stability in a swirl-stabilised gas turbine burner with respect to both neat liquid fuel burn and liquid fuel substitution ratio.
6. Characterise, by means of intermediate combustion species chemiluminescence and luminosity flame images, the flame properties (appearance and structure) of the range of fuel combinations listed in (3).
7. Determine and compare the profile of regulated post combustion emissions, namely NO_X, CO and UHC, from multiphase fuel combustion using the neat liquid fuel burn as control.
8. Utilise equilibrium chemical calculations from CHEMKIN to understand the variation in adiabatic flame temperature and volumetric heat release rate as operating conditions change in harmony with the experiments above.
9. Explore the possibility of improving the fuel flexibility of the burner to include a more oxygenated fuel, namely, glycerol by trialling glycerol/methanol blend combustion without modifying the set-up. Also, in line with the main theme of this work, investigate, by means of CH* chemiluminescence, the effect of introducing methane into the glycerol/methanol flames.

By realising these goals, the work showed not only the potential but also the limitations of multiphase fuel burn in a swirl-stabilised atmospheric burner. This included defining operability limits for the tested fuel blends as well as post-combustion emissions performance analysis.

1.5 Thesis organisation

The thesis is composed of nine chapters. Chapter 1 is the introductory chapter, providing a background and motivation for the work as well as detailing the aims and objectives of the study. Chapter 2 reviews published literature relevant to the study. This includes an overview of the state-of-the-art in gas turbine combustion; the formation as well as control of dangerous pollutants; fuels employed in gas turbine studies and; making a case for multiphase fuel combustion study in gas turbines. Chapter 3 details the experimental materials and methods employed for the study including a description of the: design and accessories of the dual fuel burner, data acquisition equipment, tested fuels and operating conditions. Also, utilised numerical tools and methods were explicated in this chapter. Chapter 4 provides the results of CFD analysis of burner air-flow and diesel/methane combustion using ANSYS Fluent software. In Chapter 5, results from experimental tests involving diesel/methane blends and diesel/syngas blends are presented and discussed. The results from equilibrium chemical kinetics modelling using CHEMKIN are also presented. Chapter 6 similarly presents and discusses the results from biodiesel/methane and biodiesel/syngas co-combustion studies. CHEMKIN analysis are also presented alongside the experimental data. Chapter 7 discusses the results obtained from glycerol combustion starting from glycerol viscosity reduction using methanol. The effect of the amount of utilised methanol for reducing glycerol viscosity on flame structure and stability over the flammability range of the blend is discussed. Also, the effect of methane introduction to the glycerol/methanol flames is highlighted. There is a general discussions Chapter – Chapter 8. It highlights the main ideas from the entire work and states areas of practical application of the work reported in this thesis. Chapter 9 is the concluding chapter. Apart from the providing a summary and concluding remarks, recommendations and suggestions for future work are stated. Over and above these, appendices are attached to the work containing additional

information like chemiluminescence image processing procedures, Matlab codes and formulae for fuel-property determination.

2

LITERATURE REVIEW

This chapter discusses relevant concepts and reviews published literature in the broad area of gas turbine combustion and in the process identifies the gap that the rest of the work sets out to fill

2.1 Basics of gas turbine combustion

Combustion is an energy generation reaction whereby fuel is oxidised to release not only thermal energy, which is the main product, but also, in some cases, light and sound energy. This exothermic reaction, which essentially converts chemical energy into heat, starts and continues as long as the fuel and oxidiser (in flammable concentrations) as well as sufficient heat are available. In addition to energy, during combustion, new products are formed as the fuel and oxidiser react. The major combustion products are mainly a combination of the fuel and oxygen as in the well-known complete combustion of hydrocarbons to form water and carbon dioxide. Minor combustion products (emissions) also result. For instance, in the combustion of gasoline in air, nitrogen, which makes up a substantial part of air could combine with oxygen to form oxides of nitrogen (NO_X). Also, incomplete combustion leads to emissions of carbon monoxide and unburnt hydrocarbons. These minor combustion products - NO_X, unburnt hydrocarbons and carbon monoxide are present in parts per million (ppm) concentrations yet are very dangerous. They will be discussed subsequently in the context of their production, dangers, and control. For now, the art and science of combustion in the gas turbine will be considered.

It has been mentioned that heat is one of three requirements if combustion is to occur and be sustained. Interestingly, heat is also a product of combustion and this explains why, as long as fuel and air are available, combustion carries on. In fact, continuous combustion is the basis of energy generation in the gas turbine engine. Unsurprisingly

then, the gas turbine combustion chamber is designed to ensure sustained and steady combustion of a mixture of fuel (which may be gaseous or liquid) and compressed atmospheric air, the oxidant.

For every air-fuel mixture at a given temperature and pressure, there is a concentration range within which, in the presence of an ignition source, combustion can take place – this is known as the flammability limits. Below the lower bound of this range (the lean limit), the air lacks sufficient fuel to burn. Conversely, above the upper flammability limit or rich limit, the mixture ceases to burn because of inadequate oxidation.

There exists a fuel-air ratio (FAR), the stoichiometric fuel-air ratio, for which complete combustion of the fuel occurs and it is associated with the highest flame temperatures. This stoichiometric value is unique for each fuel and comparison of systems operating on different fuels are done using normalised ratios like the equivalence ratio, φ, defined as the fuel-air ratio normalised with respect to the stoichiometric fuel-air ratio. Therefore, for all fuels, a value of $\varphi < 1$, indicates a fuel-lean mixture whereas $\varphi > 1$, corresponds to a fuel-rich mixture.

The conventional gas turbine combustion chamber design is shown in Fig. 2.1. Three zones are evident: the primary zone that anchors the generated flame and by means of the swirler creates a toroidal flow reversal zone that aids in heat recirculation to facilitate continuous combustion; the intermediate zone that serves to ensure complete oxidation of any products of incomplete combustion emanating from the primary zone; the dilution zone which ensures attainment of the desired pattern factor (temperature distribution profile) acceptable to the downstream component, the turbine nozzle [24].

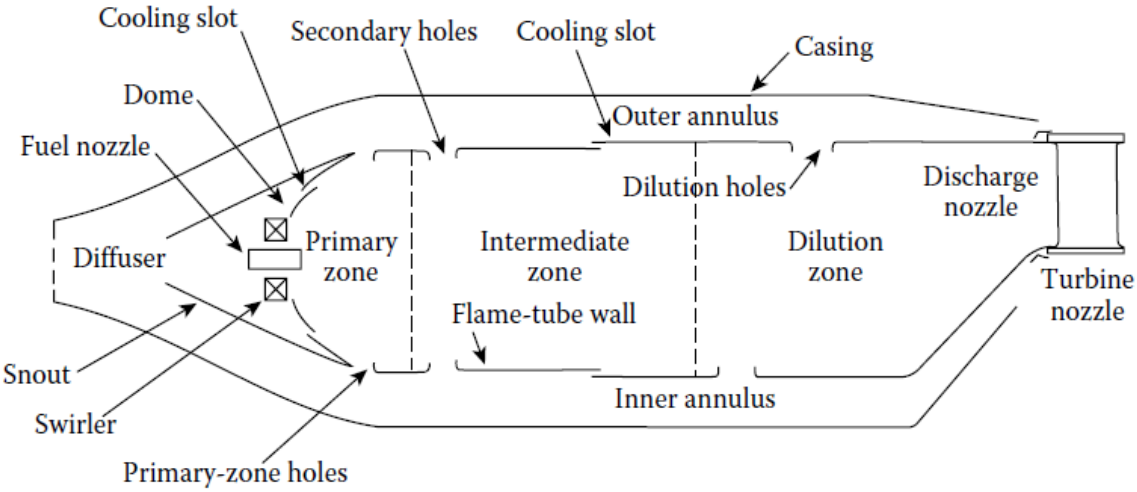

Fig. 2.1. Schematic of a gas turbine combustion chamber, reproduced from [24].

The type of combustion attained in a gas turbine depends on whether or not the fuel and air mix prior to being introduced into the combustion chamber. Consequently, "non-premixed" combustion occurs if the fuel and oxidiser enter the combustion chamber separately. The rate with which the fuel and oxidiser mix controls the reaction rate so that the flame created is called a diffusion flame. Diffusion-flame combustors, because of their reliable performance and reasonable stability, are widely employed in gas turbine engines. A key disadvantage of this method of combustion is that burning occurs at near stoichiometric conditions so that high temperatures are encountered and consequently thermal NO_X emissions become an issue [25, 26]. The unacceptably high thermal NO_X emissions associated with non-premixed combustion meant that, with the advent of strict regulations, another approach was necessary. Several solutions to pollutant-emission reduction in gas turbines has been proffered and [27] highlights a number of them for aero engines for which legislations are most stringent. A number of the new concepts involve some level of premixing between fuel and oxidiser upstream of the combustion chamber. In the extreme case, complete mixing of the fuel and oxidiser is done before burning takes place – "premixed" combustion. Perhaps the most common of the pre-mixed combustion strategies is the so-called lean-premixed (LPM) combustion otherwise called lean-premixed pre-vaporized (LPP) combustion when liquid fuels are used. This method has been demonstrated to all but eliminate the formation of thermal NO_X since combustion occurs with excess air hence keeping temperatures relatively low [28]. Nevertheless,

the apparent gain in terms of NO_X mitigation is curtailed by accompanying thermoacoustic combustion instabilities which may cause pronounced pressure oscillations capable of damaging the combustor [29]. The features unique to LPM combustors that make them especially susceptible to combustion instabilities have been elaborated by [30]; the nature and methods for suppressing instability has equally been analysed [29, 31, 32].

In the majority of practical applications though, neither pure premixed nor non-premixed combustion occurs alone. Either by design or by operating circumstances, "partially premixed" combustion, where a fuel-rich mixture enters the reaction zone before additional oxidant is provided, occurs in practical gas turbine systems and their performance has been studied [33, 34].

2.2 Gas Turbine fuels

One of the attractions of the gas turbine for power generation is its ability to efficiently burn a wide range of fuels owing to its combustion system design. With increasing global environmental concerns, fuel flexibility for power generating systems assumes even greater importance as the quest for higher efficiencies and lower emissions necessitates switching from traditional fuels to alternatives, some of which are carbon-neutral fuels. A number of gaseous and liquid fuels have been used successfully in the gas turbine hence the classification that is adopted in this section is to divide them between the two phases and the focus of the review is on the more common fuels in each group. Whereas developments in integrated gasification combined cycle (IGCC) plants employing coal gasifier and fluidised bed combustion make the use of pulverised solid fuels possible [35], this section is limited to a review of only gaseous and liquid fuels for gas turbines combustion.

2.2.1 Gaseous fuels

The two main classes of gaseous fuel comprise those industrially manufactured and those that are naturally occurring. In the latter group belongs natural gas (which is predominantly comprised of methane with traces of volatile hydrocarbons and inert gases) and the high calorific value petroleum gases, propane and butane, made of

volatile hydrocarbons. The industrially manufactured gaseous gas turbine fuels are either of medium or low calorific values with a wide range of properties [36]. Gasified coal falls into this category as are process gases – by-product gases with an extensive range of composition with methane, carbon monoxide and hydrogen the main constituents. Also known as syngas, process gases are the end product of the process of coal gasification in IGCC plants and in the thermal/chemical conversion of biomass – making it, in a sense, a renewable fuel.

2.2.1.1 Natural gas

Natural gas is a mixture of multiple gases including over 80% methane and minor amounts of ethane, propane, nitrogen, carbon dioxide and even hydrogen sulphide [37]. Natural gas and its variant liquefied natural gas (LNG), which has been liquefied to aid transportation, are the most commonly used stationary gas turbine fuels. This extensive use has been attributed to its abundance, competitive cost and little or no content of corrosive elements like sulphur. Also, of all fossil fuels, the combustion of natural gas generates the least carbon dioxide emissions because the lighter hydrocarbons in it contain more hydrogen thus producing more water than CO_2 when burnt. LNG in particular has low amounts of inert and non-methane gases so that, compared to natural gas, it has a slightly higher lower heating value (LHV) and Wobbe number. The non-methane gases like ethane, propane and butane are more valuable than natural gas and because they liquefy first in the process of converting natural gas to LNG, they are easily removed and utilised. The Wobbe index (WI) is a measure of the gas fuel flexibility on a gas turbine. It is calculated as the ratio of the LHV of the fuel to the square root of its specific gravity and used for comparing energy release from gaseous fuels with different compositions. Liu *et al.* [38] demonstrated that the Siemens dry low emissions SGT-300-1S machine is fuel flexible to the tune of a WI range from 15 to 49 MJ/Sm^3 (units: megajoules per standard metre cubed) without major combustor modifications making possible fuel diluent injection and/or fuel swap. It is the goal of the present work to exploit this extensive fuel flexibility of the gas turbine to include multiphase fuel burn.

2.2.1.2 Syngas

Syngas is sourced from material which could either be of recent biological origin such as wood or organic waste (biomass) or of fossil origin like coal [39]. Syngas obtained from biomass is considered a renewable fuel and the gasification process could be achieved by either of two thermo-chemical ways: subjecting the feedstock to high temperatures or by employing a catalyst at much lower temperatures. The latest gasification technologies for biomass-to-energy conversion can be found in Pereira *et al.* [40]. The extensive gas fuel burn capability of gas turbines makes possible the utilisation of lower calorific value fuels like syngas. Syngas is an alternative fuel that has been satisfactorily employed in gas turbine combustion studies such as [41, 42]. It is generally composed of H_2, CO, CO_2, CH_4, N_2 and steam; the presence and concentration of each constituent depending on the feedstock and synthesizing technique employed. The inert nature of N_2 and the diluting effects of CO_2 and steam diminishes, oftentimes significantly, the calorific (heating) value of syngas compared to natural gas. The reduction in heating value causes an increase in volume of syngas combusted if similar power output is to be achieved [43]. Combustor chamber modification is required in order to accommodate this increased fuel volume resulting in a perturbing of combustion zone properties and associated operational issues like blowout and flashback [44].

2.2.2 Liquid fuels

Whereas the majority of land-based gas turbines burn gaseous fuel, aviation gas turbine engines run exclusively on liquid fuels. There is simply not enough room in aviation machines for the large volume of fuel required if gaseous fuels are used as weight is a huge consideration. In this section, liquid fuels for aviation engines will be considered first and then the traditional and renewable stationary gas turbine fuels will be reviewed. Generally, light distillate liquids such as kerosene are used for aerospace applications and heavy distillates are reserved for industrial gas turbines.

2.2.2.1 Conventional aviation turbine fuels

Gas turbines for propulsion typically operate with top-quality liquid jet fuels having a well-defined and narrow range of properties. The fuel specifications are strictly governed by the American Society for Testing and Materials (ASTM) International and

the British Ministry of Defence (MOD) in ASTM D1655 [45] and MOD DS91-91 respectively. Two kerosene-type commercial aviation turbine fuels (jet fuels) are widely used today: Jet A-1 with a freeze point of –51°C and Jet A which freezes at –45°C [46]. The evolution of jet fuels over the years in the context of safety, supply security and refining capability have been extensive [47]. It is impossible to define the exact composition of Jet A/A-1 because it is a complex mixture of mainly hydrocarbons with varied constituents depending on the crude source and manufacturing process [45]. Over 70% of the fuel is made up of paraffins, with straight chain, branched chain isoparaffins and cycloparaffins or napthalenes present as well as less than 25% aromatics besides traces of sulphur, nitrogen and oxygen containing hydrocarbons [48]. However, knowledge of the exact composition of jet fuel is not really important as jet fuel requirements are 'operational' properties related to the intended application (fit-for-purpose) so that fuels meeting the same specification even if chemically different will function in a similar way [49].

2.2.2.2 Alternative jet fuels

Jet fuels are obtained from simple distillation of crude oil and treated to remove active sulphur species [47]. Recently, quite a few alternatives sourced from renewable sources have become involved with energy supply, energy security and aviation emissions some of the most important reasons for seeking alternative jet fuels [50]. Efforts to develop such alternatives are coordinated by the Commercial Aviation Alternative Fuels Initiative (CAAFI) and the agreement is that any developed fuels should be 'drop-in' fuels, requiring no adaptation of the existing turbine fuel system [51].

Depending on the feedstock, alternative jet fuels fall under two categories: 'synthetic' fuels and 'renewable' or 'bio-jet' fuels [52]. The synthetic type is derived from fossil sources like coal and natural gas. In one approach, the raw material is first pyrolysed to syngas then through the Fisher-Tropsch (FT) process, it is converted to liquid hydrocarbons resulting in CTL (coal-to-liquids) or GTL (gas-to-liquids). FT synthetic fuels have low aromatic and olefin content but are rich in *n*-paraffins and *iso*-paraffins hence the name 'synthetic paraffinic kerosene' (SPK). Renewable carbon-containing materials like biomass could also undergo the process to yield BTL (biomass-to-liquid) fuels. Biomass from plant sources like algae, camelina, jatropha and from animal fats (tallow) are hydroprocessed (a combination of hydrotreating and hydroisomerising)

to yield renewable or bio-jet fuels – commonly known as 'Hydroprocessed Renewable Jet' (HRJ) or 'Hydroprocessed Esters and Fatty Acids' (HEFA) or Bio-SPK [52-54].

The first alternative aviation fuel approved for blending with conventional jet fuel for commercial transport was coal-derived by SASOL in South Africa and used in Johannesburg. At the time of approval, the maximum blend limit of the SPK with conventional refined jet fuel was set at 50% [55]. Since then, HEFA derived from animal and vegetable oils and SASOL's fully synthetic fuel, a blend of up to five synthetic streams, have received approval as alternative aviation fuels. Also, there are several efforts devoted to the evaluation of alcohol-to-jet (ATJ) blend components where alcohol, for instance ethanol, is dehydrated into ethylene then polymerised into a hydrocarbon in the kerosene fuel boiling range [56].

For all its advantages including good thermal stability, clean burning and reduction in CO_2 emissions, synthetic kerosene, because of its low aromatic content, displays poor lubricity and a tendency to cause leaks by shrinking ageing seals. Consequently, SPKs for use in service are blended with conventional fuels, with an aromatics content of 8% being a minimum requirement for the blended fuel [48, 50-52].

2.2.2.3 Conventional fuels for stationary gas turbines

For obvious reasons, stationary gas turbine fuels are not as stringently regulated emissions-wise as their aerospace counterparts. Weight, space requirement and low temperature performance characteristics are not top priority instead, cost and availability are important. Consequently, residual oils, or heavy fuel oils, may be utilised after treatments like washing, inhibition and filtration. However, light distillates and diesel fuels are the more commonly used liquid fuels in stationary gas turbines. The most prevalent is diesel fuel, a petroleum fraction produced in conventional distillation operations, also used in the transportation sector. Liquid fuels for stationary gas turbines remain popular as alternative to gaseous fuels particularly in areas having plenty of crude oil or inadequate natural gas infrastructure [57].

2.2.2.4 Bio-liquid fuels for stationary gas turbines

Vegetable oils, animal fats or waste cooking oils can be converted to Fatty Acid Methyl Esters (FAME) by the process of transesterification. This process involves reacting glyceride and alcohol in the presence of a catalyst to yield a mixture of fatty acid esters

and an alcohol [58]. Because the process is fairly simple from the technical standpoint, production of FAME can be carried out at decentralised production units close to raw material source. Over 350 oil producing crops including rapeseed (canola), sunflower, peanut, soybean, palm oil are used in FAME production [46]. Others are inedible oils like jatropha curcas, castor, camelina, micro algae and genetically engineered plants like poplar and switchgrass as well as waste or recycled oil [59, 60]. 'Carbon neutral' FAME has properties similar to those of petrodiesel (fossil diesel) and as such a mixture of fatty acid methyl esters is often called biodiesel.

It is believed that feedstock alone accounts for 75% of the overall biodiesel production cost [60] therefore feedstock selection is crucial to the economics of the process. Variation in chemical and physical properties among biodiesel fuels from different feedstocks are well highlighted in [61]. The performance and emission characteristics of biodiesels from several feedstocks have been analysed [62] and there seems to be an origin-performance correlation. Moreover, attempts have been made to classify biodiesel into three generations [60]. Those produced with edible oils via transesterification are classed as 'first generation'. Crop residues and non-food crops may also be converted to biofuel through a number of advanced processing technologies to form 'second generation' biofuels. Among the second generation type are Fischer-Tropsch diesel produced via biomass-to-liquid conversion; green diesel produced via catalytic hydrotreatment of vegetable oils to form hydrotreated vegetable oil or HVOs; white diesel formed by hydrotreating 100% waste cooking oil and hybrid biodiesel where vegetable oil is co-processed with petro-derived raw materials [63, 64]. A 'third generation' feedstock namely microalgae was also identified and appears to be a dependable source of high oil-yielding biomass [60]. It has to be noted, though, that the use of first, second or third generation tags does not connote any sort of superiority or otherwise of the properties of biodiesel obtained from the feedstock and the meanings of these terms may be imprecise and variable [61]. Governments like the EU specify use of third generation biodiesel as fuel so as to avoid the food vs fuel conflict.

2.3 Fuel introduction into combustor

2.3.1 Atomisation

Fuels burn only in the vaporised state and depending on the volatility of a fuel, the extent of vaporisation required for burning to commence is different. Gaseous fuels obviously do not require elaborate injection systems to attain vaporisation. Liquid fuels, in contrast, need one and achieving vaporisation for gas turbine liquid fuels often starts with increasing the surface area by shattering the bulk liquid into tiny droplets (or spray) in a process known as atomisation and commonly attained in a device designated as an atomiser or nozzle or injector. The extent of atomisation hence the rate of vaporisation achieved determines the effectiveness of fuel-air mixing and consequently overall combustion performance including efficiency and emissions. Understanding and controlling atomisation and spray characteristics is an essential aspect of gas turbine combustion.

Among the most important measures of the extent of atomisation is the Sauter mean diameter (SMD), the diameter of a drop whose ratio of volume to surface area is considered equivalent to that of the spray [65]. An ideal atomiser would not only achieve good atomisation at a particular condition but provide consistent spray quality (SMD for example) for the entire operational range of the gas turbine. Several correlations exist for predicting SMD of liquid fuels. Alsulami *et al.* [66] cited three of the best-known correlations for pressure atomisers: Radcliffe, Jasuja and Lefebvre shown in Eq. (2.1a) to Eq. (2.1c) respectively. In the equations, σ_l is the liquid surface tension, μ_l and ν_l are the dynamic and kinematic viscosities respectively. $\dot{m}_l$, ΔP and ρ_{air} are the liquid mass flow rate, pressure drop across nozzle and air density in that order. Compared with experimental data using n-heptane, n-dodecane and toluene, [66] found that the Radcliffe correlation, Eq. (2.1a), had the closest agreement in all cases. Hence, in this work, the Radcliffe correlation was used to estimate SMD values where necessary.

$$SMD_{Radcliffe} = 7.3{\sigma_l}^{0.6}{\nu_l}^{0.2}{\dot{m}_l}^{0.25}\Delta P^{-0.4} \tag{2.1a}$$

$$SMD_{Jasuja} = 4.4{\sigma_l}^{0.6}{\nu_l}^{0.16}{\dot{m}_l}^{0.22}\Delta P^{-0.43} \tag{2.1b}$$

$$SMD_{Lefebvre} = 2.25{\sigma_l}^{0.25}{\mu_l}^{0.25}{\dot{m}_l}^{0.25}\Delta P^{-0.5}{\rho_{air}}^{-0.25} \tag{2.1c}$$

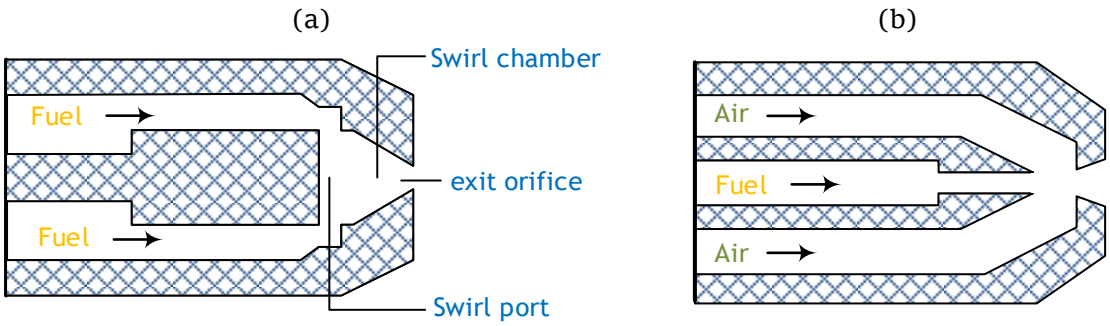

Fig. 2.2. Schematics of (a) pressure-swirl atomiser (b) plain-jet air blast nozzle

The fundamental physics behind atomisation is explained [24]: aerodynamic forces acting on the liquid surface create an external distorting force which, if greater than the consolidating surface tension force, breaks up the bulk liquid first into shreds and ligaments and then into finer droplets. Essentially what is required to overcome the surface tension of the liquid undergoing atomisation is a force such as high pressure or large shear most probably arising from velocity difference between the liquid and the surrounding air [25].

The required velocity difference can be created by accelerating either the fuel or air. Where the fuel is accelerated by forcing it (under pressure) through a tapering orifice, then it results in a pressure type or single-fluid atomiser. On the other hand, when the required shear velocity difference is met by accelerating air rather than fuel, twin-fluid atomisers arise among which are air-assist and air-blast injectors.

The most commonly used type of single-fluid atomisers is the pressure swirl atomiser (Fig. 2.2a). In this atomiser, the fuel is forced through nozzles known as swirl ports into a central swirl chamber the outlet of which is the final orifice. The swirling fuel flows through this orifice under the action of axial and radial forces to emerge as a hollow conical sheet with much wider cone angles than the plain-orifice nozzle, the simplest of the pressure atomisers. The main drawback of the pressure swirl atomiser is fuel flow rate dependence on pressure so that operational issues arise for large turndown ratios with heavy fuel injection systems for high power requirements and poor spray quality for low power conditions. Also, the narrow passageways and exit orifice run the risk of being clogged by fuel impurities.

Of the twin-fluid atomisers, the air assist and air blast nozzles stand out. Air assist atomisers are characterised by their use of relatively small amounts of high velocity air to assist in atomising liquid fuel particularly at low fuel flow rates when fuel pressure is inadequate for good atomisation. In a modification of this device, the air blast atomiser (Fig. 2.2 b) uses a larger amount of air at relatively lower velocity to achieve fuel atomisation with a relatively larger exit orifice [67]. This allows for the overall fuel pump pressure requirement to be lower than in the pressure swirl atomiser or even in the air assist nozzle. Ma *et al.* [68] with the help of laser induced florescence (LIF) and particle image velocimetry (PIV) concluded that atomising air pressure and mixing form significantly influence spray angle and spray velocity whereas these parameters are not sensitive to liquid pressure. The major drawback of the air blast nozzle is poor lean blowout performance and poor atomisation at start-up when atomizing air velocities are low. To get the best of both worlds, then, some researchers have utilised a combination of the nozzles by having a pressure-swirl nozzle designed to fit in the centreline of an air blast atomiser – a hybrid injector also known as a piloted air blast nozzle [69-71].

Worthy of mention at this point is the so-called effervescent atomiser. It is a type of twin-fluid atomiser involving the introduction of a small amount of gas (at low velocity) into the fuel somewhere upstream of the discharge orifice. The result is a two-phase bubbly flow upon arrival at the orifice. When the bubbles exit the orifice, they rapidly expand causing disintegration of the surrounding liquid into small droplets even at low air and fuel flow rates. A few advantages are apparent: atomising air can be utilised in a highly efficient manner; larger orifices can be used reducing plugging problems, and the intimate presence of air alleviates smoke and soot formation [72]. Two different configurations can facilitate injection of atomising gas into the liquid: ‘outside-in’ or ‘inside-out’ designs. In the former (Fig. 2.3a), which better suits high liquid flow rates, the liquid flows inside a perforated tube while the atomising gas is injected into the tube through holes in its wall.

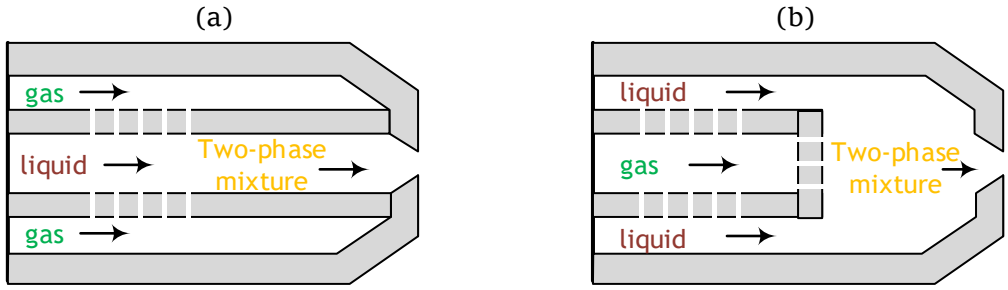

Fig. 2.3. Effervescent atomiser designs (a) outside-in configuration (b) inside-out configuration, adapted from [24, 73].

For the latter (Fig.2.3b), suited for low liquid flow rates, the gas flows inside the perforated tube and escapes outwards into the surrounding liquid. Other than these gas injection methods, [74] has highlighted several other factors that shape the flow regime inside the atomiser and the issuing spray characteristics. Also, operating parameters like injection pressure drop and atomising gas/liquid ratio have been shown to affect spray characteristics in profound ways [73, 75-78].

2.3.2 Pre-vaporisation

Another way of getting liquid fuels vaporised and ready for combustion in gas turbines is by heating it to a temperature above the boiling point of all of its hydrocarbon constituents. The aim is to completely vaporise the fuel prior to combustion without deposition of contaminants or its inherent carbon through chemical cracking at the high temperature. The advantage lies in the fact that, because no atomiser is used, fuel pressure requirement is minimal and soot formation is low. However, thermal integrity of the vaporiser tube and poor vaporisation during starting when vaporiser tube is cold will be of concern. Also, fuel scheduling during rapid acceleration must be controlled to avoid the increase in fuel flow from overcooling the tubes hence lowering evaporation rates and by extension, combustion efficiency [24, 71]. A few works have utilised what amounts to a partial pre-vaporisation approach when testing highly viscous fuels like glycerol [79] and straight vegetable oils [80].

2.4 Flame stabilisation

There are several means of stabilising flames within a flow field including sudden expansion, piloted flame and opposed jets. However, the most common techniques of flame stabilisation in gas turbine combustors are: swirl stabilisation and bluff-body stabilisation. Both achieve flame stabilisation by creating a low velocity zone of toroidal flow that recirculates hot combustion products to the primary combustion zone [81]. The two techniques can be employed simultaneously in gas turbine flame stabilisation [82]. When placed in a high-speed flow, a bluff body creates, in its wake, a recirculating zone that entrains combustion products which provides continuous ignition for the oncoming flow [83]. By this means, bluff bodies provide a mechanism for balancing, in practical combustors, the inlet velocity of premixed reactants with the relatively low adiabatic burning velocity of the mixture [84, 85].

An extensive description and analysis of the flow structures and fluid mechanics associated with bluff body flow can be found in Shanbhogue *et al.* [86]. The central toroidal flow recirculation zone created is associated with high shear stresses and strong turbulence as a consequence of vortex breakdown [25]. The recirculation currents not only aids in stabilising the flame but also causes a mixture of the incoming charge of air and fuel with the hot combustion products with the latter providing the heat required to sustain the flame.

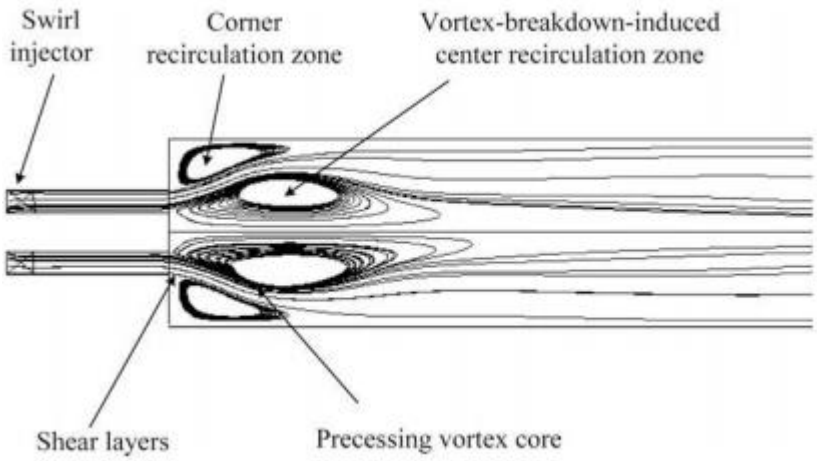

Fig. 2.4. Flow field characteristics of a typical swirl injector, reproduced from [25]

Swirlers attain this same function by imparting a tangential and radial velocity components to an otherwise axial flow [87, 88]. Huang and Yang [25] provides the schematic shown in Fig. 2.4 that characterises the flow field of a typical gas turbine swirl injector with three main structures: a central recirculation zone with a processing vortex layer surrounding it and shear layers originating from the outer edge of the inlet annulus. The incoming mixture from the shear layers bounding the central recirculation zone (CRZ) gets continuously ignited by the heat from the CRZ [89]. Reacting flows that are swirl-stabilised have been found to promote combustion efficiency and control pollutant emissions from the combustion process [90]. However, the more direct means of controlling combustion emissions in gas turbines is described in the next section after the pathways of formation of these emissions are reviewed.

2.5 Gas Turbine emissions and control

The result of all combustion processes, including that of the gas turbine burner, is energy and emissions. In the early days of the gas turbine, the overwhelming interest was in obtaining as much energy as possible, in the form of shaft power or thrust, from the gas turbine. However, the early 1970s saw a spark of interest in gas turbine emissions in the form of regulations primarily as regards oxides of nitrogen or NO_X [91]. Manufacturers quickly realised that controlled injection of water or steam into the combustion zone would meet the regulations requirement at the time without significantly perturbing machine performance or escalating the levels of other pollutants. New regulations in the 1980s pushed the permissible NO_X levels lower and further reduction by water or steam injection was possible but not without substantial negative (detrimental) impact on other emissions, GT cycle performance and part lives. Consequently, a number of alternative approaches, reviewed in Section 2.5.2, were trialled and developed. First, though, the nature and formation of emissions from conventional gas turbine combustion systems are discussed.

2.5.1 Emissions characteristics of conventional gas turbines

The major species created in the combustion of gas turbines include CO_2 and water and are present in percent concentrations. The far more hazardous species, NO_X, CO, UHC, particulates and smoke, are present only in parts per million (ppm) concentrations and are consequently designated minor species. The human and environmental health effect of such pollutants are well documented [92-94]. The so-called minor species, because of their danger, are the focus of emissions regulations which since 1980 have become increasingly more stringent.

2.5.1.1 Nitrogen oxides (NO_X)

NO_X is considered the primary pollutant in the process of combustion in gas turbine engines. NO_X describes two (of several) oxides of nitrogen: nitric oxide, NO and nitrogen dioxide, NO_2. Unlike NO_X, combustion of fossil fuels is not a major anthropogenic source of nitrous oxide (N_2O), an equally dangerous nitrogen oxide [91]. Therefore, as far as gas turbine combustion is concerned, NO and NO_2 are the regulated species. Over the past 40 years, NO_X emissions from gas turbines have been regulated, particularly by the more industrialised nations. Legislations have gradually become more stringent over the years as NO_X has been firmly linked to environmental problems like photochemical smog, acid rain and ozone layer depletion – all dangerous to human health. For instance, tropospheric ozone, one of the primary components of photochemical smog (the other being particulate matter) and formed in the lowest layer of earth's atmosphere by the combination of NO_X and volatile organic compounds in the presence of sunlight, killed between 50000 – 80000 people in China in 2015 [95]. The mechanism with which NO_X forms acid rain, produces 'bad' ozone in the troposphere and depletes 'good' ozone in the stratosphere [96].

The disastrous consequence of NO_X in the atmosphere has galvanised and sustained a wide body of research in its formation and abatement. These researches discuss three main routes of NO_X formation: thermal, prompt and fuel NO.

2.5.1.1.1 Thermal NO

The lure of lean premixed combustion in gas turbines stem from the fact that NO_X levels escalate as combustion zone flame temperatures increase in non-premixed flames. At temperatures above 1800 K, combustion air undergoes thermal dissociation which is then followed by a reaction between molecules and atoms of nitrogen and

oxygen to form the so-called thermal NO_X [57]. Via this route, a dissociated nitrogen molecule reacts with an oxygen atom (Eq. 2.2a) to produce NO at sufficiently high temperatures; a reaction that kick-starts a couple of other NO producing reactions (Eq. 2.2b and Eq. 2.2c).

$$N_2 + O \Leftrightarrow NO + N \tag{2.2a}$$

$$N + O_2 \Leftrightarrow NO + O \tag{2.2b}$$

$$N + OH \Leftrightarrow NO + H \tag{2.2c}$$

Because of the high activation energy of 314 *kJ/mol* [97] required, Eq. 2.2a is the rate-limiting reaction for the formation of thermal NO. The reaction of Eq. 2.2b, where nitrogen atoms combine with molecular oxygen, follows the first and together are known as the Zeldovich mechanism. Further, in what is known as the extended Zeldovich mechanism, the nitrogen atom generated in equation 1 reacts with an OH radical to form yet more NO via Eq. 2.2c.

Thermal NO is highly temperature dependent [98] and peaks on the fuel lean side of stoichiometric even if combustion temperatures are higher on the immediate reverse side of stoichiometric. This is because in the competition for oxygen consumption between fuel and nitrogen, the fuel is preferred [24]. The rate of formation of thermal NO is an exponential function of reaction temperature for both premixed and diffusion flames and is determined by residence time in high temperature regions [27, 91].

2.5.1.1.2 Prompt NO

Atmospheric nitrogen could also combine with oxygen via a different pathway – prompt NO_X. The reaction occurs at the flame front and is typical of hydrocarbon flames in which hydrocarbon radicals like CH interact with molecular nitrogen. The typical hydrocarbon mechanism of NO formation is shown in Eq. 2.3 and has, according to Toof [99], only ever been observed in hydrocarbon flames (never CO or hydrogen combustion).

$$CH + N_2 \rightarrow HCN + N \tag{2.3}$$

According to Lefebvre and Ballal [24], under lean-premixed conditions, HCN oxidises to NO following the sequence $HCN \rightarrow CN \rightarrow NCO \rightarrow NO$ whereas the N atom follows the second Zeldovich mechanism to arrive at NO. Prompt NO in significant quantity hardly ever forms in the post-flame zone for reasons of low concentrations of hydrocarbon radicals away from the flame front. Correspondingly, within the flame zone, formation of NO increases under rich combustion conditions because the presence of high concentrations of hydrocarbon radicals supports the mechanism [57]. Consequently, in practical combustion systems which often operate fuel-lean or close to stoichiometric conditions, the contribution of prompt NO to total NO emissions is likely small [100].

2.5.1.1.3 Fuel NO

Unlike the thermal and prompt routes of NO formation where atmospheric nitrogen is involved, the fuel NO route involves oxidation of a fraction of nitrogen contained in combusted fuel. Fuels with organically bonded nitrogen – also known as fuel-bound nitrogen, FBN – are especially susceptible to generating fuel NO during combustion. These fuels typically contain ammonia [57]. Fuels with low FBN content are much more efficient at producing NO than those with higher proportions of FBN [99] albeit significant amounts of FBN, like in crude or residual oils, must be present for oxides of nitrogen to be formed via this route. Depending on the extent of nitrogen conversion which is sensitive to reactant stoichiometry [101], fuel NO is the dominating route of NO formation for fuels containing a good proportion of FBN [24]. Naturally, diesel and biodiesel have very low nitrogen levels. As such, the potential of NO formation via the fuel NO pathway is negligible [102]. In the case of biodiesel, the average nitrogen concentration is 0.02% and the current main biodiesel source – vegetable oil – does not contain any nitrogen [103].

2.5.1.2 Carbon monoxide (CO) and unburnt hydrocarbons (UHC)

When complete combustion of carbon-containing fuels occur, one of the end products is carbon dioxide. In the event of incomplete combustion, CO and UHC are among the products formed. The significance of incomplete combustion is that UHC and CO, because they possess unreleased chemical energy, impact negatively on combustion efficiency and hence on turbine specific fuel consumption, SFC – an important measure of gas turbine efficiency. CO, a colourless, non-irritating gas impairs oxygen transport by blood and can result in vital tissue damage (including the central nervous

system and myocardium) in humans [104]. The highly dangerous CO is associated with incomplete combustion which may be due to inadequate burning rates in the primary zone, inadequate mixing, chilling effects of liner coolant, and/or insufficient residence time [105]. Formation of CO occurs mainly within the flame zone so that a potent way of tackling it is to allow sufficient residence time for conversion to CO_2. Therefore, important gas turbine combustor design considerations for minimizing CO include combustor length and the provision of dilution air introduction points in the combustor downstream of the primary zone [57]. With such designs, GE claims that its conventional gas turbine combustion systems operating in steady state produces less than 10 ppmv CO at all but very low loads [106].

Similar to CO, emission of UHCs are an indication of incomplete combustion of fuel occasioned by inadequate burning rates. Any fuel droplets or vapour that are not consumed within the combustor hot core may not have the chance to burn out owing to the chilling effects of cooling air downstream of the hot primary zone. UHC emissions can be eliminated by enhanced atomisation for liquid fuels as well as improved mixing rates within the primary combustion zone [24, 105]. Again, like in the case of CO, emissions of UHC, other than at low (part) loads, are minimal for modern combustors with good wall cooling techniques and combustion efficiencies in excess of 99% common [24].

2.5.1.3 Smoke and Particulate Matter

Carbonaceous material emitted from the exhaust of gas turbine engines are often referred to as soot, non-volatile particulates or smoke. Often these terms are used interchangeably but it is important to note that smoke could be made up of particulates and other emissions. When particulate matter settles on a surface, it is called soot. Individual particles making up these emissions are typically 10 – 80 nm in diameter each [57]. Smoke has been grouped, alongside ash and erosion as well as corrosion products, as a component of particulates and defined as the visible portion of filterable particulate matter [106]. The smoke number, an empirical value reported on a scale of 0 to 100 gives an indication of the level of this emission from gas turbine combustion systems; plumes are not visible for smoke numbers approaching 100. [106, 107] suggest that soot morphology is a function of engine power levels and fuel properties and combustor design. These two factors have been analysed in clearer detail by [24]: At low pressures, for pressure atomisers, fuel is distributed over the

entire combustion zone whereas at high pressures, it tends to concentrate within the soot-forming region next to the fuel nozzle. Also, because polycyclic aromatic hydrocarbons (PAHs) initiate the growth of soot particles, fuels with no aromatic compounds produce virtually no soot. Particulate formation, from nucleation to oxidation, is a complex process the explication of which has been undertaken in [57]. The human health effects of PM include lung cancer, cardiovascular and respiratory system diseases [108, 109].

2.5.2 Emissions control strategies

A number of factors influence pollutant formation in the gas turbine combustion process. These include: primary zone temperature and equivalence ratio, extent of homogeneity in primary zone fuel-air mix, residence time in the primary zone, liner wall quenching characteristics, and for liquid fuels, degree of atomisation [24]. Probably, the single most important factor influencing pollutant emissions from gas turbine combustion systems is primary zone flame temperature. Relatively low temperatures tend to favour formation of CO whereas at high temperatures, NOx emissions become the dominant concern. This fact is aptly illustrated in Fig. 2.5 where only within the narrow range of temperatures between 1670 K and 1900 K, are the levels of CO and NO_X below 25 and 15 ppmv respectively.

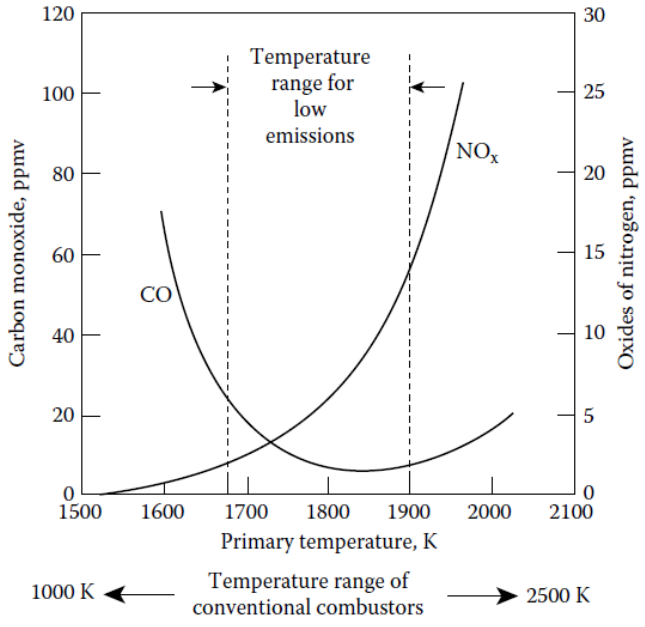

Fig. 2.5. NO_X and CO emissions as a function of GT primary zone temperature [24]

However, efforts to improve thermal efficiency and engine specific fuel consumption has driven turbine entry temperatures (TETs) higher so that the range of temperatures for low emissions indicated in Fig. 2.5 shrinks to the right making temperature control within this narrower band over the entire power range of the engine the main issue, and NO_X the principal pollutant of interest.

Again, referring to Fig. 2.5, an effective NO_X control means would be flame temperature reduction. In conventional gas turbine combustors, water/steam injection achieves substantial NO_X reduction by introducing a heat sink into the hot flame zone. A widely used NO_X control strategy, water injection is done through a number of separate nozzles at the combustor head or via additional passages in the fuel nozzle. Effective as it is, there are practical limits to this technology including the overall economics of the process and increase in CO and UHC emissions [24, 106]. Also, it will be impractical for aviation gas turbines as weight and volume are crucial in such engines. As a result, other ways of reducing primary zone flame temperature without resorting to potentially corrosive diluent injection – known as dry low- NO_X (DLN) techniques – were pursued.

With the knowledge that highest flame temperatures are associated with burning at or close to stoichiometric values, the goal became to keep fuel-air ratio away from the stoichiometric quantities. Practically this may be achieved by initiating combustion with excessive air (lean burn) or with less than stoichiometric amount of air (rich burn). For the former, early approaches involving diffusion flames was to employ lean head end (LHE) combustion liners that divert air towards the flame end thereby leaning out the flame zone, reducing flame length and residence time – all beneficial for NO_X reduction. LHE liner technology proved to be limited in terms of the extent of decrement in primary zone equivalence ratio hence attainable NO_X reduction and is further associated with high CO emissions [106].

For more effective control of equivalence ratio, premixed combustion systems were developed whereby a strongly fuel-lean mixture could be created prior to entering the combustor. Although problems of flame stability are encountered, this so-called ultra-lean premixed combustion yields very low NO_X emissions, typically less than 15 ppmv at 15% oxygen with natural gas as fuel [110]. However, with liquid fuels, premature

autoignition may occur if fuel/air is premixed since such fuels have shorter ignition delay times than natural gas at typical gas turbine inlet conditions [57]. Consequently, alternative approaches like lean direct injection (LDI), and lean prevaporized, premixed (LPP) combustion strategies are being developed for gas turbines operating on liquid fuels. The operation of these systems and their individual merits and drawbacks are highlighted in [27].

In a different approach, the so-called rich-burn quick-quench lean-burn (RQL) technology starts out with burning a fuel-rich mixture (typically with φ between 1.2 and 1.8) which ensures combustion stability then keeps flame temperatures relatively low by employing a quench section downstream of the rich zone which in turn switches rapidly to lean combustion (typically of φ between 0.5 and 0.7) to avoid thermal NO formation [27].

Combustion stoichiometry and flame temperature may also be controlled by utilising fuel injection in multiple locations within the combustor in an approach known as fuel staging [111]. A few ways of realising this have been developed including axially staged combustors where fuel injection zones are placed in axial directions and the double annular combustors where radial fuel staging strategy is used.

It is clear that the above NO_X abatement strategies are in situ combustion control approaches. There are a few control modes that are utilised post combustion. Selective catalytic reduction (SCR) converts NO_X in the gas turbine exhaust stream to molecular nitrogen and water by reacting it with ammonia or urea in the presence of a catalyst usually vanadium pentoxide [112]. Another post combustion NO_X mitigation strategy is exhaust gas recirculation (EGR). Flame temperature is reduced as cooled exhaust gases, low in O_2 but high in H_2O and CO_2 of higher heat capacity, is introduced into the primary zone. However, because an intercooler between the exhaust and inlet is required, its application in simple cycle gas turbines appears impossible. EGR has been associated with the so-called flameless combustion in which not only are emissions minimised but also combustion stability is improved and noise reduced [113].

As has been reviewed so far, there is evidently a number of conscious approaches in existence for NO_X abatement in gas turbine combustors. However, there are no such direct CO and UHC control mechanisms since these pollutants are a consequence of

incomplete combustion. Modern engines operating at high overall pressure ratio and TET in order to increase thermal efficiency and decrease engine specific fuel consumption attain very high combustion efficiencies so that CO and UHC emissions are indirectly yet effectively handled.

Controlling the amount of particulate matter emissions from turbine exhausts typically involve control of fuel composition by various treatments including washing, filtration, centrifuging, electrostatic precipitation or by the use of inhibitors [114]. Smoke and soot reduction often involves not only creating better fuel atomisation to reduce local residence time but also injecting significant amounts of high velocity air into the soot-forming, fuel rich zone – achievable by the use of air blast or air assist fuel nozzles [115].

2.6 Studies on alternative fuel performance in gas turbines

Greening the energy generation process in internal combustion (IC) engines has, in the recent past, been of interest to numerous researchers. The relatively recent and deep interest in this area is occasioned by at least three factors: rapid depletion of fossil (conventional) fuel reserves meaning that the huge energy demands of the future must be met, at least partly, with alternative sources; environmental sustainability which necessitates improvement on the levels of dangerous emissions resulting from the combustion process; and the potential economic (operating cost) benefits. Consequently, the viability of renewable fuels and blends of renewables and conventional fuels in IC engines has been evaluated by several studies.

The review in this section covers published work whose broad aim consists in the evaluation of the performance of unblended biofuels used as complete replacement to traditional fuels on gas turbines. In most cases, results of such performance analysis are compared with those of a standard fuel tested under the same or similar conditions. The performance parameters of top concern to the researchers are spray characteristics of liquid alternative fuels as well as NO_X and CO emissions. Further, for the liquid alternatives, different operating conditions, injection modes and burner geometries are reported as is the effect of physical properties of fuels on performance parameters.

2.6.1 Bio-liquids

2.6.1.1 FAME

A number of studies have investigated the potential use of biodiesel as complete replacement for diesel in gas turbine engines. For instance, [116] using a pressure type atomiser, investigated the combustion properties of palm methyl ester (PME) and concluded that it behaves largely like diesel in terms of NO_X level dependence on excess air ratio or atomised particle size as well as adiabatic flame temperature. Atomised to similar SMD values as diesel, PME was reported to improve soot and NO_X emissions (compared with diesel flame emissions) highlighting its potential as an alternative fuel for gas turbines. Also, [117] investigated the combustion characteristics and emissions performance of palm biodiesel (PME) in a swirl gas turbine burner with an air blast atomiser. The results of the study obtained via PDA, flame imaging and a Tocsin 320 gas analyser suggests that, compared to diesel and Jet A-1 fuel, lean combustion of PME is associated with higher values of SMD but lower NO_X emissions per unit mass of fuel consumed. Further, Chong and Hochgreb [118] sought to know how rapeseed methyl ester (RME) performs in gas turbine combustion compared to Jet A-1 fuel. They employed a 6 kW swirl burner and utilised PDA, PIV and flame imaging techniques to compare the spray characteristics of both fuels injected using a twin-fluid atomiser of the air blast type. The results indicate that RME sprays have droplet concentration and volume fluxes four times that of Jet A-1 implying that vaporisation of Jet A-1 is far more rapid than RME so that the resulting flame reaction zones are markedly different. Further, [119] evaluated the atomisation characteristics of rapeseed methyl ester (RME). Under lean conditions, they found RME to exhibit larger droplet sizes and concentrations yet no visible soot radiation compared to diesel. Also, NO_X emissions were reportedly lower in RME combustion compared to diesel flames. The effect of operational condition, namely, air-to-liquid ratio in twin fluid atomisers on the performance of alternative fuels was shown to be important. Sequera *et al.* [120] focused on understanding the effect of atomising air flow rate in air blast injectors on NO_X and CO emissions when biodiesel and diesel-biodiesel blends undergo combustion under gas turbine conditions. The results indicate a direct relationship between atomising air flow rate and NO_X/CO formation, a consequence of better atomisation at higher air-to-liquid mass ratios (ALR). SMD

reduction with increase in ALR has also been reported as a result of increased shear [121]. Such effects became increasingly negligible as ALR increased above 4.

There is, therefore, a huge body of evidence supporting the efficacy of FAME as an alternative gas turbine fuel based on exploration of its spray and combustion properties in relation to diesel.

2.6.1.2 Glycerol

In the course of the common biodiesel production process, transesterification, glycerol is generated as a by-product. In fact, it has been found that glycerol (IUPAC name: propane-1,2,3-triol) makes up between 10 and 20% of the total volume of biodiesel produced at any one time [122]. Value-added uses are currently being sought for glycerol as it is largely considered a waste product. Its poor combustion properties and relatively low heating value renders glycerol unappealing as fuel in combustion systems. Even so, there have been a few combustion experiments utilising crude and pure glycerol. U. S. Pharmacopeia (USP) grade glycerol combustion was tested [79] in a 7 kW prototype high-swirl burner and crude glycerol in an 82 kW refractory lined furnace with NO_X emissions being 20 times higher in the latter compared to the former. Better performance was noted with glycerol flames – stable at higher excess air ratios compared to propane and No. 2 fuel oil. Whereas the traditional fuels showed unstable combustion at equivalence ratios (ER) < 0.45, the USP grade glycerol, preheated to 93°C, showed optimal combustion stability between ER of 0.37 and 0.44. Jiang and Agrawal [123] tested the combustion of USP grade (with 99+% purity) glycerol combustion with and without methane using a so-called flow-blurring nozzle which is essentially an air-blast injector that allows a portion of the atomising air into the fuel tube creating a turbulent two phase flow inside the tube and the orifice. The efficacy of this nozzle in permitting unheated straight glycerol combustion was noted as was the flame structure variation with changes in fuel combinations. Also, [124] studied both the atomisation characteristics of glycerol using two different air-assist atomisers and the emissions from co-combustion of glycerol with natural gas and hydrogen in a laboratory furnace fired by a swirl burner. With the glycerol preheated to 80°C, optimal atomiser operating conditions and the influence of these conditions on post combustion emissions were noted. Muelas *et al.* [125] using an air-assist atomiser installed in a semi-industrial furnace simulating real boiler conditions, trialled crude glycerol (preheated to 80°C) combustion as well as its blends with

acetals. The blending improved the combustion behaviour of crude glycerol in terms of stability range, flame stability and CO emissions. Steinmetz *et al.* [126] investigated the particulate matter, acrolein and other volatile organic compound emissions that arising from methylated, demethylated and technical glycerol combustion; the fuels being preheated to 45°C, 120°C and 120°C respectively to reduce viscosity and facilitate pumping. Methylated glycerol referring to one with 10 – 20% methanol (b.p 65°C hence the lower preheating value) among other impurities. They used a pressure atomiser for the methylated glycerol, noting it is more commonly used in package boilers for which they envisage crude glycerol usage as fuel. The 82 kW refractory lined furnace of [79] was used for the experiments and the main conclusions were that, whereas acrolein and VOC emissions are not important, potentially corrosive particulate matter are a problem if crude glycerol with soluble catalyst is deployed in boiler applications.

Based on the foregoing, there has been an interest in utilising, as fuel in combustion systems, the vast amounts of glycerol generated as a result of biodiesel production. However, the majority of the studies employed fuel pre-heating and in the single case without pre-heating, a non-standard atomiser was utilised – calling for additional operational costs and substantial retrofitting of the engine. A gap exists, then, in investigating glycerol usage in gas turbine combustion without significant modification of the engine.

2.6.1.3 Straight vegetable oils

Moreover, there has been interest in utilisation of straight vegetable oils (SVO) in gas turbine engines largely in a bid to expand the fuel flexibility of the gas turbine and potentially save the cost of processing SVO to biodiesel. Prussi *et al.* [127] tested straight sunflower oil heated to 130°C in a Capstone C30 micro gas turbine delivering 29 kW of electrical power and compared the emissions therefrom with diesel burn. The turbine utilises three air-assisted injectors at different air-to-liquid ratios. The results showed that while comparable CO emissions were recorded, NO_X emissions increased two-fold in the case of the unrefined bio-oil compared to diesel. In addition, 5% more volume of fuel is consumed and 30% extra pump power is required in the case of the sunflower oil compared to diesel. Kun-Balog and Sztankó [128] used crude rapeseed oil heated to 80°C, for viscosity and surface tension reduction, as fuel in a Capstone C30 micro-gas turbine injecting it with a plain jet air blast atomiser

generating 15 kW thermal power. Using similar experimental base equipment, it would seem that the idea was to improve on the work of [127] by striving to achieve better NO_X emissions results. Kun-Balog and Sztankó [128] found that, with oil preheating and atomisation with superheated steam instead of air, equivalent emissions of CO and UHC and 60% less NO_X was possible in comparison with diesel. Chiaramonti *et al.* [129] trialled straight rapeseed oil preheated to 120°C for viscosity reduction in a model Garett GTP 30-67 gas turbine engine delivering 25 kW at full load. Flame out was reported at temperatures below 120°C but at that temperature, CO emissions were similar to diesel combustion at 20°C. However, under the same conditions, CO emissions rose by 118% compared to diesel. It was also noted that very low NO_X emissions, which did not differ significantly across tested fuels, occurred. The feasibility of using both pure jatropha oil and jatropha biodiesel as gas turbine fuels was investigated by [130] in an atmospheric swirl burner with diesel as the reference. The combustion air temperature was set at 400°C and the fuel line was maintained at 30°C, 60°C and 120°C for diesel, jatropha oil and jatropha biodiesel respectively while an air-assist pressure swirl atomiser was employed. Comparable NO_X emissions but higher CO emissions were reported with the straight oil and biodiesel compared with the reference fuel. Józsa and Kun-Balog [131] combusted crude rapeseed oil in an atmospheric LPP burner with an air blast nozzle to the tune of 15 kW thermal power output and compared the resulting stability emissions data with diesel at the same power output. Combustion air into the burner was maintained at 400°C and oil temperature was 150°C. Despite preheating, it was noted that crude rapeseed oil failed to ignite at start-up and after being aided by diesel, rapeseed oil flames showed relatively narrow stability limits. Greater CO but lesser NO_X emissions were attained comparing rapeseed oil with diesel combustion. Whereas the main goal in utilising SVOs in gas turbines was to explore its feasibility as fuel, it cannot be ignored that the requirements for attaining comparable emission performance with conventional fuels are not attractive. The attendant energy and equipment costs of a feedwater pump, steam generator and desalinated water required for possible steam blast atomisation as well as the fuel preheating system probably makes less economic sense than prior refining of the oil.

It would appear that the key physical property of liquid fuel alternatives is viscosity. Consequently, a number of researches have sought to correlate it with atomiser and

ultimately combustion performance. It was demonstrated by [80] that reducing fuel viscosity improves spray atomisation quality leading to faster evaporation and more complete combustion. A DG4M-1 micro gas turbine equipped with a pressure-swirl atomiser was utilised. Vegetable oil (commercially available as liquid frying fat) within 20 – 120°C temperature range was the fuel tested with diesel as the benchmark. CO emissions, it was found, demonstrates a linear relationship with oil viscosity which in turn is directly proportional to temperature. This is in line with other data [132] which highlighted experimentally that in the case of biodiesel from vegetable oil (VO) and animal feedstock using an air-blast atomiser, CO and NO_X emissions are mainly a function of the extent of fuel atomisation and the effectiveness of the fuel/air mixing process. Crucially, it was noted that a 70-30 diesel-VO blend performed as well as biodiesel from the two feedstocks in terms of SMD and emissions suggesting that the cost of VO processing to biodiesel can be potentially saved. In addition, Panchasara and Agrawal [133] demonstrated that enclosed flame vegetable oil spray droplet diameters mean and RMS axial velocity have a direct relationship with fuel inlet temperature. Smaller droplet size distribution, was claimed, leads to lower emissions of CO and NO_X since it results in premixed combustion as larger droplets tend to burn in diffusion flame mode. The dynamic viscosity of crude Jatropha oil at 40°C is over seven times that of diesel and Deshmukh *et al.* [134] claims this is why higher injection delays and shorter penetration lengths are experienced with Jatropha compared to diesel. The higher viscosity of the biofuel was also blamed for its poor atomisation and the intact liquid core observed even at an injection pressure of 160 *MPa* using a diesel injection system. The air core size of hollow liquid cone sheet formed by pressure swirl atomisers have been found to decrease with an increase in liquid viscosity [135]. This was corroborated by Wimmer and Brenn [136] who further hypothesised that the decreasing air core radius increases the film thickness hence causing a higher throughput of liquids as viscosity increase albeit within a range of moderate liquid viscosities. However, high liquid viscosity prevents the fluid from forming large spray cone angles which in turn impacts negatively on the efficiency of the liquid breakup process [137]. The deterioration in spray quality with increase in fluid viscosity was also noted by Li *et al.* [138] for the air-assist type injector based on experiments with heavy fuel oil. Nevertheless, it is observed that with the air-assist type injector, beyond certain critical values (GLR of 0.05 and momentum flux ratio of 4), liquid properties including viscosity do not significantly affect atomisation

[139, 140]. Not just in pressure and twin-fluid atomisers, fluid viscosity plays an important part in fuel atomisation even in hybrid atomisers. Fan *et al.* [141] utilised the air-assist pressure swirl atomiser to inject jatropha oils. The trend of atomisation dependence on fluid viscosity continued but for a couple of anomalies at points of transition from laminar to turbulent flow. However, flame radiation intensity strongly correlated with liquid viscosity.

2.6.2 Syngas

In order to validate syngas as a potential gas turbine fuel, the combustion-related characteristics of syngas in terms of blowout, flashback, autoignition and emissions characteristics have been assessed by several researchers. Blowout occurs when the flame detaches from its anchor location and is physically moved (blown out) of the combustor; flashback occurs when the flame physically propagates upstream of where it is supposed to be anchored into premixing passages that may not be designed for high temperatures; autoignition is similar to flashback but it is not caused by flame propagating upstream of its anchor point. Instead it is the result of spontaneous ignition of the mixture. The operability issues as it pertains to syngas and the effect of fuel composition has been evaluated in detail by [142]. The main conclusion was that the behaviour of gaseous fuel mixtures, as in syngas, can be very different from the individual components such that parameters like flame speed and ignition delay times are impacted, with hydrogen content a major factor. Laminar flame speed, a determinant of the propensity for flame flashback or blowout, has been studied for syngas. Dong *et al.* [143] and Fu *et al.* [144] using Bunsen burners reported that in H_2/CO syngas, over a broad range of equivalence ratios, the laminar flame speed of the mixture with air increases with the H_2 fraction thereby extending the blow-off limit significantly. Similar effect has been reported using gas turbine type burner [145]. In like manner, [146] noted that syngas with high hydrogen concentration has lower lean blowout limits demonstrating the effectiveness of hydrogen addition to enhance flammability. However, the higher flame speeds associated with syngas suggests the increased possibility of flashback if DLN technique is introduced to a syngas powered turbine [147].

It has been found that a key feature of syngas combustion is that unlike methane, combustion pulsation seems to be virtually non-existent regardless of the ratio of H_2 and CO in the syngas [40, 43]. However, as the concentration of H_2 increases, NO_X emissions correspondingly increase while recording overall low CO emissions [44]. Any of CO_2, N_2 or steam could be utilised as diluents to effectively tackle emissions from syngas flames with the level of NO_X reduction being a function of the diluent's heat capacity [148].

As noted elsewhere, using syngas as fuel in a combustion system designed for gas turbines will necessitate modifications in the combustion system. This is due to the lower calorific value of the fuel compared with natural gas and modifications to accommodate changes in mass flow rate, fuel delivery system, fuel nozzles and the combustion chamber are important if comparable efficiencies are to be attained [149].

2.6.3 The growing case for ammonia

The road toward green energy technology has led down many pathways. One of the more recent routes involves renewable hydrogen production and utilisation – the so-called "hydrogen economy". A widely researched means of renewable hydrogen production is through water electrolysis with solar power [150]. The potential for renewable hydrogen production from wind-generated electricity has also been studied as in [151]. Similarly, Rahmouni *et al.* [152] and Schoenung and Keller [153] researched the feasibility of a combination of both sources of renewable electricity (wind and solar) for hydrogen production in Algeria and California respectively. A concise review of the processes of renewable hydrogen generation can be found in [154, 155] and a comparison of available options is presented in [156].

Once generated, renewable hydrogen has to be chemically stored due to the extremely low volumetric energy density of pure hydrogen and the potential safety and infrastructure cost issues associated with its distribution on a global scale [157]. Chemical storage of hydrogen on a large scale will necessitate employing carbon or nitrogen as the main hydrogen carriers using CO_2 [158] or N_2 [159] to arrive at carbon or nitrogen-based fuels. Interestingly, it would seem that in the overall energy balance analysis – a function of the energy cost of synthesising a fuel and the energy content

of the fuel – nitrogen-based renewably derived fuels (ammonia in particular) compare favourably with their carbon-based counterparts [160].

Of the nitrogen-based fuels derived from renewable hydrogen, the so-called "green ammonia" is the most important. It is so-called because the traditional, energy-intensive method of combining nitrogen with hydrogen to form ammonia – the Haber-Bosch process – rife with CO_2 production, is bypassed rendering the entire process carbon free. Basically, the process involves the electrochemical synthesis of ammonia starting with water electrolysis and considerable progress has been achieved in this field [161, 162].

As to the utilisation and performance of ammonia in gas turbine combustion, a few studies have been conducted. Hayakawa *et al.* [163] investigated ammonia/air premixed flame stability at different equivalence ratios as well as emissions performance in a swirl burner. With increasing equivalence ratio, NO concentration reportedly decreased but NH_3 emissions increased; adoption of swirling flow improved flame stability without recourse to any additives. Similar experiments were reported for ammonia blended with methane [164] and with hydrogen [165]. A few numerical investigations on the subject could be found in [166-169]. In the experimental cases, ammonia-hydrogen blend is associated with high NO_X emissions and a narrow operational range whereas the blend with methane suffers from flame instabilities at medium swirl numbers suggesting that further investigations particularly in the area of injection strategies are necessary if ammonia or blends of it with other fuels is to be employed for gas turbine combustion. The feasibility of this can be seen in [170] where with an optimised injection strategy, direct injection of urea is effective in reducing NO_X emissions in a biodiesel-fuelled diesel engine.

Apart from converting it to green ammonia that can be used in modified gas turbines [171], hydrogen, can be stored and used in a number of other forms that are yet nitrogen-based. The feasibility of three of such forms, namely, aqueous ammonium hydroxide and urea (AHU), aqueous ammonia and ammonium nitrate (AAN) and aqueous urea and ammonium nitrate (UAN) as gas turbine fuels have been discussed in [172]. In their aqueous forms, these are known as monofuels, capable of being ignited without any additives as they inherently contain both an oxidiser and a reducer (fuel) part. The nature of UAN has been investigated [173] and the mechanism

of its combustion discussed [174] and so has the thermal decomposition of AAN [175] and the sort of fuel ignition process required for these fuels [176].

Potentially then, in the near future, as the hydrogen economy gathers momentum, nitrogen-based hydrogen carriers may play an important role in the energy generation process as the goal remains to cut down on global CO_2 production while ensuring energy security.

2.7 Simultaneous combustion of multiple fuels in IC engines

It has been established that the ever-growing energy demand across the world cannot be met by conventional sources which, themselves, are rapidly depleting. Alternative energy sources have been widely explored and in certain cases, mature technologies now exist for exploiting these options. For example, ethanol and biodiesel now enjoy combustion applications in practical internal combustion engines albeit as blend components [177]. This section details the wide variety of research into utilisation of fuel blends in compression ignition engines (Table 2.1) and in the gas turbine engine (Table 2.2). The list in both tables have been sampled from published research in the last ten years and is by no means exhaustive particularly in the diesel engine case. Liquid/liquid blends in CI engines commonly substitute biodiesel for diesel wholly or partially. Results show that, compared to standard diesel, biodiesels as a result of their inherent oxygen content, burn with lesser amounts of HC, soot and CO emissions [178]. As to the impact biodiesel combustion has on NO_X emissions, opinion is polarised. Thangaraja *et al.* [179] summarises that 85% of published researches in this area report an increase in NO_X when biodiesels instead of standard diesels are burned; 5% are of the opposite view whereas 10% of the investigations suggest that NO_X levels remain same. For the liquid/gas fuel blends utilised in the CI engines cited, a popular injection strategy is to “fumigate” the combustion air stream with the gaseous fuel in the intake manifold and then supply the liquid fuel (which often serves as pilot flame) by direct injection. Regardless of the injection strategy, all published work on the subject agree that multiphase fuel combustion is feasible in CI engines. However, the effect on engine performance parameters and emissions is not unanimous. This is not surprising given, as shown in Table 2.1, the variety of engine

types and operating conditions utilised by different studies even as is the case in single phase burn.

As for the gas turbine engine, the majority of studies in simultaneous fuel combustion involves blends of fuels in the same phase (liquid/liquid and gas/gas). These single-phase dual fuel combustion cases abound ranging from diesel and glycerol blends to wood liquefied in alcohols. The appeal/attraction of multiphase combustion in diesel engines but not in gas turbines is because, oftentimes, the replacement fuel in diesel engines is one, like natural gas, which burns cleaner than the traditional fuel. However, the inherent assumption that gas turbines run on natural gas is a generalisation. OEMs often equip gas turbines with liquid fuel atomisation systems to permit utilisation of diesel in areas without gas supply infrastructure or with inconsistent gas supply [57]. Besides, micro gas turbines widely used for distributed electricity generation or stand-by applications mostly run on liquid fuels [127, 128].

Consequently, there has been a few researches into the simultaneous combustion of liquid and gas fuels under gas turbine conditions. Perhaps the earliest multiphase fuel combustion attempts were published in 2017 [180, 181]. Kurji *et al.* [180] carried out an experimental study on the combustion of CO_2/CH_4/Diesel and CO_2/CH_4/ biodiesel mixtures. The goal of CO_2 addition to the fuel mixes, the study said, was to improve emissions performance by acting as a diluent. Low CO and NO_X emissions were reported with the biodiesel blend performing better emissions wise. However, in the work, a constant liquid fuel flow rate was reported and it was unclear which of the liquid fuels that applied to. If it applies to both, then given the different heating values of the liquids, power output is not maintained and the emissions comparison is hardly justifiable. Also, any beneficial effect of CO_2 dilution may have been attained by sacrificing ignition and stability efficiency as mooted in the paper. Sidey and Mastorakos [181] on their part, investigated the dual-fuel flame structure and stability of ethanol-methane flames in air using OH* chemiluminescence, OH-PLIF and Mie scattering. A widening of the reaction zone and changes in the stabilisation behaviour were reported when the dual-fuel flames were compared to either methane only or neat ethanol burn.

Table 2.1. Sample of multi fuel combustion in IC engines in the last decade

Fuels tested	*Engine type*	*Injection strategy*	*Power output*	*Research interest*	*Researcher(s)*	*Date*
Biogas-diesel and biogas-biodiesel	Model four-cylinder engine with displacement of 2476 cm^3	Biogas premixed with intake air, gas pressure 0.4 MPa; liquid fuel was pilot fuel at 12 MPa	46 kW at 4000 rpm	Influence of dual fuel burn on emissions and engine performance	Yoon and Lee [182]	2011
Ammonia and diesel	Four-cylinder engine with displacement of 4500 cm^3	Ammonia injected into the intake air; DI of diesel	66 kW at 1000 rpm	Combustion and emissions performance compared to conventional operation	Reiter and Kong [183]	2011
Syngas and diesel	Single-cylinder engine with displacement volume of 661 cm^3	Primary fuel, syngas, fed by a gas carburettor into the intake manifold; diesel used as pilot	5.2 kW at 1500 rpm	Engine and emissions performance at different syngas (H_2/CO) compositions compared with conventional operation	Sahoo *et al.* [184]	2012
Jatropha biodiesel and diesel	One cylinder with displacement volume of 780 cm^3	DI of fuel blends at 20 – 20.5 MPa	7.4 kW at 1500 rpm	Combustion and emissions characteristics as well as performance evaluation	Chauhan *et al.* [185]	2012
Ethanol and diesel	Six-cylinder with displacement volume of 8400 cm^3	Ethanol injected into intake manifold; DI of diesel as pilot	206 kW at 2200 rpm	Engine performance under dual-fuel mode	Sarjovaara *et al.* [186]	2013
Hydrogen and butanol-biodiesel blends	Single-cylinder with displacement volume of 773 cm^3	Hydrogen injected into intake air; DI of liquid fuel blend at 18 MPa	836 kW at 2500 rpm	Effect of hydrogen addition on post combustion emissions	Sukjit *et al.* [187]	2013
CNG, diesel and waste cooking oil derived biodiesel	Six-cylinder with displacement volume of 6728 cm^3	The oils were the pilot fuels and CNG was injected into the intake manifold	132.7 kW at 2100 rpm	Combustion and exhaust emissions evaluation	Mohsin *et al.* [188]	2014
LPG and diesel	Six-cylinder with displacement volume of 5900 cm^3	LPG fumigated into the intake air stream with diesel as pilot	162 kW at 2500 rpm	Combustion and exhaust emissions evaluation	Surawski *et al.* [189]	2014
Rapeseed methyl ester and diesel	Three-cylinder with displacement of 1028 cm^3	Liquid direct injection at maximum pressure of 150 MPa	15 kW at 3600 rpm	Combustion and emissions performance	Magno *et al.* [190]	2015
EN5590 diesel EN228 gasoline	Model single cylinder with displacement of 390 cm^3	Direct injection (DI) of up to 220 MPa for diesel and port fuel injection (PFI) for gasoline	80 kW/l	Emissions and fuels consumption reduction	Martín *et al.* [191]	2016

Table 2.1. Sample of multi fuel combustion in IC engines in the last decade, *continued*.

Fuels tested	*Engine type*	*Injection strategy*	*Power output*	*Research interest*	*Researcher(s)*	*Date*
Diethyl ether, karanja methyl ester and biogas	Single-cylinder with displacement volume of 662 cm^3	Biogas inducted into intake air; the other two injected into cylinder with biodiesel as the pilot at 20 MPa	4.4 kW at 1500 rpm	Combustion and emissions performance evaluation	Barik and Murugan [192]	2016
Ethanol and rubber seed oil methyl ester/rubber seed oil/diesel	Single cylinder with displacement volume of 661.5 cm^3	DI of the diesel/biofuel as pilot and fumigation of ethanol at 0.6 MPa	4.4 kW at 1500 rpm	Combustion and emissions characteristics as well as performance evaluation	Geo *et al.* [193]	2017
Diesel and synthetic biogas	Single cylinder with displacement volume of 630 cm^3	DI of the diesel as pilot at 24 MPa and intake port injection (fumigation) of biogas	4.5 kW at 1500 rpm	Combustion and emissions characteristics as well as performance evaluation	Aklouche *et al.* [194]	2017
Blends of oils from peels of orange and lemon fruit with diesel	1-cylinder engine with stroke length of 110 mm	DI of fuel blends at 40 and 60 MPa	3.5 kW at 1500 rpm	Combustion and emissions as well as performance evaluation	Ashok *et al.* [195]	2018
Jatropha biodiesel and turpentine oil	1-cylinder with stroke length of 110 mm	DI of fuel blend at 21 – 23 MPa	3.7 kW at 1800 rpm	Combustion and emissions performance	Dubey and Gupta [196]	2018
Hydrogen and diesel	Four-cylinder engine of displacement volume of 5200 cm^3	Hydrogen premixed with intake air at 0.4 MPa; DI injection of diesel as well as diesel pilot at 70 – 110 MPa	20 kW at 1500 rpm	Combustion and emissions performance	Dimitriou *et al.* [197]	2019
Hydrogen and diesel	Single-cylinder with a displacement volume of 40.1 cm^3	Port injection of hydrogen; DI of diesel	5.2 kW at 1500 rpm	Combustion stability and unregulated emissions investigation	Sharma and Dhar [198]	2019
Hydroxy gas (mix of hydrogen and oxygen) and diesel	Single-cylinder engine with displacement volume of 661 cm^3	Gas supplied into the air intake manifold; DI of diesel at 21 MPa	3.5 kW at 1500 rpm	Engine performance and post combustion emissions evaluation	Sharma *et al.* [199]	2020
Ethanol/diesel and ethanol/biodiesel (neem)	Single-cylinder engine with displacement volume of 661 cm^3	Carburettor supply of primary fuel (ethanol) to intake air and DI of pilot diesel/biodiesel at 21 MPa	3.5 kW at 1500 rpm	Engine performance and post combustion emissions evaluation	Gawale and Naga Srinivasulu [200]	2020
n-butanol/coal to liquid (CTL)	Single-cylinder modified from a four-cylinder engine	n-butanol premixed with intake air at 3 MPa; DI of CTL s ignition source at 100 MPa	1.44 kW at 1400 rpm	Combustion and emissions characteristics evaluation	Zhang *et al.* [201]	2020

Table 2.2. Sample of multi fuel combustion tests in gas turbine type combustors in the last decade.

Fuels tested	*Engine type*	*Injection strategy*	*Power output*	*Equivalence ratio*	*Research interest*	*Researcher(s)*	*Date*
CH_4, CO_2 and O_2	Model swirl burner	Partially premixed	10 – 30 kW	0.5 - 1	Flame stability and operability with oxyfuel combustion	Kutne *et al.* [202]	2011
Blends of jatropha biodiesel and diesel	IS/60 rovers gas turbine	-	44 kW	Variable	Feasibility of jatropha biodiesel as GT fuel	Rehman *et al.* [203]	2011
Wood liquefied in poly hydroxyl alcohols	Swirl burner	Air-blast atomiser		Variable	Feasibility of liquefied wood as GT fuel	Seljak *et al.* [204]	2012
N_2, CO_2, steam and syngas (H_2 and CO)	Model GE7EA industrial gas turbine; 1 atm, 500°C inlet conditions	-	60 kW	Variable	Combustion performance of syngas and effect of dilution of other gases	Lee *et al.* [42]	2012
Biodiesel and vegetable oil blends	Garett GTP 30-67 micro gas turbine	Pressure atomiser	0 – 25 kW	Variable	Exhaust emissions performance in comparison with diesel	Chiaramonti *et al.* [129]	2013
Rapeseed and sunflower oil and Jet A1 kerosene blends	Capstone micro gas turbine model C30	Air-blast atomiser	15, 25 kW	Variable	Exhaust emissions investigation	Chiariello *et al.* [205]	2014
Butanol and Jet A blends	University of Oklahoma propulsion Lab gas turbine	-	30 kW	0.18 – 0.33	Performance and emission characterisation	Mendez *et al.* [206]	2014
Biodiesel and pyrolysis oil blends	Generic swirl burner	Pressure atomiser	3 – 60 kW	0.5 – 1.4	Emissions performance with alternative fuels	Kurji *et al.* [207]	2016
CO2/CH4/biodiesel and CO2/CH4/diesel	Model swirl burner	Pressure atomiser	20 kW	1.4 – 2.2	Multiphase combustion trial in gas turbines	Kurji *et al.* [180]	2017
Jet A-1 and hydrotreated renewable jet fuel blends	Gas turbine swirl burner (Cardiff GTRC)	Pressure atomiser	41 kW	0.8 – 1.1	Operability and fuel performance of gas turbine with the fuel blend	Buffi *et al.* [208]	2017
Ammonia and methane	Gas turbine swirl burner (Cardiff GTRC)	Premixed	30 kW	0.8 – 1.45	Flame stability and emissions study	Valera-Medina *et al.* [164]	2017
Butyl butyrate and ethanol blends	Aero engine-based GT burner with intake pressure (0 – 7 MPa) and inlet temperature up to 600 K	-	-	variable	Gaseous and PM emissions study	Chen *et al.* [209]	2017

Table 2.2. Sample of multi fuel combustion tests in gas turbine type combustors in the last decade, *continued*.

Fuels tested	*Engine type*	*Injection strategy*	*Power output*	*Equivalence ratio*	*Research interest*	*Researcher(s)*	*Date*
Ethanol and methane	Model atmospheric bluff-body burner	Pressure atomiser; Partially premixed	Variable	variable	Flame structure and stability investigation	Sidey and Mastorakos [181]	2017
Jatropha biodiesel and diesel blends	Model swirl GT with inlet temperature of 600 K	Air-blast atomiser	40 kW	0.5 – 2.0	Operability and emissions performance of gas turbine with the alternative fuels	Bhele *et al.* [210]	2018
Fast pyrolysis bio-oil and ethanol blends	Capstone micro gas turbine model C30 LF	Pressure swirl atomiser	5 – 20 kW	Variable	Investigation of viscous fuel use as blend component in micro gas turbine	Buffi *et al.* [211]	2018
n-heptane and methane	Model atmospheric bluff-body burner	Pressure atomiser; Partially premixed	Variable	0.31 – 0.66	Flame structure and stability characteristics of dual fuel flames	Sidey and Mastorakos [212]	2018
Hydrogen-ammonia blends	Gas turbine swirl burner (Cardiff GTRC)	Premixed	39.3 kW	0.9 – 1.4	Investigating the complexity of burning ammonia in blends with hydrogen	Valera-Medina *et al.* [213]	2019
Diesel and glycerol	Micro gas turbine	Pressure atomiser	3 – 6 kW	Variable	Combustibility and characteristics of glycerol combustion emissions	Seljak and Katrašnik [214]	2019
Natural gas and n-heptane	Model atmospheric bluff-body burner	Pressure atomiser; Partially premixed	Up to 6 kW	Variable	Temperature distribution and reaction zone characteristics	Evans *et al.* [215]	2019
Diesel and syngas	Model swirl burner	Pressure atomiser	6 – 20 kW	0.7	Multiphase combustion trial in gas turbines	Agwu and Valera-Medina [216]	2020
Methane and ammonia blends	50 kW model swirl burner	Premixed and non-premixed	50 kW	Variable	Emissions production and control in methane-ammonia flames	Okafor *et al.* [217]	2020

However, the contribution of the liquid fuel to overall power output in the dual-fuel cases was at most 4%. With the liquid fuel flow rate maintained throughout the study, the dual phase flames were obviously delivering a much higher heat output compared to the neat ethanol flame. On top of that, global equivalence ratios varied widely throughout the tests. Consequently, comparison of optical emissions, including luminosity images and chemiluminescence, are not ideal. Nevertheless, these early studies highlighted, even if tentatively, the feasibility and potential benefits of multiphase fuel burn under gas turbine conditions. A year later, in 2018, Sidey and Mastorakos [212] investigated, using the same enclosed bluff-body burner as in [181], the stabilisation characteristics of *n*-heptane/methane flames. Using *n*-heptane in place of ethanol was not only an expansion of the fuel-flexibility of the multiphase combustion process but also a shift towards a better representation of practical systems (that mostly utilise non-oxygenated fuels). They reported improved flame stability as well as flame structure differences with increasing amounts of gas in the oxidiser stream. However, as was the case in [181], the overall heat output in the contrasted tests was not maintained. For instance, the flame stability (interpreted in terms of blowout velocity at flame extinction) of a given flow rate of *n*-heptane was compared with those of the same flow rate of *n*-heptane burning in a stream of air premixed with increasing quantities of methane. This is tantamount to observing that more oxygen is required for combustion as the quantity of fuel increases. The same criticism can be placed on the work of Evans *et al.* [215] who basically added hydrogen to the fuel mix of the work in [212] and imaged the resulting flame using a couple of flame visualisation techniques. Measurements were taken at varying heat outputs and gas flow rates which makes comparison of flame optical emissions spurious.

In spite of the drawbacks highlighted, these previous works on multiphase fuel burn in gas turbine combustor rigs provide data that could be used as validation targets in turbulent dual-fuel combustion modelling. The present study aims to add to this limited database by trialling the co-combustion of practical fuels – diesel, biodiesel, methane and syngas – under gas turbine conditions. Taking into account the identified shortcomings of previous research, comparisons of the combustion characteristics of single phase and the multiphase fuel flames of the listed fuels were made at equitable operating conditions.

2.8 Chapter summary

The quest for transitioning from traditional fuels to renewable alternatives or increased utilisation of the latter in the power generation industry is occasioned by at least three factors: rapid depletion of fossil (conventional) fuel reserves meaning that the huge energy demands of the future must be met, at least partly, with alternative sources; environmental sustainability which necessitates improvement on the levels of dangerous emissions resulting from the combustion process; and the potential economic (operating cost) benefits. Consequently, the viability of renewable fuels and blends of renewables and conventional fuels in internal combustion engines has been evaluated by several studies as highlighted in this Chapter. Over the years, a wide variety of fuels have been tested. Even if some tests appear to be only academic, the point made is that the fuel flexibility of combustion systems is constantly being expanded. This is as true for the diesel engine as it is for the gas turbine.

Unlike in the aviation sector, fuel regulations in the realm of industrial (stationary) gas turbines are less prescriptive and machine overall weight is not an important factor so that there is greater room for flexibility in fuel choice and deployment. As a result, biofuels from different sources and in different physical phases are widely studied for possible application in stationary gas turbines. There is even a growing interest in tapping into the so-called “hydrogen economy” such that nitrogen-based hydrogen carriers like ammonia and derivatives of it have been investigated for potential future use as gas turbine fuels.

Evidently, considerable research has been undertaken in relation to alternative fuels and their utilisation in energy generation process in the internal combustion engine. However, in the gas turbine engine, unlike in the diesel engine, studies investigating multiphase fuel combustion operation is severely limited. Present study fills that gap by trialling and characterising the combustion of several multiphase fuel combinations of diesel, biodiesel, methane and syngas in a swirl stabilised gas turbine combustor. Over and above that, the feasibility of burning blends of methanol/glycerol with and without methane using the same set-up as the previous fuels will be explored.

3

MATERIALS AND METHODS

This Chapter describes the materials and methods used in achieving the results reported in the rest of the work. It includes both experimental and numerical methodology description.

3.1 Experimental materials

Experiments in this thesis were carried out in the spray combustion bay in the Thermofluids Lab of Cardiff University. The bay houses an optically accessible 20 kW swirl-stabilised gas turbine relevant burner. Previously, Kurji [218] used the spray combustion rig for part of his PhD experiments with limited success, reporting operational difficulties and inefficiencies when burning liquid fuels. Upstream of the atomiser was a liquid accumulator that utilised compressed nitrogen to pressurise the fuel. Preliminary tests showed that the components upstream of the nozzle, in the existing set-up, were unwieldy with liquid spray flames capable of being sustained for only very short durations (<1 min) at a time. To overcome these issues, a simpler and more efficient set-up was designed capable of sustaining spray flames for upwards of forty-five minutes at a time. In Section 3.1.1 and 3.1.2, the burner together with its upstream components are described. In later sections, the data acquisition equipment and the fuels used in the experiments are detailed.

3.1.1 Burner

The burner set-up is made up of combustion air inlets and plenum; a liquid fuel line; an axial swirler; a pressure atomiser and the combustion chamber. The atomiser and swirler is presented in photographical form in Fig. 3.1 while an engineering drawing of entire set-up is in Fig. 3.2 and Fig. 3.3.

(a) **(b)**

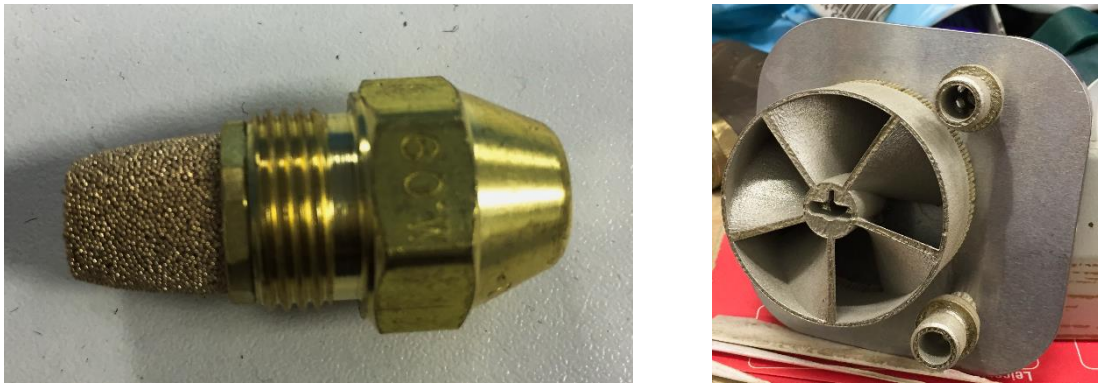

Fig. 3.1. Pictures of (a) pressure atomiser and (b) axial swirler.

A 2-D section with detailed dimensions and annotations is provided in Fig. 3.3. Where utilised, gaseous fuel is supplied to one of the air inlets via a hose installed perpendicular to that air inlet conduit. Each of the three 19 *mm* (outer diameter) gas fuel and air inlets passes the air or air/gas mixture into the burner plenum which has the axial swirler fitted to its end.

The axial swirler, Fig. 3.1(b), has a tip diameter, D_s, of 50 mm and a hub diameter, D_h, of 16 mm. It has five swirl vanes each about 2 *mm* thick. The angle of swirl, θ, is 60° so that from Eq. (3.1), the approximate geometric swirl number (S_N) is 1.24.

$$S_N = \frac{2}{3}\left[\frac{1-(D_h/D_s)^3}{1-(D_h/D_s)^2}\right]\tan\theta \tag{3.1}$$

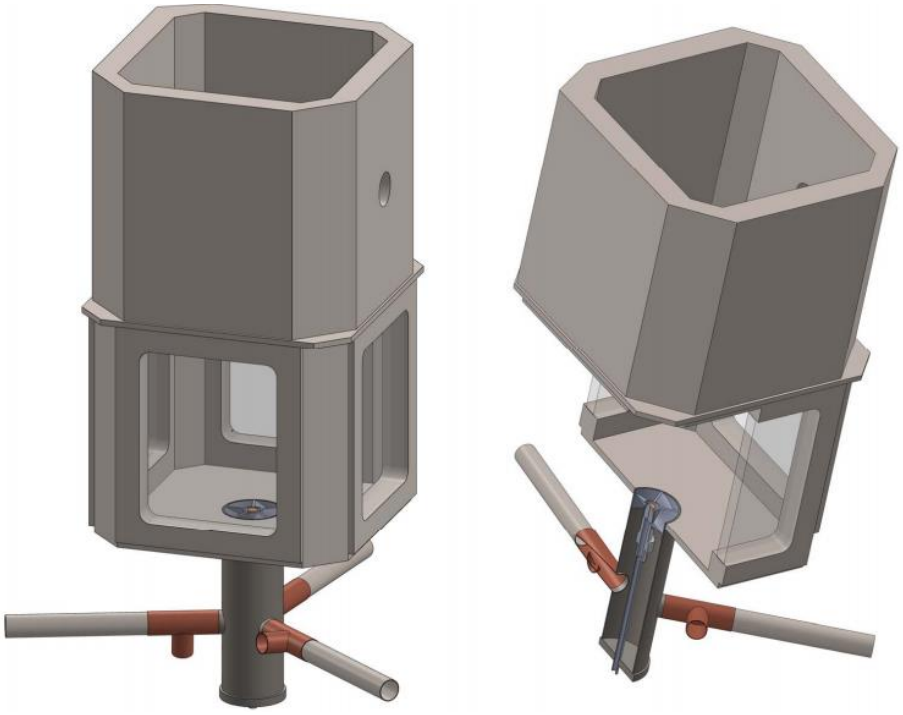

Fig. 3.2. 3D CAD of burner set-up.

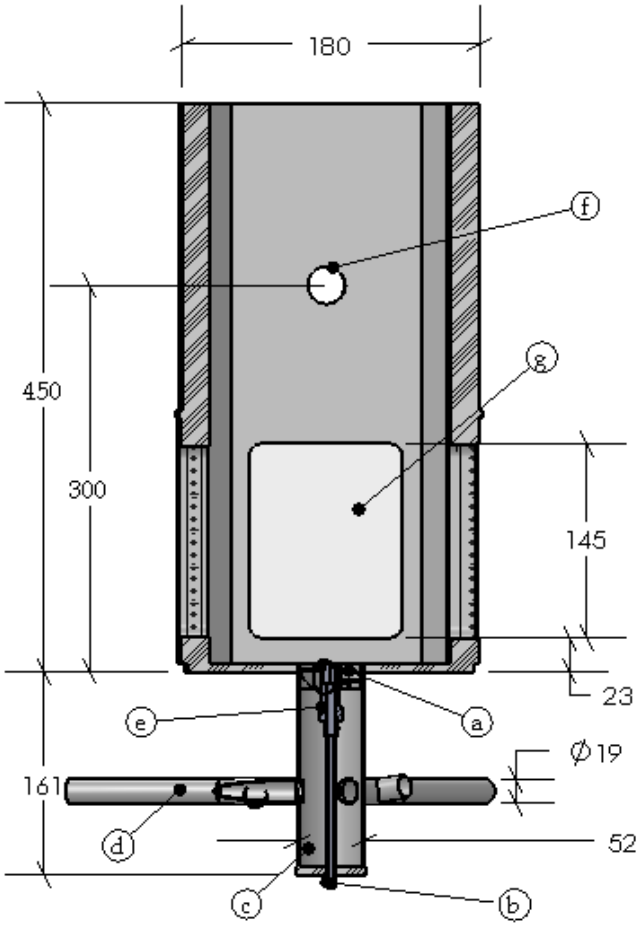

Fig. 3.3. Burner 2D section view showing (a) axial swirler (b) liquid fuel line (c) inlet plenum (d) combustion air/methane inlet (e) pressure atomiser (f) emissions probe slot (g) quartz window. All dimensions in millimetres.

The liquid fuel atomiser utilised throughout the experiment is a Delavan 0.4 GPH 60°W pressure-swirl nozzle. It has the smallest orifice (~0.23 *mm*) of all Delavan nozzles and was selected because of the relatively low liquid flow rates encountered in the study. Pressure-type nozzles are designed to deliver optimum atomisation (spray quality) over a narrow range of the stipulated flow capacity – in this case 0.4 GPH. The nozzle was earlier shown in Fig. 3.1(a). The chamber where combustion takes place has a square cross-section of sides 180 x 180 *mm* and height of 450 *mm* with a 100 x 145 *mm* transparent quartz window on each of its four sides. The base of each quartz window is 23 *mm* from the dump plane of the combustor, thus no optical access is possible below that point.

3.1.2 Burner upstream components

Upstream of the burner are fuel storage and delivery systems as well as flow measurement and control devices. The liquid fuel storage and delivery system is shown in Fig. 3.4. It consists of a fuel tank and a pipe system along the lines of which are fluid flow devices: a filter just downstream of the tank followed by a pump then a non-return valve. The liquid fuel pump is a Walbro GSL392 inline fuel pump and by using a Fuelab 52501 fuel pressure regulator, the mass flow controller (MFC) receives the liquid at 0.85 MPa. Only the set fuel flow rate gets across the MFC to the nozzle; the rest bypasses the regulator and flows back to the tank. The MFC is a Bronkhorst mini CORI-FLOW M14 type with a rated accuracy of ±0.2% of indicated reading.

Methane and air were supplied to the burner plenum at room temperature and metered by variable area rotameters in the range 1-12 l/min for methane and 30-150 l/min as well as 40-440 l/min for air with accuracies of ±1.25% FSD for the lower flow range and, ±5% FSD for the higher flow range. Air flow was split between the two meters to avoid operating close to the limits of the device thereby minimising associated errors. Consequently, the rotameters, were used between 40% and 80% of their maximum volume.

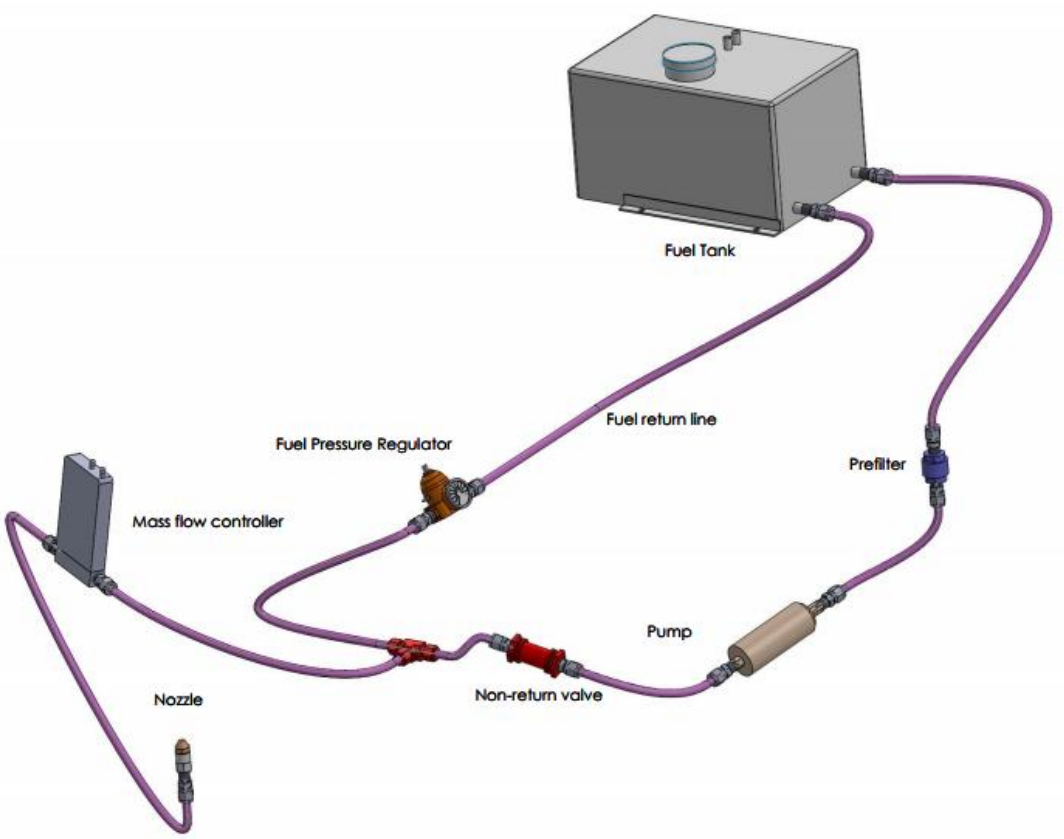

Fig. 3.4. Layout of burner upstream components

Syngas flow rate was controlled by means of a Bronkhorst El-flow Prestige MFC with a rated accuracy of ±0.5%. As earlier mentioned, the gases – combustion air and syngas – were premixed prior to combustion by introducing them simultaneously into the burner inlet air plenum. The charge undergoes further mixing as it passes through the swirler.

3.1.3 Data acquisition equipment and settings optimisation

3.1.3.1 Optical emissions

For flame chemiluminescence measurements, a LaVision Imager Intense CCD camera – model IRO25 (HB0769) – coupled with a LaVision IRO Intensifier (25mm V7670U-70-P43) was used with a 60 *mm* focal length AF Micro-Nikkor (f/2.8) lens. The camera was focused at the centreline of the burner capturing a plane that is ±50 *mm* in the radial direction and 140 *mm* in the axial direction from the base of burner optical window; the setup resulted in a resolution of 0.124 *mm*/pixel. C_2* and CH* chemiluminescence emissions were acquired by separately fitting bandpass filters of

515 *nm* (FWHM = 10 *nm*) and 430 *nm* (FWHM = 10 *nm*), respectively, on the lens. The rationale behind targeting these species is explained in Section 3.2.1.

Parametric studies were carried out to determine how imaging equipment settings, namely intensifier gain and gate pulse width, affect measured intermediate combustion species chemiluminescence intensity. CH* and C_2* species chemiluminescence measurements were taken for diesel as well as biodiesel flames at flow rate in the top range of the test matrix. The emissions intensity signals from a 13.5 kW diesel flame at an equivalence ratio of 0.8 are shown in Fig. 3.5. 250 images captured at 10 Hz from the camera were time averaged and the maximum intensity in the averaged image is plotted against the gain setting in Fig. 3.5 for three different gate pulse widths. At image intensifier gain values above 50, there is a rapid increase in the maximum species chemiluminescence intensity signal from the CCD. The gradient of this intensity signal vs gain curve gets steeper as gate pulse width increases. The biodiesel flames produced CH* and C_2* chemiluminescence intensity images having an average signal value equal to one-third that of diesel flames of the same power output. Also, as seen in Fig. 3.5, the C_2* species intensities from the diesel flame is about 1.5 times the CH* species intensity at intensifier gains above 50 at the same equipment settings.

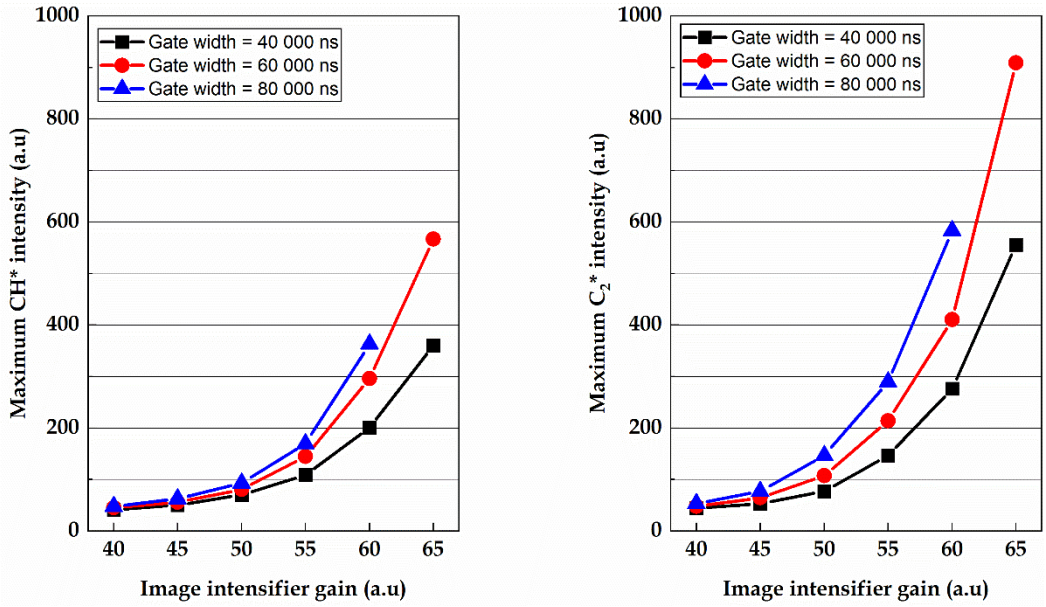

Fig. 3.5. Chemiluminescence image intensity variation with intensifier amplification at different gate pulse widths.

To identify the ideal settings for CH* and C_2* species chemiluminescence intensity measurement that is consistent for both liquid fuels, the C_2* species emissions from the diesel flames must be used to set the top limit on equipment parameters. This top limit must be selected to avoid CCD pixel saturation which would cause some image information to be lost and potentially damage the CCD sensors. The goal, then, was to select a gate width and gain value that does not oversaturate the CCD pixels (>4096 counts) from C_2* signal for a diesel flame.

In Fig. 3.6, the maximum pixel count in the C_2* species chemiluminescence intensity signal from a set of 250 frames is plotted for six gain settings and three gate pulse widths. The encircled point in Fig. 3.6 (80 000 ns gate width and gain of 60) was selected as the maximum intensity of C_2* species in any of the 250 captured images does not saturate the CCD pixel sensor. It represents a point, among the evaluated cases, where CCD signal is maximised while maintaining relatively low amplification (gain) thereby avoiding clipping and reducing noise in the resulting image. The selected imaging equipment setting was tested for biodiesel flames and found to yield meaningful signals.

For each experimental condition, 250 images were captured at 10 Hz. This number of images was selected by analysing a set of 600 images. The average integral intensity of successive images up to a total of 600 were then compared with the global average.

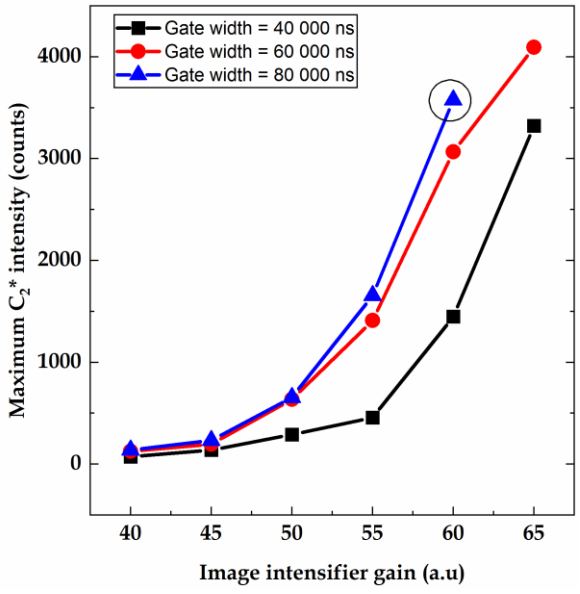

Fig. 3.6. Optimal equipment settings selection

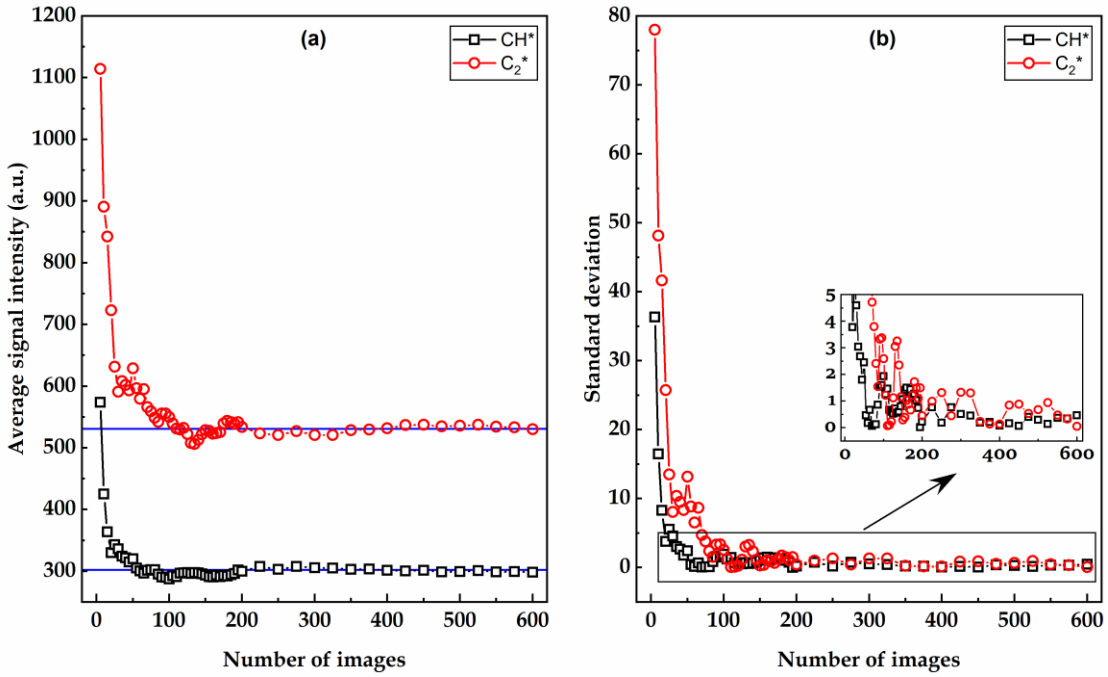

Fig. 3.7. Chemiluminescence signal intensity variation based on number of captured images

The trend is shown in Fig. 3.7(a) and the average of the 600 images is represented by the two blue horizontal lines, one for each of CH* and C_2* species. The standard deviation of each point from the global average is shown in Fig. 3.7(b). From both figures, at >200 images, there is insignificant deviation from the mean value. Therefore, each chemiluminescence test taken in the entire experimental campaign was based on a set of 250 images.

Combustion is generally associated with the emission of light known as flames. Light radiation, being a primary property of most flames, provide a means of obtaining qualitative information about the combustion process. In this study, broadband flame luminosity images from diesel blends and biodiesel blends were captured using an Olympus OM-D E-M5 Mark II camera with a M.Zuiko Digital 45 *mm* f/1.8 lens with an exposure time of 1/8000 s. Flames from the glycerol blends were captured using a Xiaomi POCOPHONE F1 camera with a focal length of 4.15 *mm* and f/2.2 lens.

3.1.3.2 Post combustion emissions

The post combustion emission measurements of NO and NO_2 (or NO_X), CO and UHC were done using Testo 350 XL emissions analyser with the emissions probe situated at the centreline of the burner, 300 mm from the nozzle orifice plane. The equipment draws flue gas through the probe into the gas preparation unit where it is suddenly cooled to 4 – 8^{o}C precipitating condensation. The dry gas is then filtered and passed to the gas sensors which then issue a signal. The manufacturers [219] specify that for NO_X and CO measurements, the instrument works on the principle of ion-selective potentiometry in which gas diffused into an electrochemical sensor reacts with a selected electrode depending on the target gas. This reaction creates a potential difference with respect to the counter electrode and, with a resistor connected across the electrodes, current proportional to the concentration of the gas is generated. The HC sensor consists of a pair of precision resistive thermal devices (RTDs) covered with two different coatings. One is covered with a catalyst that causes an exothermic reaction in the presence of a catalyst; the other is covered with an inert coating and acts as a reference. Both RTDs are heated to about 510^{o}C to increase catalytic reaction rate. With hydrocarbons present, the catalytic RTD will have a higher heat value than the reference thereby providing a means of measuring HC emissions.

The emissions analyser was programmed to sample flue gas for a duration of two minutes at a measuring rate of three seconds for each test condition resulting in a total of forty readings per experimental run. It was noted that both emissions readings stabilised well before the last twenty readings; the average of the last twenty readings is reported in this work. A rinse time of five minutes followed the completion of each programmed run of the device prior to commencement of a new run to avoid "saturating" the sensors hence causing output to drift. For the emissions reported, the equipment has an overall measurement uncertainty of ±6 % of the indicated reading. The oxygen reference was set at 15% for the tests.

3.1.4 Fuels tested

In Table 3.1 are physical and chemical properties of the fuels tested in this work. The fossil diesel used in the study is of the BS EN590 standard. The biodiesel was obtained from Olleco (UK) who state it is methyl esters from lipid sources produced as per EN 14214 standard. The same batch of the liquid fuels were used throughout.

Table 3.1. Selected properties of utilised fuels

Property	Diesel	Biodiesel	Methanol	Glycerol	Methane	Syngas
Approximate chemical formula	$C_{16}H_{34}$[a]	$C_{19}H_{36}O_2$[d]	CH_4O	$C_3H_8O_3$	CH_4	-
Lower Heating Value, LHV(MJ/kg)	43[b,c]	37[e]	20[f]	16[i,j]	50[m]	44
Density at 15^{0}C (kg/m^3)	850[a,b]	880[d]	795[f]	1261[i,k]	0.656[m]	0.671
Kinematic viscosity (mm^2/s) at 25^{0}C	3.50	6.75	0.59[g]	965.8[l,*]	-	-
Flash point (^{0}C)	52[b]	160[d]	11[h]	177[k]	-188	-
Stoichiometric fuel-air ratio (w/w)	0.070	0.080	0.155	0.191	0.058	0.068

[a-m] refer to Refs [62, 79, 119, 122, 220-228] in that order.
*the value is reported at 20^{0}C.

Derived from waste cooking oil, the biodiesel can be classified as second-generation type according to [60]. Methanol was obtained from Source Chemicals and had a purity of 99.85% and the vegetable glycerine (called “glycerol” in the rest of this work) was of 99.5% purity. It is important to note that the name “glycerol” applies only to the pure chemical compound propan-1,2,3-triol but given the stated purity of the vegetable glycerine utilised, it has been designated as glycerol in this work. Utilised methane was of CP grade and obtained from BOC Limited. The surrogate syngas (simply referred to as ‘syngas’ elsewhere) composition was 10% hydrogen, 10% carbon monoxide and 80% methane all by volume. Based on mole fraction composition, the density, lower heating value and stoichiometric fuel/air ratio for the syngas shown in Table 3.1 were determined. Relevant theory/formulae regarding the calculation of properties of syngas as well as power output and equivalence ratio determination is given in Appendix A.

The choice of diesel, biodiesel, methane and syngas are borne out of the fact that they are all, as highlighted in Chapter 2, practical gas turbine fuels of both renewable and non-renewable type. Testing with gas turbine relevant fuels elevates the work from being just academic to one having practical relevance. Also, experimenting with the different fuels and combinations under comparable operating conditions allows for common combustion characteristics and any fuel-specific trends to be identified. Further, the interest in glycerol stems from the real and present need for finding value-added uses for glycerol which as discussed in Section 2.6.1.2 is recently being

produced in surplus owing to the upscaling of biodiesel manufacture. Methanol, a major contaminant of crude glycerol obtained from biodiesel synthesis, was utilised primarily for glycerol viscosity reduction to enable pumping and atomisation as the same experimental rig as with the other fuels was utilised for its combustion. Also, by blending with methanol – a major contaminant of crude glycerol – the blend is representative of the crude product. Overall, the intention of the present work, both in terms of fuel choice and processing as well as injection strategy, is to be as representative as possible of real systems.

3.1.5 Experimental operating conditions

Except where otherwise noted, the fuel combinations and other operating conditions are as listed in Table 3.2 and Table 3.3. In all test cases, except where otherwise stated, the fuels were combined to deliver a total heat output (THO) of 15 kW based on the lower heating value (LHV) of the fuels as in Table 3.1. The ratio of liquid to gaseous fuel for the THO delivered was varied from 100/0 to 70/30 in steps of 10%. The fuel combinations were based on heat output share ratio. For instance, a 90/10 combination means that 90% of the overall heat output is set to be supplied by the liquid fuel and the balance obtained from the gaseous fuel. This method of splitting combusted fuels in multiphase burning was used in [229-231] and advantageous for this study because it means a fairly constant air flow rate for all test conditions (see Table 3.2 and Table 3.3). Consequently, cold flow characteristics are more or less maintained across the different test cases. Mathematically, the *THO* is calculated according to Eq. (3.2) in which $\dot{m}$ represents the mass flow rate of fuel and the subscripts l and g represent liquid and gas respectively.

Table 3.2. Operating conditions for diesel/gas flames

Liquid/gas fuel proportion	Diesel-methane/air flow rates (g/s)			Diesel-syngas/air flow rates (g/s)			Pressure drop across nozzle (MPa)
	Diesel	Methane	Air	Diesel	Syngas	Air	
100/0	0.35	0	7.19	0.35	0	7.19	0.85
90/10	0.32	0.03	7.21	0.32	0.03	7.19	0.70
80/20	0.28	0.06	7.23	0.28	0.07	7.19	0.54
70/30	0.25	0.09	7.25	0.25	0.10	7.19	0.35

Table 3.3. Operating conditions for biodiesel/gas flames

Liquid/gas fuel proportion	Biodiesel-methane/air flow rates (g/s)			Biodiesel-syngas/air flow rates (g/s)			Pressure drop across nozzle (MPa)
	Biodiesel	Methane	Air	Biodiesel	Syngas	Air	
100/0	0.41	0	7.28	0.41	0	7.28	0.85
90/10	0.37	0.03	7.29	0.37	0.03	7.27	0.75
80/20	0.33	0.06	7.30	0.33	0.07	7.26	0.60
70/30	0.29	0.09	7.31	0.29	0.10	7.25	0.38

The air flow rates listed in Table 3.2 and Table 3.3 represent air flows for combustion at a global equivalence ratio (ER) of 0.7. The air flow rate is obtained from Eq. (3.3) in which all symbols and subscripts have their previously defined or usual meanings and φ_{global} refers to global equivalence ratio.

$$THO = (LHV_l \times \dot{m}_l) + \left(LHV_g \times \dot{m}_g\right) \tag{3.2}$$

$$\dot{m}_{air} = \frac{\dot{m}_g \times AFR_{Stoic,g} + \dot{m}_l \times AFR_{Stoic,l}}{\varphi_{global}} \tag{3.3}$$

Given that a pressure atomiser was employed for diesel injection and that the pressure upstream of the MFC was maintained, reducing flow rates across the MFC resulted in decreasing pressure drop across the nozzle as shown in Table 3.2 and Table 3.3. As liquid flow rates reduce, the valve of the MFC progressively closes thereby increasing the fluid pressure loss. With the loss of pressure in this manner, trials conducted at flow rates corresponding to liquid/gas ratios below 70/30 were of very poor spray quality thereby adversely affecting combustion efficiency. Consequently, the chemiluminescence and emissions tests carried out with the liquid fuels listed in Table 3.2 and Table 3.3 were limited to the range stated therein.

3.2 Experimental methodology

3.2.1 Chemiluminescence

Because combustion environments are dangerous and restrictive, non-intrusive flame diagnostics techniques enjoy wide application in flame analysis since they yield fairly accurate results while providing safe access to the hostile environment. Chemiluminescent measurement is one of such techniques providing reliable information about the operating conditions of a combustion process without any external influence on the flame. Chemiluminescence refers to light emitted by molecules chemically created in an excited energy state when they undergo radiation to relax to a lower energy state [232]. Key chemiluminescent species in hydrocarbon-air flames are CH*, OH*, C_2* and CO_2* [233, 234].

The reactions producing these excited radicals involve intermediate combustion species. The characteristic wavelengths and the reactions leading to the formation of these species are shown in Table 3.4 which is reproduced from [235]. OH* species have been identified as being formed through three reactions listed as R1, R2 and R3 in Table 3.4. CH* species on the other hand are formed via the pathways shown by R4 and R5. The other two species, C_2* and CO_2* are formed via reactions R6 and R7 respectively.

Table 3.4. Reactions producing chemiluminescence radicals

Radical	Relevant reactions		Wavelength (nm)
OH*	R1:	$CH + O_2 \rightarrow CO + OH^*$	282.9, 308.9
	R2:	$H + O + M \rightarrow OH^* + M$	
	R3:	$OH + OH + H \rightarrow OH^* + H_2O$	
CH*	R4:	$C_2H + O_2 \rightarrow CO_2 + CH^*$	387.1, 431.4
	R5:	$C_2H + O \rightarrow CO + CH^*$	
C_2*	R6:	$CH_2 + C \rightarrow {C_2}^* + H_2$	513, 516.5
CO_2*	R7:	$CO + O + M \rightarrow {CO_2}^* + M$	350 - 600

Fig. 3.8 reproduced from [236] shows the chemiluminescence spectra for natural gas combustion in air with the CH* and C_2* species clearly prominent. Similar investigation has been carried out by other such studies [237] as well as industrial scale experiments using combustors from OEM's like Alstom (EV-10) [238] and Siemens (SGT-700/800) [239]. It should be noted, though, that the excess energy contained in an excited molecule is not wholly removed by chemiluminescence. Inter-molecular reaction or a non-reactive collision (called quenching collision since it occurs without emission of light) may lead to energy loss in an excited species. However, the spontaneous emission of light that is out of proportion to that expected from thermal emission has been utilised as a 'signature' for flames. Commonly, and as demonstrated in Fig. 3.8, a relationship between equivalence ratio and radiation intensity associated with one or several of the key radicals is established and used in combustor flame monitoring [240, 241].

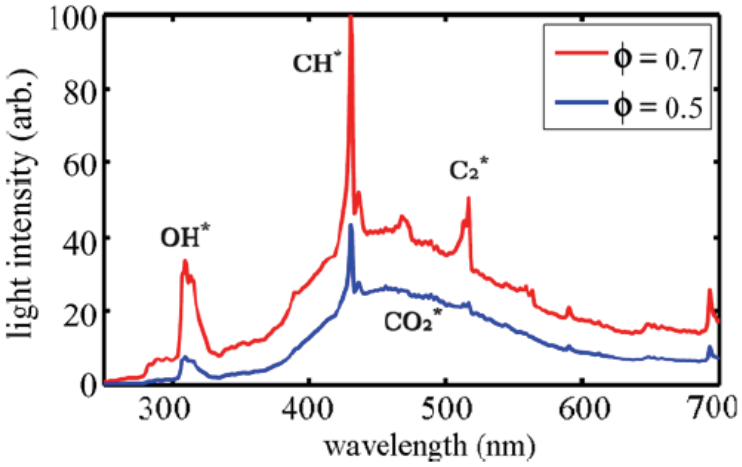

Fig. 3.8. Typical chemiluminecsence spectra of natural gas-air flame at different equivalence ratios (ϕ). Reproduced from [236].

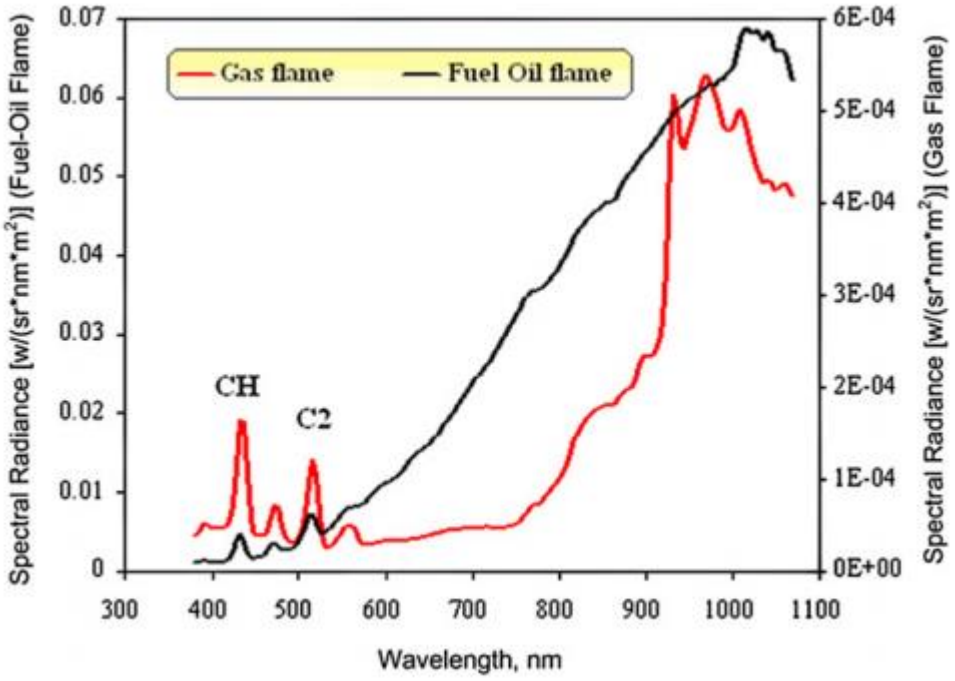

Fig. 3.9. Emission spectra of oil and gas flames. Reproduced from [235]

The species targeted in this study - C_2* and CH* - were selected because not only are they good indicators of heat release rate in hydrocarbon flames but also their emission spectra are prominent in gas/oil fuelled combustors with clearly identifiable peaks at the selected bandwidths [119, 234, 235, 242, 243]. A spectra for gas and oil flames is pictured in Fig. 3.9.

The intensity of light emitted via chemiluminescence by species like C_2* and CH* can be accurately detected if broadband light emission is filtered out. Accordingly, for CH* chemiluminescence intensity measurement, a bandpass filter centered at 430 *nm* was utilised, and for C_2*, a filter centred at 515 *nm* was used.

3.2.1.1 Chemiluminescence data interpretation and analysis

As mentioned and justified in Section 3.1.3.1, 250 images per set were captured using the LaVision imaging set-up described in the same section. DaVis 7.0 software provided not just an interface between the imaging system and a computer but also provided required image processing capability. Temporal averaging, background correction and cropping of the raw chemiluminescence images were done using DaVis 7.0. Preliminary processing and presentation of chemiluminescence intensity images

often involve these methods [244, 245]. Further, chemiluminescence, being a line-of-sight technique, includes radiation from both in front and behind the focal length of the camera lens [246]. The line-of-sight images require reconstruction in order to extract an exact spatial distribution of the radicals. Different tomographic techniques such as Abel deconvolution, onion peeling and filtered back projection methods have been developed for this purpose [247]. Among these, the Abel deconvolution technique using the Abel inversion method provides a concise and exact solution for two-dimensional rendition of radical distributions in an axisymmetric flame [247]. The Abel inversion of chemiluminescence images in this work was adapted from a MATLAB code developed by Runyon [82] based on an open source MATLAB algorithm by Killer [248] which in turn was based on an Abel inversion method described by Pretzler [249]. Runyon [82] explained that "this Abel inversion is based on a Fourier-series-like expansion which projects the radial pixel intensity distribution function onto a theoretical 2-D plane through cosine expansions". As earlier mentioned, a key assumption in the Abel inversion method is that the flame is symmetric about a central axis. The atomiser and swirler used in the experiments imparts a conical shape on the flame for the most part and only the temporally averaged image is used for Abel inversion therefore the assumption of an axisymmetric flame is deemed valid in this work. A sample of the Abel deconvolution code used in this work is shown in Appendix B.

In order to compare the chemiluminescence intensity levels of single phase and different multiphase fuel combustion tests, the concept of integral intensity was utilised. In this work, integral intensity refers to the pixel-wise sum of all chemiluminescence intensity values across a temporally averaged and background-corrected image. Related to this and adapted from [237], the magnitude of signal intensity fluctuation from frame to frame has also been used to compare different operating points in the context of flame stability.

3.3 Numerical tools and methods

3.3.1 Chemical kinetics modelling

To provide a computational idea of adiabatic flame temperature and volumetric heat release rate of the different experimental tests, CHEMKIN-PRO software was utilised

[250]. The equilibrium model was used and solutions were based on an adaptive grid of 1000 points in all cases. The chemical kinetics mechanism used for diesel fuel modelling was created by Lawrence Livermore National Laboratory [251]. The reaction mechanism comprises of 323 chemical species with n-C_7H_{16} selected as diesel surrogate. The biodiesel mechanism used was developed by the CRECK modelling group [252] and comprises of 177 species and 2904 reactions. Although biodiesel combustion kinetics involve several hundred to thousands of species, the reduced mechanism of Ranzi *et al.* [252] achieves reasonable simulation accuracy of main combustion properties [253].

3.3.2 Turbulent flow simulation

Modelling swirling or rotating flows is challenging because they are highly turbulent and associated with unsteady motion in which there is a wide fluctuation in both time and space of transported quantities like mass and momentum. The range of length and time scales involved in practical turbulent flows like swirl combustion, especially given its chaotic and transient nature, makes it impractical to resolve all the relevant flow scales using direct numerical solutions [254].

As a result, two approaches of modelling the behaviour of turbulent flows are mainly used in engine studies: (1) Scale resolving simulations like the Large Eddy Simulation (LES). In LES, the largest flow structures (eddies) are resolved in part of the computational domain – capturing local unsteadiness in that region of the flow – while eddies smaller than the mesh are modelled and (2) Reynolds Averaged Navier-Stokes simulation (RANS) which models all turbulence offering a steady-state simulation of turbulent flows. Despite the potential of yielding less accurate solutions than LES, RANS models – because of the smaller computational cost and the fact that most practical flow applications demand only time-averaged solutions – are favoured [255]. Som *et al.* [256] showed that the prediction accuracy of global spray characteristics like liquid and vapour penetration length, mixture fraction and flame lift-off length by LES is not very dissimilar from RANS models when compared to similar experimental data from Sandia National Laboratories.

In this work, the finite-volume based commercial CFD package, ANSYS Fluent was utilised to simulate swirl reacting and non-reacting flows. It incorporates models for

spray injection, atomisation and break up, turbulence and droplet collision and coalescence whilst enabling atomiser design in terms of injection-property specifications like fuel flow rate, orifice diameter, upstream pressure, and spray half angle. In view of the foregoing paragraph, a RANS model (realizable $k-\varepsilon$) was employed to describe the flow field. The governing equations were solved implicitly using the finite volume method in which a second order scheme was used for spatial discretization.

3.3.2.1 Governing equations

For all flows, Ansys Fluent solves conservation equations for mass and momentum. As the current calculation involves species mixing or reaction and heat transfer, the species conservation equation and conservation equation for energy are also solved. Further, since the non-premixed combustion model was used, the conservation equation for mixture fraction and its variance are solved as well and transport equations are also solved since the flow is turbulent.

The Reynolds Averaged Navier-Stokes equations of motion are written in conservation form as follows. All equations in this section are from the Ansys Fluent theory guide.

Continuity equation:

$$\frac{\partial \rho}{\partial t}+\frac{\partial}{\partial x_i}(\rho u_i)=\dot{\rho}^s \tag{3.4}$$

Conservation of momentum equation:

$$\frac{\partial}{\partial t}(\rho u_j)+\frac{\partial}{\partial x_i}(\rho u_i u_j)=\frac{\partial}{\partial x_i}\left[\mu\left(\frac{\partial u_i}{\partial x_j}+\frac{\partial u_j}{\partial x_i}\right)\right]-\frac{\partial p}{\partial x_j}+\rho g_i+\dot{F}^s+\frac{\partial}{\partial x_j}(\rho\overline{u_i{}'u_j{}'}) \tag{3.5}$$

Conservation of energy equation:

$$\frac{\partial}{\partial t}(\rho h_0) + \frac{\partial}{\partial x_i}(\rho u_i h_0) = \frac{\partial}{\partial x_i}\frac{k_m + k_t}{c_p}\left[\frac{\partial(h_0 - u^2/2)}{\partial x_i} - \sum_j h_j \frac{\partial X_j}{\partial x_i}\right] - \frac{\partial}{\partial x_i}\sum_j h_j J_{ji} + \frac{\partial p}{\partial t} - \frac{\partial}{\partial x_i}(\tau_{ik} u_k) + S_h + \dot{Q}^s \quad (3.6)$$

Conservation of species equation

$$\frac{\partial}{\partial t}(\rho Y_i) + \frac{\partial}{\partial x_i}(\rho u_i Y_i) = \frac{\partial}{\partial x_i} J_i + R_i + \dot{\rho}^s \delta_i \quad (3.7)$$

The net source of chemical species i due to the reaction is computed as the sum of the Arrhenius reaction sources over the N_R reactions in which the species participate:

$$R_i = M_{w,i} \sum_{r=1}^{N_R} R_{i,r} \quad (3.8)$$

For the r-th reaction written generally as:

$$\sum_{i=1}^{N} \nu'_{i,r}\ M_i \underset{k_{b,r}}{\overset{k_{f,r}}{\Leftrightarrow}} \sum_{i=1}^{N} \nu''_{i,r}\ M_i \quad (3.9)$$

For a non-reversible reaction, the molar rate of formation and destruction of species i in reaction r is calculated by the equation below where Γ presents the net effect of third bodies on the reaction rate.

$$R_{i,r} = \Gamma\left(\nu''_{i,r} - \nu'_{i,r}\right).\left[k_{f,r} \prod_{j=1}^{N} \{C_{j,r}\}^{\eta'_{j,r} + \eta''_{j,r}}\right] \quad (3.10)$$

Γ is defined by:

$$\Gamma = \sum_{j}^{N_r} \gamma_{j,r} C_j \tag{3.11}$$

For liquid fuel combustion, the Discrete Phase Model (DPM), which calculates the trajectories of motion for individual particles was utilised. The model predicts the particle trajectories of the discrete phase by integrating the transport equation written in Lagrange form (for x-direction):

$$\frac{du_p}{dt} = F_D(u - u_p) + \frac{g_x(\rho_p - \rho)}{\rho_p} + F_x \tag{3.12}$$

Where F_x represents additional forces like the "virtual mass" force – the force required to accelerate the fluid surrounding the particle and given by:

$$F_x = \frac{1}{2}\frac{\rho}{\rho_p}\frac{d}{dt}(u - u_p) \tag{3.13}$$

The term $F_D(u - u_p)$ on the other hand is the drag force per unit mass of the particle and is given by:

$$F_D = \frac{18\mu}{\rho_p {d_p}^2}\frac{C_D Re}{24} \tag{3.14}$$

Turbulent dispersion of the DPM is modelled by stochastic tracking (discrete random walk) in which the interaction of a particle with a succession of discrete fluid phase turbulent eddies is simulated. It accounts for local variations in flow properties and recommended over the alternative – cloud tracking model – for use in complex geometry. Fluent predicts the trajectories of the turbulent flow using the mean fluid phase velocity, $\bar{u}$, in the trajectory equation (Eq. 3.12). Integrating this equation in time yields the particle velocity at each point along its trajectory, with the trajectory itself predicted by:

$$\frac{dx}{dt} = u_p \tag{3.15}$$

Equations similar to (Eq. 3.12) and the above are solved in each coordinate direction to predict the trajectories of the discrete phase. Assuming that the term with the body force stays constant over each small interval of time, and linearizing any other forces acting on the particle, the trajectory equation can be simplified as:

$$\frac{du_p}{dt} = \frac{1}{\tau_p}(u - u_p) \tag{3.16}$$

Liquid spray droplet size distribution is represented using the Rosin-Rammler expression with the entire range of sizes divided into an adequate number of discrete intervals; each represented by a mean diameter for which trajectory calculations are done. The mass fraction of droplets of diameter greater than d is given by

$$Y_d = e^{-(d/\bar{d})^n} \tag{3.17}$$

3.3.2.2 Model boundary conditions

Calculations were performed for four different compositions of diesel/methane as in Table 3.2. A finite-volume based commercial CFD code – Ansys Fluent 2019 R1 – was employed for the study. The combustion simulation was carried out in Ansys Fluent with the injections settings of the discrete phase model enabling atomiser design in terms of injection-property specifications like fuel flow rate, orifice diameter, upstream pressure, and spray half angle; the selected atomiser was pressure-swirl type and the number of streams tracked was 200. Also, as previously mentioned, the turbulent dispersion of the droplets is modelled by stochastic tracking using the discrete random walk model with a random eddy lifetime. The liquid fuel was designated as the primary fuel stream and methane, the secondary fuel stream.

The boundary conditions: a mass flow inlet and a pressure outlet were appropriately defined as in Table 3.5. Monitors of mass-weighted averages of the H_2O and CO_2 at the combustor outlet were set and together with the discrete phase mass in domain and evaporated mass, good convergence was determined.

Table 3.5. Boundary conditions

Oxidiser	
Type	Air
Constituents	21% O_2; 79% N_2
Inlet temperature	300K
Inlet pressure	1 atm
Flow rate	variable
Liquid Fuel	
Type	Diesel
Formula	$C_{10}H_{22}$
Inlet temperature	300 K
Upstream pressure	variable
Flow rate	variable
Gaseous Fuel	
Type	Methane
Formula	CH_4
Inlet temperature	300 K
Upstream pressure	1 atm
Flow rate	variable
Outlet	
Type	Pressure outlet
Pressure	0 atm

3.4 Chapter summary

The materials used in the experiments reported in this work were highlighted in this Chapter. This included a description of the burner system; the utilised fuels and their properties; the fuel injection methods; and the fuel combinations. The measurements taken and the methods used in optimising, obtaining and processing data from the experiments were also explicated. In addition to the experimental methodology, the numerical methods and its underlying principles have been discussed in this Chapter.

4

DUAL FUEL COMBUSTION MODELLING

In this Chapter, numerical modelling of the combustion domain including non-reacting and reacting flow behaviour is investigated using the commercial CFD software Ansys Fluent.

4.1 Introduction

Preliminary experiments were carried out on the combustor to determine operating conditions that are practicable. The working operating conditions are detailed in Chapter 3. In this Chapter, the combustion of one of the fuel combinations – diesel/methane – has been modelled using Ansys Fluent 2019 R1 with the combustion domain being a full-size model of the actual burner. The axial swirler which impacts the air/gas fuel through it is incorporated into the calculation as is the experimental liquid fuel injection strategy – pressure-swirl atomisation.

The aim is to model the burner operation particularly in terms of non-reacting flow dynamics – the gas flow pattern and how operating conditions affect it as well as the diesel spray characteristics as operating conditions change. Over and above these, reacting flow parameters like temperature distribution and emissions characteristics were numerically investigated. Together, these offer an insight into expected conditions that may not be evident in practice.

4.2 Mesh Independence Study

The geometry forming the computation domain, Fig. 4.1 (a), was designed using Solidworks 2019. The numerical modelling was carried out on a student version of Ansys Fluent. This version limits the number of cells in a mesh to 512, 000.

As such, three different meshes were generated with 381 081, 424 719 and 506 856 cells. As shown in Fig. 4.1, care was taken to refine the mesh in the area containing the swirler in order to better capture flow behaviour in that region.

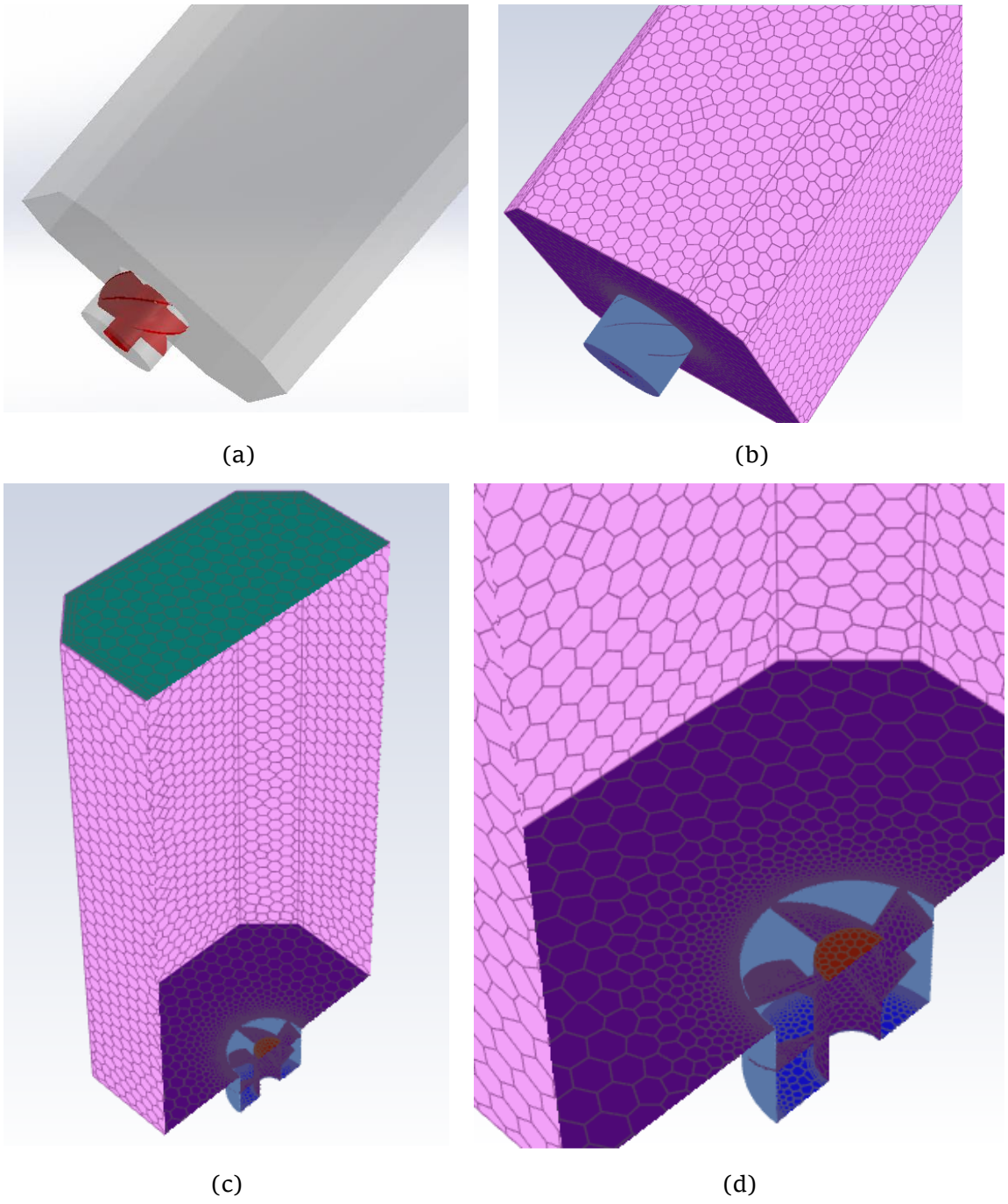

Fig. 4.1. (a) Solidworks CAD model of burner showing swirler (b, c, d) meshing with Fluent

Ansys Fluent's task-based workflow for watertight geometries was utilised for meshing using the following steps: CAD import, surface mesh, geometry description, flow-volume extraction and then volume meshing. In each of the three mesh sizes, grid size was refined in the area containing the swirler (see Fig. 4.1(d)) to better capture fluid dynamics there and the grid quality was over 0.25 in all cases.

Reacting flow simulation was carried out on the three models to determine the extent to which the computational solution depends on the number of cells in the mesh. The total temperature distribution along the axis of the burner from the nozzle orifice point to the centre of the combustor outlet was used as the indicator. The calculation result, shown in Fig. 4.2, reveals that there is hardly any difference in burner axial temperature distribution as the number of cells in the grid varied. The mesh with 506 856 elements was ultimately used for calculations.

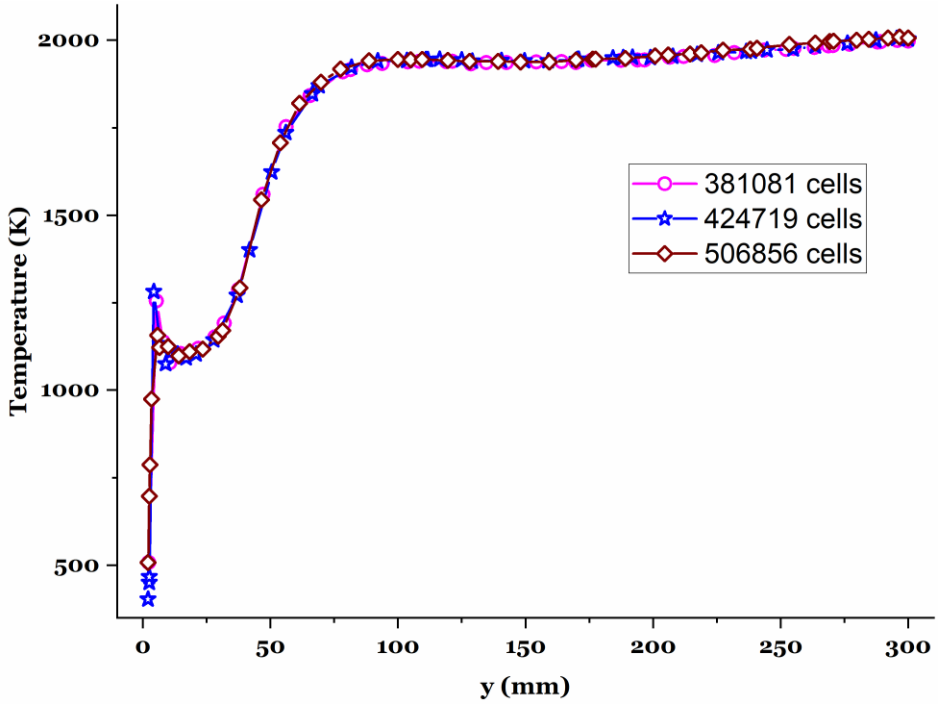

Fig. 4.2. Total temperature distribution along combustor axis

4.3 Calculation convergence criteria

Residual monitors were not used to monitor convergence. Instead, DPM and surface report definitions were used as recommended by [257]. DPM report definition was created to track the total mass present in the domain and the mass of the evaporated droplets. Also, the mass weighted average of H_2O and CO_2 on the outlet of the combustor was plotted as a surface report definition. From the plots in Fig. 4.3, which are the convergence history of the different parameters for the 100/0 case, it can be concluded that the solution is converged because the spray and flow products tracked are constant. Similar plots are available in Appendix C for the other test cases.

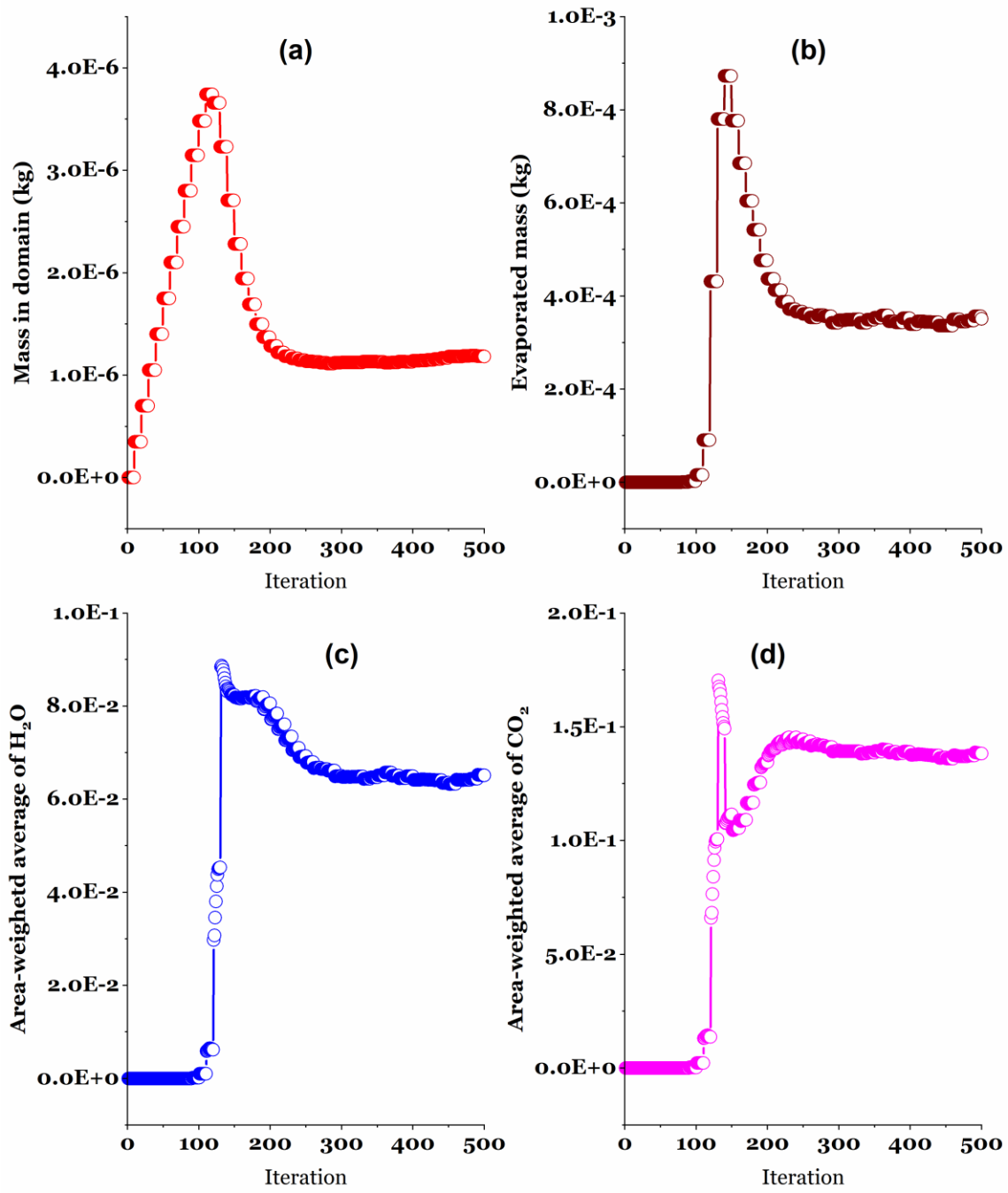

Fig. 4.3. Convergence history of (a) total mass in domain (b) evaporated mass (c) area-weighted average of H_2O and (d) area-weighted average of CO_2

4.4 Analysis of gas flow through swirler

A key component of the gas turbine combustor utilised for the experimental studies is the 5-vane axial swirler that is fitted with its top surface flush with the nozzle exit plane and dump plane of the burner. The swirler imparts a spiralling pattern to the air flow as it passes through the swirler as seen in Fig. 4.4 which are the velocity streamlines as seen from (a) an isometric perspective (b) the burner outlet and (c) a plane clipped midway through the burner and normal to its longitudinal axis.

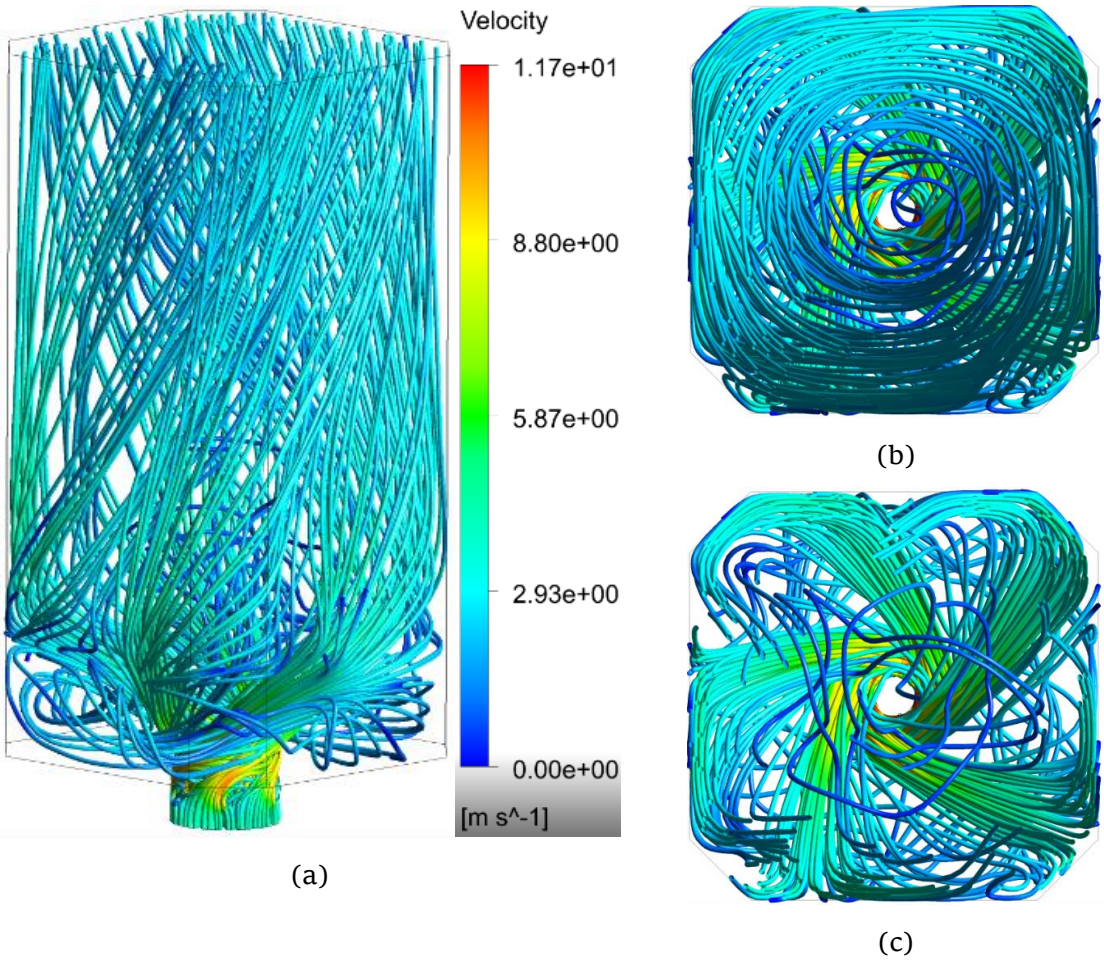

Fig. 4.4. Effect of swirler on air flow through it

Fig. 4.4 (a) shows that the flow gets twisted as it exits the swirler onto the dump plane of the combustor. The spiralling of the flow is clearly observable from the top view (c). In addition, (a) shows that around the bottom edges of the burner, relatively low-velocity random flow circulation occurs. Also, this is noticeable in and around the centre of the burner in the clipped plane (c). The creation of flow recirculation zones in the combustion domain as a result of the swirling flow is the essence of utilising a swirler in gas turbine combustion. These zones enable a recirculation of the hot combustion products so that the incoming fuel/air mixture can be ignited, anchored and sustained. The velocity vector contours shown in Fig. 4.5, for the different LGRs used in the experiment and on a plane along the longitudinal axis of the burner, reveal that air flow through the swirler results not only in the creation of a central recirculation zone but also an outer recirculation zone at the edges of the burner.

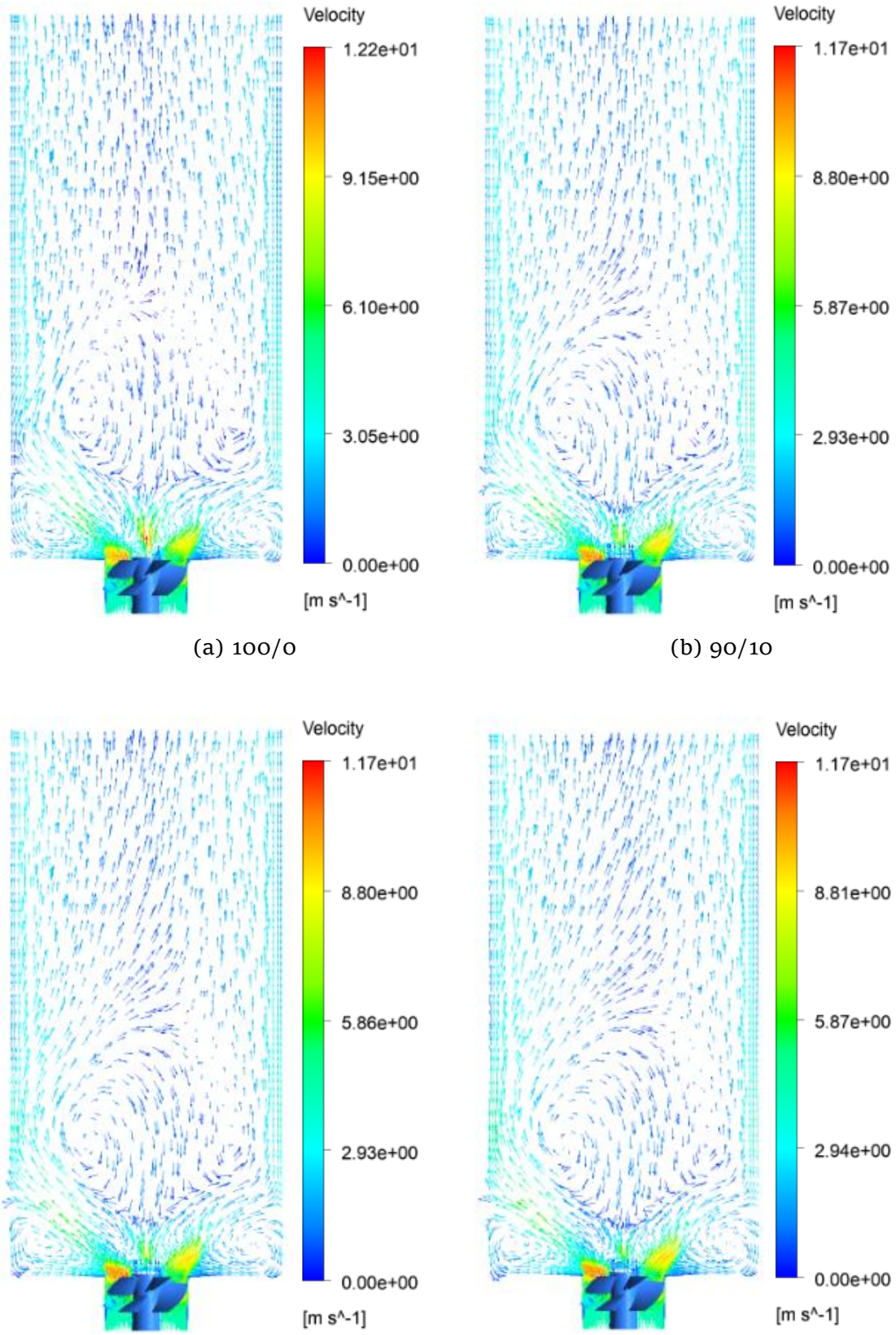

(a) 100/0 (b) 90/10

(c) 80/20 (d) 70/30

Fig. 4.5. Velocity contours at the flow rates for the different experimental LGRs

One-equation turbulence models will be inadequate for the non-equilibrium turbulent flow conditions in these recirculation zones thereby further supporting the use of two-equation models for this study. It is important that the flow dynamics across the test cases be approximately maintained if comparisons among the cases are to be deemed valid. This appears to be the case for all the experimental instances given the not-too-different fluid flow rates involved. The range of velocities in all of the four instances stays more or less the same. It is clear from Fig. 4.6 that as the fluid mass flow rate increases so does the velocities in all its components. Therefore, if as is the case for the experiments, the goal is to maintain non-reacting flow conditions in order to ensure that any differences in combustion results are due to LGR variation, the overall flow rate in through the swirler cannot vary greatly.

The trend in the graph of Fig. 4.6 is reflected in the vector contours of Fig. 4.7 which depicts the flow circulation at one flow rate and at 1.5 times as well as twice that flowrate. Also, the size of the recirculation zone changes considerably as air flow rates alter. This is shown in Fig. 4.7 which is the vector contours at different flow rates.

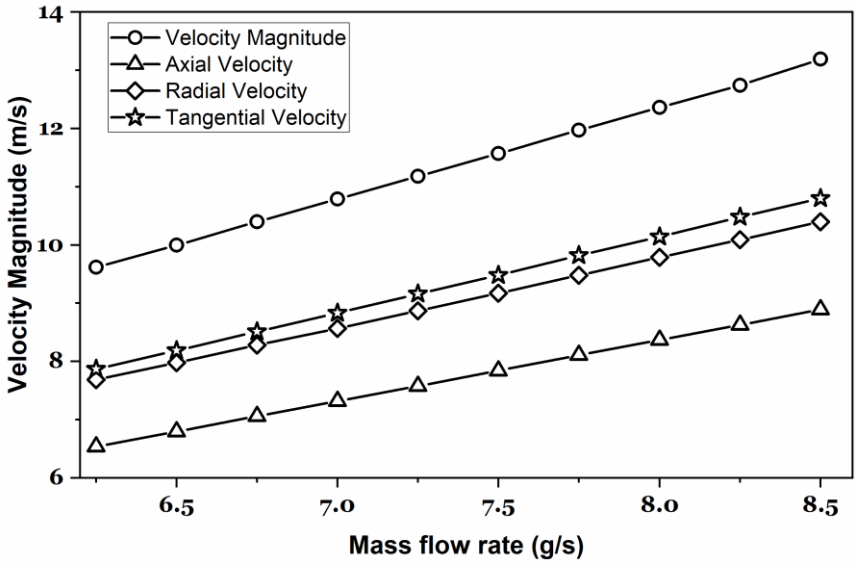

Fig. 4.6. Effect of mass follow rate through swirler on different velocity components.

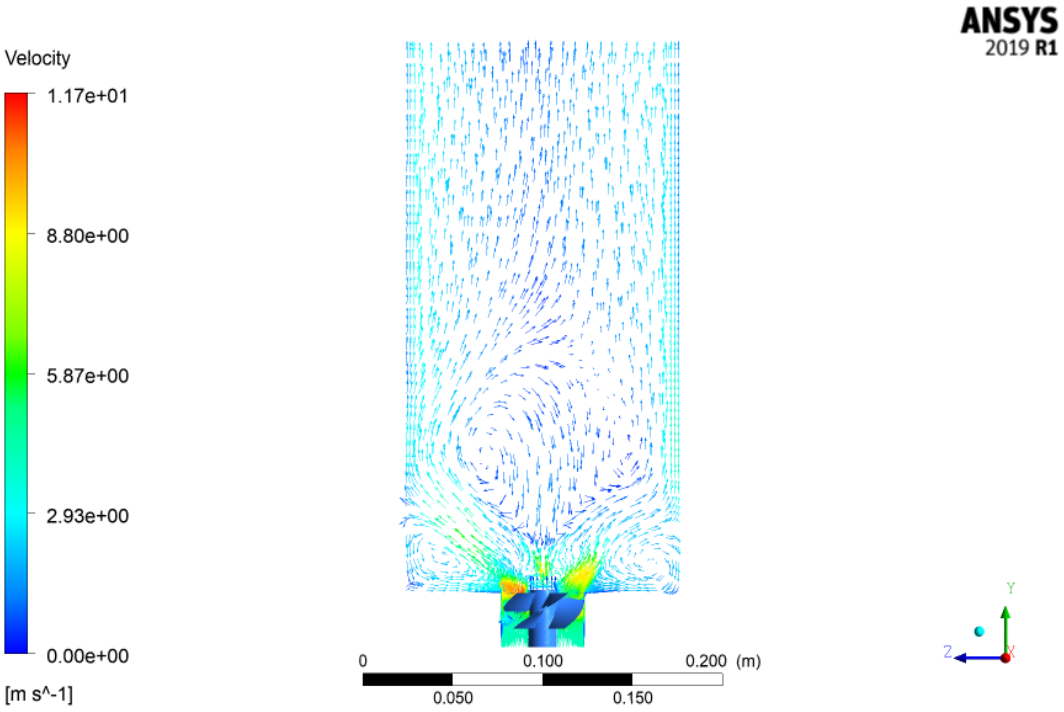

90/10 flowrate at experimental condition

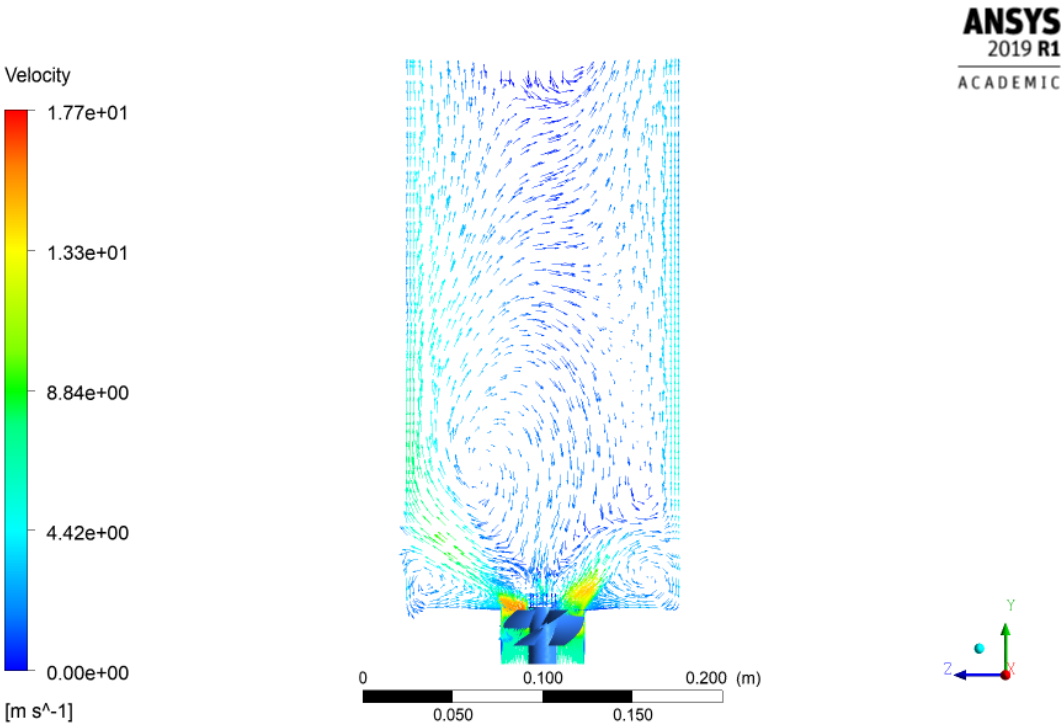

90/10 at 1.5 times the air flowrate

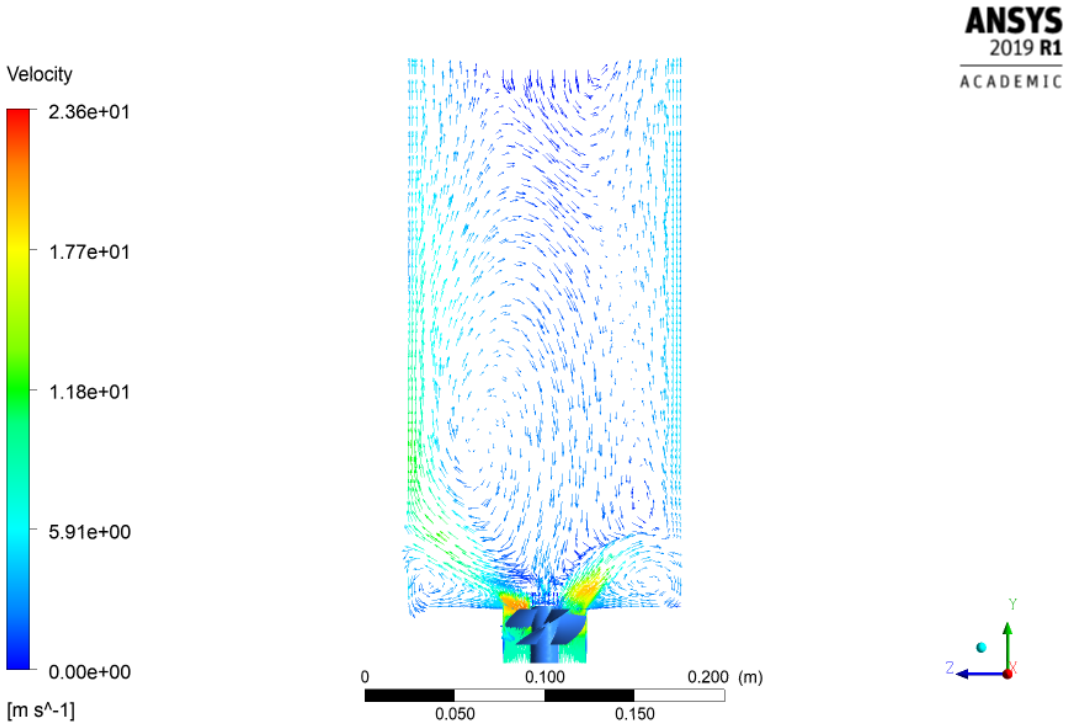

90/10 at twice the air flowrate

Fig. 4.7. Velocity contours at different flow rates.

4.5 Liquid fuel spray characteristics

The behaviour of the evaporating diesel spray was modelled taking into account the changes in flow rate and pressure drop as LGR varies. To predict the behaviour of the diesel spray as it exits the pressure-swirl nozzle, Ansys Fluent's discrete phase model is used including, as highlighted earlier, a secondary model for spray break-up simulation. The interest here is mainly the trajectory and flow characteristics of the spray droplets as it exits the atomiser. The discrete phase (diesel spray) was modelled as being dispersed in the continuous phase and the coupling between the two phases and its impact on the discrete phase behaviour was included.

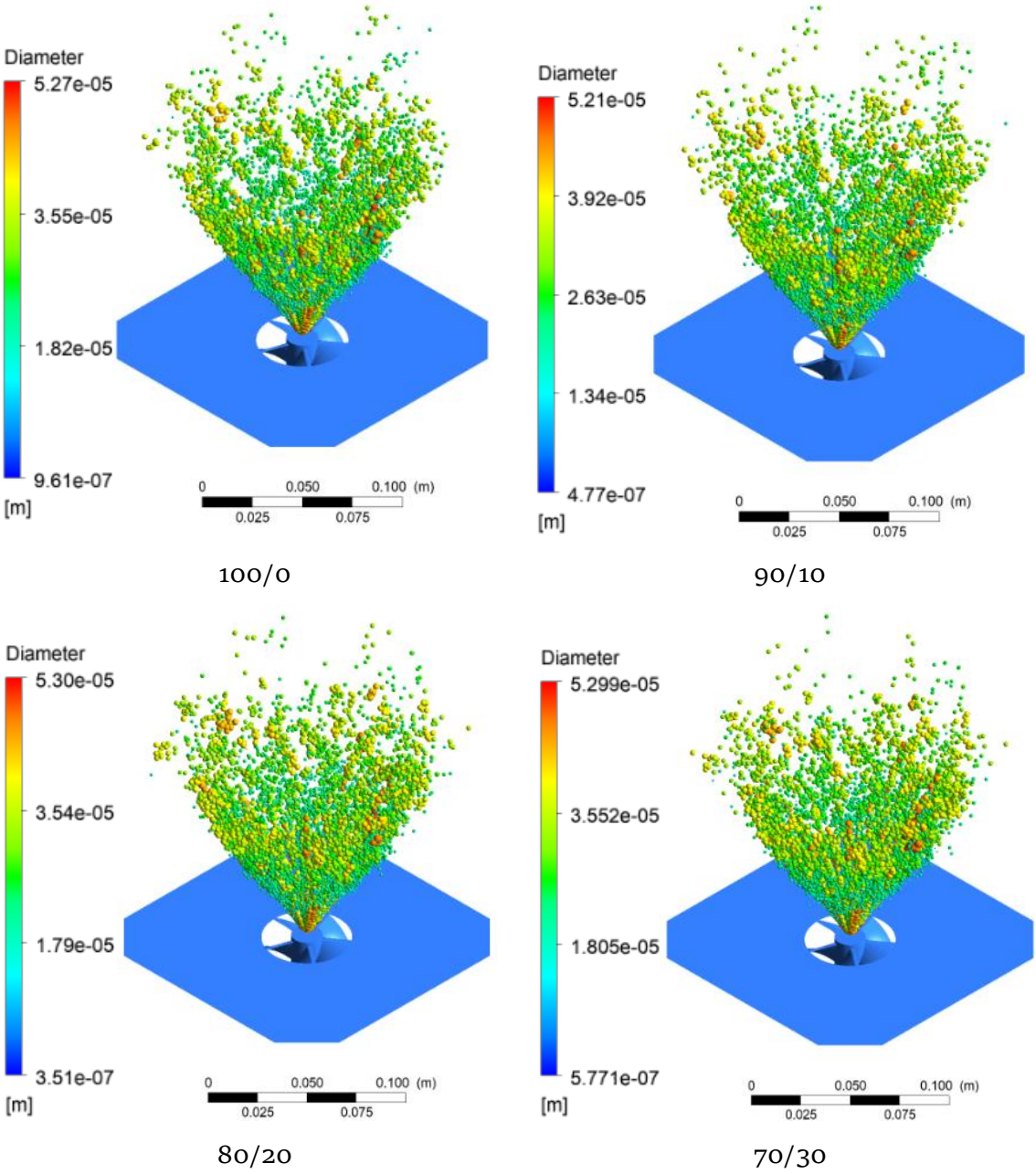

Fig. 4.8. Diesel spray droplet diameter symbolised by balls sized by the droplet diameter.

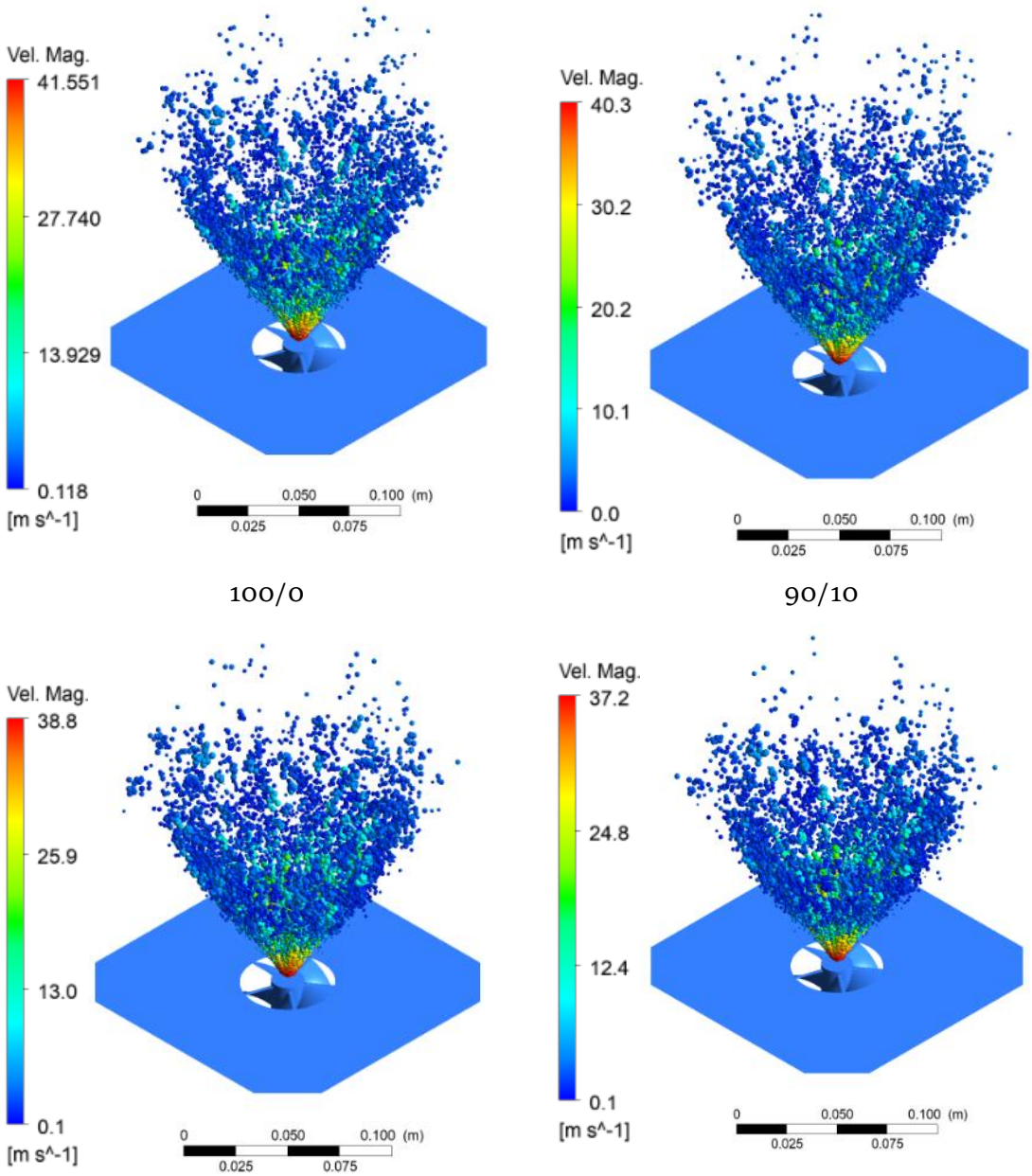

Fig. 4.9. Diesel spray droplet velocity magnitude symbolised by balls sized by the droplet diameter.

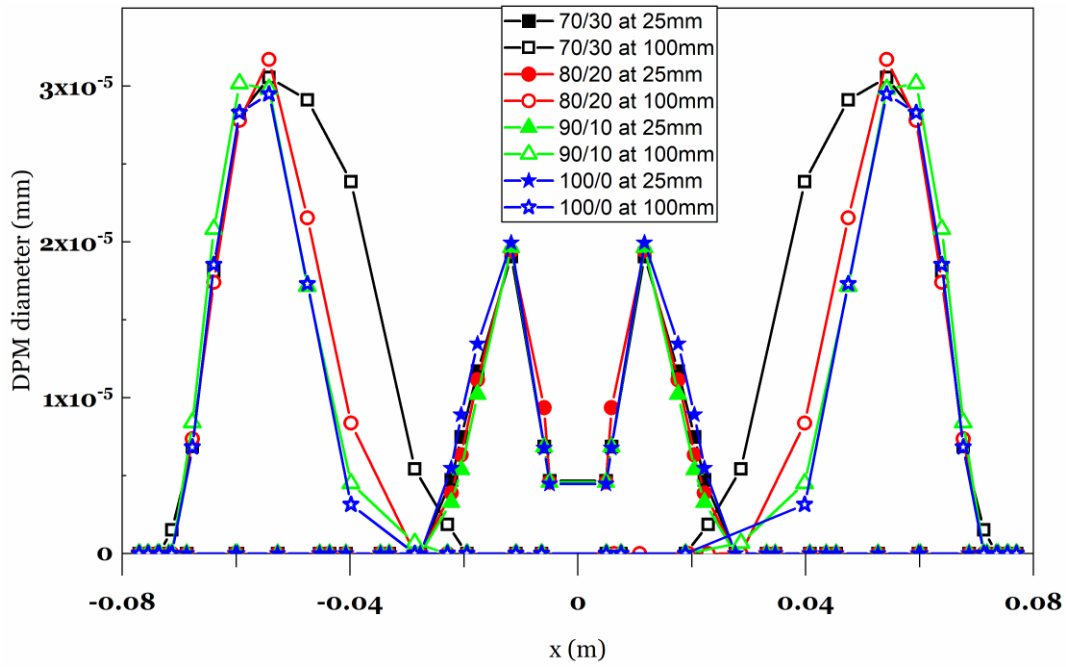

Fig. 4.10. Spatial distribution of diesel spray droplets at different test conditions

The diesel spray droplet size and velocity distribution are shown in Fig. 4.8 and Fig. 4.9 respectively. The spray is formed around a 60° cone with the vertex at the tip of the nozzle. This dimension is selected for the simulation as it is the same as the nozzle angle used for experimental studies. As expected, the spray droplet velocities are highest at the nozzle exit plane and are observed to drop considerably further downstream. The droplet diameters, on the other hand, appear to be more uniformly distributed in the spray across all test conditions. As shown in Fig. 4.10, at a plane 25 mm from the nozzle exit plane, diesel spray diameter distribution is similar from 100/0 to 70/30 diesel flowrates. The droplets are concentrated around an approximately 20 mm radius from the nozzle orifice. However, as observed in Fig. 4.10, further downstream of the orifice, at a plane 100 mm from it, the spatial distribution of the spray becomes different as flowrates alter. While the outer extent is similar in all cases, the hollow centre without any droplets gets wider as flowrates increase. Comparing 100/0 with 70/30, it can be seen that droplets in the latter occupy a wider area than in the former with the difference occurring in the inner boundary of the spray.

Additional spray characteristics are graphed in Fig. 4.11. These include the spray droplet evaporation/devolatization rate, D32 – the representative diameter of the

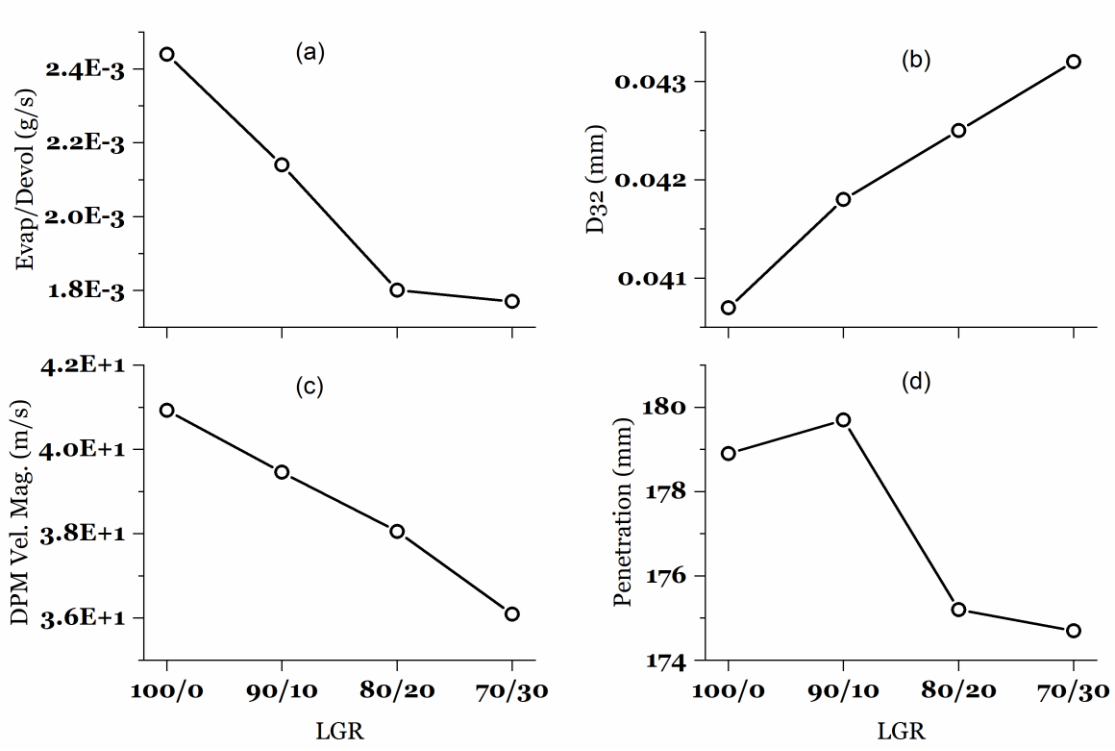

Fig. 4.11. Spray droplet characteristics (a) evaporation/devolatisation rate (b) D32 (c) DPM velocity magnitude (d) penetration.

spray, the spray maximum velocity magnitude and the maximum penetration. The values plotted are the average values for the spray. The trend of spray evaporation/devolatization rate show that despite the previously noted distribution over an increasingly larger area as LGR decrease, the droplets have a faster evaporation rate as LGR increases. This is probably due to a combination of the other plotted factors. Take the D32, it is observed to steadily increase as conditions change from 100/0 to 70/30. As the representative diameter of diesel droplets increase so does the difficulty in evaporation. Also, at higher LGRs, droplets enjoy deeper penetration possibly driven by the associated higher initial velocities.

4.6 Temperature distribution

One key evidence of combustion reactions is a change in flow temperature. The temperature contours of combustion of diesel and different compositions of diesel/methane is shown in Fig. 4.12. The plane on which the contours are shown is one that is along the centre of the longitudinal axis of the burner. The contours show that with addition of methane to the reaction, a region of low temperature around the

nozzle exit plane develops. It would seem that it is in this region that the ultra-lean methane component of the fuel burns. This combustion regime provides heat in addition to that from recirculation currents to support the combustion of diesel further downstream.

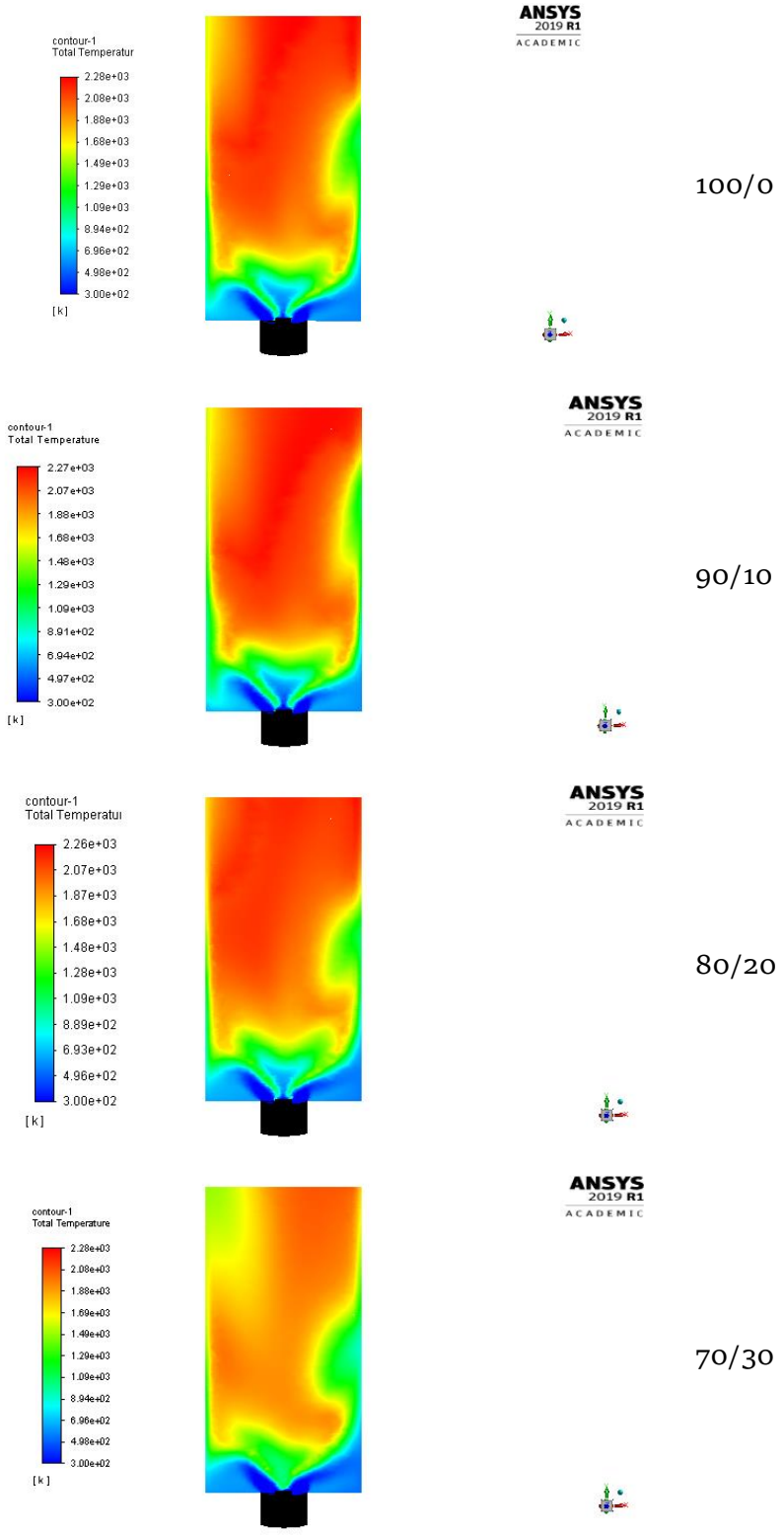

Fig. 4.12. Temperature contours of diesel/methane flames at different compositions

The temperature contours are a picture of the temperature distribution in the tested cases painted along a single plane across the longitudinal axis of the combustor. Whereas it offers a good representation of the reaction zone along that plane, it has to be borne in mind that the combustion of diesel and diesel/methane blends is a three-dimensional turbulent process hence the non-uniform temperature distribution particularly at the edges of the plane.

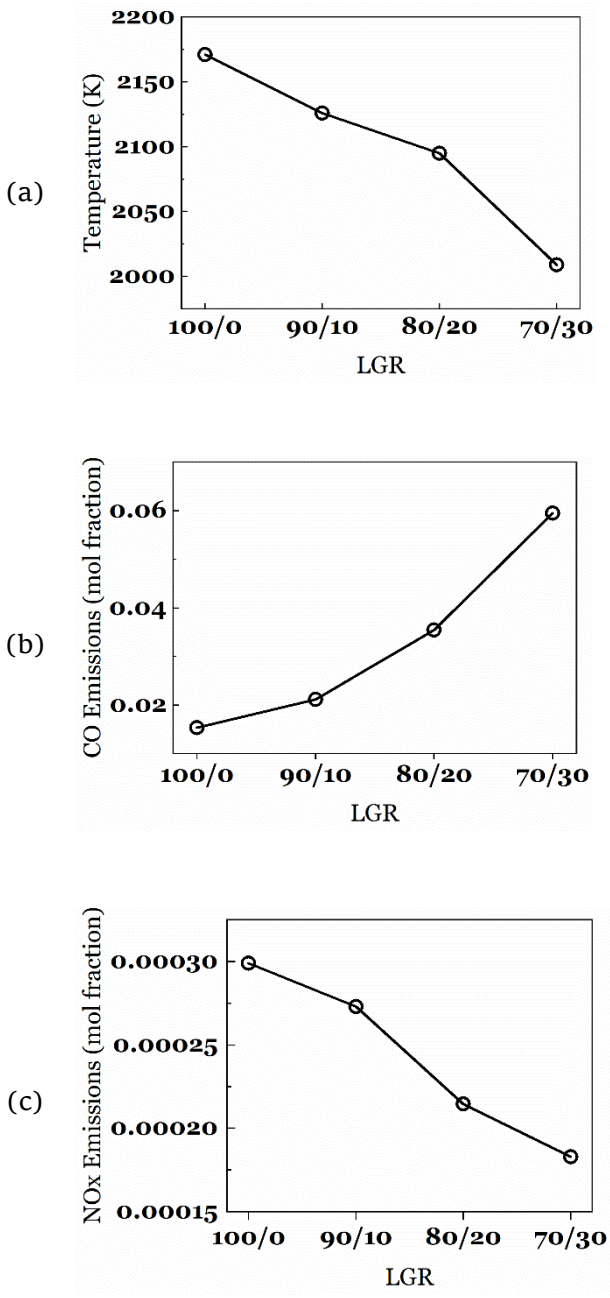

Fig. 4.13. Mass-weighted average of (a) temperature (b) CO emissions and (c) NOx emissions at combustor outlet plane.

Comparing the temperature, or indeed pollutant emissions, at a single point may thus be misleading. Consequently, the mass-weighted averages at the combustor outlet of temperature, NO_X and CO emissions has been utilised for the sake of comparison. The mass weighted averages of these parameters at the combustor outlet is shown in Fig. 4.13.

Fig. 4.13 shows that the temperature and NO_X emissions data follow the same trend – decreasing as LGR decreases. The temperature trend is consistent with the previous observation regarding evaporation rate, spray penetration and spray SMD values. The observed trend in these parameters is such that they, individually or when combined, cause flame temperature trend shown. The flame temperature in turn determines NO_X emissions especially as the thermal NO_X model dominates in the simulation. As for CO emissions: diesel spray droplets increase in size as gas fraction increases leading to a lower evaporation rate. As evaporation timescales increase, combustion becomes increasingly inefficient leading to a rising CO emissions trend. If only trends are considered and not the absolute values of these emissions, there is good agreement of the computer simulations with experimental studies for diesel/methane combustion which are discussed further in Chapter 5.

4.7 Chapter summary

This chapter set out to numerically model the combustor utilised in the experiments and to simulate experimental conditions. The main information derived from the simulation were: swirler impact on gas flow through it; liquid spray characteristics and temperature distribution in the burner as well as prediction of regulated emissions.

Take the effect of the swirler on air flow. It was observed that the swirler imparts a spiralling pattern to the flow as it passes through it creating not only a central but also outer recirculation zones. In line with the theory, these zones serve to anchor and stabilise the flame by causing flow recirculation currents that entrain hot combustion products. It was also noted that the mass flow rate through the swirler affects the magnitude of the flow velocity components – increasing mass flowrates causes increased axial, radial and tangential velocities. It is therefore important, if non-

reacting flow dynamics is to be maintained, to keep overall flow rates through the swirler fairly constant. This knowledge informed the operational conditions selected for the subsequent experiment – keeping air flow rates fairly unaltered whilst maintaining power and equivalence ratio.

As for the liquid fuel spray, it was observed that as operating conditions change, spray droplet diameter and the spatial distribution of the droplets are altered. So does other parameters like spray velocity, evaporation rate and penetration. Of these, spray droplet size and evaporation are key in combustion. An increase in the representative diameter of droplets – D32 – was observed with decreasing LGR and, unsurprisingly, this was accompanied by a steady decrement in spray evaporation rate.

One key feature from the temperature contours plotted along a plane on the longitudinal axis of the burner is that with the addition of methane to the combusting diesel spray, a low temperature combustion regime develops just downstream of the nozzle exit plane likely dominated by ultra-lean methane burn. The mass-weighted averages at the combustor outlet of reaction temperature reveals that with the addition of methane, temperatures drop. Also, mass-weighted averages of CO and NO_X emissions show an increase in the former and a decline in the latter as LGR decreases. The trends of these emissions are consistent with the experimental results as presented in Chapters 5 – 7.

In conclusion, this Chapter offered insight into the flow dynamics and thermal distribution aiding with experimental decisions and understanding of outcomes. For instance, the considerable difference in flow dynamics as flowrate through swirler is altered informed the experimental decision to keep flow rates approximately constant.

5

DIESEL/METHANE AND DIESEL/SYNGAS COMBUSTION

This chapter presents and discusses the results obtained from the simultaneous combustion of blends of diesel/methane as well as diesel/syngas in a swirl-stabilised gas turbine relevant combustor rig.

5.1 Introduction

There is no shortage of experimental and numerical studies on combustion of blends of different fuels in a single phase in gas turbines. The goal of such studies is not only to determine the impact of multi-fuel combustion on emissions performance but also to improve the fuel flexibility of the gas turbine which is a workhorse for power generation across the world. However, studies on multiphase fuel combustion in gas turbine engines are severely limited whereas there exists a need, in view of energy security challenges, to investigate the potential expansion of the fuel flexibility of the gas turbine in this manner. In fact, one of the main gas turbine OEMs claim to, at present, have engines with dual-phase fuel capability allowing continuous operation even as fuels are switched with plans for further expansion [222]. In such systems it is important that the flame dynamics during the changeover period, however brief it lasts, be understood to avoid stability and extinction issues. Further, such knowledge will be useful for multiphase fuel combustion in gas turbines where gas/liquid fuels are continuously combusted or in staged combustion modes involving multiphase fuels. To that end, Chapters 5 and 6, utilises fundamental flame diagnostics methods to explore simultaneous combustion of liquid and gaseous fuels in a 20 kW gas turbine relevant burner.

In this Chapter, optical and flue gas emissions from the co-combustion of three blends of each of diesel/methane and diesel/syngas are presented alongside that of neat

diesel combustion. The optical emissions are C_2* and CH* species chemiluminescence from the resultant single and multiphase fuel flames and provide information about the heat release rate, reacting flow dynamics and flame stability of the reacting flows. The flue gas emissions presented are those of NO_X, CO and unburnt hydrocarbons (UHCs) and have been discussed in the context of chemical kinetic analysis as well as diesel spray characteristics. Over and above the foregoing, flame luminosity images of the tested fuel combinations are presented providing a visual comparison of the combustion zone as test conditions change.

Combustion tests were carried out at a constant global equivalence ratio of 0.7 and at a total heat output of 15 kW except for flammability range determination. Initially, the delineation of the limits of stable flame operation for two dual phase fuel combustion cases were determined and are presented in comparison to neat diesel burn.

5.2 Limits of Stable Flame Operation

Prior to taking measurements of optical and post combustion emissions, the ranges of stable flame operation for single and workable dual phase combustion of diesel/methane and diesel/syngas were determined. The method used in delineating the region of stable burning in the combustion experiments was adapted from that outlined in Lefebvre and Ballal [24] which involves carrying out a series of extinction tests and noting the lean and rich extinction limits of the combusted fuel. Consequently, diesel/methane and diesel/syngas flames were established at different total heat outputs (THO) and for each THO, combustion air flow rate was gradually increased until flame extinction occurred – the lean limit.

Also, after re-establishing the flame at the same THO, the air flow rate was gradually reduced up to the rich extinction point so as to determine the corresponding rich limit. The results for the diesel/methane flame are presented in Fig. 5.1 while that of the diesel/syngas flame are plotted in Fig. 5.2.

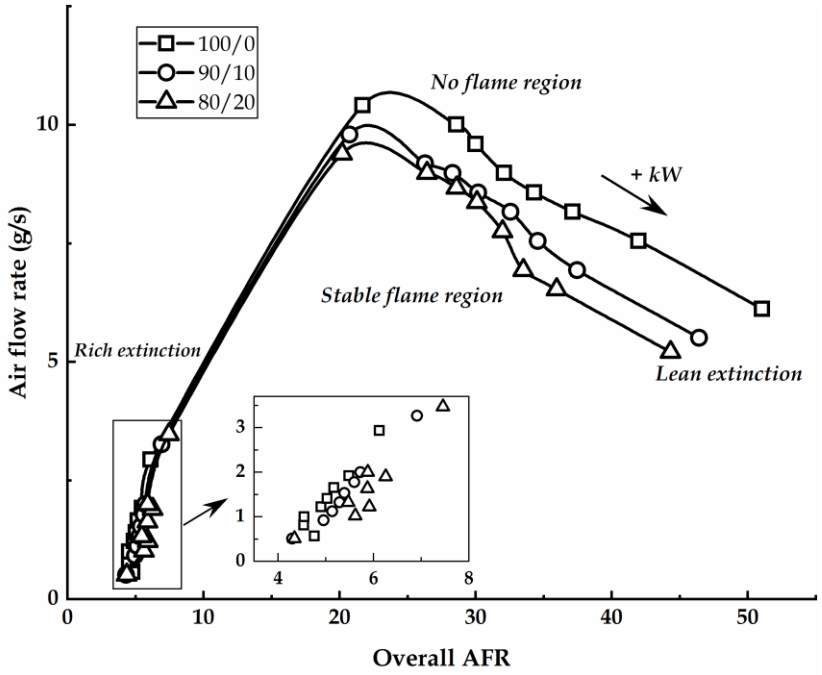

Fig. 5.1. Limits of stable flame operation for different diesel/methane blends

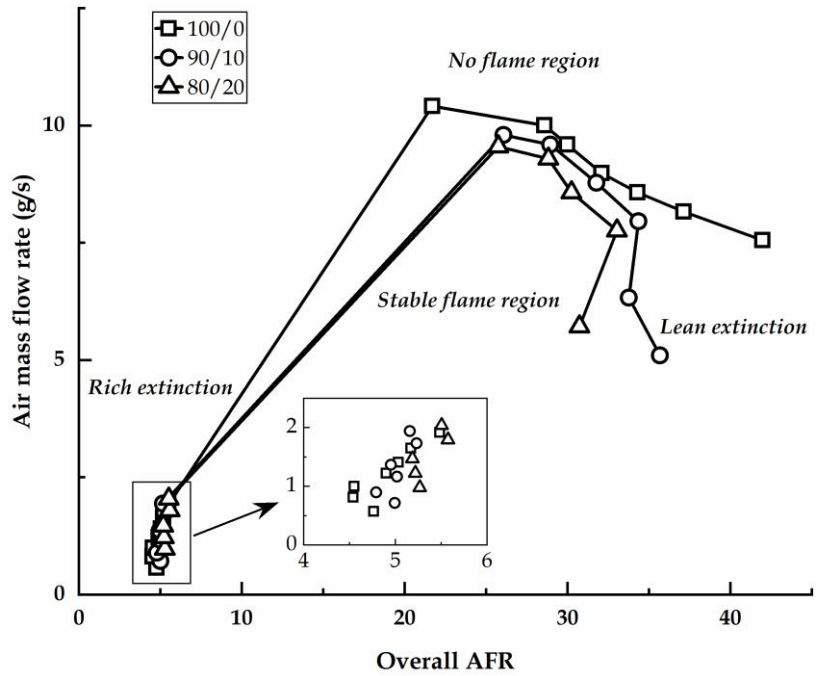

Fig. 5.2. Limits of stable flame operation for different diesel/syngas blends

Each data point on the 'lean' section of both plots indicates the air mass flow rate and overall air-to-fuel ratio (AFR) attainable for a specific power output delivered by the neat diesel fuel or some combination of diesel and gas fuel. There is also a corresponding point for rich extinction at the same power output in the 'rich' section of the plots. The plotted power output range for diesel/methane combustion is from 6 – 20 kW in increments of 2 kW. As for diesel/syngas, the considered heat output range are 6 – 18 kW in steps of 2 kW for the 100/0 case; 8 – 18 kW in steps of 2 kW for the 90/10 case; and 10 – 18 kW in steps of 2 kW for the 80/20 case. Stable flames were difficult to establish and impossible to sustain at 6 and 8 kW for the 80/20 diesel/syngas case over a reasonable range of air flow rates hence their exclusion in the plot. The same was true for a heat output of 6 kW for the 90/10 diesel/syngas case. These difficulties were absent for diesel/methane combustion signalling a difference in the reacting flow characteristics of methane and the selected syngas mixture. However, a 70/30 mix of both fuel combinations suffered from the same stability issues and therefore stability range data was not acquired from that blend.

In both Fig. 5.1 and Fig. 5.2, the area beneath each curve represents the region of stable burning for the particular fuel combination represented by the curve. Outside the region enclosed by the curve, no flame can be sustained at the specified power output. Also, for both diesel/methane and diesel/syngas combustion, flame stability limits is observed to decrease as LGR decreases from 100/0 to 80/20. The increasingly greater momentum of the swirling stream of gas fuel/air as air flow rate is increased causes the rate of diffusion of diesel spray droplets from the combustion zone to exceed the rate of recirculation of hot combustion products necessary to sustain the flame. As LGR decreases, this occurs sooner as the comparatively larger diesel spray particles require longer evaporation timescales and hence the hot combustion products are not as rapidly formed as in the finer spray of the 100/0 case.

The claim of declining spray evaporation rate as LGR reduces is supported by Fig. 4.11(a). And apart from Fig. 4.11 (b), Fig. 5.3 shows that diesel spray droplet size gets increasingly bigger as LGR decreases. Fig. 5.3 graphs the trend of diesel spray quality, in terms of Sauter mean diameter (SMD) as LGR changes. Decreasing the liquid flow rate causes a reduction in pressure drop across the nozzle as highlighted in Table 3.2.

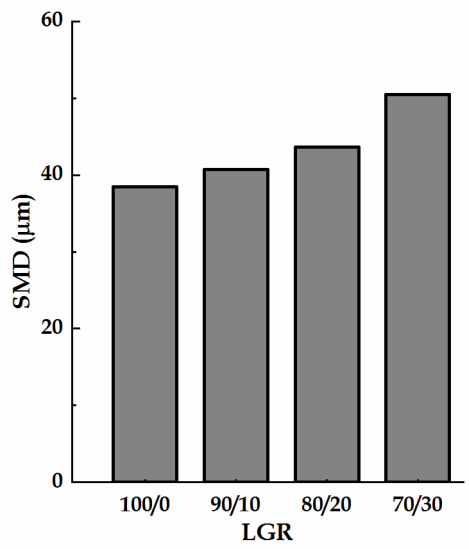

Fig. 5.3. Diesel SMD variation with increase in gas ratio of combusted fuel as predicted using Radcliffe's correlation.

This in turn leads to a loss in spray atomisation quality as evinced by the increase in SMD values (Fig. 5.3). Radcliffe's SMD correlation equation (Eq. 2.1a), proven in [66] to best predict Sauter mean diameter (SMD) of spray droplets for the type of nozzle utilised in the present study, was used to estimate the variation of SMD as liquid flow rates change based on the fuel combinations tested.

Apart from the foregoing analysis on the influence of atomisation quality variation, alteration in reacting flow dynamics as the gaseous fuel is introduced into the diesel spray may also be contributing to the reduction in stability limits shown in Fig. 5.1 and Fig. 5.2. This is because the distribution of the intermediate C_2* and CH*, shown in Fig. 5.4 and Fig. 5.5, suggests that with more than 10% syngas or methane present, combustion reactions commence and end faster with greater reactivity away from the burner centreline and more towards the edges of the burner. Although the chemiluminescence images of Fig. 5.4 and Fig. 5.5 represent a single equivalence ratio, highlighting the reaction flow dynamics as test conditions change. One of the impact lessons is that reaction near or around the burner centreline diminishes as LGR decreases. Hence the diesel spray, initially concentrated within a 60° cone angle around the burner centreline, has to diffuse to or around the burner edges in order to participate in the reaction. The finer spray particles in the 100/0 case would be superior in this regard compared with the 90/10 and 80/20 cases.

As a consequence of the above discussed factors namely, inferior atomisation quality as LGR decreases and reaction flow dynamics that prove increasingly unfavourable for stable flame operation with reducing liquid fuel spray, the attainable stability range in dual phase fuel combustion is worse off than neat diesel burn. The noted contraction in the range of air-fuel ratios over which stable flames exist as fuel LGR changes must not be misconstrued as being same for flame stability at a particular operating point. In fact, as shown later, diesel flame stability improves when co-combusted with 20% or 30% gas. Nevertheless, the reduction in stable flame operating range is undesirable for gas turbine combustors and, given the explanation offered, a different injection strategy for the liquid fuel that does not significantly alter atomisation quality as flow rates change like the air-blast nozzle may yield improved results.

5.3 Optical Emissions

A false colourmap representation of the distribution of C_2* and CH* species in diesel and diesel/methane flames at 15 kW and equivalence ratio (ER) of 0.7 are shown in Fig. 5.4. The images are normalised to the highest intensity for each species across the entire range of fuel blends shown. Likewise, Fig. 5.5 shows the chemiluminescence emissions of C_2* and CH* species in diesel and diesel/syngas flames at 15 kW and ER of 0.7 normalised to the highest emissions intensity for each species.

In both figures, whereas both species have a U-shaped distribution about the centreline of the burner for the 100/0 case, in the multiphase cases, the distribution of C_2* and CH* species assume more of a V-shape with the species spreading further away from the burner centreline towards the edges and all but separating in the middle for the 80/20 and 70/30 cases. A possible explanation for this, and supported by [258, 259], is that the central recirculation zone is weakened while the outer recirculation zone is strengthened as the local equivalence ratio of the of the swirling flow increases with increase in gas fraction in fuel mix.

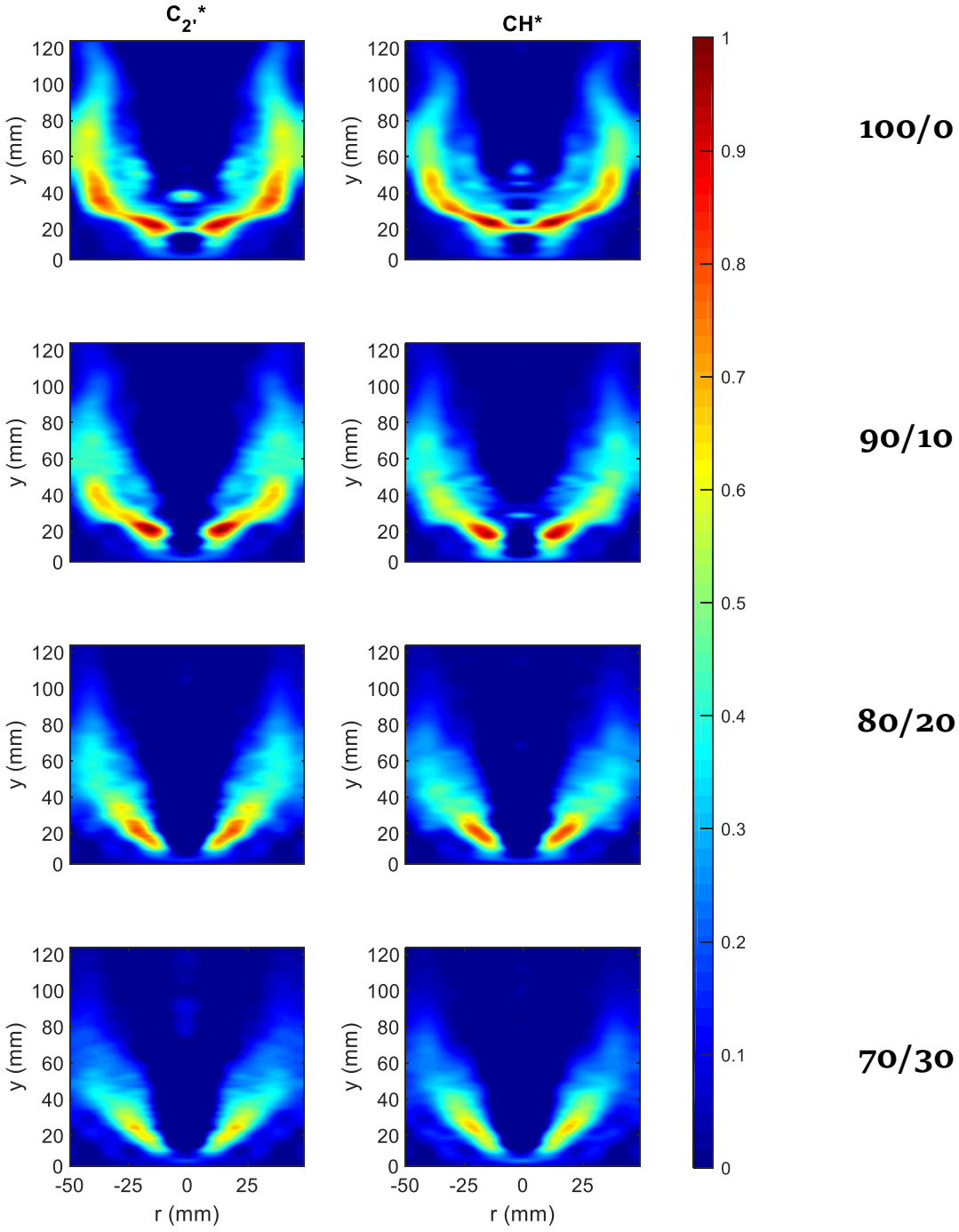

Fig. 5.4. Abel deconvoluted images of C_2* (left column) and CH* (right column) species from diesel/methane flames normalised to the highest intensity in each category. Flow is from bottom to top.

Evans *et al.* [215] noted similar appearance in swirling n-heptane-NG/H_2 flames claiming that fuel was being drawn out from the inner reaction zone to the outer branch of the flame and the findings here are in agreement.

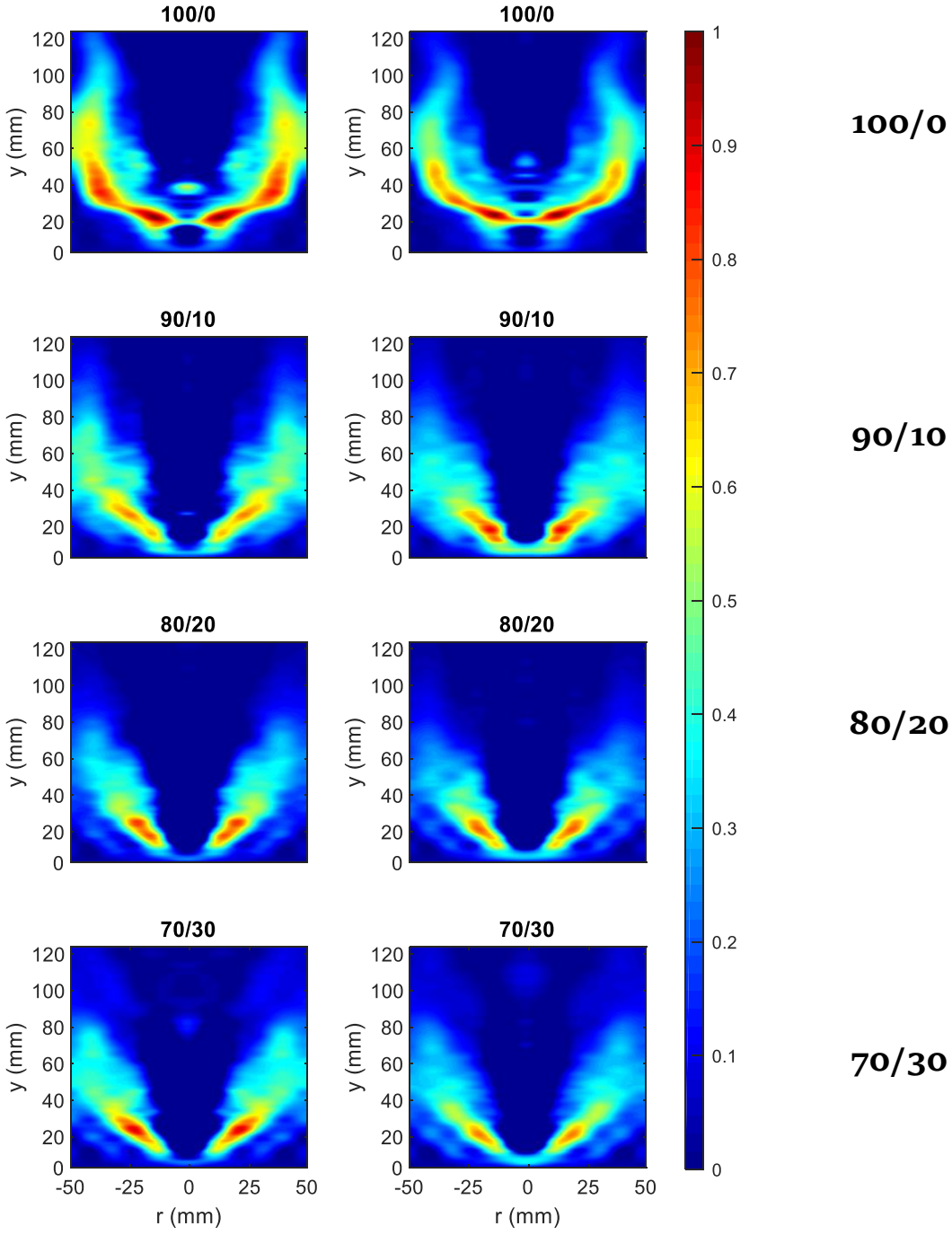

Fig. 5.5. Abel deconvoluted images of C_2* (left column) and CH* (right column) species from diesel/syngas flames normalised to the highest intensity in each category. Flow is from bottom to top.

Also, it appears that in the multiphase combustion cases, the reaction zone is closer to the nozzle orifice plane compared to 100/0 case. Thus it would seem that introduction of gaseous fuel into the burning diesel spray causes a quicker onset of C_2*/CH*-forming reactions as higher concentrations of these species are evident well before the 20 mm axial position in the multiphase cases compared to the 100/0 case. Moreover, the reactions forming the intermediate combustion species, appear not only to start sooner but also to end quicker in the multiphase cases in relation to the 100/0 case as evident in the axial distribution of the species in both Fig. 5.4 and Fig. 5.5. This is likely due to the fact that the lower liquid flow rates at 70/30, for instance, has poorer spray quality than the flowrate at 100/0 given the atomiser employed (as shown in Fig 5.3) thereby requiring a longer evaporation timescale, a fact corroborated by the predictions from Ansys Fluent shown in Fig. 4.11(a) and Fig 4.11(b).

Increasing the gas content of each fuel blend is also accompanied by a decrease in the volumetric heat release rate and maximum flame temperature as shown by chemical kinetics analysis (Fig. 5.6). The trend of flame temperature variation seen in Fig. 5.6(b) agrees with that of Fig. 4.13(a). C_2* and CH* species chemiluminescence are reasonably good indicators of heat release rate and the intensity variation of these species from Fig. 5.4 and Fig. 5.5 appear to generally support the trend of Fig. 5.6 (a). Assuming that the heat release rate at a particular instance is a function of the integral intensity (II) of either the C_2* or CH* radicals at that instance, the temporal variation of the rate of heat release from the flames were determined. This approach is similar to that in [237] and as samples, the variation of C_2* species integral intensity across the duration of the 250 captured images is shown for the diesel/methane 100/0 case in Fig. 5.7 (a) and for the 70/30 case in Fig. 5.7 (b). The corresponding CH* species integral intensity is shown in Fig. 5.7 (c) and Fig. 5.7 (d). In the same manner, the temporal variation of the intermediate species integral intensity is shown in Fig. 5.8.

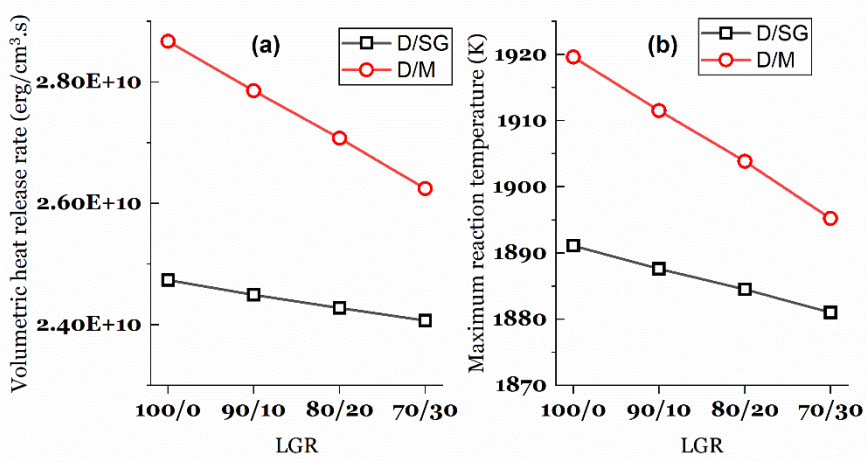

Fig. 5.6. Chemical kinetic analysis of diesel/methane and diesel/syngas combustion showing (a) volumetric heat release rate and (b) maximum flame temperature.

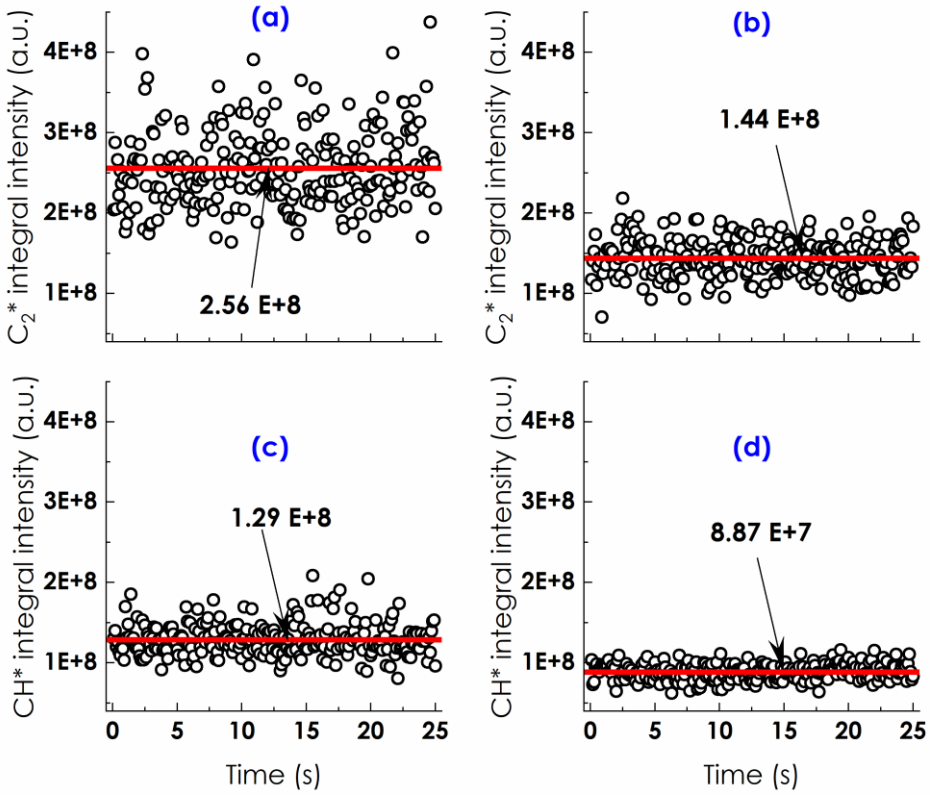

Fig. 5.7. Temporal variation of C2* species integral intensity for (a) 100/0 (b) 70/30 and CH* species integral intensity for (c) 100/0 (d) 70/30 diesel/methane flames.

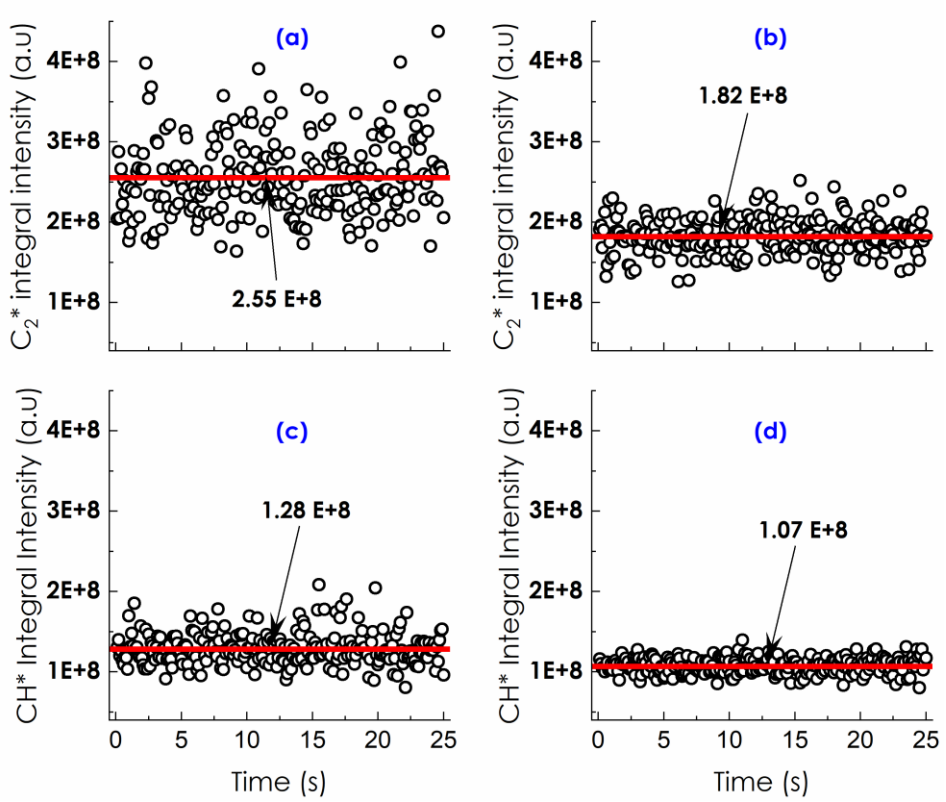

Fig. 5.8. Temporal variation of C2* species integral intensity for (a) 100/0 (b) 70/30 and CH* species integral intensity for (c) 100/0 (d) 70/30 diesel/syngas flames.

The solid red horizontal line in each graph represents the average integral intensity of the particular set of 250 images. As this average value varies across fuel blends, a simple standard deviation of each data set is inadequate to enable comparison of the temporal variability of heat release rate across the tested fuel compositions. Instead, the coefficient of variation, the ratio of the standard deviation of each data set to the corresponding mean value has been utilised as shown in Fig. 5.9. The multiphase combustion cases, based on Fig. 5.9, show lesser fluctuation in heat release rate fluctuation as gas ratio of combusted fuel increases. Lesser fluctuation in heat release rate promotes a more stable flame. For the diesel/methane blend, the curves of Fig. 5.9 (a) indicate an approximately 4% improvement in flame stability comparing the 90/10 case to the 70/30 from the heat release rate fluctuations of both chemiluminescence species. For the diesel/syngas blend, the extent of flame stability improvement is predicted differently by the two species. C_2* species indicate a 13% rise while the CH* species indicate a 9% increase in flame stability comparing the 90/10 dual-phase case with the 70/30 case.

The improvement in flame stability as gas is introduced to the combustion process, it would appear, based on the flame luminosity images shown in Fig. 5.11, is a function of the preferential combustion of methane near the base of the flame. This is evidenced by the blue flame close to the nozzle orifice that increases in size as gas content of fuel mix is increased. The earlier reaction, closer to the nozzle orifice plane, at 20% or more gas ratios compared with the 100/0 case favours the formation and entrainment of hot combustion products near the root of the flame that recirculate and thereby enhance stability of the flame.

Unlike the diesel/methane blends, diesel/syngas stability across the four cases is non-monotonic. Neat diesel combustion delivers a more stable flame than a 90/10 diesel/syngas based on Fig. 5.9 (b). The reason for this may be due to the chemistry of the syngas used. It would seem that the ultra-lean gas fuel mixture with the intake air in the 90/10 case is not as capable as the 80/20 or 70/30 cases in forming a distinct combustion regime next to the nozzle orifice (see Fig. 5.11).

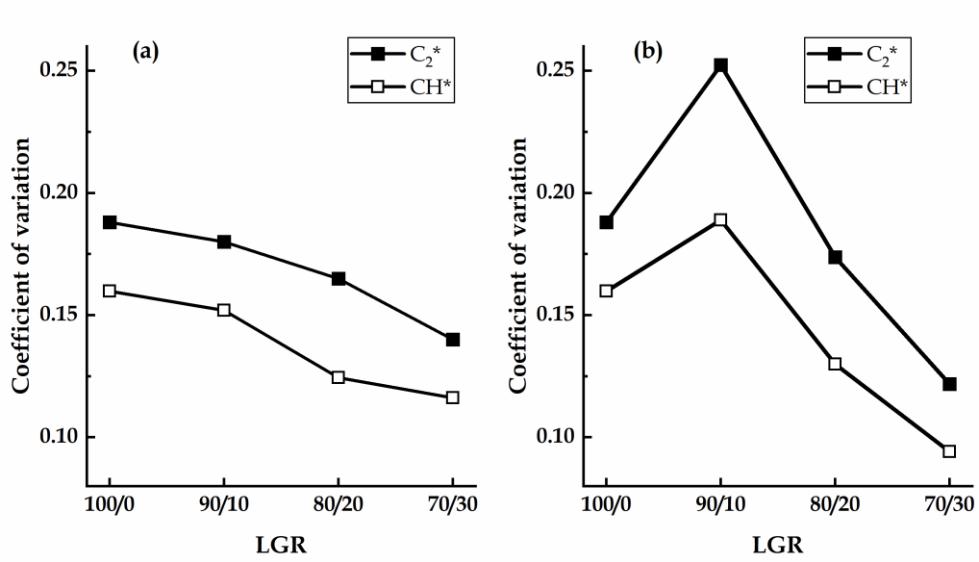

Fig. 5.9. Comparison of temporal fluctuation of heat release rate for (a) diesel/methane and (b) diesel/syngas flames at different LGRs.

Instead, the small amount of gas, due to its nature, diffuses quickly and reacts further downstream of the combustion zone thereby not contributing to hot gas recirculation in the same manner as the 80/20 or 70/30 case. At the higher gas fractions of 80/20 and 70/30, there is sufficient gas in the air stream to create a gas combustion regime early on in the process in the manner of the methane blends. This was also evident in observation of the flames.

5.4 Post combustion emissions

The flue gas emissions from the co-combustion of diesel/methane (D/M) and diesel/syngas (D/SG) is shown in Fig. 5.10. The error bars are the 6% uncertainty in the readings as stated by the calibration document from the manufacturer. The gradual and then rapid rise in CO emissions as diesel fuel fraction decreases is attributable to several inter-related factors. First, as mentioned previously, the reduction in diesel flow rate as LGR is altered causes a variation in pressure drop across the nozzle which in turn results in poorer liquid fuel atomisation.

Poor liquid fuel atomisation is associated with relatively larger droplets which require comparatively more time for evaporation and combustion. Additionally, the alteration in reacting flow dynamics discussed in the previous section, exacerbates the CO problem as gas fuel partly replaces diesel in the fuel mix.

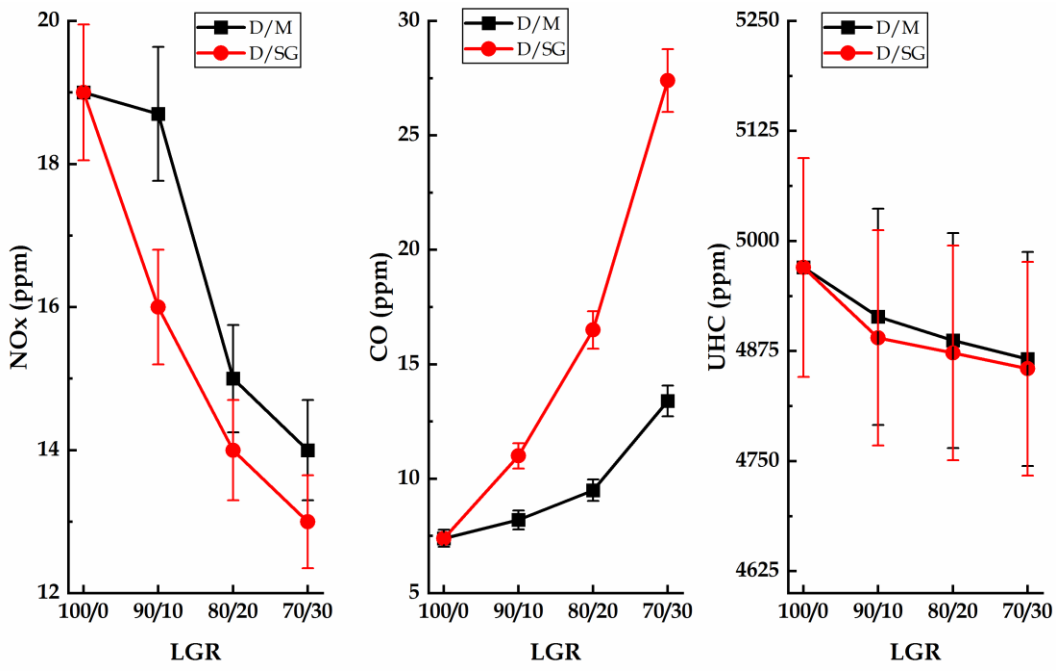

Fig. 5.10. Post combustion emissions of (a) NO_X (b) CO and (c) Unburnt hydrocarbons (UHC) for diesel/methane (D/M) and diesel/syngas (D/SG) flames at different liquid-gas ratios.

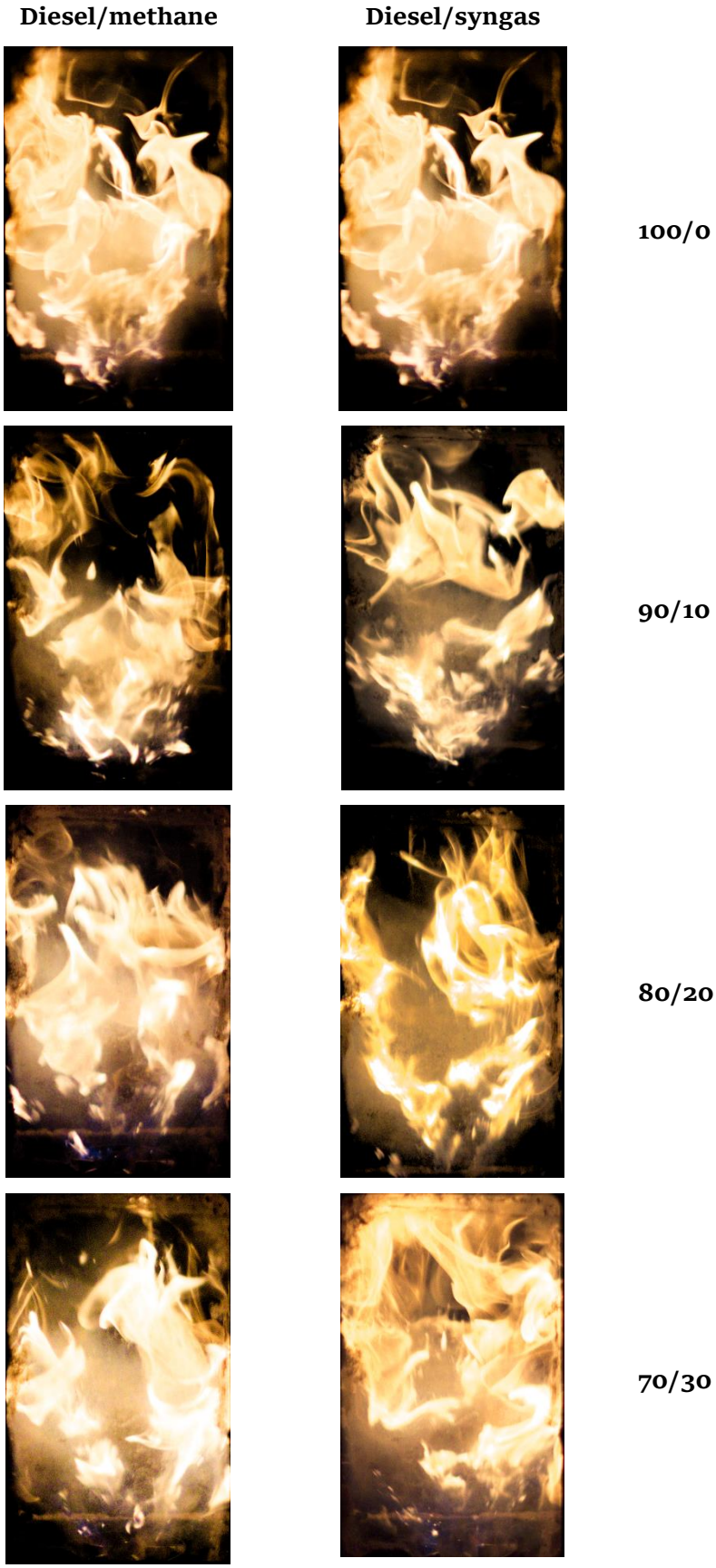

Fig. 5.11. Flame luminosity images of diesel/methane and diesel/syngas flames.

Second, the heat release rate trend of Fig. 5.6 (a), supported by the intermediate combustion species average intensity variation in Fig. 5.7 and Fig. 5.8, suggests a reduction in adiabatic flame temperature as diesel/syngas ratio changes from 100/0 to 70/30. The chemical analysis simulation supports this as shown in Fig. 5.6 (b). The decreasing adiabatic flame temperatures as gas ratio in fuel blend increases contributes to the graphed variation in CO emissions.

The conditions elaborated in the foregoing that prove unfavourable for CO oxidation, serve to lower NO_X emissions. Lower adiabatic flame temperature arising from reduction in heat release rate together with shorter residence times indicated by the shorter reaction zones as gas ratio in fuel blend increases causes a steady reduction in NO_X emissions as shown in Fig. 5.10 (a).

The trend of unburnt hydrocarbons (UHC) shown in Fig. 5.10 (c) is unusual. Commonly, UHCs follow the same gradient as CO emissions because both are products of inefficient combustion. However, as pointed out earlier, two combustion regimes are apparent particularly at 20% and 30% gas ratios (see the luminosity images of Fig. 5.11). One is the lean gas combustion in the vicinity of nozzle orifice. Musculus *et al.* [260] showed that very lean mixtures near the injector can result in high UHCs yet low CO. The second combustion regime apparent from the luminosity images, is diesel spray entrained in potentially oxygen-vitiated recirculating air. Combined with relatively poorer atomisation, attainable flame temperatures lessen as gas ratio increases. Prior studies have shown that relatively low temperature combustion regimes in flames can result in opposite gradients for CO and UHC emissions [261]. A combination of these factors seems to be responsible for the UHC and CO emissions relationship observed in the present study.

5.5 Chapter summary

Three blends each of diesel/methane and diesel/syngas were separately combusted in a model swirl-stabilised gas turbine combustor to experimentally study multiphase fuel burn in combustion turbines. Range of stable flame operation, flame stability and post combustion emissions comparisons were made between the neat diesel combustion and the multiphase co-combustion cases. Apart from the instance of

determining the stable operating range, the multiphase fuel mix and air combination was selected to deliver a power output of 15 kW at a global equivalence ratio of 0.7. Also, a numerical study was conducted using CHEMKIN to establish trends in heat release rate and adiabatic flame temperature. The main findings from the study are:

1. Both diesel/methane and diesel/syngas co-combustion in a swirl-stabilised gas turbine burner using the strategy described in this work reduces the achievable range of stable flame operation compared with neat diesel combustion.
2. At the chosen operating point – 15 kW overall heat output at a global equivalence ratio of 0.7 – flame stability, determined by the extent of the temporal fluctuation of C_2* and CH* species chemiluminescence, is improved when diesel flow rate is reduced to allow 20 – 30% of the overall heat output to be supplied by the gaseous fuel. However, heat release rate is sacrificed as suggested by chemical kinetics analysis as well the observed intensity variation of the aforementioned intermediate combustion species.
3. NO_X emissions are steadily reduced whereas CO emissions are increased as gaseous fuel partly replaces diesel in the combustion process. Interestingly, UHC emissions follow an opposite gradient to CO emissions and this has been attributed to the reacting flow dynamics occasioned by the fuel injection strategy utilised.

6

BIODIESEL/METHANE AND BIODIESEL/SYNGAS COMBUSTION

This chapter presents and discusses the results obtained from co-combustion of waste cooking oil-derived biodiesel and either methane or syngas in a 20 kW swirl-stabilised gas turbine relevant combustor.

6.1 Introduction

In addition to that in the preceding Chapter, further experiments in multiphase fuel combustion was carried out. In this case, biodiesel derived from waste cooking oil was simultaneously combusted in methane and syngas mixtures using the same experimental set-up as in Chapter 5.

Capable of being sourced from several different feedstock including edible and non-edible oils, waste or recycled oil, and animal fat, biodiesel has been widely tested in combustion engines either wholly or as blend component with the fossil fuel. The extensive interest in utilising biodiesel as a whole or partial replacement for fossil diesel stems from its apparent renewability and comparable engine performance with the conventional fuel. Also, with fossil fuels ever depleting, the need for alternative energy sources has never been greater.

Despite having an energy density that is 14% less than that of fossil diesel, biodiesel, with an inherent oxygen content of about 10%, burns cleaner than fossil diesel and potentially reduces harmful emissions [60, 62]. Expectedly, there is no shortage of published literature on biodiesel production, its chemical and physical properties, as well as the emissions from its combustion in power generating systems.

Further, there are numerous studies on the combustion of blends of biodiesel with both liquid and gaseous fuels in the compression-ignition engine. However, literature on the simultaneous combustion of biodiesel and gaseous fuels in continuous flow devices like the gas turbine is severely limited if available. This work addresses this lack of data.

The results presented in this Chapter are based on the combustion of neat biodiesel spray in air and also in air premixed with either methane or syngas. The approach is the same as in the last chapter, viz. establishing flame stability limits; utilising optical emissions in the form of C_2* and CH* species chemiluminescence as well as flame luminosity images to explore reacting flow dynamics and flame stability. Also post combustion emissions of NO_X, CO and unburnt hydrocarbons (UHCs) from the flames are analysed. Consistent with the last Chapter, tests were conducted at an overall heat output of 15 kW and a fairly lean global equivalence ratio of 0.7.

6.2 Limits of stable operation

The same method used in the previous Chapter is used here to delineate the region of stable burning in the biodiesel/methane and biodiesel/syngas combustion experiments. Flames at heat outputs of 6, 8, 10, 12, 14 and 16 kW were established, and for each heat output, the air flow rate was gradually increased until flame extinction occurred. Also, after re-establishing the flame at the same heat output, the air flow rate was gradually reduced up to the rich extinction point which was noted as well. This process was repeated for the aforementioned levels of power output for the 100/0 and 90/10 cases. The 6 kW test was omitted for the 80/20 case as a stable flame could not be sustained at the corresponding fuel flow rates due to deterioration of spray quality with reduction in biodiesel flowrate. Similarly, combustion of the 70/30 case proved to be highly inefficient at the lower range of heat output up to 12 kW. The fuel lean and fuel rich extinction points result in the curves of Fig. 6.1 for three different fuel combinations. As it was with diesel, there is, in Fig. 6.1, a reduction in the region of stable burning – the area under each curve – as methane replaces biodiesel as a fraction of the thermal power output.

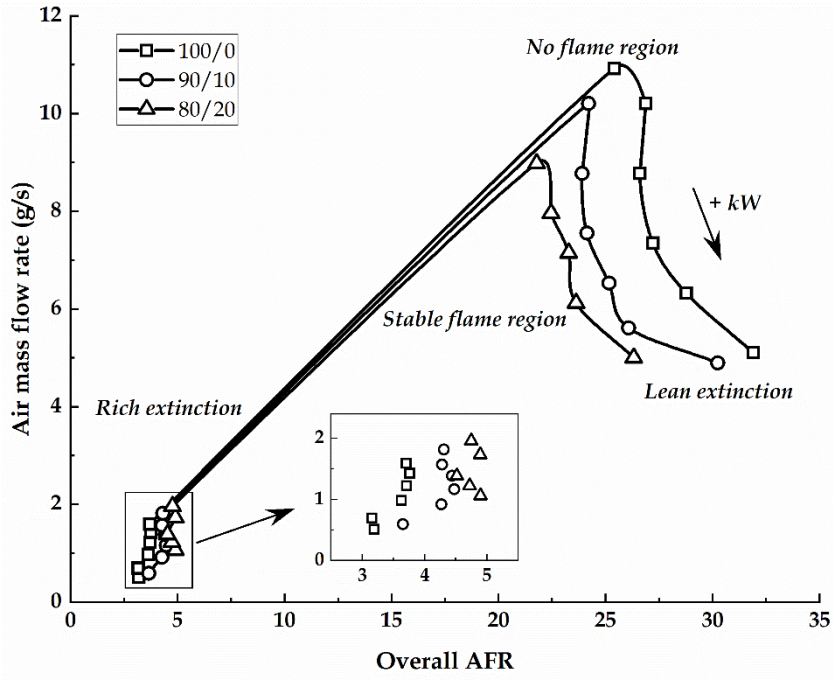

Fig. 6.1. Limits of stable flame operation for different biodiesel/methane blends

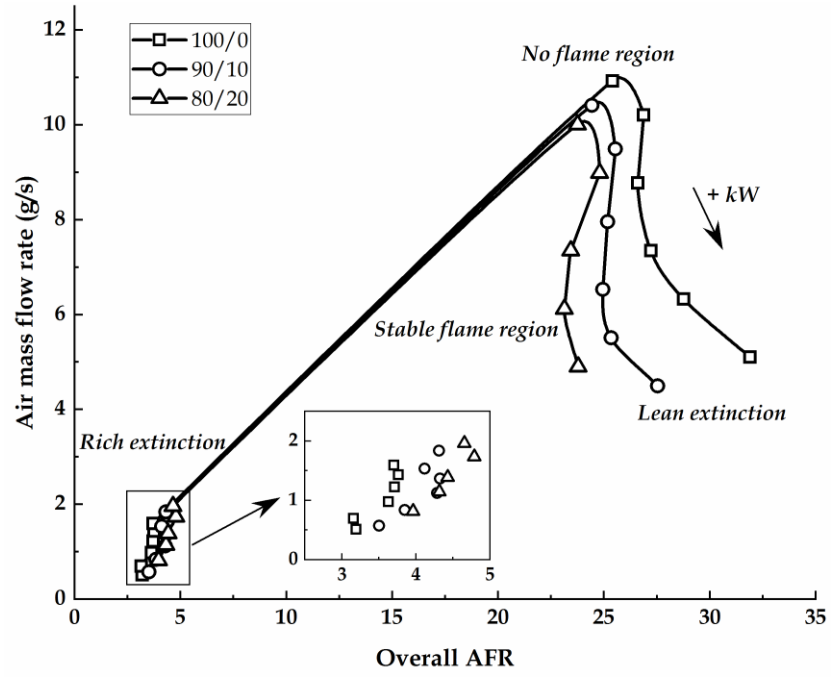

Fig. 6.2. Limits of stable flame operation for different biodiesel/syngas blends

Further, as the fraction of methane increases in the fuel combination, the flame stability limit (in terms of overall AFR) becomes narrower, particularly in the lean region. Over the same thermal power outputs listed in the foregoing, the range of stable flame operation for biodiesel/syngas flames was determined and shown in Fig. 6.2. Again, the trend is the same: decreasing limits of stable burning as LGR decreases.

There are at least two reasons for the reduction in flame stability as combustion shifts from a single (liquid) fuel to dual (liquid/gas) fuel. The first involves the changes in reacting flow dynamics as the swirling gaseous flow rate is increased and will be further discussed in Section 6.3 in the light of optical emissions. The other reason for the contraction of stability range as gas percentage in fuel mix increases is the loss in liquid atomisation quality as liquid flow rate decreases. Decreasing the liquid flow rate to accommodate gas introduction to the system causes a reduction in pressure drop across the nozzle as highlighted in Table 3.3. The resulting trend of SMD values as LGR changes, shown in Fig. 6.3, means that liquid fuel evaporation rate is reduced as is the combustion rate which in turn leads to a decrease in the amount of recycled heat and chemical species necessary for anchoring and stabilising the flame. With simultaneously increasing droplet size and less support for combustion as LGR decreases, the flames reach extinction point faster.

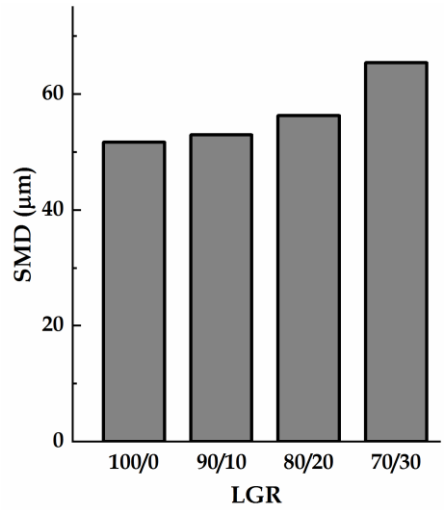

Fig. 6.3. Biodiesel SMD variation with increase in gas ratio of combusted fuel calculated using Radcliffe's correlation.

Also, as noted in the last chapter, it has previously been observed by [258, 259] that swirl-stabilised reacting flows have increasingly weaker central recirculation zones as the local swirling fuel/air ratio increases. This might be contributing to the observed contraction in flame stability range as gas flow rate increases since the strength of the recirculation zone is important for flame sustenance.

Compared with the diesel/gas tests in Chapter 5, lower AFRs are observed with biodiesel/gas experiments. The greater overall AFRs recorded for diesel/gas flames are not indicative of wider stability limits in comparison with biodiesel/gas flames. The oxygenated nature of biodiesel means that a greater quantity of it is burnt to generate the same power output as the diesel/gas fuel thereby driving down its overall AFR.

The general reduction in stability limits observed in both diesel/gas and biodiesel/gas tests highlights an important operational consideration if multiphase fuel combustion is to be employed in swirl-stabilised combustion systems following the strategy utilised in this work: flames will not stay alight over as wide a range of AFRs as it would for neat liquid fuel burn. Consequently, it is recommendable as noted previously, to trial a different fuel injection strategy.

6.3 Optical emissions

6.3.1 Flame luminosity and chemiluminescence

The C_2* and CH* species chemiluminescence images in Fig. 6.4 are for biodiesel/methane flames established at an overall heat output of 15 kW and global equivalence ratio, φ_{global}= 0.7. The corresponding intermediate combustion species chemiluminescence for biodiesel/syngas flames is shown in Fig. 6.5. The chemiluminescence images in both figures have been normalised to the maximum intensity in each species category.

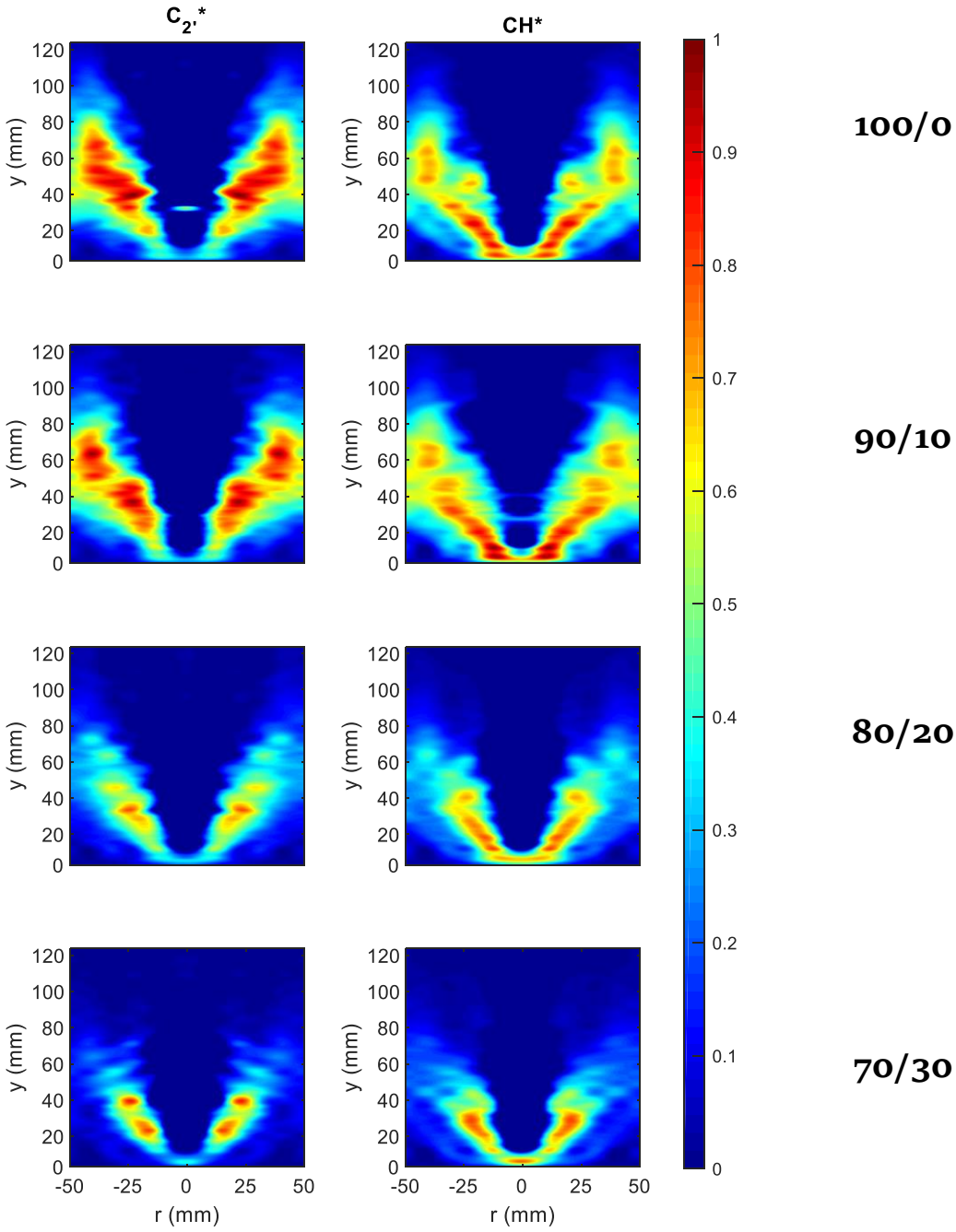

Fig. 6.4. Abel deconvoluted images of C_2* (left column) and CH* (right column) species from biodiesel/methane flames normalised to the highest intensity in each category. Flow is from bottom to top

Both chemiluminescence species images show a reduction in intensity and area as gas content of fuel mix increases when considering the dual phase cases. As in the diesel/gas flames, the distribution of the C_2* and CH* species for the biodiesel/gas flames follow a V-shape around the burner centreline with decreasing intensity as LGR decreases.

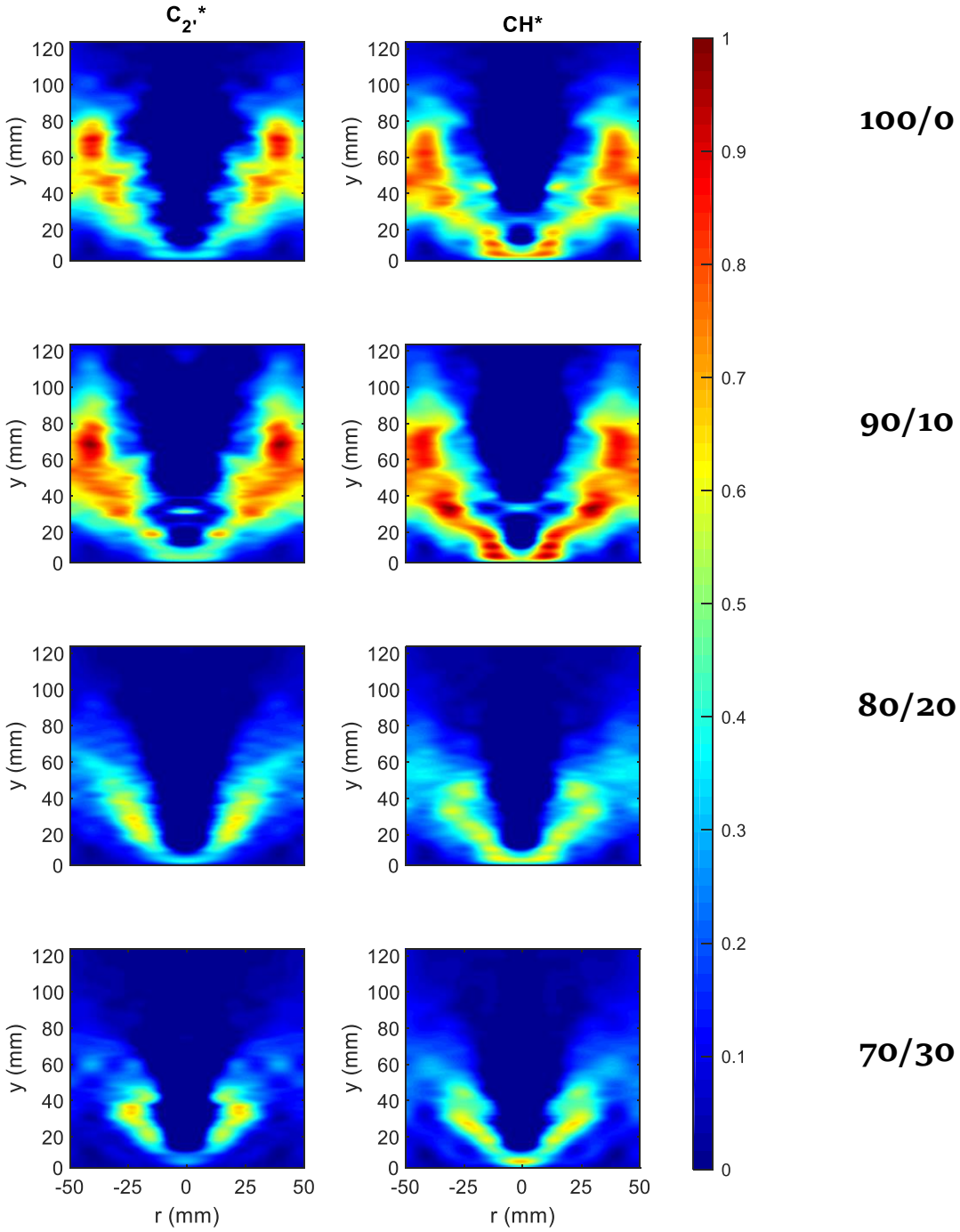

Fig. 6.5. Abel deconvoluted images of C_2* (left column) and CH* (right column) species from biodiesel/syngas flames normalised to the highest intensity in each category. Flow is from bottom to top.

The flame luminosity images (Fig. 6.6) appear to show first a wrinkling and then a seemingly turbulent separation of reacting flow that appears to worsen as liquid/gas fuel composition is altered from 100/0 to 90/10 and beyond.

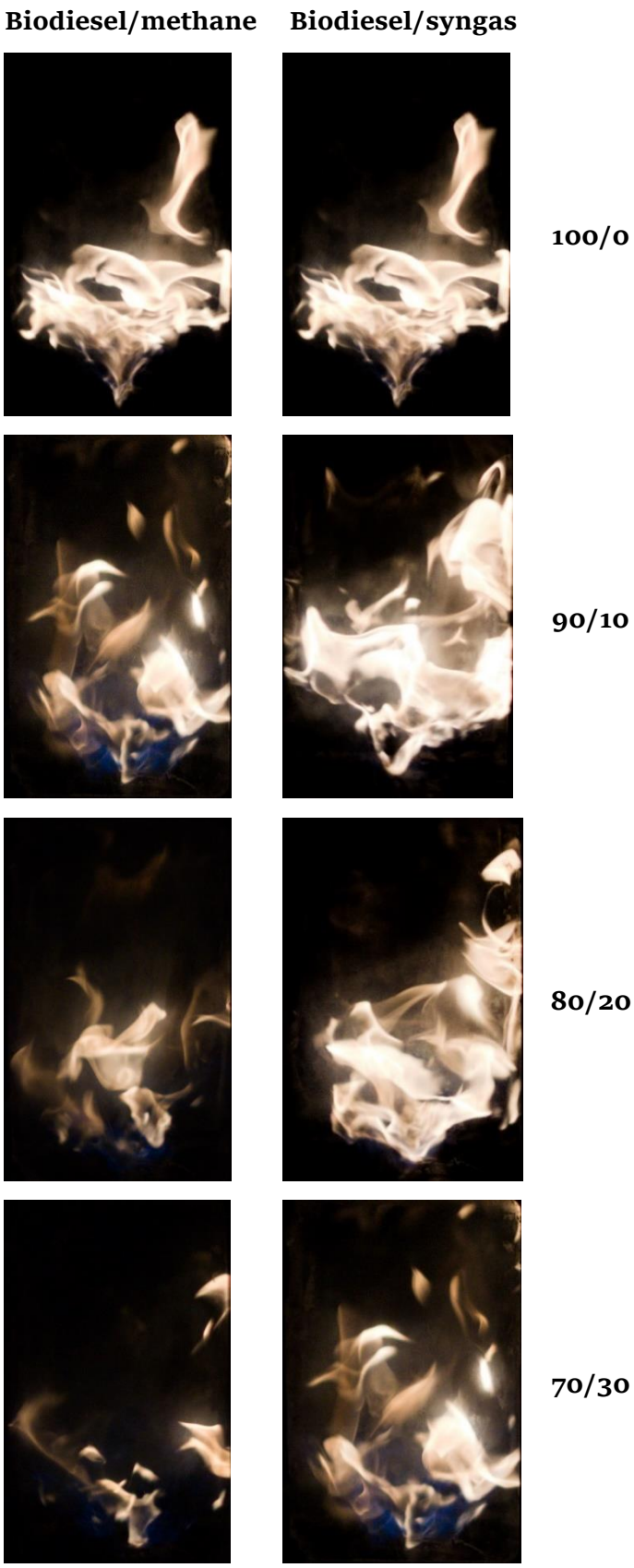

Fig. 6.6. Biodiesel/methane and biodiesel/syngas flame luminosity images

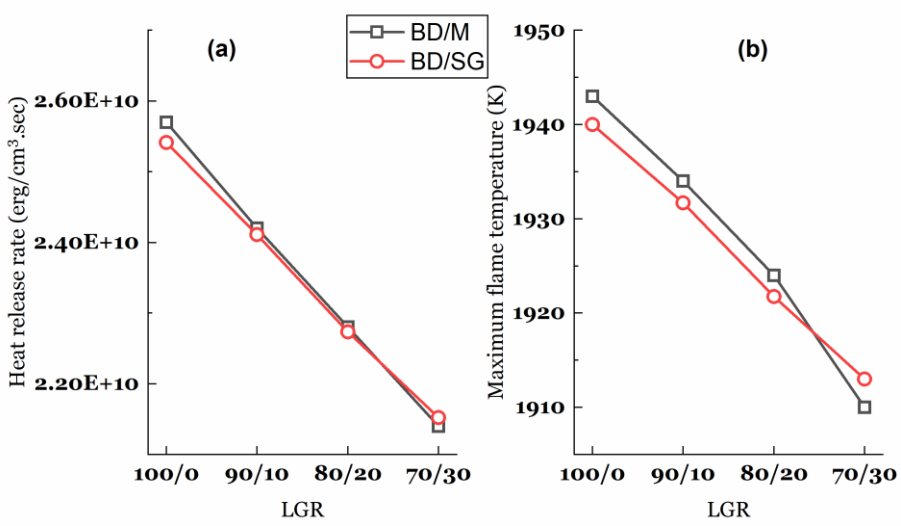

Fig. 6.7. Chemical kinetic analysis of biodiesel/methane (BD/M) and biodiesel/syngas (BD/SG) combustion showing (a) volumetric heat release rate and (b) maximum flame temperature

Compared with the diesel/gas flames shown in Chapter 5, biodiesel-related flames are less luminous hence better captured by the imaging equipment used for the luminosity pictures. Consequently, it is more obvious in Fig. 6.6 than in the corresponding figure in the last Chapter that with the introduction of gas fuel, a blue flame region close to and around the flame nozzle exit plane is formed suggesting the formation of a locally lean, predominantly gaseous combustion region.

The chemical kinetics calculations reveal, as shown in Fig. 6.7, that volumetric heat release rate and maximum flame temperature both decrease as gas ratio in fuel blend increases. The import of this (in relation to flame stability and emissions) will be made apparent in Sections 6.33 and 6.4 respectively. In summary, these decrements in heat release rate and flame temperature are consistent with the chemiluminescence images shown earlier.

6.3.2 Reaction zone properties

The biodiesel/gas flames were observed to, unlike the diesel-related flames (particularly the diesel/syngas ones), be well-confined in the burner with generally

shorter flame lengths. This is noticeable in the flame luminosity images. Therefore, additional analysis on the biodiesel/gas chemiluminescence images was possible providing further comparison between the reaction zone properties of single and dual phase cases.

This analysis involved converting the chemiluminescence images to binary images (Fig. 6.8 and Fig. 6.9) using Matlab. Matlab's Otsu thresholding method was used to determine which pixels are designated white or black. The Otsu thresholding method is suitable here because it selects a threshold value that minimises the intraclass variance of the black and white pixels. The threshold value was determined separately in the 100/0 image for each of the two chemiluminescence species and subsequently held constant across the test cases in each category. The aim of 'binarising' the images based on a set threshold value is to characterise the reaction zone.

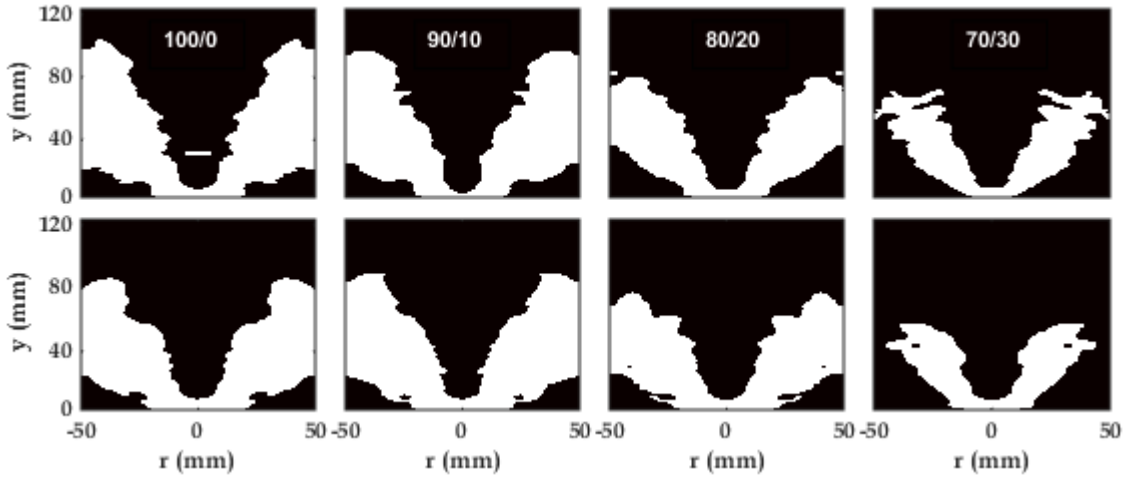

Fig. 6.8. Binary images of C2* (top row) and CH* (bottom row) chemiluminescence in biodiesel/methane flames at different liquid/gas ratios. Flow is from bottom to top.

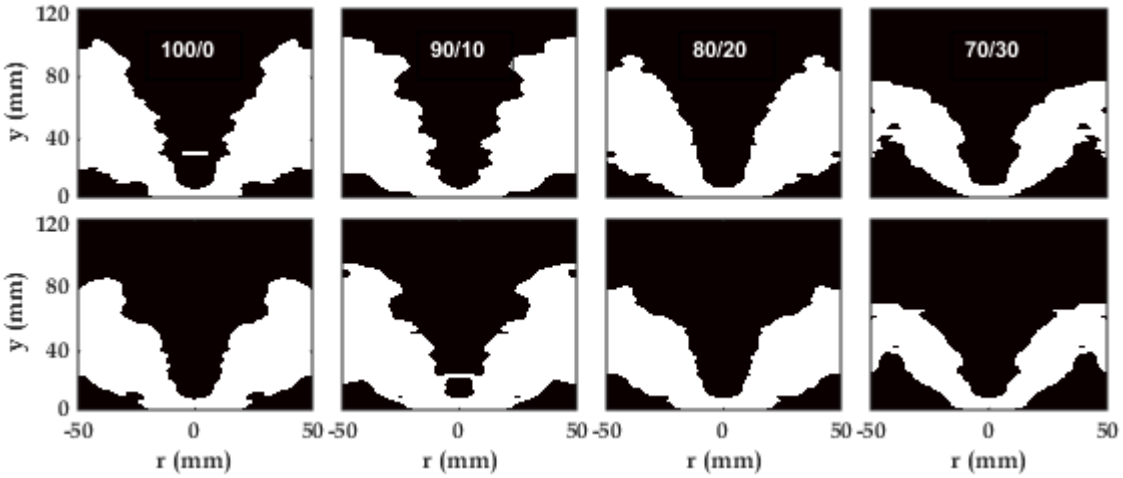

Fig. 6.9. Binary images of C2* (top row) and CH* (bottom row) chemiluminescence in biodiesel/syngas flames at different liquid/gas ratios. Flow is from bottom to top.

Having converted it to binary images, the sum of the unity pixels in the images is designated as the reaction zone (RZ) area whereas the distance between the uppermost unity pixel to the lowermost is regarded as the RZ length in each case. A quantitative description of the variation in RZ properties is shown in Fig. 6.10. The graphs of Fig. 6.10 suggest that the 90/10 biodiesel/gas combustion zone properties are not significantly different from neat biodiesel combustion. This suggests that, apart from the highlighted reduction in stable operational range, multiphase fuel burn in gas turbine combustors is possible without notable disturbance of the RZ at low gas fractions (up to 10% in this case). The reason for this is probably because at very low percentages in the intake air, the gas mixture is too fuel-lean to form a distinct combustion regime as is possible at higher gas fractions. This was noticeable in the physical observation of the flames. Instead of forming its own combustion zone, the ultra-lean gas at 90/10 LGR diffuses into the diesel spray and combusts therein. As a consequence, the RZ properties of the biodiesel/gas flames at an LGR of 90/10 is approximately the same or even slightly greater (particularly with the biodiesel/syngas blend) to that of neat biodiesel (LGR = 100/0) combustion as seen in Fig. 6.10.

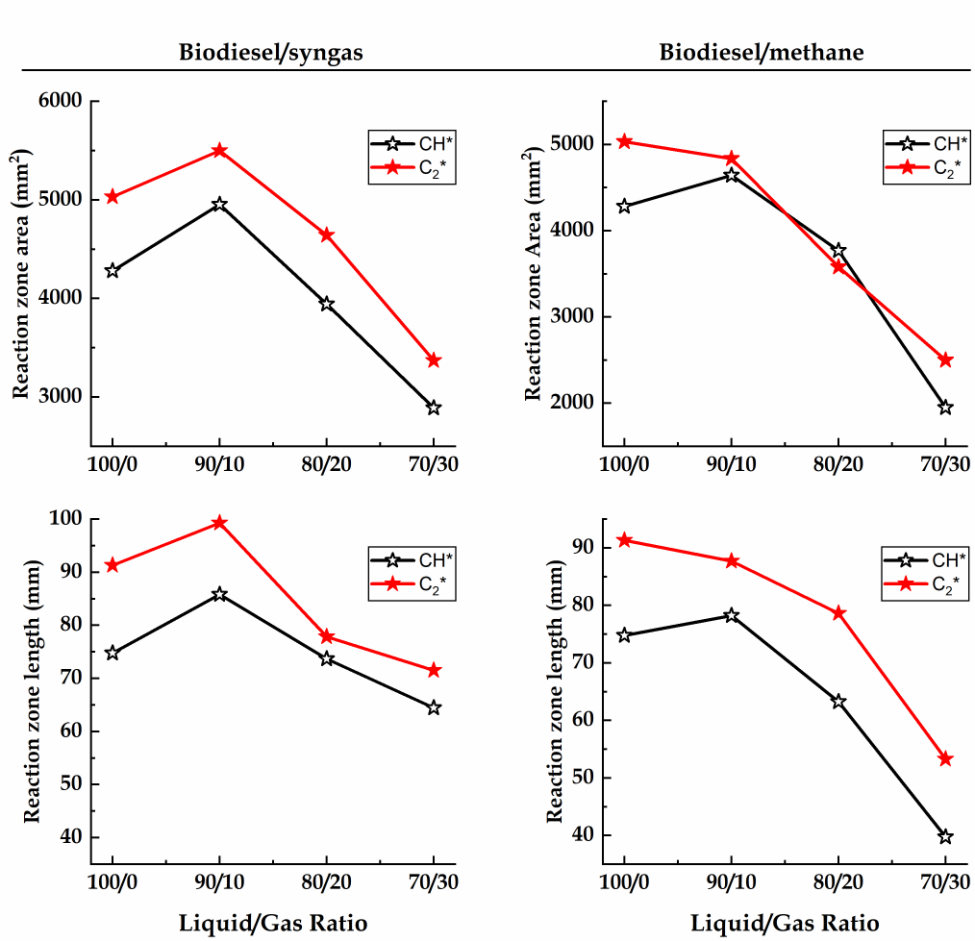

Fig. 6.10. Reaction zone area and reaction zone length of 15 kW biodiesel/methane and biodiesel/syngas flames.

As gas fractions increase beyond 10%, at LGRs of 80/20 and 70/30, the gas is capable of forming and maintaining a distinct combustion zone at the root of the biodiesel flame. With this formation of a relatively hot zone close to the base of the burner, the biodiesel spray is forced to commence combustion earlier than at no or low gas fractions. And with the biodiesel deteriorating in spray quality with decreasing LGR, combustion efficiency is lessened and even made worse as the air available for reaction further downstream of the gas combustion zone is vitiated in oxygen. All of these factors contribute to decreased reactivity and flame residence time in the combustion process which causes the reduction in RZ area and length seen in Fig. 6.10 further showing that the intermediate combustion species, C_2* and CH*, are reasonably good indicators of the RZ of flames.

6.3.3 Flame Stability

The temporal variation of the integral intensity of the chemiluminescence radicals can be assumed, similar to the approach in Ballester *et al.* [237], to be indicative of the variation of heat release rate from the flames. On this basis, the C_2* and CH* species integral intensity variation across the duration of the chemiluminescence imaging for each of the tested fuel combinations was calculated and compared. Samples of this fluctuation in the rate of heat release is shown in Fig. 6.11 and Fig. 6.12.

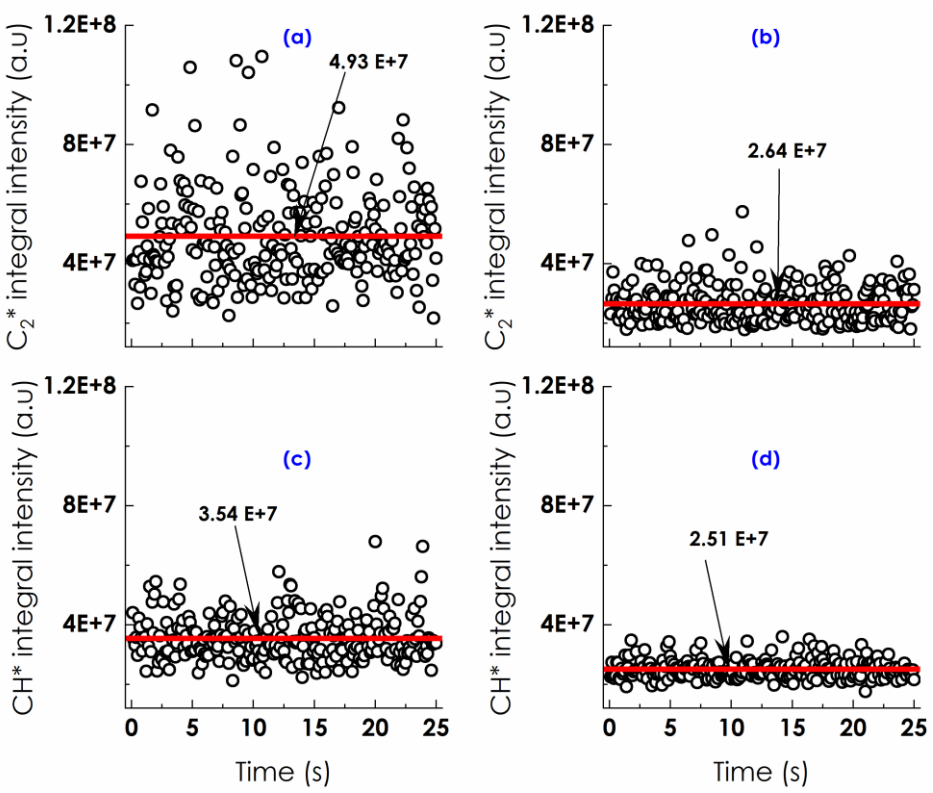

Fig. 6.11. Temporal variation of C_2* species integral intensity for (a) 100/0 (b) 70/30 and CH* species integral intensity for (c) 100/0 (d) 70/30 biodiesel/methane flames.

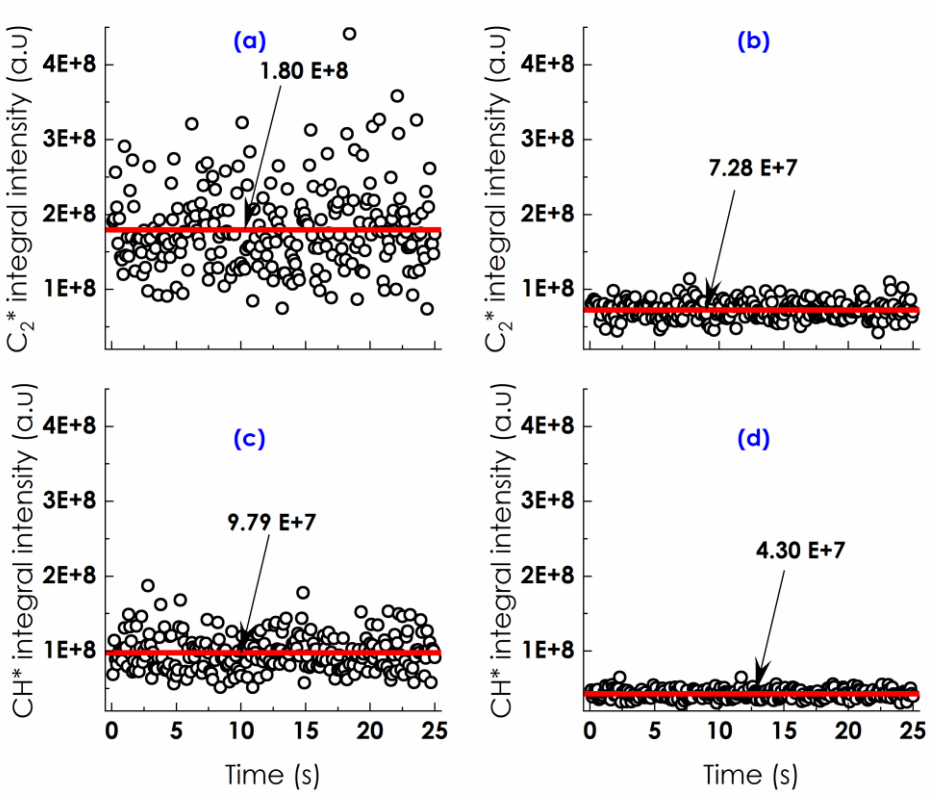

Fig. 6.12. Temporal variation of C_2* species integral intensity for (a) 100/0 (b) 70/30 and CH* species integral intensity for (c) 100/0 (d) 70/30 biodiesel/syngas flames.

The C_2* species integral intensity variation over time for the biodiesel/methane flame is shown for the 100/0 case in Fig. 6.11 (a) and for the 70/30 case in Fig. 6.11 (b). The corresponding data for the CH* species is shown in Fig. 6.11 (c) and Fig. 6.11 (d) respectively. Likewise, Fig. 6.12 displays the data for biodiesel/syngas in the same order as in Fig. 6.11. The solid horizontal red line in each figure indicates the integral intensity of the average of the 250 images. As the average varies widely across the test cases, comparison of the data variability based on standard deviation is inadequate.

Therefore, the coefficient of variation (standard deviation normalised by mean value) has been employed. This is shown in Fig. 6.13 and points to lesser fluctuation in heat release rate as the percentage of gas in the multiphase fuel combustion cases increases. Decreased fluctuation in the rate of heat release indicates an improvement in flame stability. Based on the CH* species HRR fluctuation, there is an approximately 8% improvement in flame stability comparing the 90/10 blend with the 70/30 blend

in both biodiesel/gas combustion tests. Comparing the same multiphase blends using C_2* species HRR fluctuation, there is an improvement of about 6% and 15% in the biodiesel/methane and biodiesel/syngas blends respectively. So, essentially, going for higher gas content in multiphase fuel burn under gas turbine conditions increases the flame stability. The greater flame stability noted here as must not be confused with the range of flame stability which was, in Section 6.2, observed to contract as gas ratio in fuel mix increases. Also, it is evident from Fig. 6.13 (b) that the 90/10 blend of biodiesel/syngas, as was the case with the same blend of diesel/syngas, is worse off in flame stability than the neat liquid fuel combustion. This difference in behaviour compared to the biodiesel/methane blend might be down to the composition of the syngas employed. At the low gas fraction of 90/10 LGR, without being of sufficient quantity to form a distinct reaction zone, the volatile hydrogen component potentially increases the unsteadiness of the flame by reacting amid the liquid spray molecules.

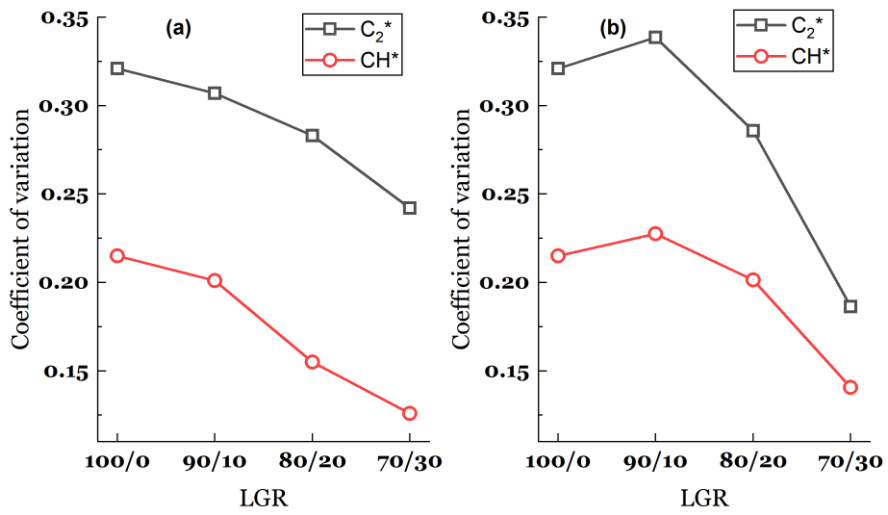

Fig. 6.13. Comparison of temporal fluctuation of heat release rate for (a) biodiesel/methane and (b) biodiesel/syngas flames at different LGRs.

6.4 Post combustion emissions

The NO_X, CO and UHC emissions from the four blends of each of biodiesel/methane and biodiesel/syngas are presented in Fig. 6.14 with the error bars being the 6% uncertainty in the readings as stated by the calibration document from the manufacturer. As highlighted elsewhere, NO_x emissions are known to be heavily reliant on flame temperatures for which heat release rate is important [71]. On the basis of the optical emissions observed, there is a steady decrement in the heat release rate from the flames with increase in the gaseous fuel component of the blend supplied for combustion. The contended reduction in the rate of heat release is supported by chemical kinetic analysis (Fig. 6.7) which also shows a decrease in flame temperature as LGR decreases.

Compared with UHC emissions, very little CO emissions accompany the co-combustion of biodiesel/methane and biodiesel/syngas. In the particular case of the biodiesel/methane combustion, the UHC and CO emissions have opposite gradients whereas in the biodiesel/syngas cases (90/10 and over) where they do demonstrate same gradient, the CO emissions are very minimal (<2 ppm).

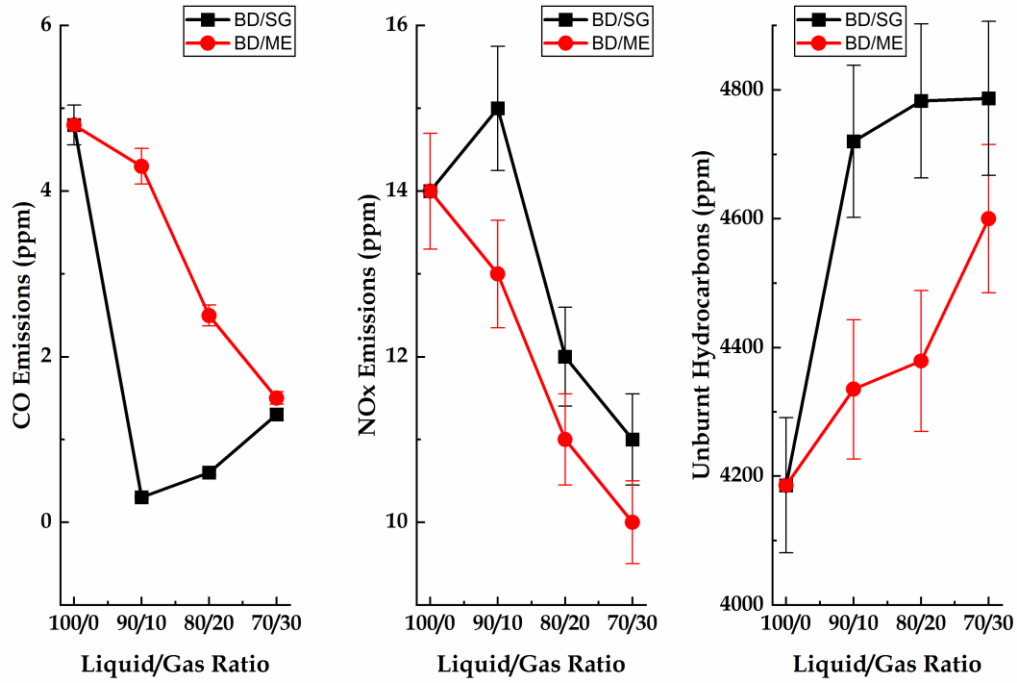

Fig. 6.14. Post combustion emissions from biodiesel/methane (BD/ME) and biodiesel/syngas (BD/SG) flames at different liquid-gas ratios.

Biodiesel/gas flames, very much like the diesel/gas flames in the last Chapter generally appears to burn in two combustion regimes if injected in the manner of this work. One combustion regime is dominated by lean premixed gas combustion, identifiable by the blue flame near and around the burner dump plane in the luminosity images (Fig. 6.6). The other is the orange-coloured liquid fuel-intensive diffusion regime which occurs further downstream and sustained in vitiated air, with some premixed oxygen having supported the methane combustion.

Assuming all of the gas was consumed, the resulting recirculating flow could contain, compared with the bulk combustion air in the 100/0 case, as much as 30% less oxygen for the liquid diffusion flame. Two things thus happen simultaneously: lean combustion of methane close to nozzle orifice plane and biodiesel spray burning in recirculating vitiated air. This may result in high UHCs and low CO emissions in line with the findings of Musculus et al [260]. Over and above that, as liquid flow rates drop with increasing gas ratio, the SMD of biodiesel droplets generated by the atomiser increases (Fig. 6.3) leading to longer timescales for evaporation and subsequent combustion. The chemiluminescence and binary images showed that at higher gas ratios, there appears to be a diminishing of the reaction zone so that the longer time required for the relatively larger droplets to vaporise and undergo combustion is unavailable. As a consequence, the unburned hydrocarbons emissions increase. Further, the opposite gradient observed for the two emissions in the 90/10 biodiesel/syngas case has been associated with the presence of relatively low temperature combustion regimes in flames [261].

6.5 Chapter summary

Biodiesel derived from waste cooking oil was combusted in a model swirl-stabilised gas turbine engine using a pressure atomiser to inject the fuel into the combustion chamber. Similarly, in the same combustor, different blends of biodiesel and methane or syngas, combined to deliver the same power output as in the neat biodiesel fuel test were combusted. The aim was to study multiphase fuel combustion in gas turbines using the fuels mentioned. The range of stable flame operation, flame stability,

reacting flow characteristics and post combustion emissions from the neat biodiesel combustion was compared with the multiphase combustion cases. The main findings from the study are:

1. Multiphase fuel combustion results in a reduction in the range of stable flame operation compared with neat liquid fuel combustion. The reduction in achievable stability limits is greater as gas ratio of fuel blend increases.
2. Chemiluminescence imaging of C_2* and CH* species in the flames show a variation in combustion zone properties as fuel compositions change. Among the biodiesel-gas dual fuel flames, the reaction zone area and length reduces as gas fraction increases suggesting an overall reduction in reactivity in the combustion zone. Equilibrium chemical kinetics calculations support this by predicting decreasing volumetric heat release rate and diminishing maximum flame temperature as gas fraction in fuel mix increases.
3. The temporal variation of radical chemiluminescence integral intensity suggest that multiphase fuel burn of biodiesel/gas in a swirl-stabilised gas turbine combustor promotes flame stability.
4. Flame luminosity images provide additional information on the reacting flow dynamics as gas fuel is introduced into the combustion air. Two combustion regimes become apparent with the gas fuel inclined to combust near and around the nozzle exit plane and the liquid fuel reacting further downstream.
5. Post combustion emissions of NOx, CO and UHC are impacted as methane or syngas partly replaces biodiesel in the combustion process.

7

EXPERIMENTS ON GLYCEROL COMBUSTION

In this chapter, the feasibility of glycerol as a blend component in gas turbine fuelling is explored. The fundamental combustion characteristics of single phase and multiphase blends of glycerol and other fuels is investigated using CH* species chemiluminescence primarily.

7.1 Introduction

Recently, the role of biodiesel as fuel in the energy industry has grown primarily because it is a sustainable fuel with proven performance in internal combustion engines. Produced to the appropriate standard (ASTM 6751 in the US and EN 14214 in Europe), biodiesel is accepted as a blend component with fossil diesel in the US and EU and is part of the energy mix globally [262, 263]. For instance, the blend mandate of biodiesel with fossil diesel in both Brazil and Argentina currently stands at 10% [264] while that of Indonesia stands at 20% in the transport and power sectors [265]. Buoyed by public opinion and driven by government support through favourable policies, subsidies and incentives [266], worldwide biodiesel production and use has soared over the last ten years [267, 268].

This upsurge in the production and use of biodiesel has, however, also resulted in an unprecedented amount of glycerol production. Glycerol being a by-product of the popular process of biodiesel synthesis – transesterification of animal fats or oily seeds [269]. It is estimated that 10 – 20% of the weight of biodiesel produced via the transesterification route is made of glycerol [122]. Thus, with increase in biodiesel production comes a rise in glycerol generation. In fact, the contribution of biodiesel process to glycerol production grew from 9% in 1999 to 64% in 2009 [270].

Crude glycerol from biodiesel synthesis by transesterification contains methanol as a major impurity and salts, water, free fatty acids and non-glycerol organic material as minor impurities [271]. The presence of a substantial amount of methanol in crude glycerol is because it is employed in excess of the required quantity in the transesterification reaction to ensure complete conversion of the reactants to biodiesel [272]. Although the methanol may be recovered and reused in the process, it is not often the case as it is cheaper to use a fresh supply [122].

When refined to high levels of purity, glycerol enjoys extensive use as raw material in food and pharmaceutical industries [273]. However, the recent upscale in glycerol production causes a surplus in supply which results in a shortfall in its demand in these industries hence its value. For instance, Yang *et al.* [274] notes that the price of refined glycerol in the US fell from $0.70 to $0.30 per pound in 2007 following the expansion of biodiesel production with crude glycerol prices falling from $0.25 to $0.05 per pound in the same time. Therefore, finding alternative value-added uses for glycerol is important as it will improve the economics of the biodiesel supply chain since biodiesel, as it stands, still requires huge government support to be competitive in the energy market [275].

A potential value-added alternative use of glycerol, explored in this Chapter, is its utilisation as fuel for gas turbines without significant modification of the combustor. A continuous flow engine with extensive fuel flexibility and available in micro (<200 kW) size, the gas turbine lends itself to such investigation. However, combustion of glycerol for useful thermal power generation is unattractive. For one, its physical properties notably high viscosity makes for inefficient flow through pipes and other narrow passageways that make up a typical fuel delivery system. This also impacts fuel atomisation – liquid spray breakup – as the flow exits a nozzle orifice; spray atomisation quality being directly related to combustion efficiency. Also, glycerol has a relatively low heating value. Typically about 16 MJ/kg, the lower heating value of glycerol is approximately half that of biodiesel and roughly 44% that of fossil diesel. This relatively poor energy density means a greater volume of glycerol needs to be combusted to obtain the same level of heat output as the more common fuels. Previous studies have tried to tackle these challenges by fuel preheating, use of novel nozzle designs and operating at low power output.

The present study attempts to circumvent the use of fuel preheating for viscosity reduction as it results in not just fuel coking [276, 277] but also, as discussed in Section 7.3, a considerable amount of heat loss that could potentially render the process impractical. Instead, to reduce glycerol viscosity, blending with methanol – a major impurity of crude glycerol from the transesterification process – was utilised. Again, to be more practical, the same nozzle as with the previous experiments discussed in Chapters 5 and 6 was maintained. When single phase burn had been achieved, in keeping with the theme of this thesis, the effect of introducing methane to the glycerol/methanol flames was investigated.

The overarching goal here was to investigate the feasibility of burning, in the unmodified combustion rig, a representation of crude glycerol and its blend with methane while simultaneously exploring its flame characteristics over the stable operating range. This was done through CH* species chemiluminescence imaging as well as by flame luminosity imaging. This allowed for an estimation and comparison of reaction zone properties like flame area, aspect ratio and lift-off height as equivalence ratio and blend composition were varied. Also, the intermediate combustion species chemiluminescence imaging allowed for flame stability comparisons based on the temporal fluctuation of species integral intensity. Post combustion emissions, however, were not measured because at the time of carrying out this study, the emissions analyser had failed.

To begin with, the Section 7.2 discusses why glycerol preheating prior to combustion, as done in many previous studies, is impractical. In Section 7.3, the basis for viscosity reduction by mixing with a thinner fuel is discussed and the choices of mixture fractions are made.

7.2 Demerits of preheating glycerol for viscosity reduction

Glycerol viscosity at 25^{o}C is 276 times that of fossil diesel at the same temperature (see Table 3.1). Therefore, to utilise it in an engine system designed for diesel would be impossible as pure glycerol would simply clog the pipes through which diesel was pumped and certainly the even narrower passageways in the injector. Nearly all published research on glycerol combustion overcame this problem by preheating (see

section 2.6.1.2). This involves raising the glycerol temperature by between 20°C and 70°C, presumably starting at room temperature. The problem with this is not just the associated fuel coking problems and the extra equipment required but also the heat loss involved in the process.

Fig. 7.1 shows the amount of heat required (in kW) to achieve different levels of glycerol temperature increment for every 1 kW power output from the fuel. Eq. (1) correlates power output with fuel flow rate based on its lower heating value (LHV). Eq. (2) calculates the heat requirement (Q) for a desired temperature change (ΔT) with c being the specific heat capacity of the liquid.

From Fig. 7.1, up to about 1% of the power output from the combustion of glycerol is spent on preheating if that is done to the levels reported in previous studies. Over and above this preheating heat loss is the heating equipment capital and maintenance cost. Besides these, preheating is associated with fuel coking problems as reported in earlier glycerol combustion studies. Granted, the heat requirement for preheating may not necessarily or in its entirety be an additional expense in the process as it could be obtained from exhaust gases in a form of heat recuperation.

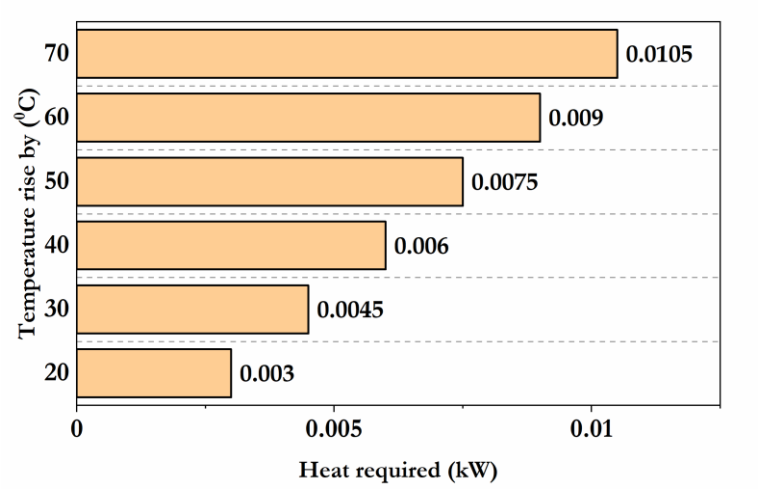

Fig. 7.1. Heat requirement for preheating glycerol to obtain 1 kW power from the fuel.

Nevertheless, as the exhaust heat has other more productive uses, the present study attained glycerol viscosity reduction by diluting the fuel with methanol rather than by fuel preheating. This eliminated all the aforementioned drawbacks of preheating and since, as noted previously, methanol is major contaminant of glycerol obtained from biodiesel synthesis hence, utilising it for thinning glycerol makes for a fuel blend that bears some likeness to crude glycerol obtained from the transesterification process. The target, then, was to generate methanol/glycerol blends with viscosities comparable to diesel at temperatures that diesel fuel may be practically utilised. This is further discussed in Section 7.3 after a theoretical analysis of liquid mixture viscosity determination and its temperature dependence.

7.3 Glycerol viscosity reduction

Liquid fuel viscosity at ambient pressure is known to decrease with an increase in temperature as well as by the addition of a low viscosity liquid diluent. Several correlations have been formulated to describe kinematic viscosity (ν) relationship with temperature (T) for liquids including the Arrhenius-type equation, the Andrade equation, the Avramov and Milchev equation and the Vogel-Fulcher-Tammann (VFT) equation. Generally, the equations take the form $\ln \nu = A + f(T)$ where $f(T)$ is an analytical function of temperature. Of these three parameter correlations, the VFT equation formulated as in Eqn. 7.1, has previously been found to be satisfactory in predicting the viscosity of glycerol [278], diesel [279] and methanol [280].

$$\ln \nu = A + \frac{B}{T + C} \tag{7.1}$$

Table 7.1. Fitting parameters for viscosity-temperature relationship

	A	B	C (K)
Glycerol [227]	-9.3998	2911.2	-118.2
Methanol [281]	-6.7562	2337.24	84.0853
Diesel [279]	-2.384	574.351	-140.27

In Eqn. (7.1), ν is the kinematic viscosity in units of mm^2/s of the liquid at temperature T in units of *Kelvin* whereas A, B and C are fitting parameters that are empirically determined. The values for these fitting parameters for the liquids considered are presented in table 7.1 having been taken from published literature that carried out extensive analysis based on experimental data to reasonably high levels of accuracy. Whereas the provided adjustable parameters leave ν in kinematic viscosity units (mm^2/s) for diesel, it renders that of glycerol and methanol in dynamic viscosity units of $mPa.s$. This is easily converted to kinematic viscosity by multiplying with the corresponding liquid density at the particular temperature.

For the blends of glycerol and methanol used in this work, Chevron's mixing rule based on the concept of the viscosity blending index (VBI) was utilised in predicting blend viscosity. The blend viscosity from the Chevron rule is a function of the volume fraction (V) of each constituent of the mixture and calculated according to Eqn. 7.2(a-c).

$$VBI_i = \frac{\log \nu_i}{3 + \log \nu_i} \tag{7.2 a}$$

$$VBI_{mixt.} = \sum_{i=1}^{n} V_i \times VBI_i \tag{7.2 b}$$

$$\nu_{mixt.} = 10^{\left(\frac{3 \times VBI_{mixt.}}{1 - VBI_{mixt.}}\right)} \tag{7.2 c}$$

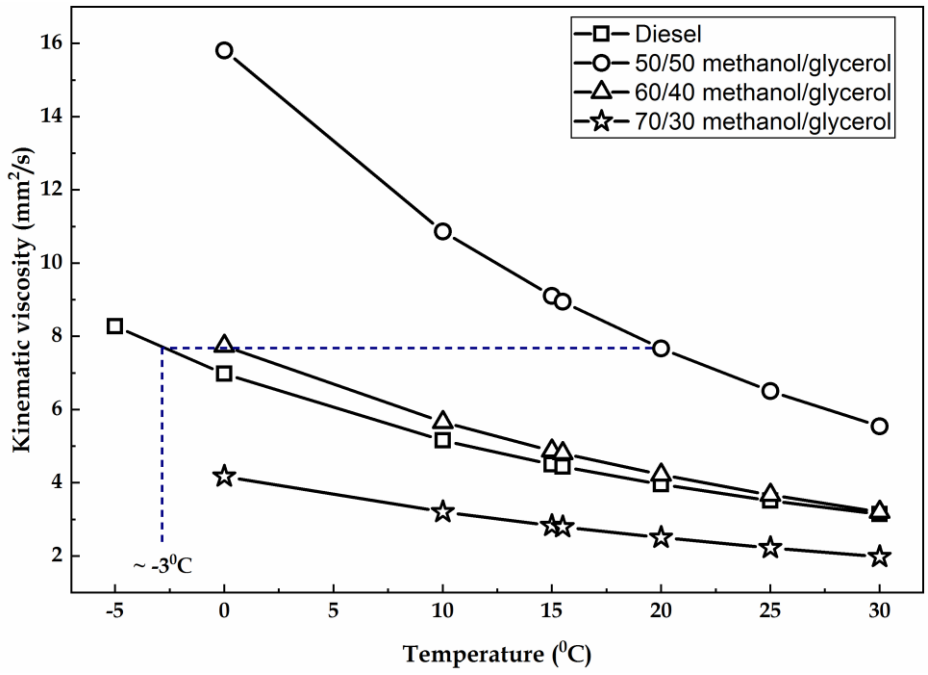

Fig. 7.2. Liquid and liquid mixture viscosity variation with temperature

The viscosity data graphed in Fig. 7.2 shows that a 60/40 (by volume) blend of methanol/glycerol is very similar to that of diesel over a wide range of temperatures. However, because the goal of the study was to utilise as much glycerol as possible, tests were carried out at 50/50 (by volume) methanol/glycerol mix rationalising that it has the same viscosity at 20°C as diesel at -3°C (Fig. 7.2). There will be no qualms burning diesel at -3°C with the existing experimental set-up. Nevertheless, in the interest of equipment safety and being that glycerol/methanol use in the burner is tantamount to entering uncharted territory, initial tests erred on the side of caution by using a 70:30 blend of methanol and glycerol.

7.4 Optical Emissions from methanol/glycerol combustion

7.4.1 Flame luminosity images

Initial trials showed that the reaction zone length of the methanol/glycerol blends were considerably shorter than those of diesel or biodiesel. Therefore, to situate the flame well within the region of optical access of the burner, the fuel nozzle was moved upward by about 20 *mm*. This was the sole modification made to the burner set-up for both the 70:30 and 50:50 cases and allowed for the reacting flow to be captured maximally. Besides that, the mixture flow rate through the nozzle was set so as to deliver a power output of 6 *kW* in both cases. The equivalence ratio (ER) of the flames was varied to capture the flame appearance over the widest possible stable range.

Fig. 7.3 shows the flame luminosity images for both cases over the identified flame stability range (between ER =0.29 and ER = 0.51). At ER = 0.51, the 70:30 blend presents with a long narrow flame that appears to be separated from the nozzle orifice plane. This separation becomes more evident as ER increases above 0.51 and eventually leads to flame blow out at ER>0.6. As air flow rate increases (decreasing ER), the 70:30 methanol/glycerol flame transitions from the narrow and separated-from-nozzle flame to a broader shape showing less separation from the nozzle. This transition point occurs at ER = 0.36. At 0.29>ER>0.36, the flame appears to be quite stable with no apparent changes in its shape or structure. Below ER = 0.29, however, the flame becomes flatter and highly unstable leading to lean extinction at an ER<0.23.

The 50:50 case does not demonstrate the extensive variation in flame shape seen in the 70:30 case as ER decreases neither does it undergo considerable lift-off prior to rich extinction. Both of these phenomena are markers of flame stability and their relative insignificance in the 50:50 flames in comparison with the 70:30 blend suggests that the greater glycerol content of the former improved the flame stability.

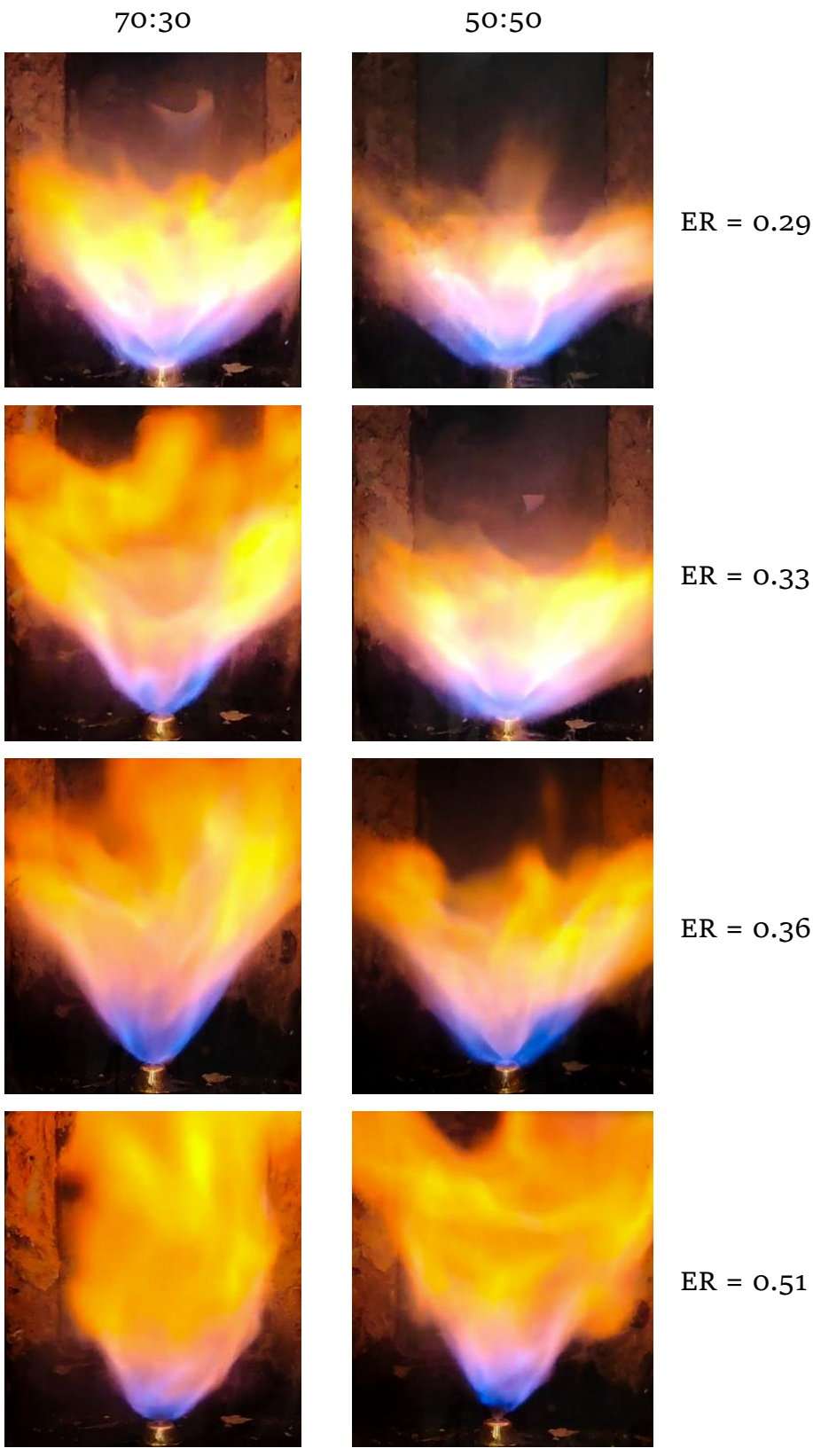

Fig. 7.3. Methanol/glycerol flame luminosity at different equivalence ratios

7.4.2 CH* species chemiluminescence

In this section, the CH* species chemiluminescence from 70:30 and 50:50 methanol/glycerol flames are presented highlighting the species distribution and reacting flow dynamics using CH* chemiluminescence.

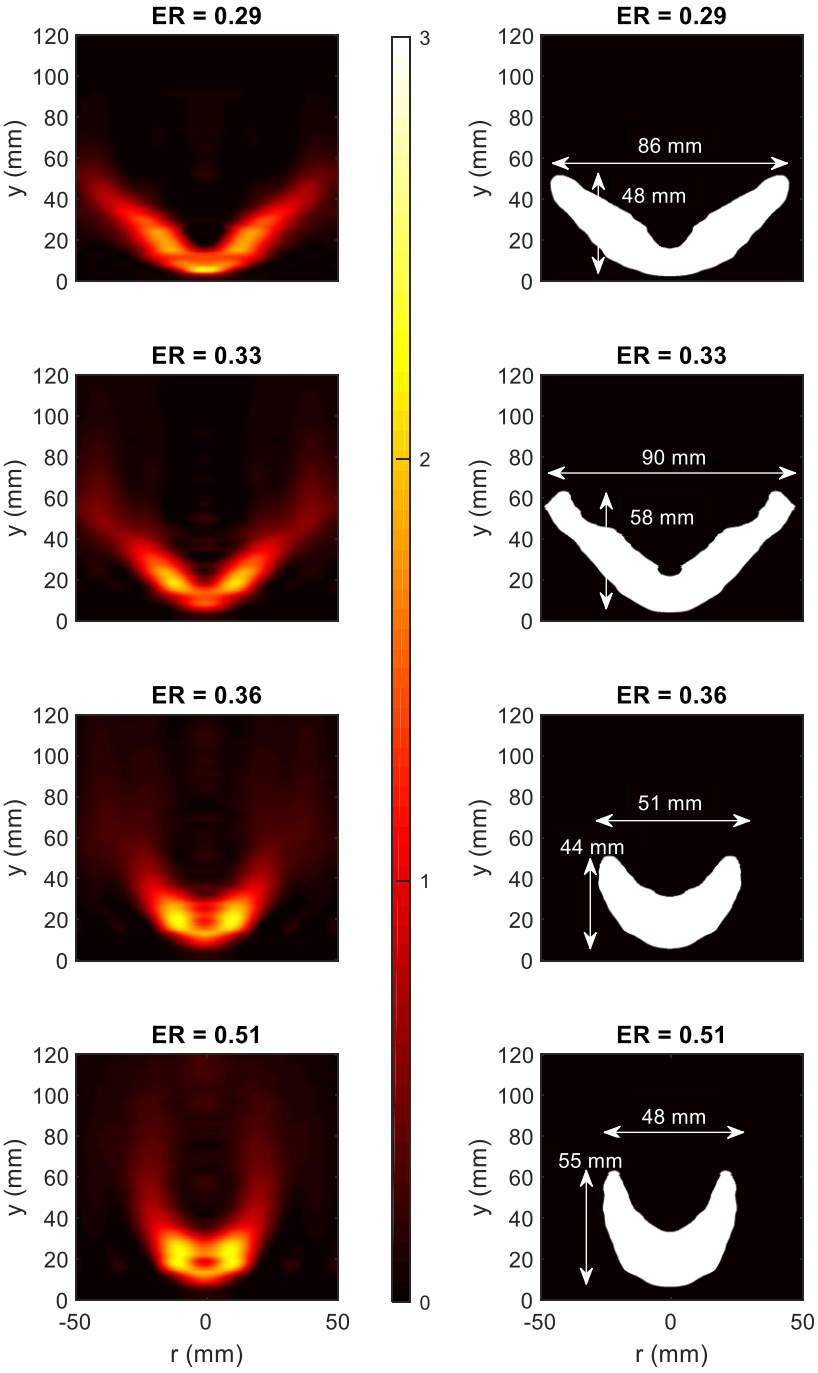

Fig. 7.4. Left column: Abel deconvoluted chemiluminescence images of CH* species in 70:30 methanol/glycerol flames at different equivalence ratios. Right column: Corresponding binary images. Flow is from top to bottom.

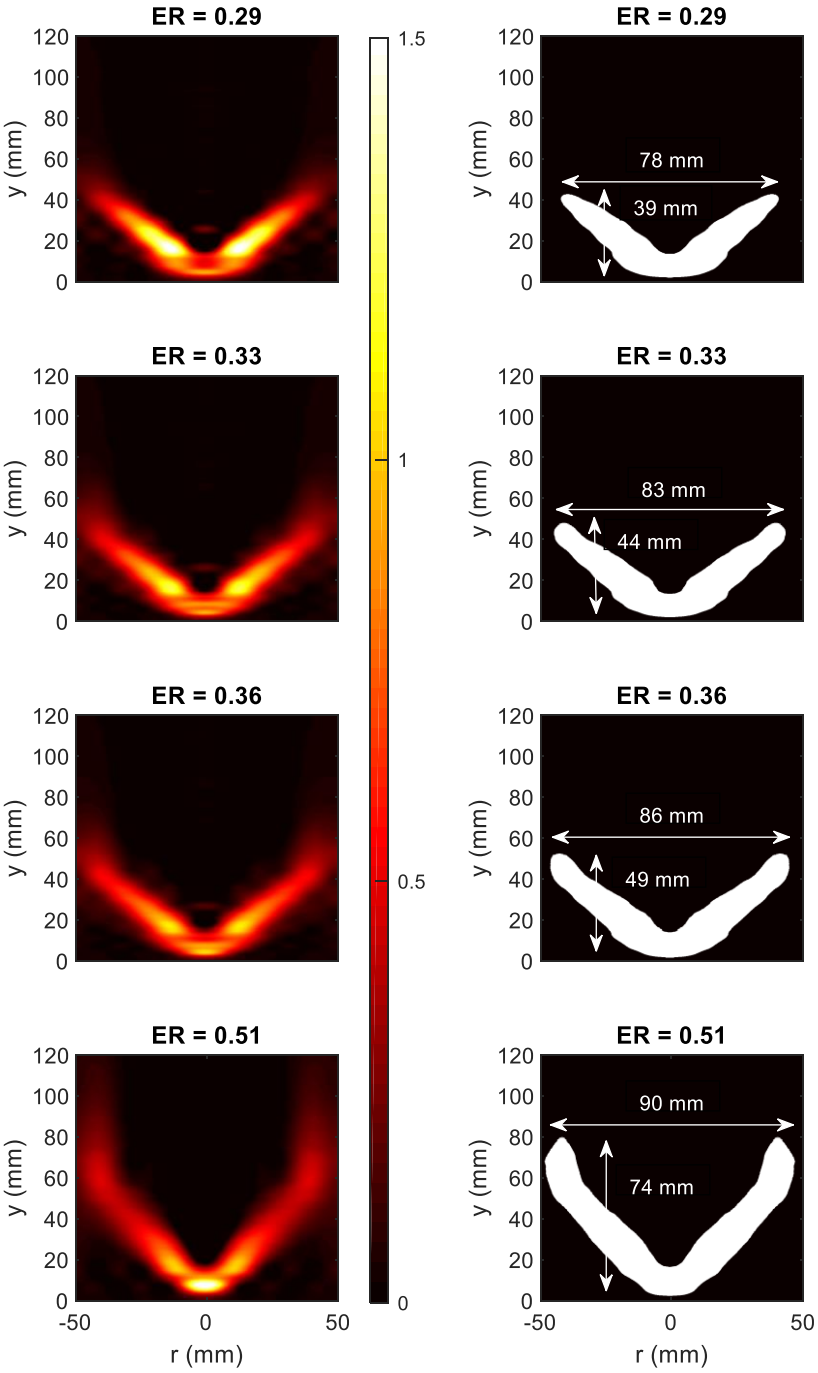

Fig. 7.5. Left column: Abel deconvoluted chemiluminescence images of CH* species in 50:50 methanol/glycerol flames at different equivalence ratios. Right column: Corresponding binary images. Flow is from top to bottom.

Fig. 7.4 shows the CH* species chemiluminescence from the 70:30 methanol/glycerol flame whereas Fig. 7.5 displays that of the 50:50 blend for corresponding ERs. Each figure is accompanied by a binary equivalent obtained from MATLAB processing as explained in Section 6.3.2.

7.4.2.1 Reaction zone properties

In addition to the reaction zone area and reaction zone aspect ratio (width/length), the variability in flame lift-off height has been highlighted in Fig. 7.6. As shown in the binary images of Fig. 7.5, the reaction zone length is estimated as the distance between the uppermost and lowermost unity pixels whereas the reaction zone width is represented by the distance between the unity pixels at the lateral edges of the binary image.

The reaction zone area is modelled as the sum of the unity pixels in the binary image while the flame lift-off height is considered to be the vertical distance, in the binary image, from the lowermost unity pixel to the $y = 0$ point on the image. Fig. 7.6 shows that a 70:30 blend of methanol and glycerol generates flames whose reaction zone properties vary widely as equivalence ratio is altered. The 50:50 blend of the same fuels, however, do not show such wide variation in reaction zone properties as air flow rate is changed. This observation is consistent with the flame luminosity images in which flame shape was noted to vary much more significantly with changes in ER for the 70:30 blend than for the 50:50 blend. Also, there was appreciable flame lift-off especially at the higher end of the practicable ER range for the 70:30 case relative to the 50:50 case and this, again, is in agreement with the data obtained from flame luminosity images.

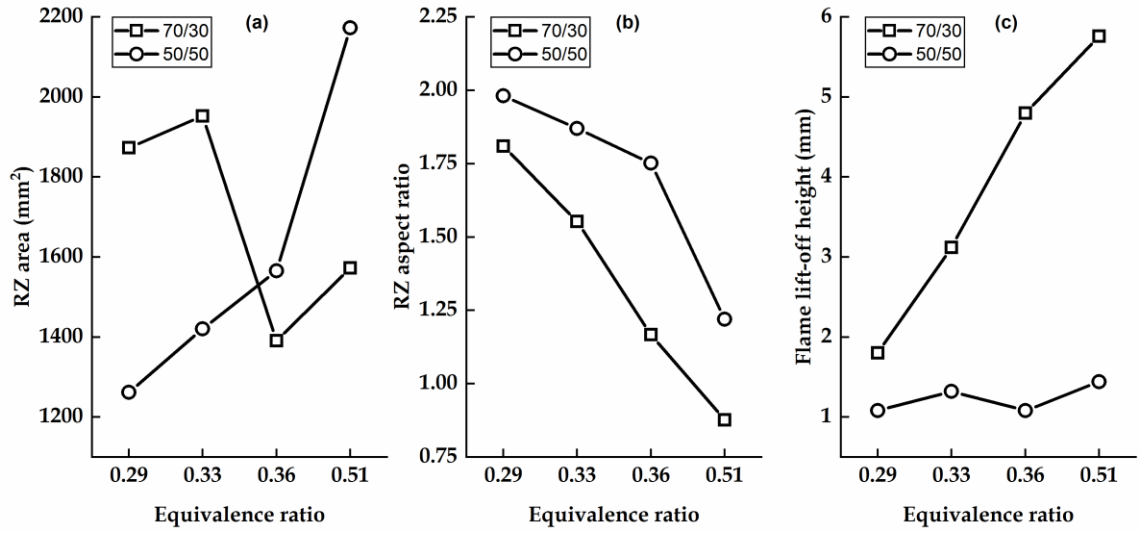

Fig. 7.6. Reaction zone (RZ) properties of methanol/glycerol blends

7.4.2.2 Flame stability

In the same manner as reported in Chapters 5 and 6, the stability of methanol/glycerol flames from the two blends (70:30 and 50:50) have been analysed. The idea, as noted previously, is to sum up the chemiluminescence species intensity for each of the 250 captured images and evaluate the temporal variation of each sum with the overall average intensity.

A greater variation of the intensity of the intermediate combustion species over the capture period would be indicative of a lesser stable flame. As an example, the temporal variation of the CH* species chemiluminescence intensity for the 70:30 case is shown in Fig. 7.7.

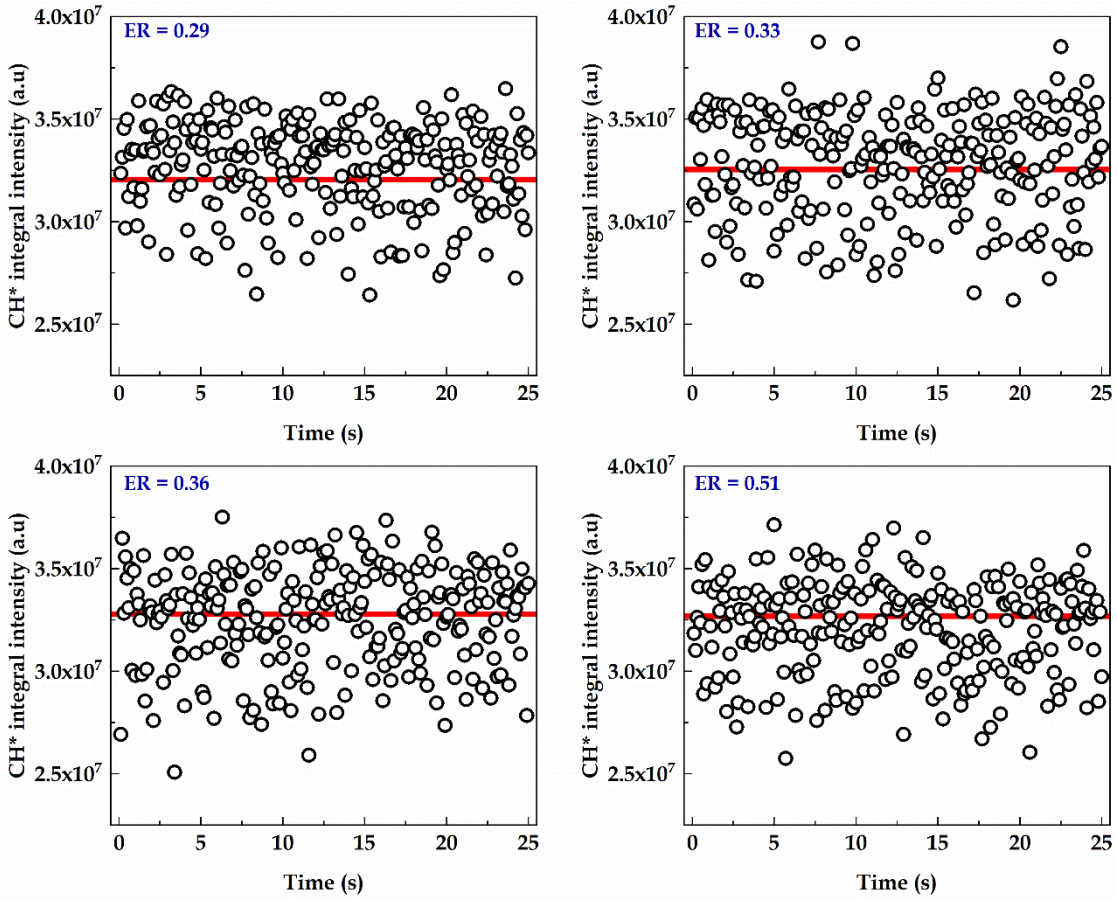

Fig. 7.7. Temporal variation of CH* species integral intensity from 70:30 methanol glycerol flames at different ERs

The solid red line in Fig. 7.7 indicates the average CH* species chemiluminescence intensity for the 250 images. This does not appear to vary very much as ER changes in each of the two test categories. However, across the two categories of tests (i.e. 70:30 and 50:50), there is a greater variation in the average CH* species chemiluminescence intensity.

Consequently, to enable a fair comparison of both sets of tests, the so-called coefficient of variation, *CoV* (standard deviation divided by mean) is used. The resulting data is shown in Fig. 7.8. From there, it is observed that flame stability is improved slightly as ER increases and that a 50:50 blend of methanol/glycerol generates flames that are of greater stability than a 70:30 blend across the range of stable flame operation of the fuels. This is in agreement with the observation from the flame luminosity images and the chemiluminescence images.

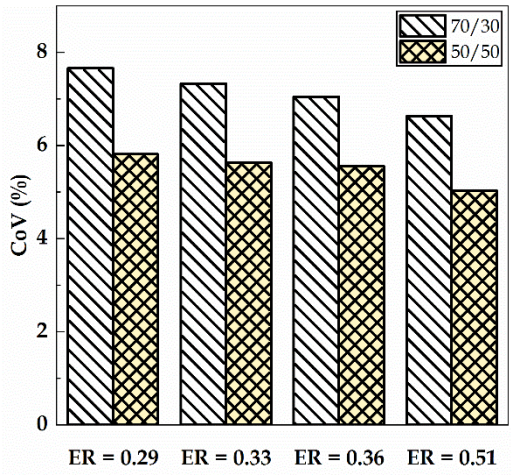

Fig. 7.8. CH* species chemiluminescence CoV for 70:30 and 50:50 methanol glycerol flames

7.5 Multiphase combustion trials

7.5.1 CH* species chemiluminescence imaging

Further tests were carried out by introducing 0.023 g/s of methane into the burning spray of methanol/glycerol for the 70:30 blend as well as the 50:50 blend. This adds an extra 1 kW to the heat output. The ER designations are maintained as before: considering the liquid fuel blend only.

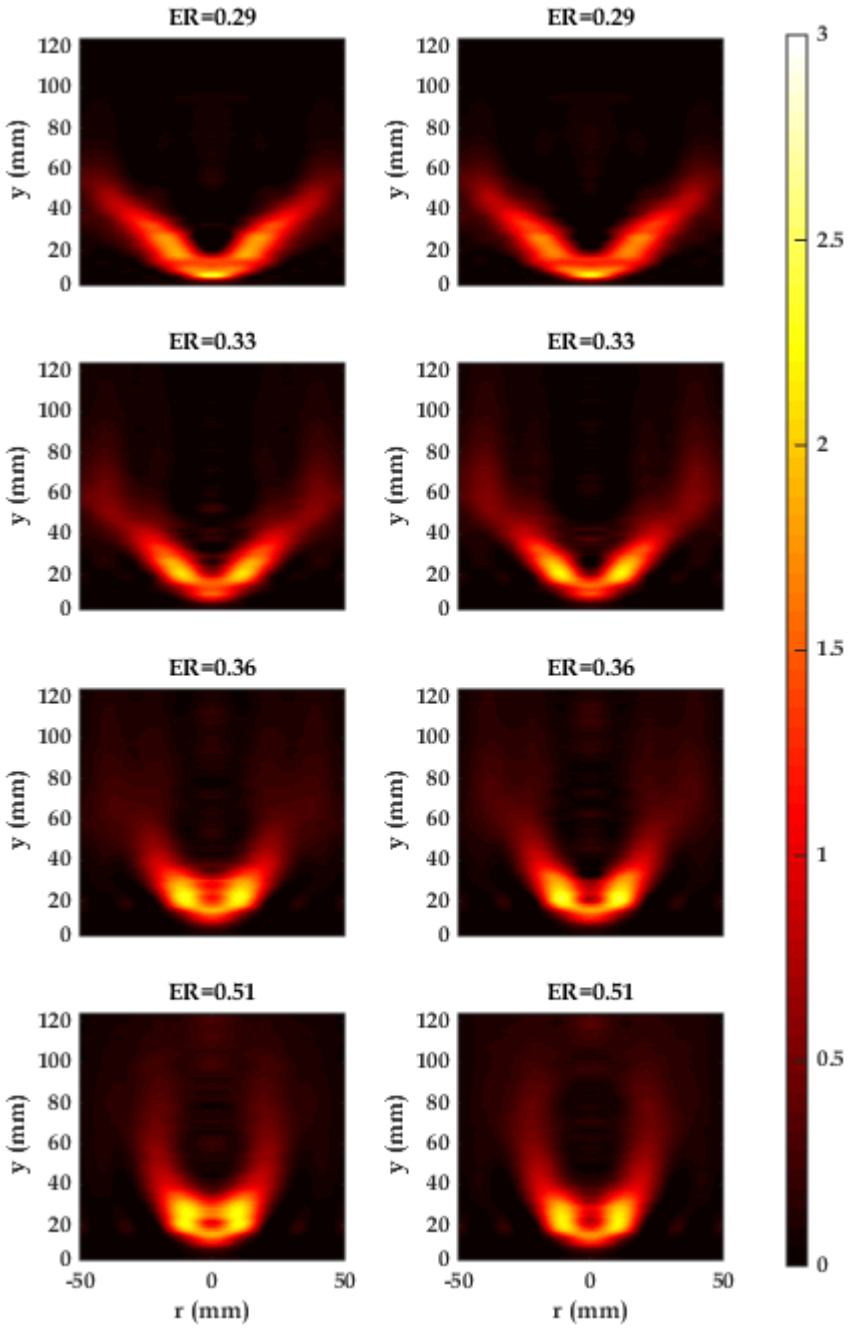

Fig. 7.9. Left column: Abel deconvoluted CH* chemilumnescence images of 70:30 methanol/glycerol flames at different ERs. Right column: Corresponding images for multiphase case with methane.

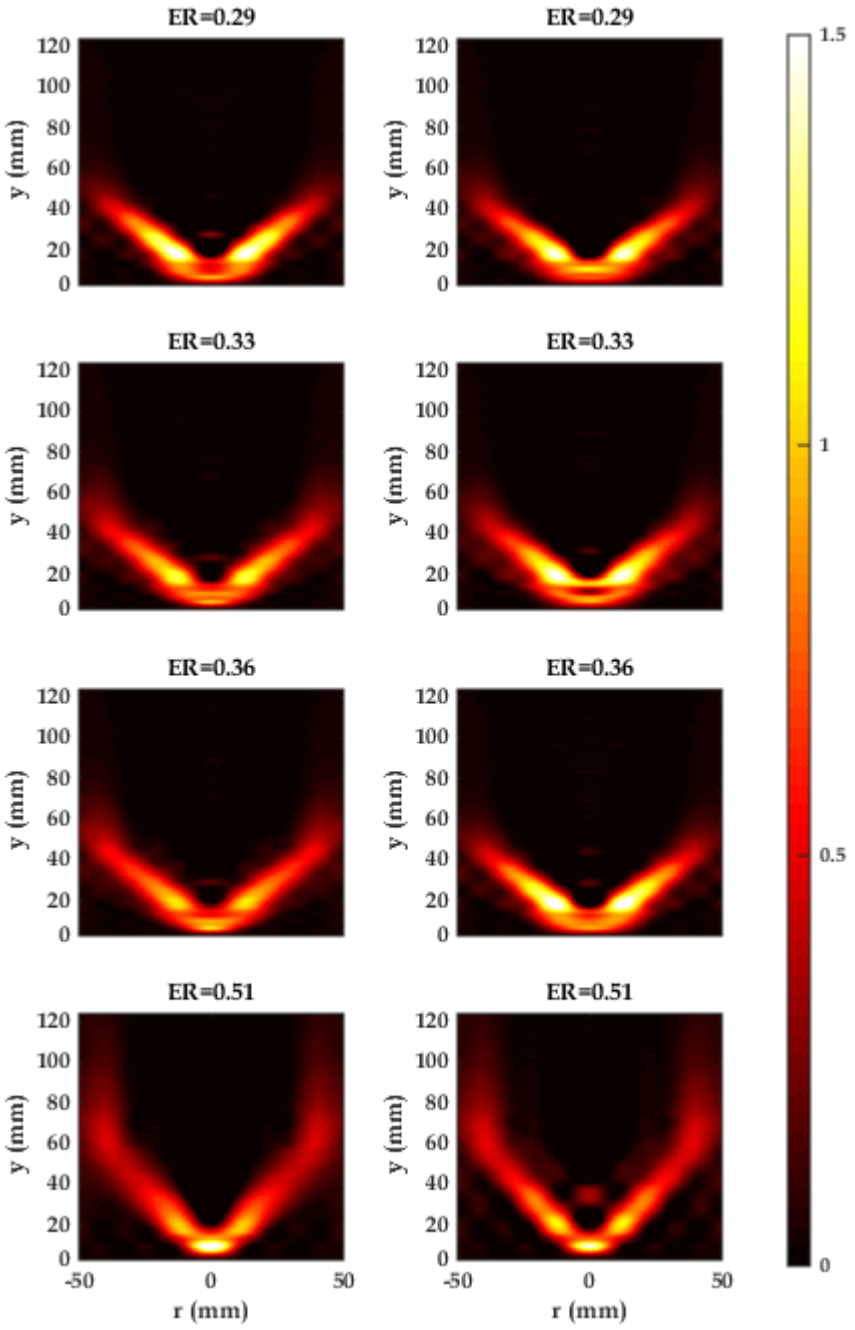

Fig. 7.10. Left column: Abel deconvoluted CH* chemiluminescence images of 50:50 methanol/glycerol flames at different ERs. Right column: Corresponding images for multiphase case with methane.

The aim was to, in continuation of the main theme of this work, study the effect of multiphase fuel combustion on gas turbine combustor performance using CH* species chemiluminescence. Fig. 7.9 presents the CH* species chemiluminescence images for the 70:30 blend of methanol/glycerol with methane (left column) and without methane (right column).

The ERs stated on each image does not refer to the global ER but that of the blend of liquid fuels. The corresponding CH* species chemiluminescence images for the 50:50 blend is shown in Fig. 7.10.

It would appear from the images that introducing methane into the methanol/glycerol flames does not result in a considerable difference in CH* species distribution or intensity. The next section offers a quantitative evaluation of the effect of methane injection into the flames of the liquid blend in the context of reaction zone area, aspect ratio, flame lift-off height and flame stability.

7.5.2 Reaction zone properties and flame stability

The RZ characteristics of the fuel combinations with methane (w CH_4) are shown in Fig. 7.11. These have been derived, similar to Section 7.4.2.1, from binarisation of the chemiluminescence images. The corresponding methanol/glycerol flame characteristics without methane (w/o CH_4) as in Fig. 7.6 are included in Fig. 7.11.

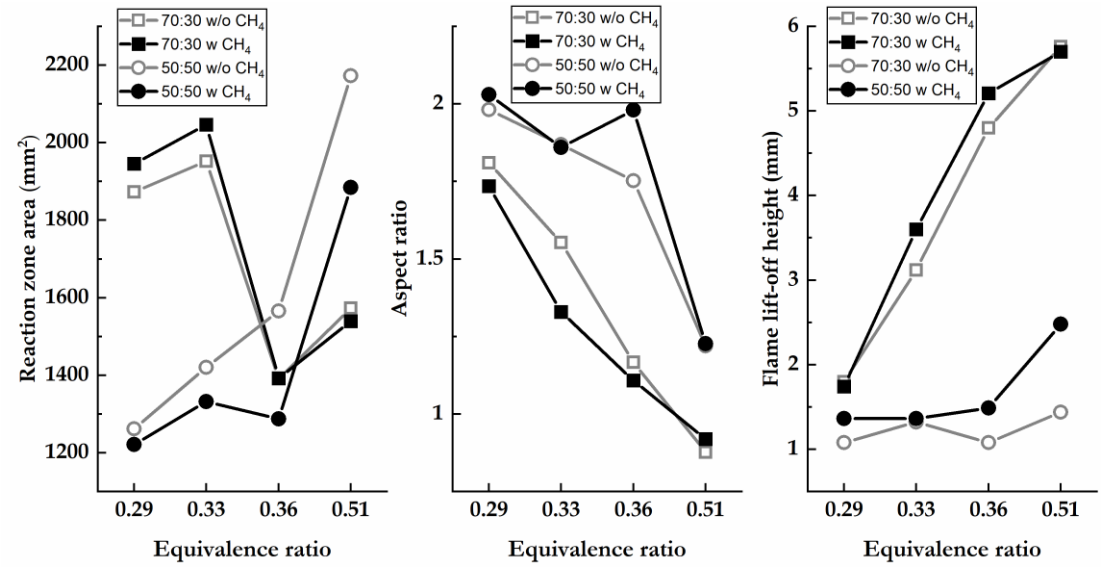

Fig. 7.11. Flame characteristics of multiphase combustion of methanol/glycerol blends with methane compared with single phase combustion.

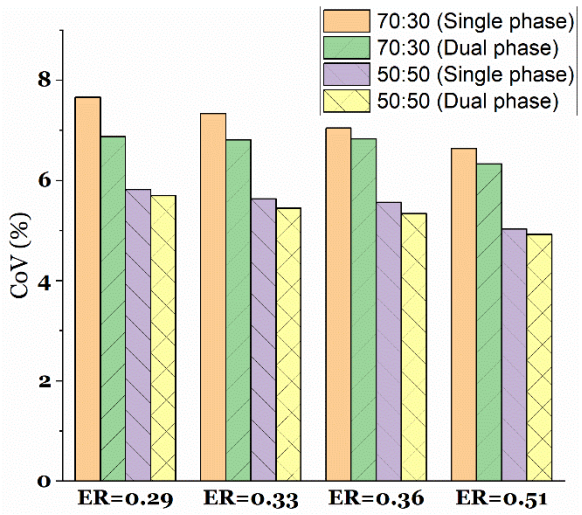

Fig. 7.12. Flame stability comparison between single phase and multiphase combustion.

Comparing the single phase and dual phase combustion cases, there is very little difference in flame presentation particularly in the 70:30 case. This is also evident in the multiphase combustion chemiluminescence images shown earlier. More significant variation in reaction zone area and flame lift-off height was observed in the 50:50 methanol/glycerol combustion with methane compared with the liquid fuel blend combustion. Reaction zone area decreases over the four conditions tested with the multiphase fuel combustion compared with single phase combustion. The most significant difference in flame lift-off height for the 50:50 case occurred in the highest ER tested. Leaner conditions should therefore be the target for this sort of blend in practice. However, this lift-off height is minimal compared to that experienced by the 70:30 blend at the same conditions.

Further, using the same approach as in Section 7.4.2.2, the flame stability for the single phase and dual phase combustion cases were compared in Fig. 7.12. It appears that addition of methane to the combustion of glycerol blends only leads to marginal improvement in flame stability in both blends. This trend – higher portion of gas in fuel lowers CoV – agrees with earlier work.

7.6 Chapter summary

As interest in biodiesel production and utilisation in combustion system grows, so does the production of glycerol. Extensive purification of glycerol is required for most of the current applications of this by-product of one of the most popular biodiesel production processes. To improve cost-effectiveness while maximising glycerol utilisation, alternative uses of crude glycerol must be explored. A major contaminant in glycerol obtained from biodiesel synthesis via transesterification of animal fats and oil vegetables is methanol which is used in excess in the process. To roughly simulate and simultaneously improve crude glycerol combustion properties, methanol was blended with pure glycerol and tested as fuel in a model swirl-stabilised gas turbine combustor. A 70:30 blend of methanol and glycerol as well as a 50:50 blend was combusted in the model burner with only minor modification of the set-up. The main findings from the study are:

1. Mixing methanol with glycerol improves the viscosity of glycerol and a 60:40 (by volume) blend of methanol/glycerol has very similar viscosity to diesel over a practical temperature range.
2. Lean and rich flame extinction range for 70:30 (by volume) and 50:50 methanol/glycerol blends occurs at low equivalence ratios (approximately 0.2 – 0.6).
3. A 50:50 blend of methanol/glycerol shows greater flame stability compared with a 70:30 methanol/glycerol blend as evidenced by flame luminosity and from CH* species chemiluminescence data analysis.
4. Simultaneous combustion of the tested methanol/glycerol blends with methane does not significantly alter flame characteristics or flame stability. Marginal improvement in flame stability was recorded across both blends with the addition of methane.

8

GENERAL DISCUSSION

This chapter highlights the main points that stand out from the conducted research and presents the author's position regarding practical application of the research.

8.1 Multiphase fuel combustion in gas turbines: operability

Stable flames in a gas turbine relevant burner were achieved with different liquid and gas fuel blends. Conventional fuels like diesel and methane as well as alternatives like biodiesel, syngas, methanol and glycerol were all successfully trialled by injecting the liquid fuels with a pressure-swirl atomiser and premixing the gaseous one with the combustion air. The fuels were combined based on the concept of energy share ratio in such a manner that a desired power output was achieved partly by the heat content of the liquid fuel and partly by the gaseous fuel. Two keys areas of operability were investigated: flammability limits and flame stability in multiphase fuel combustion.

8.1.1 Flammability limits

The following figures (Fig. 8.1 and Fig. 8.2) exemplify the alteration in the range of stable flame operation as combustion mode is changed from neat liquid fuel burn to an 80/20 liquid/gas ratio (LGR) dual-phase burn for diesel and biodiesel blends with methane and syngas. Both Fig. 8.1 and Fig. 8.2 are obtained from flame extinction data for an overall thermal power output of 12 kW from diesel/methane, diesel/syngas, biodiesel/methane and biodiesel/syngas flames; the trend is similar over a wide range of thermal power outputs. Consistently, it is observed that simultaneous combustion of the listed liquid and gaseous fuel combinations in a 15 kW burner following the injection strategy described in the work reduces the range of stable flame operation.

There are two inter-related factors that causes the observed reduction in flammability limits. First, the liquid fuel injection strategy utilised induces a decrease in pressure drop across the nozzle as LGR decreases which in turn leads to a deterioration of liquid spray quality from the nozzle. Associated with this loss in spray quality is a decline in the rate of spray evaporation. Burning rates are thus negatively affected – a fact supported by chemical kinetics calculations which indicate a reduction in the rate of heat release as LGR decreases. Thus, as the liquid fuel is partly replaced by gaseous fuel, the rate of heat generation which is important for sustaining flames diminishes and as a result flammability limits reduce. The second reason for this observed reduction in limits of flammability is about the variation of the reacting flow dynamics as LGR is altered. From the intermediate combustion species chemiluminescence images obtained, it was observed that as liquid flow rates decrease and gas flow rates increase, the reaction zone shifts away from the central axis of the burner towards the edges. This would mean that the liquid fuel spray which is initially concentrated within a 60° cone around the burner centreline (based on the atomiser design) has to diffuse to the edges of the burner in order to be consumed. Diffusion of the spray to the preferred reaction zone is made more difficult as the spray droplet sizes are larger and the evaporation timescales greater with decreasing LGR. As a consequence, the limits of stable flame operation are curtailed as LGR decreases.

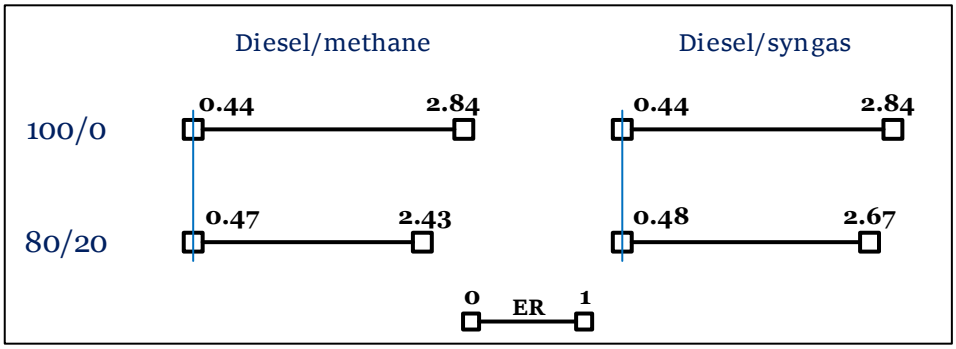

Fig. 8.1. Diesel/methane and diesel/syngas ER range at different LGRs.

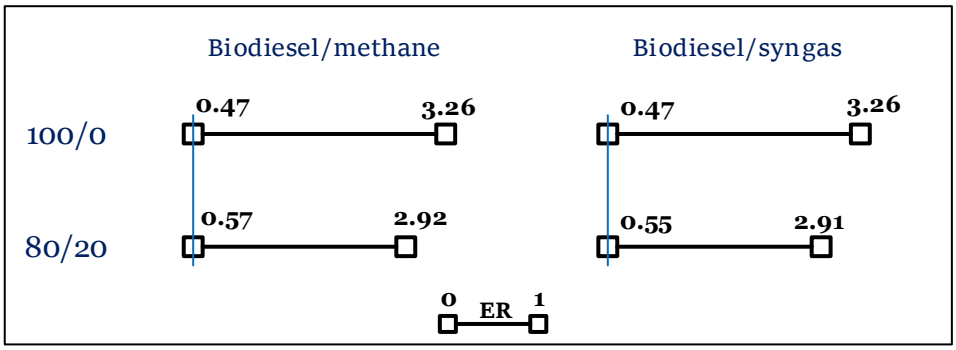

Fig. 8.2. Biodiesel/methane and biodiesel/syngas ER range at different LGRs.

Reduction in stability limits at both the fuel-rich and fuel-lean ends of the range implies a quicker onset of flame instability phenomena like flashback and blow-out should operation shift in either direction. This is an undesirable attribute as the operational domain of gas turbine engines, for reliability and safety reasons, must be as far away from the onset of any instabilities that potentially lead to flame-out.

8.1.2 Flame stability

As for flame stability at a particular operating point, an equivalence ratio of 0.7 and a total power output of 15 kW for the diesel/gas and biodiesel/gas cases, the temporal variation of the rate of heat release was key. Flames are more stable when the fluctuation of the rate of heat release from the combustion process is minimal. Comparisons of these fluctuations were made for the different multiphase fuel combustion tests using the species chemiluminescence data. Although the magnitude varied, the trend stayed the same in all cases: a steady improvement in flame stability with increasing gas content in fuel blend.

The reason for the improvement in flame stability with increase in gas content of fuel mix is because of the formation and growth of a gas combustion regime as gas fraction in combusted fuel grows. This gas combustion regime being locally lean is predominantly blue in appearance and is situated just downstream of the liquid fuel nozzle exit plane. Its formation and location introduce heat early on in the combustion zone which, in addition to the recirculated heat due to the swirling flow, promotes liquid fuel flame anchoring and stabilisation. Improved flame stability is observed when the multiphase cases are compared with the neat liquid fuel burn except in the 90/10 cases involving syngas where neat liquid fuel combustion is superior in terms

of flame stability. This anomalous behaviour was attributed to the nature of syngas. It would seem that at the low gas fraction offered by 90/10, the formation of a separate gas-dominated combustion zone for blends involving syngas is not possible allowing majority of the gas to escape and react further downstream. This perturbs the liquid fuel spray reaction zone thereby impacting on flame stability.

The other tested fuel combination, a 50/50 and 70/30 (by volume) blend of methanol/glycerol was not co-combusted with a gaseous fuel over a range of LGRs. However, a quantity of methane amounting to approximately 14% of the total heat output was co-combusted with each of the blends. The blends were each set to deliver 6 kW of thermal power and a total heat output of 7 kW with methane addition. As with the other fuels, the introduction of methane led to improvement in flame stability in both blends albeit marginally in this case. The stand-out feature from an operational perspective with the combustion of the glycerol blends was the range of stable flame operation attainable. Flames of this fuel blend remained alight only within an equivalence ratio range of 0.2 – 0.6. This is interesting because, even though it is a comparatively narrow range, stable ultra-lean combustion was possible with the glycerol blend. Burning what is inherently a highly oxygenated fuel blend in ultra-lean conditions augurs well for emissions. Another interesting observation from the methanol/glycerol/methane flames related to stability, was the extensive variation in aspect ratio and a significant lift-off of the flame from its anchor point next to the nozzle (when operating at the upper end of the stability range). The prolonged flame detachment before blow-out was more noticeable in the 70/30 methanol/glycerol blend compared to the 50/50 blend indicating that methanol, as opposed to glycerol, may be responsible for the phenomenon. Given the relatively small range for which stable flames are obtainable from the blends, adequate control of equivalence ratio is therefore important if the blend is deployed in practical systems.

8.2 Multiphase fuel combustion in gas turbines: emissions

Post combustion emissions of CO, NO_x and UHC were reported for the tested fuel blends except for the glycerol tests. In both the multiphase diesel/gas and biodiesel/gas combustion cases, emissions of NO_x consistently declined as gas fraction in the blend increased. This is down to decreasing flame temperatures and residence time as noted in chemical kinetics and chemiluminescence data. For the same reason,

CO emissions are on the increase with increasing gas content in combusted fuel for both diesel blends and the biodiesel/syngas blend. However, for the biodiesel/methane case, CO emissions consistently decrease as LGR decreases. It is difficult to suggest any reason for this behaviour but it has to be noted that very small CO emissions result from the biodiesel blends (<5 ppm) – close to the lower limit of the measuring equipment.

UHC emissions show a decline as LGR decreases in the diesel/methane and diesel/syngas flames but an increase in the biodiesel blends. By comparison, the UHC emissions dwarf the CO emissions in both cases and in some instances assume an opposite gradient to CO emissions. The relatively high UHC emissions from the flames are likely due to the fact that with the formation of a distinct gas combustion regime next to the nozzle, downstream air becomes poorer in oxygen content leading to combustion inefficiency in the form of UHC which is further worsened by the degradation of liquid fuel spray quality as LGR decreases.

8.3 Emerging lessons and perspective

Energy consumption is both the stimulus for and consequence of economic development. As a result, energy security – the uninterrupted availability of energy – is to the economy of nations what food security is to their health. However, economic expansion has an inverse relationship with the quantity of non-renewable energy reserves. At the same time, never has the need to green the energy industry been more urgent. As such, alternative sources of energy particularly those of the renewable kind have been explored to avoid over-reliance or complete dependence on a single source. Accordingly, fuel flexibility is an increasingly attractive attribute of secondary energy generators such as the combustion turbine.

The present study has shown that the fuel flexibility of the gas or combustion turbine is not limited to the single-phase blends of different fuels that previous studies have focused on. The present study demonstrates the feasibility of multiphase fuel combustion by trialling several liquid/gas fuel blends with minimal or no experimental rig modification. It further showed that comparable, and in some cases, even better post-combustion emissions performance result from multiphase fuel burn

when compared with neat liquid fuel combustion. And whereas the range of stable flame operation is reduced in multiphase combustion cases, flame stability at a stable operating point is improved as the rate of liquid fuel substitution for gaseous fuel is increased.

All three sets of experiments on multiphase fuel combustion in a gas turbine relevant combustor, reported in Chapters 5, 6 and 7, merit consideration for practical application in gas turbine settings. However, one stands out as more remarkable than others for reasons of novelty. Glycerol combustion for energy generation is not new but often it is made ready for the process by preheating. Besides causing undesirable issues such as fuel coking, preheating results in energy losses that far outweigh the energy gains from combusting the glycerol. In Chapter 7 it was proved that it is technically feasible to utilise glycerol as fuel in combustors designed to work with conventional fuels and, crucially, without preheating. Of course, blending with methanol was necessary for viscosity reduction but crude glycerol from biodiesel production typically contains a good amount of methanol which is not economically attractive to recover. Methanol itself can be synthesised from renewable hydrogen and CO_2 captured from atmospheric air [282, 283] making the liquid fuel blend not just entirely renewable but also one that is partly derived from waste (glycerol and CO_2 are mostly process by-products and largely considered wastes). And since the methanol/glycerol flame is stable in the ultra-lean region, controlled addition of gas fuel will improve glycerol/methanol heat output without either driving overall ER above 1 or, as the present work shows, significantly perturbing other combustion characteristics. It would appear, then, that there exists sound technical, economic and environmental cases for glycerol/methanol blend utilisation in practical gas turbines.

Also, biodiesel/gas co-combustion appears primed for deployment in existing systems. Not only does co-combustion of biodiesel and methane result in lower CO and NO_X emissions (also lower compared to fossil diesel) with increasing gas ratio but also the flexibility of decentralising biodiesel production stations offers an additional advantage. If the biodiesel plants are sited where gas lines are accessible, then this can be tapped and co-combusted with the biodiesel in a combustion turbine for distributed power generation. Distributed generation – where power generation is close to the load [284]– is touted as the best solution for meeting electricity needs of the developing world because it circumvents the large capital investments required

for grid infrastructure [285]. Utilisation of biodiesel/gas in combustion turbines for distributed generation will find wide application in Nigeria, for instance, where there is no shortage of biodiesel feedstock in areas with gas infrastructure [286].

The future of gas turbine fuelling, taking into account environmental sustainability and energy security, lies in increasing the relevance of alternatives like biodiesel and glycerol/methanol and propping them up with gases in a multiphase combustion approach. However, there is a key limitation in the present work. The experiments were conducted under atmospheric conditions whereas real gas turbines operate under elevated temperature and pressure conditions. Multiphase combustion performance under these conditions needs to be investigated. Also, it will be interesting to determine the effect of the secondary air system in actual gas turbines on emissions, particularly UHCs and CO.

9

CONCLUSIONS AND FUTURE RESEARCH

This chapter summarises the work carried out and reported in this thesis. It also offers, as a consequence of the present study, a few recommendations for future research.

9.1 Conclusions

The main goal of this work was to design and implement co-combustion of liquid and gaseous fuels in a swirl-stabilised model gas turbine combustor. This would serve to expand the fuel flexibility of the gas turbine to include multiphase fuel burn while allowing for the effect of such multiphase fuel combustion on flame characteristics and emissions performance to be investigated.

Consequently, a gas turbine relevant burner system was designed and successfully ran on blends of diesel/methane, diesel/syngas, biodiesel/methane and biodiesel/syngas. The experimental set-up allowed a stable combustion of up to a 70/30 combination of the liquid/gas fuel. Fuel combination was based on energy share ratio such that a 70/30 liquid-gas-ratio (LGR) meant that the liquid fuel flow rate was set to deliver 70% of the desired overall thermal power output while the gas was supplied at a rate that delivers 30% of the overall power output; the thermal power output being based on the LHV of the fuels.

The results showed that a 90/10 blend of the above listed fuels proved to have a narrower flame stability range than the corresponding neat liquid fuel combustion. The 80/20 blend of the fuels demonstrated even narrower flame stability range compared to the 100/0 and 90/10 cases suggesting that, with the injection strategy employed, increasing the gas content in dual phase gas turbine combustion results in a decrement in the range of stable flame operation.

Conversely, for the above listed fuel combinations and at an overall thermal power output of 15 kW and a global equivalence ratio of 0.7, flame stability was found to improve among the multiphase cases as LGR decreased i.e. as gas fuel contribution to thermal power output increased. An estimation of the flame stability was made using the temporal variability of the integral intensity of both CH* and C_2* species chemiluminescence from the flames.

Further, both CH* and C_2* species chemiluminescence showed a variation in signal intensity as fuel LGR was altered. Among the multiphase cases, a reduction in signal intensity was observed as LGR decreased. Also, the Abel deconvoluted images, obtained by mathematically resolving the raw chemiluminescence images, showed consistent variation in shape as fuels changed from neat liquid fuel burn to dual phase fuel combustion cases. This points to a variation in reacting flow dynamics as combusted fuel composition changes.

Moreover, measurements of post combustion emissions from diesel/methane, diesel/syngas, biodiesel/methane and biodiesel/syngas flames were taken. It was observed that, to a greater or lesser extent, NO_X emissions decreased and CO emissions increased as LGR was decreased from 100/0 to 70/30 in steps of 10. Compared to CO emissions, very high unburned hydrocarbon emissions were observed and, in some cases, the CO and UHCs were of opposite gradients. These effects on emissions was attributed to a combination of the following (1) variation in liquid fuel spray atomisation quality (2) changing reacting flow dynamics and temperature distribution in the combustion zone occasioned by the apparent separate combustion regimes of liquid and gas fuels.

Besides the aforementioned fuel blends, this work trialled the combustion of two blends of methanol/glycerol (70/30 and 50/50 by volume) with only minimal modification of the experimental set-up. Notably, unlike in several previous studies on glycerol combustion, fuel preheating was not applied in the present study and a standard pressure-swirl fuel injector was utilised. It was observed that the stable operating range of these fuel blends was in the fuel-lean region, roughly between 0.2 and 0.6 equivalence ratios. The 50/50 blend showed greater flame stability than the 70/30 blend across four points selected within the stable operating range with flame stability improving with increase in equivalence ratio in both blends. Further, simultaneous combustion of the tested methanol/glycerol blends with methane was

found to not significantly alter flame characteristics and resulted in improved flame stability albeit marginally.

Reaction zone properties of methanol/glycerol flames namely reaction zone area, flame aspect ratio and lift-off height show greater variation over the stable operating region for the 70/30 blend compared with the 50/50 case. In both cases, at the higher end of the range of stable flame operation, flames were observed to undergo considerable lift-off and separation from the nozzle prior to blow-out; this was more evident in the 70/30 case than in the 50/50 case as previously noted. Addition of methane to the combustion of the liquid fuel blend in air influenced this phenomenon only marginally in the 70/30 category and in all but one of the 50/50 cases.

The main significance of this work lies in its use of standard parts in a representative combustor to carry out multiphase combustion of practical fuels. This, as far as the author is aware, is the first such work in the area. It covered system operability range and factors affecting it as well as regulated emissions performance (i.e. NO_X and CO).

9.2 Recommendations for future research

In the entirety of the experimental study forming this thesis, liquid fuels were introduced into the combustion chamber via a pressure-swirl nozzle while the gaseous fuel was premixed with the combustion air upstream of the nozzle. It will be interesting to investigate the effect of utilising a different injection strategy. For instance, an air-blast nozzle or an air-assist pressure atomiser for liquid fuel injection may affect spray quality as LGR decreases in such a manner that a 60/40 and/or a 50/50 blend of diesel/gas and biodiesel/gas combustion can be achieved and explored. Also, an effervescent atomiser can be employed and with that, the gas fuel can possibly be partly or wholly bubbled into the liquid fuel in the mixing chamber for atomisation purposes. Of course, with twin-fluid atomisers, the right liquid to atomising gas ratio is crucial for atomiser efficiency and if the combustion air is tapped off for fuel atomisation, both the reacting and non-reacting flow dynamics including flame front stabilisation will be perturbed to some extent. These would need investigating as well.

It will also be interesting to, with the present set-up or indeed with any other injection strategy, image the temperature distribution of the reaction zone area of the different

fuels tested. This could be achieved using nonlinear excitation regime two-line atomic fluorescence (NTLAF) which is a promising two-dimensional thermometry technique for turbulent sooty flames. Information from this could aid in further understanding the unusual CO and UHC relationship encountered in the present study.

Moreover, as mentioned in Chapter 8, the present study was carried out under atmospheric conditions and at best represents the primary combustion zone of a real gas turbine. Future work in this area should attempt similar experiments under gas turbine conditions – elevated temperature and pressure as well as the utilisation of secondary air systems.

Further, the scope of research in multiphase fuel burn in combustion turbines could be expanded to include investigation of the impact of simultaneous liquid and gas fuel burn on combustion noise. Combustion noise has become increasingly relevant in gas turbines as other noise sources have been partly solved by advances in materials and design. There are two main elements to direct combustion noise: one being a determination of the nature of the unsteady heat release in turbulent flames and the other is the generation of noise by these heat release rate fluctuations [287]. The former has been shown in the present study, through multiple intermediate combustion species chemiluminescence, to vary in a consistent manner as LGR is altered in multiphase fuel burn. The latter is an acoustic problem requiring measurements involving velocity, pressure, density and temperature fluctuations. And, taking it a step further, determining how this acoustic phenomena scales with the unsteady heat release fluctuation data is worth investigating.

References

[1] BP. *BP Statistical Review of World Energy*, 2019.

[2] BP. *BP Statistical Review of World Energy*, 2018.

[3] U.N. *World Economic Situation and Prospects 2018*, 2018.

[4] Yu Y, Zhang N, and Kim JD. *Impact of urbanization on energy demand: An empirical study of the Yangtze River Economic Belt in China.* Energy Policy, 2020. **139**.

[5] Kouton J. *Information Communication Technology development and energy demand in African countries.* Energy, 2019. **189**.

[6] Paramati SR, Bhattacharya M, Ozturk I, and Zakari A. *Determinants of energy demand in African frontier market economies: An empirical investigation.* Energy, 2018. **148**: p. 123-133.

[7] IEA. *Energy Access Outlook 2017 from poverty to prosperity*, 2017.

[8] EIA. *International Energy Outlook 2019 with projections to 2050*, 2019.

[9] Le T-H and Nguyen CP. *Is energy security a driver for economic growth? Evidence from a global sample.* Energy Policy, 2019. **129**: p. 436-451.

[10] Winzer C. *Conceptualizing energy security.* Energy Policy, 2012. **46**: p. 36-48.

[11] Narula K and Reddy BS. *Three blind men and an elephant: The case of energy indices to measure energy security and energy sustainability.* Energy, 2015. **80**: p. 148-158.

[12] ASME. *Reversal of fortune: production of gas turbines for electric generation takes an unexpected turn*. Mechanical Engineering, 2017. **139**(06).

[13] Agwu O and Eleghasim C. *Mechanical drive gas turbine selection for service in two natural gas pipelines in Nigeria.* Case Studies in Thermal Engineering, 2017. **10**: p. 19-27.

[14] ASME. *Anticipated but Unwelcome*. Mechanical Engineering, 2018. **140**(06).

[15] Soares C, *Gas Turbines*, in *Gas Turbines*. 2015. p. 1-40.

[16] Jansohn P, *Overview of gas turbine types and applications*, in *Modern Gas Turbine Systems*. 2013. p. 21-43.

[17] GE. *Powering a new record at EDF: 9HA.01 sets efficiency world record*, [GEA32885], 2016.

[18] Bochenek K and Basista M. *Advances in processing of NiAl intermetallic alloys and composites for high temperature aerospace applications.* Progress in Aerospace Sciences, 2015. **79**: p. 136-146.

[19] ASME. *Global gas turbine news*. Mechanical Engineering, 2017. **139**(12).

[20] Krewinkel R. *A review of gas turbine effusion cooling studies.* International Journal of Heat and Mass Transfer, 2013. **66**: p. 706-722.

[21] Rajendran R. *Gas turbine coatings – An overview*. Engineering Failure Analysis, 2012. **26**: p. 355-369.

[22] Huth M and Heilos A, *Fuel flexibility in gas turbine systems: impact on burner design and performance*, in *Modern Gas Turbine Systems*. 2013. p. 635-684.

[23] GE. *Addressing Gas Turbine Fuel Flexibility*, [GER4601], 2011.

[24] Lefebvre AH and Ballal DR. *Gas Turbine Combustion: Alternative fuels and emissions*. 3rd ed. 2010: CRC Press Taylor & Francis Group.

[25] Huang Y and Yang V. *Dynamics and stability of lean-premixed swirl-stabilized combustion.* Progress in Energy and Combustion Science, 2009. **35**(4): p. 293-364.

[26] Gazzani M, Chiesa P, Martelli E, Sigali S, and Brunetti I. *Using Hydrogen as Gas Turbine Fuel: Premixed Versus Diffusive Flame Combustors*. Journal of Engineering for Gas Turbines and Power, 2014. **136**(5).

[27] Liu Y, Sun X, Sethi V, Nalianda D, Li Y-G, and Wang L. *Review of modern low emissions combustion technologies for aero gas turbine engines*. Progress in Aerospace Sciences, 2017. **94**: p. 12-45.

[28] Gokulakrishnan P, Ramotowski MJ, Gaines G, Fuller C, Joklik R, Eskin LD, Klassen MS, and Roby RJ. *A Novel Low NOx Lean, Premixed, and Prevaporized Combustion System for Liquid Fuels*. Journal of Engineering for Gas Turbines and Power, 2008. **130**(5).

[29] Cohen JM, Banaszuk A, Hibshman JR, Anderson TJ, and Alholm HA. *Active Control of Pressure Oscillations in a Liquid-Fueled Sector Combustor*. Journal of Engineering for Gas Turbines and Power, 2008. **130**(5).

[30] Dhanuka SK, Temme JE, and Driscoll JF. *Lean-limit combustion instabilities of a lean premixed prevaporized gas turbine combustor*. Proceedings of the Combustion Institute, 2011. **33**(2): p. 2961-2966.

[31] Lieuwen T, Torres H, Johnson C, and Zinn BT. *A Mechanism of Combustion Instability in Lean Premixed Gas Turbine Combustors*. Journal of Engineering for Gas Turbines and Power, 2001. **123**(1): p. 182-189.

[32] Rashwan SS, Nemitallah MA, and Habib MA. *Review on Premixed Combustion Technology: Stability, Emission Control, Applications, and Numerical Case Study*. Energy & Fuels, 2016. **30**(12): p. 9981-10014.

[33] Xue H. *NOx emissions in n-heptane/air partially premixed flames*. Combustion and Flame, 2003. **132**(4): p. 723-741.

[34] Zhang K, Ghobadian A, and Nouri JM. *Comparative study of non-premixed and partially-premixed combustion simulations in a realistic Tay model combustor*. Applied Thermal Engineering, 2017. **110**: p. 910-920.

[35] Oh H-T, Lee W-S, Ju Y, and Lee C-H. *Performance evaluation and carbon assessment of IGCC power plant with coal quality*. Energy, 2019. **188**.

[36] Gökalp I and Lebas E. *Alternative fuels for industrial gas turbines (AFTUR)*. Applied Thermal Engineering, 2004. **24**(11-12): p. 1655-1663.

[37] Walsh PP and Fletcher P. *Gas turbine performance*. 2nd ed. 2004: Blackwell publishing.

[38] Liu K, Alexander V, Sanderson V, and Bulat G. *Extension of Fuel Flexibility in the Siemens Dry Low Emissions SGT-300-1S to Cover a Wobbe Index Range of 15 to 49 MJ/Sm3*. Journal of Engineering for Gas Turbines and Power, 2013. **135**(2).

[39] Demirbas A. *Combustion characteristics of different biomass fuels*. Progress in Energy and Combustion Science, 2004. **30**(2): p. 219-230.

[40] Pereira EG, da Silva JN, de Oliveira JL, and Machado CS. *Sustainable energy: A review of gasification technologies*. Renewable and Sustainable Energy Reviews, 2012. **16**(7): p. 4753-4762.

[41] Lee MC, Seo SB, Chung JH, Kim SM, Joo YJ, and Ahn DH. *Gas turbine combustion performance test of hydrogen and carbon monoxide synthetic gas*. Fuel, 2010. **89**(7): p. 1485-1491.

[42] Lee MC, Seo SB, Yoon J, Kim M, and Yoon Y. *Experimental study on the effect of N2, CO2, and steam dilution on the combustion performance of H2 and CO synthetic gas in an industrial gas turbine*. Fuel, 2012. **102**: p. 431-438.

[43] Chacartegui R, Torres M, Sánchez D, Jiménez F, Muñoz A, and Sánchez T. *Analysis of main gaseous emissions of heavy duty gas turbines burning several syngas fuels.* Fuel Processing Technology, 2011. **92**(2): p. 213-220.
[44] Delattin F, Lorenzo GD, Rizzo S, Bram S, and Ruyck JD. *Combustion of syngas in a pressurized microturbine-like combustor: Experimental results.* Applied Energy, 2010. **87**(4): p. 1441-1452.
[45] International A. *Standard Specification for Aviation Turbine Fuels*. 2017.
[46] Rochelle D and Najafi H. *A review of the effect of biodiesel on gas turbine emissions and performance.* Renewable and Sustainable Energy Reviews, 2019. **105**: p. 129-137.
[47] Maurice LQ, Lander H, Edwards T, and Harrision WE. *Advanced aviation fuels: a look ahead via a historical perspective.* Fuel, 2001. **80**: p. 747-756.
[48] Blakey S, Rye L, and Wilson CW. *Aviation gas turbine alternative fuels: A review.* Proceedings of the Combustion Institute, 2011. **33**(2): p. 2863-2885.
[49] Vozka P and Kilaz G. *A review of aviation turbine fuel chemical composition-property relations.* Fuel, 2020. **268**.
[50] Riebl S, Braun-Unkhoff M, and Riedel U. *A Study on the Emissions of Alternative Aviation Fuels.* Journal of Engineering for Gas Turbines and Power, 2017. **139**(8).
[51] Wilson GR, Edwards T, Corporan E, and Freerks RL. *Certification of Alternative Aviation Fuels and Blend Components.* Energy & Fuels, 2013. **27**(2): p. 962-966.
[52] Hui X, Kumar K, Sung C-J, Edwards T, and Gardner D. *Experimental studies on the combustion characteristics of alternative jet fuels.* Fuel, 2012. **98**: p. 176-182.
[53] Gutiérrez-Antonio C, Gómez-Castro FI, de Lira-Flores JA, and Hernández S. *A review on the production processes of renewable jet fuel.* Renewable and Sustainable Energy Reviews, 2017. **79**: p. 709-729.
[54] Wei H, Liu W, Chen X, Yang Q, Li J, and Chen H. *Renewable bio-jet fuel production for aviation: A review.* Fuel, 2019. **254**.
[55] Yang J, Xin Z, He Q, Corscadden K, and Niu H. *An overview on performance characteristics of bio-jet fuels.* Fuel, 2019. **237**: p. 916-936.
[56] Zhang C, Hui X, Lin Y, and Sung C-J. *Recent development in studies of alternative jet fuel combustion: Progress, challenges, and opportunities.* Renewable and Sustainable Energy Reviews, 2016. **54**: p. 120-138.
[57] Lieuwen TC and Yang V. *Gas Turbine Emissoins*. 2013: Cambridge University Press.
[58] Chiong MC, Chong CT, Ng J-H, Lam SS, Tran M-V, Chong WWF, Mohd Jaafar MN, and Valera-Medina A. *Liquid biofuels production and emissions performance in gas turbines: A review.* Energy Conversion and Management, 2018. **173**: p. 640-658.
[59] Sajjadi B, Raman AAA, and Arandiyan H. *A comprehensive review on properties of edible and non-edible vegetable oil-based biodiesel: Composition, specifications and prediction models.* Renewable and Sustainable Energy Reviews, 2016. **63**: p. 62-92.
[60] Atabani AE, Silitonga AS, Badruddin IA, Mahlia TMI, Masjuki HH, and Mekhilef S. *A comprehensive review on biodiesel as an alternative energy resource and its characteristics.* Renewable and Sustainable Energy Reviews, 2012. **16**(4): p. 2070-2093.

[61] Hoekman SK, Broch A, Robbins C, Ceniceros E, and Natarajan M. *Review of biodiesel composition, properties, and specifications*. Renewable and Sustainable Energy Reviews, 2012. **16**(1): p. 143-169.
[62] Kumar N, Varun, and Chauhan SR. *Performance and emission characteristics of biodiesel from different origins: A review*. Renewable and Sustainable Energy Reviews, 2013. **21**: p. 633-658.
[63] Bezergianni S and Dimitriadis A. *Comparison between different types of renewable diesel*. Renewable and Sustainable Energy Reviews, 2013. **21**: p. 110-116.
[64] Knothe G. *Biodiesel and renewable diesel: A comparison*. Progress in Energy and Combustion Science, 2010. **36**(3): p. 364-373.
[65] Kay PJ, Bowen PJ, and Witlox HWM. *Sub-cooled and flashing liquid jets and droplet dispersion II. Scaled experiments and derivation of droplet size correlations*. Journal of Loss Prevention in the Process Industries, 2010. **23**(6): p. 849-856.
[66] Alsulami R, Windell B, Nates S, Wang W, Won SH, and Windom B. *Investigating the role of atomization on flame stability of liquid fuels in an annular spray burner*. Fuel, 2020. **265**.
[67] Lefebvre AH. *Airblast Atomization*. Progress in Energy and Combustion Science, 1980. **6**: p. 233-261.
[68] Ma R, Dong B, Yu Z, Zhang T, Wang Y, and Li W. *An experimental study on the spray characteristics of the air-blast atomizer*. Applied Thermal Engineering, 2015. **88**: p. 149-156.
[69] Jiang X, Siamas GA, Jagus K, and Karayiannis TG. *Physical modelling and advanced simulations of gas–liquid two-phase jet flows in atomization and sprays*. Progress in Energy and Combustion Science, 2010. **36**(2): p. 131-167.
[70] Watanawanyoo P, Hirahara H, Mochida H, Furukawa T, Nakamura M, and Chaitep S. *Experimental Investigations on Spray Characteristics in Twin-Fluid Atomizer*. Procedia Engineering, 2011. **24**: p. 866-872.
[71] Razak AMY. *Industrial Gas Turbines performance and operability*. 2007: Woodhead publishing limited and CRC press.
[72] Chin JS and Lefebvre AH. *A design procedure for effervescent atomizers*, in *International gas turbine and aeroengine congress and exposition*. 1993: Cincinnati, Ohio.
[73] Jedelsky J and Jicha M. *Energy conversion during effervescent atomization*. Fuel, 2013. **111**: p. 836-844.
[74] Sovani SD, Sojka PE, and Lefebvre AH. *Effervescent atomization*. Progress in Energy and Combustion Science, 2001. **27**: p. 483-521.
[75] Jedelský J and Jícha M. *Spray characteristics and liquid distribution of multi-hole effervescent atomisers for industrial burners*. Applied Thermal Engineering, 2016. **96**: p. 286-296.
[76] Zaremba M, Weiß L, Malý M, Wensing M, Jedelský J, and Jícha M. *Low-pressure twin-fluid atomization: Effect of mixing process on spray formation*. International Journal of Multiphase Flow, 2017. **89**: p. 277-289.
[77] Mlkvik M, Stähle P, Schuchmann HP, Gaukel V, Jedelsky J, and Jicha M. *Twin-fluid atomization of viscous liquids: The effect of atomizer construction on breakup process, spray stability and droplet size*. International Journal of Multiphase Flow, 2015. **77**: p. 19-31.

[78] Sovani SD, Chou E, Sojka PE, Gore JP, Eckerle WA, and Crofts JD. *High pressure effervescent atomization: effect of ambient pressure on spray cone angle.* Fuel, 2001. **80**: p. 427-435.
[79] Bohon MD, Metzger BA, Linak WP, King CJ, and Roberts WL. *Glycerol combustion and emissions.* Proceedings of the Combustion Institute, 2011. **33**(2): p. 2717-2724.
[80] Sallevelt JLHP, Gudde JEP, Pozarlik AK, and Brem G. *The impact of spray quality on the combustion of a viscous biofuel in a micro gas turbine.* Applied Energy, 2014. **132**: p. 575-585.
[81] Tong Y, Liu X, Wang Z, Richter M, and Klingmann J. *Experimental and numerical study on bluff-body and swirl stabilized diffusion flames.* Fuel, 2018. **217**: p. 352-364.
[82] Runyon JP. *Gast turbine fuel flexibility: pressurized swirl flame stability, thermoacoustics, and emissions*. 2017, Cardiff University.
[83] Chaudhuri S, Kostka S, Tuttle SG, Renfro MW, and Cetegen BM. *Blowoff mechanism of two dimensional bluff-body stabilized turbulent premixed flames in a prototypical combustor.* Combustion and Flame, 2011. **158**(7): p. 1358-1371.
[84] Kedia KS and Ghoniem AF. *The blow-off mechanism of a bluff-body stabilized laminar premixed flame.* Combustion and Flame, 2015. **162**(4): p. 1304-1315.
[85] Kedia KS and Ghoniem AF. *The anchoring mechanism of a bluff-body stabilized laminar premixed flame.* Combustion and Flame, 2014. **161**(9): p. 2327-2339.
[86] Shanbhogue SJ, Husain S, and Lieuwen T. *Lean blowoff of bluff body stabilized flames: Scaling and dynamics.* Progress in Energy and Combustion Science, 2009. **35**(1): p. 98-120.
[87] Khalil AEE and Gupta AK. *Distributed swirl combustion for gas turbine application.* Applied Energy, 2011. **88**(12): p. 4898-4907.
[88] Khalil AEE and Gupta AK. *Swirling distributed combustion for clean energy conversion in gas turbine applications.* Applied Energy, 2011. **88**(11): p. 3685-3693.
[89] Zhang W, Wang J, Lin W, Guo S, Zhang M, Li G, Ye J, and Huang Z. *Measurements on flame structure of bluff body and swirl stabilized premixed flames close to blow-off.* Experimental Thermal and Fluid Science, 2019. **104**: p. 15-25.
[90] Gupta AK, Lilley DG, and Syred N. *Swirl flows*. 1984, Turnbridge Wells, England, UK: Abacus Press.
[91] Muzio LJ and Quartucy GC. *Implementing NOx control: Research to application.* Progress in Energy and Combustion Science, 1997. **23**: p. 233-266.
[92] Mabahwi NAB, Leh OLH, and Omar D. *Human Health and Wellbeing: Human Health Effect of Air Pollution.* Procedia - Social and Behavioral Sciences, 2014. **153**: p. 221-229.
[93] Kampa M and Castanas E. *Human health effects of air pollution.* Environ Pollut, 2008. **151**(2): p. 362-7.
[94] Raaschou-Nielsen O, Andersen ZJ, Beelen R, Samoli E, Stafoggia M, Weinmayr G, Hoffmann B, Fischer P, Nieuwenhuijsen MJ, Brunekreef B, Xun WW, Katsouyanni K, Dimakopoulou K, Sommar J, Forsberg B, Modig L, Oudin A, Oftedal B, Schwarze PE, Nafstad P, De Faire U, Pedersen NL, Östenson C-G, Fratiglioni L, Penell J, Korek M, Pershagen G, Eriksen KT, Sørensen M, Tjønneland A, Ellermann T, Eeftens M, Peeters PH, Meliefste K, Wang M, Bueno-de-Mesquita B, Key TJ, de Hoogh K, Concin H, Nagel G, Vilier A, Grioni S, Krogh V, Tsai M-Y, Ricceri F, Sacerdote C, Galassi C, Migliore E, Ranzi A,

Cesaroni G, Badaloni C, Forastiere F, Tamayo I, Amiano P, Dorronsoro M, Trichopoulou A, Bamia C, Vineis P, and Hoek G. *Air pollution and lung cancer incidence in 17 European cohorts: prospective analyses from the European Study of Cohorts for Air Pollution Effects (ESCAPE)*. The Lancet Oncology, 2013. **14**(9): p. 813-822.

[95] Liu H, Liu S, Xue B, Lv Z, Meng Z, Yang X, Xue T, Yu Q, and He K. *Ground-level ozone pollution and its health impacts in China*. Atmospheric Environment, 2018. **173**: p. 223-230.

[96] Brasseur GP, Cox RA, Hauglustaine D, Isaksen I, Lelieveld J, Lister DH, Sausen R, Schumann U, Wahner A, and Wiesen P. *European scientific assessment of the atmospheric effects of aircraft emissions*. Atmospheric Environment, 1998. **132**(13): p. 2329-2418.

[97] Palash SM, Kalam MA, Masjuki HH, Masum BM, Rizwanul Fattah IM, and Mofijur M. *Impacts of biodiesel combustion on NOx emissions and their reduction approaches*. Renewable and Sustainable Energy Reviews, 2013. **23**: p. 473-490.

[98] Deng L, Jin X, Zhang Y, and Che D. *Release of nitrogen oxides during combustion of model coals*. Fuel, 2016. **175**: p. 217-224.

[99] Toof JL. *A model for the prediction of thermal, prompt, and fuel NOx emissions from combustion turbines*. Journal of Engineering for Gas Turbines and Power, 1986. **108**.

[100] Hill SC and Smoot LD. *Modeling of nitrogen oxides formation and destruction in combustion systems*. Progress in Energy and Combustion Science, 2000. **26**: p. 417-458.

[101] Folsom BA, Courtney CW, and Heap MP. *The effects of LBG composition and combustion characteristics on fuel NOx formation*. Journal of Engineering for gas turbines and Power, 1980. **102**.

[102] Hoekman SK and Robbins C. *Review of the effects of biodiesel on NOx emissions*. Fuel Processing Technology, 2012. **96**: p. 237-249.

[103] Fernando S, Hall C, and Jha S. *Nox reduction from biodiesel fuels*. Energy & Fuels, 2006. **20**: p. 376-382.

[104] Goldsmith JR and Landaw AS. *Carbon monoxide and human health*. Science, 1968. **162**.

[105] Rizk NK and Mongia HC. *Semianalytical correlations for NOx, CO, and UHC emissions*. Journal of Engineering for Gas Turbines and Power, 1993. **115**.

[106] Pavri R and Moore GD. *Gas turbine emissions and control*, 2001.

[107] (NASA) NAaSA. *Alternative Aviation Fuel Experiment (AAFEX)*, 2011.

[108] Li L, Lei Y, Wu S, Chen J, and Yan D. *The health economic loss of fine particulate matter (PM 2.5) in Beijing*. Journal of Cleaner Production, 2017. **161**: p. 1153-1161.

[109] Sosa BS, Porta A, Colman Lerner JE, Banda Noriega R, and Massolo L. *Human health risk due to variations in PM 10 -PM 2.5 and associated PAHs levels*. Atmospheric Environment, 2017. **160**: p. 27-35.

[110] Beer JM. *Combustion technology developments in power generation in response to environmental challenges*. Progress in Energy and Combustion Science, 2000. **26**: p. 301-327.

[111] Goh E, Sirignano M, Li J, Nair V, Emerson B, Lieuwen T, and Seitzman J. *Prediction of minimum achievable NO levels for fuel-staged combustors*. Combustion and Flame, 2019. **200**: p. 276-285.

[112] Skalska K, Miller JS, and Ledakowicz S. *Trends in NO(x) abatement: a review*. Sci Total Environ, 2010. **408**(19): p. 3976-89.
[113] Xing F, Kumar A, Huang Y, Chan S, Ruan C, Gu S, and Fan X. *Flameless combustion with liquid fuel: A review focusing on fundamentals and gas turbine application*. Applied Energy, 2017. **193**: p. 28-51.
[114] Soares C, *Gas Turbine Fuel Systems and Fuels*, in *Gas Turbines*. 2015. p. 317-411.
[115] Chatterjee S and Gülder ÖL. *Soot concentration and primary particle size in swirl-stabilized non-premixed turbulent flames of ethylene and air*. Experimental Thermal and Fluid Science, 2018. **95**: p. 73-80.
[116] Hashimoto N, Ozawa Y, Mori N, Yuri I, and Hisamatsu T. *Fundamental combustion characteristics of palm methyl ester (PME) as alternative fuel for gas turbines*. Fuel, 2008. **87**(15-16): p. 3373-3378.
[117] Chong CT and Hochgreb S. *Spray Combustion Characteristics of Palm Biodiesel*. Combustion Science and Technology, 2012. **184**(7-8): p. 1093-1107.
[118] Chong CT and Hochgreb S. *Spray flame structure of rapeseed biodiesel and Jet-A1 fuel*. Fuel, 2014. **115**: p. 551-558.
[119] Chong CT and Hochgreb S. *Flame structure, spectroscopy and emissions quantification of rapeseed biodiesel under model gas turbine conditions*. Applied Energy, 2017. **185**: p. 1383-1392.
[120] Sequera D, Agrawal AK, Spear SK, and Daly DT. *Combustion Performance of Liquid Biofuels in a Swirl-Stabilized Burner*. Journal of Engineering for Gas Turbines and Power, 2008. **130**(3).
[121] Chong CT and Hochgreb S. *Spray and combustion characteristics of biodiesel: Non-reacting and reacting*. International Biodeterioration & Biodegradation, 2015. **102**: p. 353-360.
[122] Quispe CAG, Coronado CJR, and Carvalho Jr JA. *Glycerol: Production, consumption, prices, characterization and new trends in combustion*. Renewable and Sustainable Energy Reviews, 2013. **27**: p. 475-493.
[123] Jiang L and Agrawal AK. *Combustion of straight glycerol with/without methane using a fuel-flexible, low-emissions burner*. Fuel, 2014. **136**: p. 177-184.
[124] Queirós P, Costa M, and Carvalho RH. *Co-combustion of crude glycerin with natural gas and hydrogen*. Proceedings of the Combustion Institute, 2013. **34**(2): p. 2759-2767.
[125] Muelas A, Remacha P, Pina A, Barroso J, Sobrino A, Aranda D, Bayarri N, Estévez C, and Ballester J. *Combustion of crude glycerol and its blends with acetals*. Experimental Thermal and Fluid Science, 2020. **114**.
[126] Steinmetz SA, Herrington JS, Winterrowd CK, Roberts WL, Wendt JOL, and Linak WP. *Crude glycerol combustion: Particulate, acrolein, and other volatile organic emissions*. Proceedings of the Combustion Institute, 2013. **34**(2): p. 2749-2757.
[127] Prussi M, Chiaramonti D, Riccio G, Martelli F, and Pari L. *Straight vegetable oil use in micro-gas turbines: system adaptation and testing*. Applied Energy, 2012. **89**: p. 287-295.
[128] Kun-Balog A and Sztankó K. *Reduction of pollutant emissions from a rapeseed oil fired micro gas turbine burner*. Fuel Processing Technology, 2015. **134**: p. 352-359.
[129] Chiaramonti D, Rizzo AM, Spadi A, Prussi M, Riccio G, and Martelli F. *Exhaust emissions from liquid fuel micro gas turbine fed with diesel oil, biodiesel and vegetable oil*. Applied Energy, 2013. **101**: p. 349-356.

[130] Hashimoto N, Nishida H, and Ozawa Y. *Fundamental combustion characteristics of Jatropha oil as alternative fuel for gas turbines.* Fuel, 2014. **126**: p. 194-201.
[131] Józsa V and Kun-Balog A. *Stability and emission analysis of crude rapeseed oil combustion.* Fuel Processing Technology, 2017. **156**: p. 204-210.
[132] Panchasara HV, Simmons BM, Agrawal AK, Spear SK, and Daly DT. *Combustion Performance of Biodiesel and Diesel-Vegetable Oil Blends in a Simulated Gas Turbine Burner*. Journal of Engineering for Gas Turbines and Power, 2009. **131**(3).
[133] Panchasara H and Agrawal A. *Effect of Enclosed Flame on Spray Characteristics and Emissions from Preheated Bio-oil Using an Air-blast Atomizer*. Energy Procedia, 2017. **110**: p. 216-222.
[134] Deshmukh D, Madan Mohan A, Anand TNC, and Ravikrishna RV. *Spray characterization of straight vegetable oils at high injection pressures.* Fuel, 2012. **97**: p. 879-883.
[135] Liu Z, Huang Y, and Sun L. *Studies on air core size in a simplex pressure-swirl atomizer.* International Journal of Hydrogen Energy, 2017. **42**(29): p. 18649-18657.
[136] Wimmer E and Brenn G. *Viscous flow through the swirl chamber of a pressure-swirl atomizer.* International Journal of Multiphase Flow, 2013. **53**: p. 100-113.
[137] Yao S, Zhang J, and Fang T. *Effect of viscosities on structure and instability of sprays from a swirl atomizer.* Experimental Thermal and Fluid Science, 2012. **39**: p. 158-166.
[138] Li Z, Wu Y, Yang H, Cai C, Zhang H, Hashiguchi K, Takeno K, and Lu J. *Effect of liquid viscosity on atomization in an internal-mixing twin-fluid atomizer*. Fuel, 2013. **103**: p. 486-494.
[139] Avulapati MM and Rayavarapu Venkata R. *Experimental studies on air-assisted impinging jet atomization.* International Journal of Multiphase Flow, 2013. **57**: p. 88-101.
[140] García JA, Lozano A, Alconchel J, Calvo E, Barreras F, and Santolaya JL. *Atomization of glycerin with a twin-fluid swirl nozzle.* International Journal of Multiphase Flow, 2017. **92**: p. 150-160.
[141] Fan Y, Hashimoto N, Nishida H, and Ozawa Y. *Spray characterization of an air-assist pressure-swirl atomizer injecting high-viscosity Jatropha oils.* Fuel, 2014. **121**: p. 271-283.
[142] Lieuwen T, McDonell V, Petersen E, and Santavicca D. *Fuel Flexibility Influences on Premixed Combustor Blowout, Flashback, Autoignition, and Stability*. Journal of Engineering for Gas Turbines and Power, 2008. **130**(1).
[143] Dong C, Zhou Q, Zhao Q, Zhang Y, Xu T, and Hui S. *Experimental study on the laminar flame speed of hydrogen/carbon monoxide/air mixtures.* Fuel, 2009. **88**(10): p. 1858-1863.
[144] Fu J, Tang C, Jin W, Thi LD, Huang Z, and Zhang Y. *Study on laminar flame speed and flame structure of syngas with varied compositions using OH-PLIF and spectrograph.* International Journal of Hydrogen Energy, 2013. **38**(3): p. 1636-1643.
[145] Daniele S, Jansohn P, Mantzaras J, and Boulouchos K. *Turbulent flame speed for syngas at gas turbine relevant conditions.* Proceedings of the Combustion Institute, 2011. **33**(2): p. 2937-2944.
[146] Littlejohn D, Cheng RK, Noble DR, and Lieuwen T. *Laboratory Investigations of Low-Swirl Injectors Operating With Syngases*. Journal of Engineering for Gas Turbines and Power, 2010. **132**(1).

[147] Daniele S, Jansohn P, and Boulouchos K. *Flashback Propensity of Syngas Flames at High Pressure: Diagnostic and Control*. in *ASME Turbo Expo 2010: Power for Land, Sea, and Air*. 2010.
[148] Renzi M, Patuzzi F, and Baratieri M. *Syngas feed of micro gas turbines with steam injection: Effects on performance, combustion and pollutants formation*. Applied Energy, 2017. **206**: p. 697-707.
[149] Gupta KK, Rehman A, and Sarviya RM. *Bio-fuels for the gas turbine: A review*. Renewable and Sustainable Energy Reviews, 2010. **14**(9): p. 2946-2955.
[150] Ziogou C, Ipsakis D, Seferlis P, Bezergianni S, Papadopoulou S, and Voutetakis S. *Optimal production of renewable hydrogen based on an efficient energy management strategy*. Energy, 2013. **55**: p. 58-67.
[151] Mohsin M, Rasheed AK, and Saidur R. *Economic viability and production capacity of wind generated renewable hydrogen*. International Journal of Hydrogen Energy, 2018. **43**(5): p. 2621-2630.
[152] Rahmouni S, Negrou B, Settou N, Dominguez J, and Gouareh A. *Prospects of hydrogen production potential from renewable resources in Algeria*. International Journal of Hydrogen Energy, 2017. **42**(2): p. 1383-1395.
[153] Schoenung SM and Keller JO. *Commercial potential for renewable hydrogen in California*. International Journal of Hydrogen Energy, 2017. **42**(19): p. 13321-13328.
[154] Hosseini SE and Wahid MA. *Hydrogen production from renewable and sustainable energy resources: Promising green energy carrier for clean development*. Renewable and Sustainable Energy Reviews, 2016. **57**: p. 850-866.
[155] Abbasi T and Abbasi SA. *'Renewable' hydrogen: Prospects and challenges*. Renewable and Sustainable Energy Reviews, 2011. **15**(6): p. 3034-3040.
[156] Nikolaidis P and Poullikkas A. *A comparative overview of hydrogen production processes*. Renewable and Sustainable Energy Reviews, 2017. **67**: p. 597-611.
[157] Lan R, Irvine JTS, and Tao S. *Ammonia and related chemicals as potential indirect hydrogen storage materials*. International Journal of Hydrogen Energy, 2012. **37**(2): p. 1482-1494.
[158] Olah GA. *Beyond oil and gas: the methanol economy*. Angew Chem Int Ed Engl, 2005. **44**(18): p. 2636-9.
[159] Zamfirescu C and Dincer I. *Using ammonia as a sustainable fuel*. Journal of Power Sources, 2008. **185**(1): p. 459-465.
[160] Grinberg Dana A, Elishav O, Bardow A, Shter GE, and Grader GS. *Nitrogen-Based Fuels: A Power-to-Fuel-to-Power Analysis*. Angew Chem Int Ed Engl, 2016. **55**(31): p. 8798-805.
[161] Kyriakou V, Garagounis I, Vasileiou E, Vourros A, and Stoukides M. *Progress in the Electrochemical Synthesis of Ammonia*. Catalysis Today, 2017. **286**: p. 2-13.
[162] Shipman MA and Symes MD. *Recent progress towards the electrosynthesis of ammonia from sustainable resources*. Catalysis Today, 2017. **286**: p. 57-68.
[163] Hayakawa A, Arakawa Y, Mimoto R, Somarathne KDKA, Kudo T, and Kobayashi H. *Experimental investigation of stabilization and emission characteristics of ammonia/air premixed flames in a swirl combustor*. International Journal of Hydrogen Energy, 2017. **42**(19): p. 14010-14018.
[164] Valera-Medina A, Marsh R, Runyon J, Pugh D, Beasley P, Hughes T, and Bowen P. *Ammonia–methane combustion in tangential swirl burners for gas turbine power generation*. Applied Energy, 2017. **185**: p. 1362-1371.

[165] Valera-Medina A, Morris S, Runyon J, Pugh DG, Marsh R, Beasley P, and Hughes T. *Ammonia, Methane and Hydrogen for Gas Turbines.* Energy Procedia, 2015. **75**: p. 118-123.
[166] Xiao H, Valera-Medina A, Marsh R, and Bowen PJ. *Numerical study assessing various ammonia/methane reaction models for use under gas turbine conditions.* Fuel, 2017. **196**: p. 344-351.
[167] Xiao H and Valera-Medina A. *Chemical Kinetic Mechanism Study on Premixed Combustion of Ammonia/Hydrogen Fuels for Gas Turbine Use.* Journal of Engineering for Gas Turbines and Power, 2017. **139**(8).
[168] Xiao H, Valera-Medina A, and Bowen PJ. *Study on premixed combustion characteristics of co-firing ammonia/methane fuels.* Energy, 2017. **140**: p. 125-135.
[169] Otomo J, Koshi M, Mitsumori T, Iwasaki H, and Yamada K. *Chemical kinetic modeling of ammonia oxidation with improved reaction mechanism for ammonia/air and ammonia/hydrogen/air combustion.* International Journal of Hydrogen Energy, 2018. **43**(5): p. 3004-3014.
[170] An H, Yang WM, Li J, and Zhou DZ. *Modeling analysis of urea direct injection on the NO x emission reduction of biodiesel fueled diesel engines.* Energy Conversion and Management, 2015. **101**: p. 442-449.
[171] Zamfirescu C and Dincer I. *Ammonia as a green fuel and hydrogen source for vehicular applications.* Fuel Processing Technology, 2009. **90**(5): p. 729-737.
[172] Elishav O, Tvil G, Mosevitzky B, Lewin D, Shter GE, and Grader GS. *The nitrogen economy: the feasibility of using nitrogen-based alternative fuels.* Energy Procedia, 2017. **135**: p. 3-13.
[173] Grinberg Dana A, Shter GE, and Grader GS. *Nitrogen-Based Alternative Fuels: Progress and Future Prospects.* Energy Technology, 2016. **4**(1): p. 7-18.
[174] Mosevitzky B, Grinberg Dana A, Shter GE, and Grader GS. *Combustion simulations of aqueous urea ammonium nitrate monofuel at high pressures.* Combustion and Flame, 2016. **166**: p. 295-306.
[175] Mosevitzky B, Shter GE, and Grader GS. *Auto-ignition of a carbon-free aqueous ammonia/ammonium nitrate monofuel: A thermal and barometric analysis.* Fuel Processing Technology, 2017. **159**: p. 363-368.
[176] Mosevitzky B, Shter GE, and Grader GS. *Effect of equivalence ratio on the thermal autoignition of aqueous ammonia ammonium nitrate monofuel.* Combustion and Flame, 2018. **188**: p. 142-149.
[177] Tutak W, Jamrozik A, Pyrc M, and Sobiepański M. *A comparative study of co-combustion process of diesel-ethanol and biodiesel-ethanol blends in the direct injection diesel engine.* Applied Thermal Engineering, 2017. **117**: p. 155-163.
[178] Tamilselvan P, Nallusamy N, and Rajkumar S. *A comprehensive review on performance, combustion and emission characteristics of biodiesel fuelled diesel engines.* Renewable and Sustainable Energy Reviews, 2017. **79**: p. 1134-1159.
[179] Thangaraja J, Anand K, and Mehta PS. *Biodiesel NOx penalty and control measures - a review.* Renewable and Sustainable Energy Reviews, 2016. **61**: p. 1-24.
[180] Kurji H, Valera-Medina A, Okon A, and Chong CT. *Combustion and emission performance of CO2/CH4/biodiesel and CO2/CH4/diesel blends in a swirl burner generator.* Energy Procedia, 2017. **142**: p. 154-159.
[181] Sidey J and Mastorakos E. *Visualisation of turbulent swirling dual-fuel flames.* Proceedings of the Combustion Institute, 2017. **36**(2): p. 1721-1727.

[182] Yoon SH and Lee CS. *Experimental investigation on the combustion and exhaust emission characteristics of biogas–biodiesel dual-fuel combustion in a CI engine.* Fuel Processing Technology, 2011. **92**(5): p. 992-1000.
[183] Reiter AJ and Kong S-C. *Combustion and emissions characteristics of compression-ignition engine using dual ammonia-diesel fuel.* Fuel, 2011. **90**(1): p. 87-97.
[184] Sahoo BB, Sahoo N, and Saha UK. *Effect of H2:CO ratio in syngas on the performance of a dual fuel diesel engine operation.* Applied Thermal Engineering, 2012. **49**: p. 139-146.
[185] Chauhan BS, Kumar N, and Cho HM. *A study on the performance and emission of a diesel engine fueled with Jatropha biodiesel oil and its blends.* Energy, 2012. **37**(1): p. 616-622.
[186] Sarjovaara T, Alantie J, and Larmi M. *Ethanol dual-fuel combustion concept on heavy duty engine.* Energy, 2013. **63**: p. 76-85.
[187] Sukjit E, Herreros JM, Dearn KD, Tsolakis A, and Theinnoi K. *Effect of hydrogen on butanol–biodiesel blends in compression ignition engines.* International Journal of Hydrogen Energy, 2013. **38**(3): p. 1624-1635.
[188] Mohsin R, Majid ZA, Shihnan AH, Nasri NS, and Sharer Z. *Effect of biodiesel blends on engine performance and exhaust emission for diesel dual fuel engine.* Energy Conversion and Management, 2014. **88**: p. 821-828.
[189] Surawski NC, Miljevic B, Bodisco TA, Situ R, Brown RJ, and Ristovski ZD. *Performance and gaseous and particle emissions from a liquefied petroleum gas (LPG) fumigated compression ignition engine.* Fuel, 2014. **133**: p. 17-25.
[190] Magno A, Mancaruso E, and Vaglieco BM. *Effects of both blended and pure biodiesel on waste heat recovery potentiality and exhaust emissions of a small CI (compression ignition) engine.* Energy, 2015. **86**: p. 661-671.
[191] Martín J, Novella R, García A, Carreño R, Heuser B, Kremer F, and Pischinger S. *Thermal analysis of a light-duty CI engine operating with diesel-gasoline dual-fuel combustion mode.* Energy, 2016. **115**: p. 1305-1319.
[192] Barik D and Murugan S. *Effects of diethyl ether (DEE) injection on combustion performance and emission characteristics of Karanja methyl ester (KME)–biogas fueled dual fuel diesel engine.* Fuel, 2016. **164**: p. 286-296.
[193] Geo VE, Sonthalia A, Nagarajan G, and Nagalingam B. *Studies on performance, combustion and emission of a single cylinder diesel engine fuelled with rubber seed oil and its biodiesel along with ethanol as injected fuel.* Fuel, 2017. **209**: p. 733-741.
[194] Aklouche FZ, Loubar K, Bentebbiche A, Awad S, and Tazerout M. *Experimental investigation of the equivalence ratio influence on combustion, performance and exhaust emissions of a dual fuel diesel engine operating on synthetic biogas fuel.* Energy Conversion and Management, 2017. **152**: p. 291-299.
[195] Ashok B, Nanthagopal K, Chaturvedi B, Sharma S, and Raj TK. *A comparative assessment on Common Rail Direct Injection (CRDI) engine characteristics using low viscous biofuel blends.* Applied Thermal Engineering, 2018. **145**: p. 494-506.
[196] Dubey P and Gupta R. *Influences of dual bio-fuel (Jatropha biodiesel and turpentine oil) on single cylinder variable compression ratio diesel engine.* Renewable Energy, 2018. **115**: p. 1294-1302.
[197] Dimitriou P, Tsujimura T, and Suzuki Y. *Low-load hydrogen-diesel dual-fuel engine operation – A combustion efficiency improvement approach.* International Journal of Hydrogen Energy, 2019. **44**(31): p. 17048-17060.

[198] Sharma P and Dhar A. *Effect of hydrogen fumigation on combustion stability and unregulated emissions in a diesel fuelled compression ignition engine*. Applied Energy, 2019. **253**.
[199] Sharma PK, Sharma D, Soni SL, Jhalani A, Singh D, and Sharma S. *Characterization of the hydroxy fueled compression ignition engine under dual fuel mode: Experimental and numerical simulation*. International Journal of Hydrogen Energy, 2020. **45**(15): p. 8067-8081.
[200] Gawale GR and Naga Srinivasulu G. *Experimental investigation of ethanol/diesel and ethanol/biodiesel on dual fuel mode HCCI engine for different engine load conditions*. Fuel, 2020. **263**.
[201] Zhang H, Guo L, Yan Y, Sun W, Li J, Wang Q, and Sun Y. *Experimental investigation on the combustion and emissions characteristics of an N-butanol/CTL dual fuel engine*. Fuel, 2020. **274**.
[202] Kutne P, Kapadia BK, Meier W, and Aigner M. *Experimental analysis of the combustion behaviour of oxyfuel flames in a gas turbine model combustor*. Proceedings of the Combustion Institute, 2011. **33**(2): p. 3383-3390.
[203] Rehman A, Phalke DR, and Pandey R. *Alternative fuel for gas turbine: Esterified jatropha oil–diesel blend*. Renewable Energy, 2011. **36**(10): p. 2635-2640.
[204] Seljak T, Rodman Oprešnik S, Kunaver M, and Katrašnik T. *Wood, liquefied in polyhydroxy alcohols as a fuel for gas turbines*. Applied Energy, 2012. **99**: p. 40-49.
[205] Chiariello F, Allouis C, Reale F, and Massoli P. *Gaseous and particulate emissions of a micro gas turbine fuelled by straight vegetable oil–kerosene blends*. Experimental Thermal and Fluid Science, 2014. **56**: p. 16-22.
[206] Mendez CJ, Parthasarathy RN, and Gollahalli SR. *Performance and emission characteristics of butanol/Jet A blends in a gas turbine engine*. Applied Energy, 2014. **118**: p. 135-140.
[207] Kurji H, Valera-Medina A, Runyon J, Giles A, Pugh D, Marsh R, Cerone N, Zimbardi F, and Valerio V. *Combustion characteristics of biodiesel saturated with pyrolysis oil for power generation in gas turbines*. Renewable Energy, 2016. **99**: p. 443-451.
[208] Buffi M, Valera-Medina A, Marsh R, Pugh D, Giles A, Runyon J, and Chiaramonti D. *Emissions characterization tests for hydrotreated renewable jet fuel from used cooking oil and its blends*. Applied Energy, 2017. **201**: p. 84-93.
[209] Chen L, Zhang Z, Lu Y, Zhang C, Zhang X, Zhang C, and Roskilly AP. *Experimental study of the gaseous and particulate matter emissions from a gas turbine combustor burning butyl butyrate and ethanol blends*. Applied Energy, 2017. **195**: p. 693-701.
[210] Bhele SK, Deshpande NV, and Thombre SB. *Experimental Investigation of Combustion Characteristics of Jatropha Biodiesel (JME) and its Diesel Blends for Gas Turbine Combustor*. Materials Today: Proceedings, 2018. **5**(11): p. 23404-23412.
[211] Buffi M, Cappelletti A, Rizzo AM, Martelli F, and Chiaramonti D. *Combustion of fast pyrolysis bio-oil and blends in a micro gas turbine*. Biomass and Bioenergy, 2018. **115**: p. 174-185.
[212] Sidey JAM and Mastorakos E. *Stabilisation of swirling dual-fuel flames*. Experimental Thermal and Fluid Science, 2018. **95**: p. 65-72.
[213] Valera-Medina A, Gutesa M, Xiao H, Pugh D, Giles A, Goktepe B, Marsh R, and Bowen P. *Premixed ammonia/hydrogen swirl combustion under rich fuel*

conditions for gas turbines operation. International Journal of Hydrogen Energy, 2019. **44**(16): p. 8615-8626.
[214] Seljak T and Katrašnik T. *Emission reduction through highly oxygenated viscous biofuels: Use of glycerol in a micro gas turbine*. Energy, 2019. **169**: p. 1000-1011.
[215] Evans MJ, Sidey JAM, Ye J, Medwell PR, Dally BB, and Mastorakos E. *Temperature and reaction zone imaging in turbulent swirling dual-fuel flames*. Proceedings of the Combustion Institute, 2019. **37**(2): p. 2159-2166.
[216] Agwu O and Valera-Medina A. *Diesel/syngas co-combustion in a swirl-stabilised gas turbine combustor*. International Journal of Thermofluids, 2020. **3-4**.
[217] Okafor EC, Somarathne KDKA, Ratthanan R, Hayakawa A, Kudo T, Kurata O, Iki N, Tsujimura T, Furutani H, and Kobayashi H. *Control of NOx and other emissions in micro gas turbine combustors fuelled with mixtures of methane and ammonia*. Combustion and Flame, 2020. **211**: p. 406-416.
[218] Kurji HJ. *Fuel Flexibility with low emissions for gas turbine engines*. 2017, Cardiff University.
[219] TESTO. Available from: http://www.testo350.com/testo-350/350anadefsx/350faqs.html. accessed: April 14, 2020.
[220] Li Z, Wang Y, Geng H, Zhen X, Liu M, Xu S, and Li C. *Effects of diesel and methanol injection timing on combustion, performance, and emissions of a diesel engine fueled with directly injected methanol and pilot diesel*. Applied Thermal Engineering, 2019. **163**.
[221] Wang Y, Wang H, Meng X, Tian J, Wang Y, Long W, and Li S. *Combustion characteristics of high pressure direct-injected methanol ignited by diesel in a constant volume combustion chamber*. Fuel, 2019. **254**.
[222] Liu K, Wood JP, Buchanan ER, Martin P, and Sanderson VE. *Biodiesel as an Alternative Fuel in Siemens Dry Low Emissions Combustors: Atmospheric and High Pressure Rig Testing*. Journal of Engineering for Gas Turbines and Power, 2010. **132**(1).
[223] Zhen X, Li X, Wang Y, Liu D, and Tian Z. *Comparative study on combustion and emission characteristics of methanol/hydrogen, ethanol/hydrogen and methane/hydrogen blends in high compression ratio SI engine*. Fuel, 2020. **267**.
[224] Duraisamy G, Rangasamy M, and Govindan N. *A comparative study on methanol/diesel and methanol/PODE dual fuel RCCI combustion in an automotive diesel engine*. Renewable Energy, 2020. **145**: p. 542-556.
[225] Verhelst S, Turner JWG, Sileghem L, and Vancoillie J. *Methanol as a fuel for internal combustion engines*. Progress in Energy and Combustion Science, 2019. **70**: p. 43-88.
[226] Setyawan HY, Zhu M, Zhang Z, and Zhang D. *Ignition and combustion characteristics of single droplets of a crude glycerol in comparison with pure glycerol, petroleum diesel, biodiesel and ethanol*. Energy, 2016. **113**: p. 153-159.
[227] Ferreira AGM, Egas APV, Fonseca IMA, Costa AC, Abreu DC, and Lobo LQ. *The viscosity of glycerol*. The Journal of Chemical Thermodynamics, 2017. **113**: p. 162-182.
[228] Mehra RK, Duan H, Juknelevičius R, Ma F, and Li J. *Progress in hydrogen enriched compressed natural gas (HCNG) internal combustion engines - A comprehensive review*. Renewable and Sustainable Energy Reviews, 2017. **80**: p. 1458-1498.
[229] Dimitriou P, Tsujimura T, and Suzuki Y. *Hydrogen-diesel dual-fuel engine optimization for CHP systems*. Energy, 2018. **160**: p. 740-752.

[230] Sarkar A and Saha UK. *Role of global fuel-air equivalence ratio and preheating on the behaviour of a biogas driven dual fuel diesel engine.* Fuel, 2018. **232**: p. 743-754.
[231] Chen Z, Wang L, and Zeng K. *A comparative study on the combustion and emissions of dual-fuel engine fueled with natural gas/methanol, natural gas/ethanol, and natural gas/n-butanol.* Energy Conversion and Management, 2019. **192**: p. 11-19.
[232] Nori V and Seitzman J. *Evaluation of chemiluminescence as a combustion diagnostic under varying operating conditions*, in *46th AIAA Aerospace Sciences Meeting and Exhibit*. 2008: Reno, Nevada.
[233] Gaydon AG and Wolfhard HG. *Flames: their structure, radiation and temperature*. 3rd ed. 1970: Chapman and Hall Ltd.
[234] García-Armingol T, Hardalupas Y, Taylor AMKP, and Ballester J. *Effect of local flame properties on chemiluminescence-based stoichiometry measurement.* Experimental Thermal and Fluid Science, 2014. **53**: p. 93-103.
[235] Ballester J and García-Armingol T. *Diagnostic techniques for the monitoring and control of practical flames.* Progress in Energy and Combustion Science, 2010. **36**: p. 375-411.
[236] Guethe F, Guyot D, Singla G, Noiray N, and Schuermans B. *Chemiluminescence as diagnostic tool in the development of gas turbines.* Applied Physics B, 2012. **107**(3): p. 619-636.
[237] Ballester J, Hernández R, Sanz A, Smolarz A, Barroso J, and Pina A. *Chemiluminescence monitoring in premixed flames of natural gas and its blends with hydrogen.* Proceedings of the Combustion Institute, 2009. **32**(2): p. 2983-2991.
[238] Guyot D, Guethe F, Schuermans B, Lacarelle A, and Paschereit CO. *CH*/OH* Chemiluminescence response of an atmospheric premixed flame under varying operating conditions*, in *ASME Turbo Expo 2010: Power for land, sea and air*. 2010: Glasgow, UK.
[239] Lantz A, Collin R, Aldén M, Lindholm A, Larfeldt J, and Lörstad D. *Investigation of Hydrogen Enriched Natural Gas Flames in a SGT-700/800 Burner Using OH PLIF and Chemiluminescence Imaging*. Journal of Engineering for Gas Turbines and Power, 2015. **137**(3).
[240] Higgins B, McQuay MQ, Lucas F, Rolon JC, Darabiha N, and Candel S. *Systematic measurements of OH chemiluminescence for fuel-lean, high pressure, premixed, laminar flames.* Fuel, 2001. **80**: p. 67-74.
[241] Trindade T, Ferreira A, and Fernandes E. *Characterization of Combustion Chemiluminescence: An Image Processing Approach.* Procedia Technology, 2014. **17**: p. 194-201.
[242] Kathrotia T, Riedel U, Seipel A, Moshammer K, and Brockhinke A. *Experimental and numerical study of chemiluminescent species in low-pressure flames.* Applied Physics B, 2012. **107**(3): p. 571-584.
[243] Morell MR, Seitzman JM, Wilensky M, Lubarsky E, Lee J, and Zinn B. *Interpretation of optical emissions for sensors in liquid fueled combustors*, in *39th Aerospace Sciences Meeting & Exhibit*. 2001: Reno, NV.
[244] Kutne P, Boxx I, Stohr M, and Meier W. *Experimental analysis of the combustion behaviour of a low calorific syngas mixture in a gas turbine model combustor*, in *3rd European Combustion Meeting*. 2007: Crete, Greece.
[245] Hardalupas Y, Panoutsos CS, Skevis G, and Taylor AMKP. *Numerical Evaluation of Equivalence Ratio Measurement Using OH* and CH* Chemiluminescence in*

Premixed IsoOctane/Air Flames, in *2nd European Combustion Meeeting*. 2005: Lovain-la-Neuve, France.
[246] Lauer M and Sattelmayer T. *Heat Release Calculation in a Turbulent Swirl Flame from Laser and Chemiluminescence Measurements*, in *14th International Symposium on Applications of Laser Techniques to Fluid Mechanics*. 2008: Lisbon, Portugal.
[247] Jeong YK, Jeon CH, and Chang YJ. *Evaluation of the equivalence ratio of the reacting mixture using intensity ratio of chemiluminescence in laminar partially premixed CH4-air flames.* Experimental Thermal and Fluid Science, 2006. **30**(7): p. 663-673.
[248] Killer C. *Abel Inversion Algorithm*. Available from: http://www.mathworks.com/matlabcentral/fileexchange/43639-abel-inversion-algorithm.
[249] Pretzler G. *A new method for numerical Abel-inversion.* Zeitschrift fur Naturforschung A, 1991. **46**(7): p. 639-641.
[250] CHEMKIN. *Reaction Design*, 2009.
[251] Mehl M, Pitz WJ, Westbrook CK, and Curran HJ. *Kinetic modeling of gasoline surrogate components and mixtures under engine conditions.* Proceedings of the Combustion Institute, 2011. **33**(1): p. 193-200.
[252] Ranzi E, Frassoldati A, Stagni A, Pelucchi M, Cuoci A, and Faravelli T. *Reduced kinetic schemes of complex reaction systems: Fossil and biomass-derived transportation fuels.* International Journal of Chemical Kinetics 2014. **46**(9): p. 512-542.
[253] Bergthorson JM and Thomson MJ. *A review of the combustion and emissions properties of advanced transportation biofuels and their impact on existing and future engines.* Renewable and Sustainable Energy Reviews, 2015. **42**: p. 1393-1417.
[254] Zienkiewicz OC, Taylor RL, and Nithiarasu P, *Turbulent Flows*, in *The Finite Element Method for Fluid Dynamics*. 2014. p. 283-308.
[255] Wegner B, Maltsev A, Schneider C, Sadiki A, Dreizler A, and Janicka J. *Assessment of unsteady RANS in predicting swirl flow instability based on LES and experiments.* International Journal of Heat and Fluid Flow, 2004. **25**(3): p. 528-536.
[256] Som S, Senecal PK, and Pomraning E. *Comparison of RANS and LES turbulence models against constant volume diesel experiments*, in *24th Annual Conference on Liquid Atomization and Spray Systems*. 2012: San Antonio, TX.
[257] ANSYS. *Ansys Fluent 18 tutorial guide*. 2017, Canonsburg, PA 15317.
[258] Valera-Medina A, Syred N, and Bowen P. *Central Recirculation Zone Visualization in Confined Swirl Combustors for Terrestrial Energy*. Journal of Propulsion and Power, 2013. **29**(1): p. 195-204.
[259] Syred N. *A review of oscillation mechanisms and the role of the precessing vortex core (PVC) in swirl combustion systems.* Progress in Energy and Combustion Science, 2006. **32**(2): p. 93-161.
[260] Musculus MPB, Miles PC, and Pickett LM. *Conceptual models for partially premixed low-temperature diesel combustion.* Progress in Energy and Combustion Science, 2013. **39**(2-3): p. 246-283.
[261] Kim D, Ekoto I, Colban WF, and Miles PC. *In-cylinder CO and UHC imaging in a light-duty diesel engine duringPPCI low-temperature combustion.* SAE Int. J. Fuels Lubri., 2009. **1**(1): p. 933-956.

[262] Mahlia TMI, Syazmi ZAHS, Mofijur M, Abas AEP, Bilad MR, Ong HC, and Silitonga AS. *Patent landscape review on biodiesel production: Technology updates*. Renewable and Sustainable Energy Reviews, 2020. **118**.
[263] Eurostat. *Energy, transport and environment statistics*, 2019.
[264] OECD/FAO. *OECD-FAO Agricultural Outlook 2019-2028*, 2019.
[265] REN21. *Renewables 2019 Global status report*, 2019.
[266] Azad AK, Rasul MG, Khan MMK, Sharma SC, Mofijur M, and Bhuiya MMK. *Prospects, feedstocks and challenges of biodiesel production from beauty leaf oil and castor oil: A nonedible oil sources in Australia*. Renewable and Sustainable Energy Reviews, 2016. **61**: p. 302-318.
[267] Naylor RL and Higgins MM. *The rise in global biodiesel production: Implications for food security*. Global Food Security, 2018. **16**: p. 75-84.
[268] Debnath D, Whistance J, Westhoff P, and Helmar M, *Consequences of US and EU biodiesel policies on global food security*, in *Biofuels, Bioenergy and Food Security*. 2019. p. 165-178.
[269] Ogunkunle O and Ahmed NA. *A review of global current scenario of biodiesel adoption and combustion in vehicular diesel engines*. Energy Reports, 2019. **5**: p. 1560-1579.
[270] Ayoub M and Abdullah AZ. *Critical review on the current scenario and significance of crude glycerol resulting from biodiesel industry towards more sustainable renewable energy industry*. Renewable and Sustainable Energy Reviews, 2012. **16**(5): p. 2671-2686.
[271] Sivasankaran C, Ramaujam PR, Balasbramanian B, and Mani J. *Recent progress on transforming crude glycerol into high value chemicals: a critical review*. Biofuels, 2019. **10**(3): p. 309-314.
[272] Sdrula N. *A study using classical or membrane separation in the biodiesel process*. Desalination, 2010. **250**(3): p. 1070-1072.
[273] Chozhavendhan S, Karthiga Devi G, Bharathiraja B, Praveen Kumar R, and Elavazhagan S, *Assessment of crude glycerol utilization for sustainable development of biorefineries*, in *Refining Biomass Residues for Sustainable Energy and Bioproducts*. 2020. p. 195-212.
[274] Yang F, Hanna MA, and Sun R. *Value-added uses for crude glycerol - a byproduct of biodiesel production*. Biotechnology for Biofuels, 2012. **5**(13).
[275] Ajanovic A and Haas R. *Economic challenges for the future relevance of biofuels in transport in EU countries*. Energy, 2010. **35**(8): p. 3340-3348.
[276] Seljak T, Širok B, and Katrašnik T. *Advanced fuels for gas turbines: Fuel system corrosion, hot path deposit formation and emissions*. Energy Conversion and Management, 2016. **125**: p. 40-50.
[277] Seljak T and Katrašnik T. *Designing the microturbine engine for waste-derived fuels*. Waste Management, 2016. **47**: p. 299-310.
[278] Yadav A, Trivedi S, Rai R, and Pandey S. *Densities and dynamic viscosities of (choline chloride+glycerol) deep eutectic solvent and its aqueous mixtures in the temperature range (283.15–363.15)K*. Fluid Phase Equilibria, 2014. **367**: p. 135-142.
[279] Yuan W, Hansen AC, Zhang Q, and Tan Z. *Temperature-dependent kinematic viscosity of selected biodiesel fuels and blends with diesel fuel*. Journal of the American Oil Chemists' Society, 2005. **82**(3): p. 195-199.
[280] Gülüm M and Bilgin A. *A comprehensive study on measurement and prediction of viscosity of biodiesel-diesel-alcohol ternary blends*. Energy, 2018. **148**: p. 341-361.

[281] DDB. Available from: http://ddbonline.ddbst.de/VogelCalculation/VogelCalculationCGI.exe. accessed: April 6, 2020.
[282] Mignard D, Sahibzada M, Duthie JM, and Whittington HW. *Methanol synthesis from flue-gas CO2 and renewable electricity: a feasibility study*. International Journal of Hydrogen Energy, 2003. **28**: p. 455-464.
[283] Bos MJ, Kersten SRA, and Brilman DWF. *Wind power to methanol: Renewable methanol production using electricity, electrolysis of water and CO2 air capture*. Applied Energy, 2020. **264**.
[284] Ackermann T, Andersson G, and Soder L. *Distributed generation: a definition*. Electric Power Systems Research, 2001. **57**: p. 195-204.
[285] Ma S and Urpelainen J. *Distributed power generation in national rural electrification plans: An international and comparative evaluation*. Energy Research & Social Science, 2018. **44**: p. 1-5.
[286] Adewuyi A. *Challenges and prospects of renewable energy in Nigeria: A case of bioethanol and biodiesel production*. Energy Reports, 2020. **6**: p. 77-88.
[287] Dowling AP and Mahmoudi Y. *Combustion noise*. Proceedings of the Combustion Institute, 2015. **35**(1): p. 65-100.

Appendix A: Relevant formula

1. Fuel flow rate for desired power output

$$fuel\ flow\ (kg/s) = \frac{power\ output\ (kW)}{LHV\ (KJ/kg)} \qquad 1\,W = 1\,J/s$$

2. Equivalence ratio

$$\phi = \frac{\left(m_f/m_a\right)_{utilised}}{\left(m_f/m_a\right)_{stoichiometric}}$$

m_a: *air mass flow rate*

m_f: *fuel mass flow rate*

3. Stoichiometric fuel-air mass ratio (Biodiesel example)

Approximate formula : $C_{19}H_{36}O_2$

Ideal combustion equation:

$C_{19}H_{36}O_2 + 27(O_2 + 3.76N_2) \rightarrow 19CO_2 + 18H_2O + 101.52N_2$

Fuel/air mass ratio for stoichiometric combustion:

$$\left(\frac{m_f}{m_a}\right)_{stoichiometric} = \frac{(19 \times 12) + (36 \times 1) + (2 \times 16)}{27[(2 \times 16) + (3.76 \times 28)]} \approx \mathbf{0.08}$$

4. Properties of gas mixtures

4.1 Mass and molar fractions

A mixture of two or more gases of fixed chemical composition is called a *non-reacting* gas mixture. The properties of the mixture may be based on the mass of each component and called *gravimetric analysis* or on the moles of each component, called *molar analysis*. For a mixture of k different gases,

Mass of mixture	*Mass fraction*	*Moles in mixture*	*Mole fraction*
$m_m = \sum_{i=1}^{k} m_i$	$m_{fi} = \frac{m_i}{m_m}$	$N_m = \sum_{i=1}^{k} N_i$	$y_i = \frac{N_i}{N_m}$
	$\sum_{i=1}^{k} m_{fi} = 1$		$\sum_{i=1}^{k} y_i = 1$

Mass and mole number for a given component are related through the molecular weight M: $m_i = N_i M_i$.
Since

$$m_m = \sum_{i=1}^{k} m_i = \sum_{i=1}^{k} N_i M_i = N_m M_m$$

Average or apparent molar mass for a mixture

$$M_m = \frac{m_m}{N_m} = \sum_{i=1}^{k} \frac{N_i}{N_m} M_i = \sum_{i=1}^{k} y_i M_i$$

Average or apparent gas constant of a mixture

$$R_m = \frac{R_u}{M_m} = \sum_{i=1}^{k} m_{fi} R_i$$

To change from mole fraction analysis to mass fraction analysis

$$m_{fi} = \frac{y_i M_i}{\sum_{i=1}^{k} y_i M_i}$$

To change from a mass fraction analysis to a mole fraction analysis

$$y_i = \frac{m_{fi}/M_i}{\sum_{i=1}^{k} m_{fi}/M_i}$$

4.2 Volume fraction

Amagat's law of additive volumes states that the volume of a gas mixture is equal to the sum of the volumes each gas would occupy if it existed alone at the mixture temperature and pressure.

$$V_m = \sum_{i=1}^{k} V_i(T_m, P_m)$$

Volume fraction of a component

$$V_{fi} = \frac{V_i(T_m, P_m)}{V_m} \quad ; \quad \sum_{i=1}^{k} V_{fi} = 1$$

For an ideal gas mixture

$$V_i = \frac{N_i R_u T_m}{P_m} \qquad \text{and} \qquad V_m = \frac{N_m R_u T_m}{P_m}$$

$$V_{fi} = \frac{V_i}{V_m} = \frac{N_i}{N_m} = y_i$$

4.3 Density of gas mixture

$$\rho_m = \sum_{i=1}^{k} \rho_i . V_{fi}$$

5. Application of gas mixture properties to Syngas

5.1 Density and LHV of syngas

Gas mix	*M* (kg/kmol)	*N*	Molar inferior calorific value at 15°C (kJ/mol)	Mole fraction × molar mass per mole (kg/kmol)	Mole fraction × molar inferior calorific value (kJ/mol)
CH4	16.04	0.8	802.69	12.83	642.15
H2	2.02	0.1	241.72	0.2016	24.17
CO	28.01	0.1	282.91	2.801	28.29
Ideal density = 0.6698 kg/m³; dividing this by a gas mixture compression factor of 0.9986 gives a real **density** of **0.6707 kg/m³**				∑15.837	∑694.62 (**43860 kJ/kg)***
				*The mass inferior calorific value is obtained by manipulating the molar one *wrt* the molar mass of gas mix	

5.2 Syngas fuel-air mass ratio calculation

Composition: $80\%CH_4; 10\%CO; 10\%H_2$

Ideal combustion equations

$$CH_4 + 2O_2 \rightarrow CO_2 + 2H_2O$$

1 *kmol* methane requires 2 *kmol* oxygen for complete combustion.
In 1 *kmol* syngas, there's 0.8 *kmol* methane which will require (0.8 × 2) *kmol* oxygen = **1.6 *kmol* oxygen**

$$H_2 + 0.5O_2 \rightarrow H_2O$$

1 *kmol* hydrogen requires 0.5 *kmol* oxygen for complete combustion.
In 1 *kmol* syngas, there's 0.1 *kmol* methane which will require (0.1 × 0.5) *kmol* oxygen = **0.05 *kmol* oxygen**

$$2CO + O_2 \rightarrow 2CO_2$$

1 *kmol* methane requires 0.5 *kmol* oxygen for complete combustion.
In 1 *kmol* syngas, there's 0.1 *kmol* methane which will require (0.1 × 0.5) *kmol* oxygen = **0.05 *kmol* oxygen**

Total oxygen required for 1 *kmol* syngas = **1.7 *kmol***

Fuel/air mass ratio for stoichiometric combustion

$$\left(\frac{m_f}{m_a}\right)_{stoichiometric} = \frac{15.837}{1.7\{32 + (3.76 \times 28)\}} = \mathbf{0.068}$$

Appendix B: Abel deconvolution technique

The Abel deconvolution method is a popular means of resolving line-of-sight images obtained from chemiluminescence. Open source MATLAB codes such as "abel_inversion.m", "compute_expansion.m" and "solve_lsq.m" are available to aid Abel deconvolution of chemiluminescence images. The listed three codes were utilised to develop a MATLAB function "HalfAbel.m" which is reproduced here for convenience to the reader. The input image to the "HalfAbel.m" function in this work is the temporally averaged, background-subtracted and cropped chemiluminescence image. These pre-processing steps were carried out using Davis 7 software by right clicking on the batch of images then selecting:

Batch processing>Group>Statistics>Average>Start processing for temporal averaging

Batch processing>Basic image arithmetic>Subtract>Start processing for background subtraction; under "Parameter" in "Operations List", input the background to be subtracted which background had been averaged as in the previous step.

Batch processing>Basic image arithmetic>Extract Rectangle>Start processing for cropping if desired.

These three levels of processing can be done simultaneously on Davis 7 and the resulting image exported as a .tif file for Abel deconvolution on MATLAB. For the integral intensities used in determining the heat release rate fluctuations in several Chapters of this work, the unprocessed chemiluminescence images exported as a .tif file was processed with the following "IntegralIntensities" code developed by the author on MATLAB. The 250 images were by default named B00001.tif up to B00250.tif hence the second line of the code.

IntegralIntensities.m

```
for n=1:250

  images{n} = imread(sprintf('B%05d.tif',n));
  II{n}=sum(images{n}(:));

end
```

Going back to the Abel deconvolution code and supposing that the Davis 7 processed image is 808 by 972 pixels in dimension with a resolution of 0.124 mm/pixel. The variables in the "HalfAbel.m" function are defined with the aid of the accompanying figure. CentXPix is the central pixel location in the image; the half image selected for analysis is either from CentXPix to left edge of image (WhichWay==1) or the opposite (WhichWay==2) whereas Image radius, R is calculated as shown in the figure below.

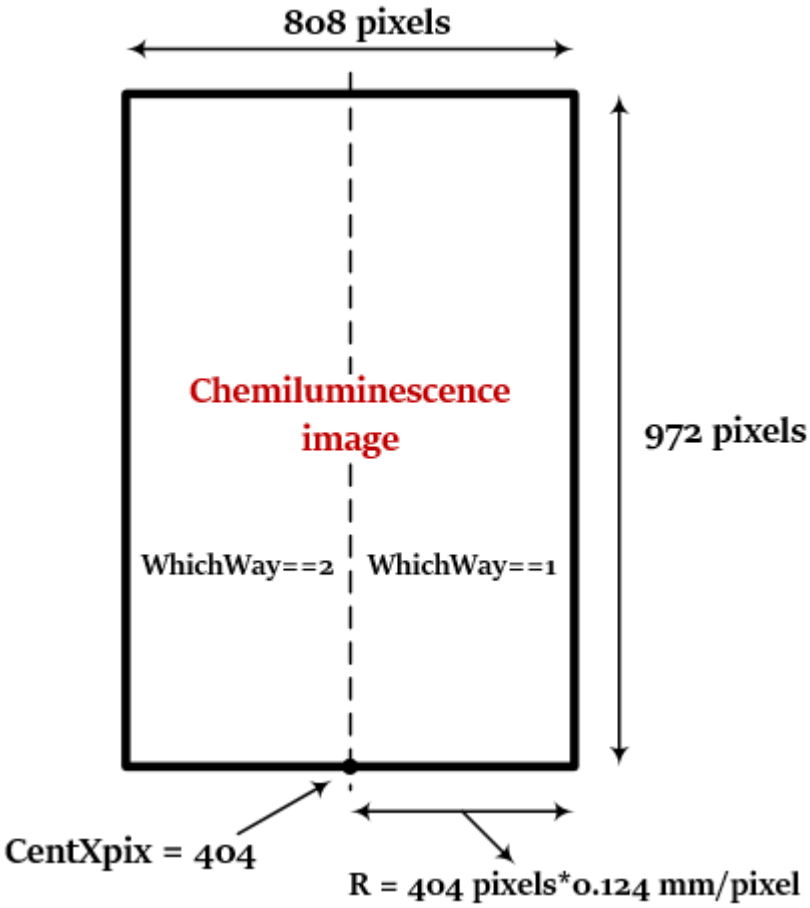

HalfAbel.m

```
function [ImAbel] = HalfAbel(Image, R, CentXPix, WhichWay)
[i j] = size (Image);
n = (j/2) + 1;
if WhichWay == 1
NewEdge = (2*(j-CentXPix));
%Initialize output image matrix
ImAbel = zeros(i, NewEdge);
k = (NewEdge/2) - 1;
%For loop cycles through each row of the input image
for z = 1:i
%Extract single image row
A = Image(z, CentXPix:j);
%Convert image row to double precision
A2 = im2double(A, 'indexed');
%Calls the Abel inversion function one row at a time with
an
%input of 5 cosinus expansions in the Fourier-series-like
%expansion
[f_rec , X] = abel_inversion(A2,R,5);
%Add the Abel deconvoluted row to the output matrix
ImAbel(z, (NewEdge/2):NewEdge) = f_rec(:,1);
%Rotate the Abel deconvoluted row about the central axis
f_rec = flipud(f_rec);
ImAbel(z, 1:k) = f_rec(2:(NewEdge/2),1);
end
end
if WhichWay == 2
NewEdge = (2*CentXPix);
ImAbel = zeros(i, NewEdge);
k = (NewEdge/2) - 1;
%For loop cycles through each row in the input image
for z = 1:i
    %Extract single image row
A = Image(z, 1:(CentXPix+1));
A = fliplr(A);
%Convert image row to double precision
A2 = im2double(A, 'indexed');
%Calls the Abel inversion function one row at a time with
an input
%of 5 cosinus expansions in the Fourier-series-like
expansion
[f_rec , X] = abel_inversion(A2,R,5);
%Add the Abel deconvoluted row to the output matrix
ImAbel(z, (NewEdge/2):NewEdge) = f_rec(:,1);
%Rotate the Abel deconvulted row about the central axis
f_rec = flipud(f_rec);
ImAbel(z, 1:k) = f_rec(2:(NewEdge/2),1);
end
end
end
```

Appendix C: Convergence criteria

Diesel/methane 90/10 blend

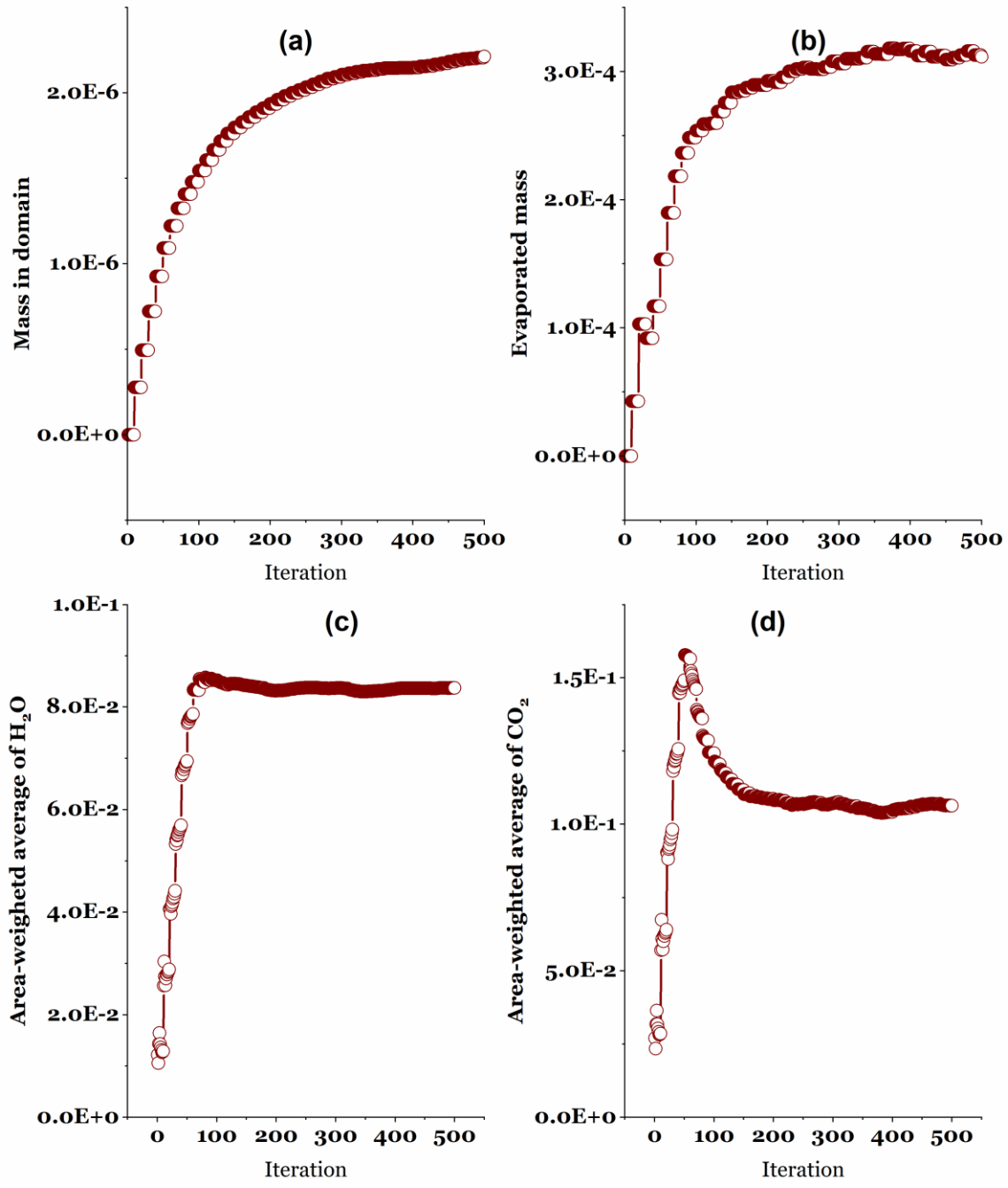

Fig. C1. Convergence history of (a) total mass in domain (b) evaporated mass (c) area-weighted average of H_2O and (d) area-weighted average of CO_2 for diesel/methane 90/10 blend.

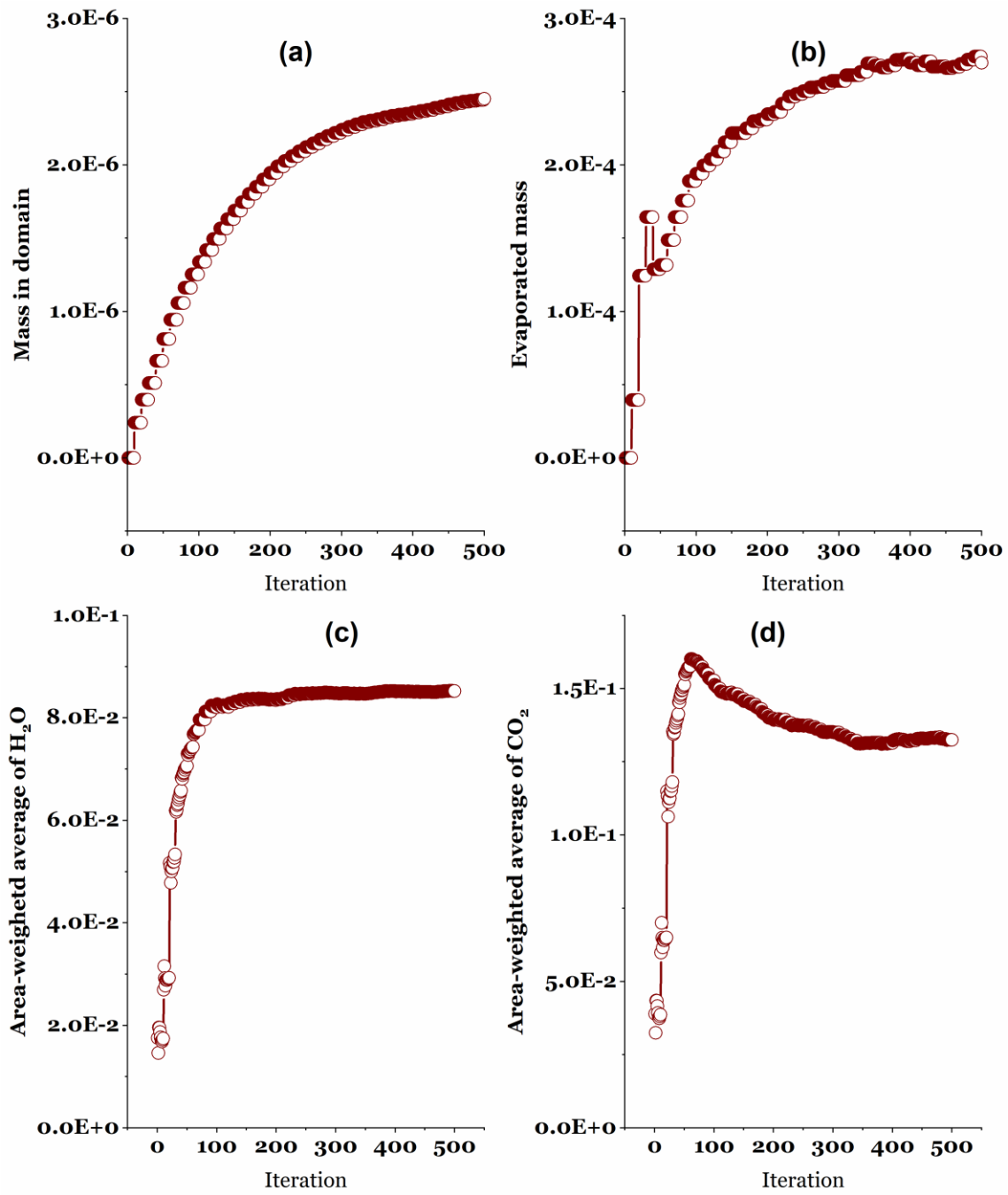

Fig. C2. Convergence history of (a) total mass in domain (b) evaporated mass (c) area-weighted average of H_2O and (d) area-weighted average of CO_2 for diesel/methane 80/20 blend.

Diesel/methane 70/30 blend

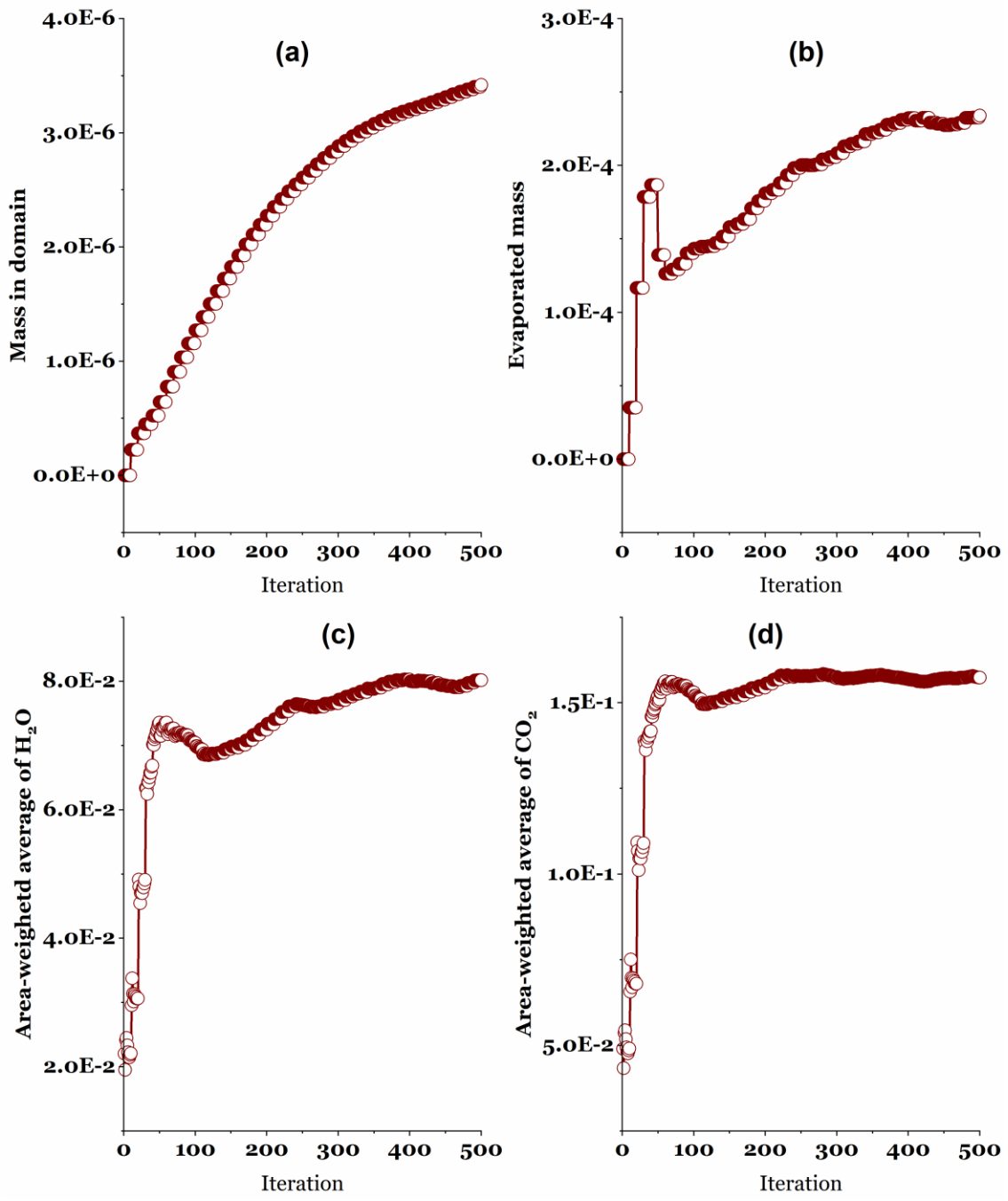

Fig. C3. Convergence history of (a) total mass in domain (b) evaporated mass (c) area-weighted average of H_2O and (d) area-weighted average of CO_2 for diesel/methane 70/30 blend.